UNIVERSITY OF BELGRADE

FACULTY OF CHEMISTRY

Slađana Z. Đurđić

Graphene and nano-structured oxides composites as components of glucose and polyphenols biosensors

Doctoral Dissertation

Belgrade, 2021.

УНИВЕРЗИТЕТ У БЕОГРАДУ

ХЕМИЈСКИ ФАКУЛТЕТ

Слађана З. Ђурђић

Композити графена и наноструктурисаних оксида као компоненте биосензора глукозе и полифенола

Докторска Дисертација

Београд, 2021.

Supervisors:

Dr. Jelena Mutić

Associate professor, University of Belgrade - Faculty of Chemistry

_____

Dr. Dalibor Stanković

Assistant professor, University of Belgrade - Faculty of Chemistry

_____

***Committee members*:**

Dr. Dragan Manojlović

Full professor, University of Belgrade - Faculty of Chemistry

_____

Dr. Goran Roglić

Full professor, University of Belgrade - Faculty of Chemistry

_____

Dr. Ľubomír Švorc

Associate professor, Slovak University of Technology in Bratislava -
Faculty of Chemical and Food Technology (Institute of Analytical Chemistry),
Slovak Republic

_____

Date: _____

Acknowledgments

I owe sincere gratitude to my mentors Dr. Jelena Mutić, associate professor at the Faculty of Chemistry - University of Belgrade, and Dr. Dalibor Stanković, assistant professor at the Faculty of Chemistry - University of Belgrade, for the proposed topic, help, encouragement and constructive advices provided during this doctoral dissertation. I would also like to thank them for their selfless commitment, constant support, and patience, which ensured my scientific success so far.

I would like to express my gratitude to Professor Dr. Dragan Manojlović, full professor at the Faculty of Chemistry - University of Belgrade, for the selfless support provided during the preparation of this doctoral dissertation, but also for the opportunity to work on my Bachelor, Master's and Doctoral studies in his laboratory. I also thank him for the company during the, now traditional, daily morning coffee and "tea", followed by constructive conversations on various topics.

I owe a special thanks to Professor Dr. Goran Roglić, full professor at the Faculty of Chemistry - University of Belgrade, for every advice, unconditional support, and patience during the preparation of present doctorate. I am most grateful for his "*countering*" which, in fact, was aimed at move my boundaries, related to science and contribution to science, to greater levels. I recognized that and made the most of it.

I would like to thank Dr. Lubomir Švorc, Associate Professor at the Faculty of Chemistry and Food Technology, University of Bratislava (Slovakia), for his consent to be a member of the Commission for the evaluation and defense of this doctoral dissertation, as well as for useful advices and assistance.

I would like to express my gratitude to my friend and colleague Dr. Vesna Stanković, research associate at IHTM, for being with me since Bachelor thesis, until today, and I believe from today. Also, thank you for the understanding and friendship provided during all these years, but also for the unreserved support during the preparation of this doctoral dissertation.

I would like to thank Dr. Biljana Dojčinović, Dr. Marija Pergal, and Vojin Krsmanović for useful advices, also to friends and colleagues from the Faculty (Filip, Igor, Daca, Đurđa, Aca, Jovana, Slađa, Branko, Slavka, Beka, Nikola, Sara and Pera) on selfless companionship, support and joint scientific achievements, as well as Simke, whose encouragement I receive every day.

I especially thank my life friends - Tamara, Kristina and Mima (as well as their husbands) for their daily love, understanding, advices, companionship and constructive criticism. I apologize to them, if I ever, mostly due to the writing and realization of this dissertation, deprived them of my love and attention.

In the end, I owe the greatest gratitude to my family, mother Branka, brother Slaviša and sister Snežana for their unconditional love, understanding and selfless sharing. Thank you for the daily support provided during the preparation of this doctoral dissertation, for the purpose of its final realization. Also, we know who would be the proudest of all today...

Slađana Z. Đurđić

Захвалница

Огромну захвалност дугујем својим менторима др Јелени Мутић, ванредном професору Хемијског факултета - Универзитета у Београду, и др Далибору Станковићу, доценту Хемијског факултета - Универзитета у Београду на предложеној теми, огромној помоћи, охрабривању и конструктивним саветима пруженим током израде ове докторске дисертације. Такође им хвала за несебично залагање, константну подршку и стрпљење, из којих је заправо проистекао сав мој досадашњи научни успех.

Велику захвалност дугујем професору др Драгану Манојловићу, редовном професору Хемијског факултета - Универзитета у Београду, на несебичној подршци пруженој током израде ове докторске дисертације, али пре свега на могућности да завршни рад, мастер и докторске студије започнем и завршим у његовој лабораторији. Такође му хвала на друштву током, сад већ традиционалног, свакодневног јутарњег испијања кафе и „чаја“, уз констуктивне разговоре о свим могућим темама.

Професору др Горану Роглићу, редовном професору Хемијског факултета - Универзитета у Београду, дугујем посебну захвалност на сваком савету, безусловној подршци и стрпљењу током израде овог доктората. Највише се захваљујем на његовом „контрирању“ које је, заправо, имало за циљ померање мојих граница везаних за науку и допринос науци. Ја сам ову добру намеру препознала и успешно искористила.

Др Љубомиру Шворцу, ванредном професору Факултета за хемију и технологију хране – Универзитета у Братислави (Словачка), се захваљујем на прихватању предлога да буде члан Комисије за оцену и одбрану ове докторске дисертације, као и на корисним саветима и помоћи у раду.

Пријатељици и колегиници др Весни Станковић, истраживачу сараднику ИХТМ-а, желим да искажем огромну захвалност на томе што је била уз мене од почетка завршног рада, па све до данас, а верујем и од данас. Такође, хвала јој на разумевању и пријатељству пруженом током свих ових година, али и за безкомпромисну подршку током израде ове докторске дисертације.

Желела бих да се захвалим др Биљани Дојчиновић, др Марији Пергал и Војину Крсмановићу на корисним саветима, затим пријатељима и колегама са Факултета (Филипу, Игору, Даци, Ђурђи, Аци, Јовани, Слађи, Бранку, Славки, Беки, Николи, Сари и Пери) на несебичном дружењу, бодрењу и заједничким научним остварењима, као и Симкету чије охрабривање слушам из дана у дан.

Посебно се захваљујем својим животним пријатељима и кумовима - Тамари, Кристини и Мими, на свакодневној љубави, разумевању, саветима, дружењу и конструктивним критикама. Извињавам им се ако сам их некад, највише због писања и реализације ове дисертације, ускратила за своју љубав и пажњу.

На крају, највећу захвалност дугујем својој породици, мајци Бранци, брату Славиши и сестри Снежани, на безусловној љубави, разумевању и несебичном дељењу. Хвала вам за свакодневну подршку пружену током израде ове докторске дисертације, у циљу њене коначне реализације. Такође, знамо ко би данас био најпоноснији...

Слађана З. Ђурђић

List of abbreviations

A - adenine
ABTS - 2,2'-azino-bis (3-ethylbenzothiazoline-6-sulfonic acid)
ABS - acetate buffer solution
Asc - ascorbic acid
BDD - boron doped diamond electrode
BPI - bioelectrochemical polyphenolic index
BRBS - Britton-Robinson buffer solution
C- cytosine
CE - counter electrode
CNT - carbon nanotubes
CPE - carbon paste electrode
CT - catechol
CVD - chemical vapor deposition
DET - direct electron transfer
DME - dripping mercury electrode
DMF - *N*,*N*-dimethylformamide
DNA - deoxyribonucleic acid
Dop - dopamine
dsDNA - double-stranded DNA
EDS - 1-ethyl-3-(3-dimethylamino- propyl) carbodiimide hydrochloride
EIS - electrochemical impedance spectroscopy
$\boldsymbol{Ep_a}$ - potential of anodic peak
$\boldsymbol{Ep_k}$ - potential of cathodic peak
EPI- electrochemical polyphenolic index
ERGO - electrochemically reduced graphene oxide
$\mathbf{FAD^+}$ - flavin adenine dinucleotide
$\mathbf{FADH_2}$ - reduced flavin adenine dinucleotide
FE-SEM - field emission-scanning electron microscopy
Fru - fructose
G - guanine
GCE - glassy carbon electrode
GNR - graphene nanoribbons
GNR@$\mathbf{Bi_2O_3}$ - graphene nanoribbons decorated with Bi_2O_3 nanoparticles
GNP - graphene nanoplatelets
GNP@$\mathbf{MnO_2}$ - graphene nanoplatelets decorated with MnO_2 nanoparticles
GO - graphene oxide
$\mathbf{GO_x}$ - glucose oxidase
HET - heterogenous electron transfer
HMDE - hanging mercury drop electrode
HOPG - highly oriented pyrolytic graphite
HSA - human serum albumin
HQ - hydroquinone
I - current intensity
$\boldsymbol{Ip_a}$ - intensities of anodic peak
$\boldsymbol{Ip_c}$ - intensities of cathodic peak
ISO - International Organization for Standardization
IUPAC - International Union of Pure and Applied Chemistry
LCD - liquid crystal display
LED - light-emitting diodes
LOD - limit of detection

LOQ - limit of quantification
Mal - maltose
M_xO_y - metal oxide
NAD^+ - reduced nicotinamide adenine dinucleotide
NADH - nicotinamide adenine dinucleotide
Naf - Nafion
NHS - *N*-hydroxysulfosuccinimide sodium salt
NMP - *N*-methyl-2-pyrrolidone
Par - paracetamol
***p*-nPh** - para nitrophenol
p_a - anodic peak
p_k - cathodic peak
PBS - phosphate buffer solution
PdI - index of polydispersity
PGE - poly(3,4-ethylenedioxy-thiophene)/graphene oxide
PMMA - polymethylmethacrylate
r - Pearson regression coefficient
RE - reference electrode
rGO - reduced graphene oxide
RSD - relative standard deviation
SEM - scanning electron microscopy
SMDE - static mercury drop electrode
SPCE - screen printed carbon electrode
SPCE/GNR@Bi_2O_3/GO_x - developed glucose biosensor
SPCE/GNP@MnO_2/TvL/Naf - developed polyphenolic index biosensor
ssDNA - single-stranded DNA
SWCNT - single wall carbon nanotube
SWV - square wave voltammetry
T- thymine
Tart - tartaric acid
TEM - transmission electron microscopy
TEMPO - (2,2,6,6-tetramethylpiperidin-1-yl)oxyl
THF - tetrahydrofuran
TvL - laccase from *Trametes Versicolor*
Uric - uric acid
WE - working electrode
XRD - X-ray diffraction
XRPD - X-ray powder diffraction

Graphene and nano-structured oxides composites as components of glucose and polyphenols biosensors

ABSTRACT

Present doctoral dissertation describes the development of novel glucose and polyphenolic index biosensors, based on a combination of graphene nanomaterials and nano-structured metal oxides. An in-depth examination of how mentioned nanomaterials separately influence the electrochemical performances of developed biosensors, as well as their synergic effect, is provided within the scope of this dissertation. In order to obtain desired working electrodes, synthesized nanocomposites were applicated on the surface of screen printed carbon electrodes (SPCEs). Cyclic voltammetry and chronoamperometry were electrochemical methods utilized for testing electrochemical performances of synthetized nanocomposites as well as the final biosensors.

Glucose biosensor was based on the modification of graphene nanoribbons (GNR) with Bi_2O_3 nanoparticles. The synthesized GNR@Bi_2O_3 nanocomposite was introduced to the surface of SPCE, in order to obtain the working electrode (SPCE/GNR@Bi_2O_3). Glucose biosensor was prepared by immobilization of glucose-oxidase (GO_x), from *Aspergillus niger*, on the surface of SPCE/GNR@Bi_2O_3, and followed by coating of the enzyme with Nafion (Naf) solution. Developed SPCE/GNR@Bi_2O_3/GO_x/Naf biosensor has been successfully applied for the quantification of glucose in a honey sample.

Polyphenolic index biosensor was constructed by modification of graphene nanoplatelets (GNP) with MnO_2 nanoparticles. In order to produce the working electrode (SPCE/GNP@MnO_2), SPCE has been modified with GNP@MnO_2 nanocomposite. The final polyphenolic index biosensor has been produced by immobilization of the laccase, from *Trametes Versicolor* (TvL), onto the SPCE/GNP@MnO_2 surface, and followed by the application of Naf. Using the developed SPCE/GNP@MnO_2/TvL/Naf biosensor, the polyphenolic index in wine was successfully determined.

Keywords: biosensors, electrochemistry, glucose, glucose-oxidase, graphene nanoplatelets, graphene nanoribbons, laccase, metal oxide nanoparticles, polyphenolic index.

Scientific field: Chemistry

Scientific subfield: Analytical Chemistry

UDC number:

Композити графена и наноструктурисаних оксида као компоненте биосензора глукозе и полифенола

РЕЗИМЕ

Представљена докторска дисертација описује развој нових биосензора за одређивање глукозе и полифенолног индекса који се заснивају на комбинацији графенских наноматеријала и наноструктурисаних металних оксида. Утицај поменутих наноматеријала на електрохемијске перформансе развијених биосензора, као и њихов синергијски ефекат, је детаљно проучен у оквиру ове дисертације. Синтетисани нанокомпозити су нанети на површину штампаних угљеничних електрода (*SPCE*) у циљу добијања радних електрода. Циклична волтаметрија и хроноамперометрија су електрохемисјке методе које су коришћене за испитивање електрохемијских перформанси синтетисаних нанокомпозита, као и финалних биосензора.

Биосензор за одређивање глукозе се заснивао на модификацији графенских нанотрачица (*GNR*) са Bi_2O_3 наночестицама. Синтетисани *GNR@*Bi_2O_3 нанокомпозит је нанет на површину *SPCE* у циљу добијања радне електроде (*SPCE/GNR@*Bi_2O_3). Биосензор за одређивање глукозе је припремљен имобилизацијом глукоза-оксидазе (*GO*$_x$) из *Aspergillus niger* на површину *SPCE/GNR@*Bi_2O_3, што је праћено превлачењем ензима са раствором нафиона (*Naf*). Развијени *SPCE/GNR@*Bi_2O_3*/GO*$_x$*/Naf* биосензор је успешно примењен за квантификацију глукозе у узорку меда.

Биосензор за одређивање полифенолног индекса се базирао на модификацији графенских наноплочица (*GNP*) са MnO_2 наночестицама. *SPCE* је модификована са *GNP@*MnO_2 нанокомпозитом у циљу конструкције радне електроде (*SPCE/GNP@*MnO_2). Биосензор за одређивање полифенолног индекса је конструисан након имобилизације лаказе из *Trametes Versicolor* (*TvL*) на површину *SPCE/GNP@*MnO_2, након чега је уследило наношење *Naf* раствора. Полифенолни индекс у узорцима вина је одређен користећи развијени *SPCE/GNP@*MnO_2*/TvL/Naf* биосензор.

Кључне речи: биосензори, електрохемија, глукоза, глукоза-оксидаза, графенске наноплочице, графенске нанотрачице, лаказа, наночестице металних оксида, полифенолни индекс.

Научна област: Хемија

Ужа научна област: Аналитичка хемија

УДК број:

Table of contents

1. Introduction

In 1962, the first electrochemical biosensor was developed and used to quantify glucose in blood. Until today, the interest in the development of biosensors for the detection of various compounds has not diminished. Electrochemical biosensors for the quantification of glucose and polyphenols, which are characterized by simple and inexpensive preparation, have found wide application in biological, chemical and environmental determination, food quality assessment, as well as in the industrial and pharmaceutical industries. Also, today it is unthinkable to determine glucose content in clinical samples without electrochemical biosensors, in order to detect diabetes and similar diseases. On the other hand, polyphenolic compounds show high antioxidant activity and protect the organism from oxidation of enzymes, proteins and genetic material by free radicals (polyphenols act as radical "scavengers"). In addition, polyphenols are characterized by biological activities such as antibacterial and anti-inflammatory, but also play an important role in defining food quality. According to this brief review, the determination of glucose and polyphenolic content in various areas is essential, and in this regard the development of simple and sensitive analytical methods for monitoring the concentration of these metabolites in different samples is of utmost importance.

Although many classical methods can be used to detect glucose and polyphenols, electroanalytical methods, especially voltametric and amperometric methods, are more dominant due to their advantages. Electroanalytical methods reflect simple instrumentation, low cost, easy operation as well as fast response, high sensitivity and selectivity of the applied sensors (working electrodes).

In fact, selecting the most suitable working electrode is one of the key steps in developing electrochemical methods. Screen printed carbon electrodes (SPCEs) are one of the most widely used electrochemical disposable sensors, due to their electrical characteristics, easy preparation, as well as the possibility of their modification by various mediators. Today, thanks to nanotechnology that enables the synthesis and application of new nanomaterials (mediators, catalysts), graphene nanomaterials, due to their unique electrochemical and physical properties, are particularly dominant and widely used in the modification of SPCE, as well as other electrochemical sensors, to improve their electrochemical performances. The combination of graphene nanomaterials with metal oxide (M_xO_y) nanoparticles that act as a catalyst, using amperometric methods, leads to the development of new electrochemical sensors/biosensors characterized by high sensitivity of determination, high selectivity, as well as the possibility of simultaneous determination.

Within this doctoral dissertation there are four major chapters: ***General part***, ***Experimental part***, ***Results and Discussion*** and ***Conclusion.***

The ***GENERAL PART*** chapter gives a brief overview of the properties of graphene, graphene production techniques, graphene nanomaterials, as well as the application of graphene. Further in the text, the characteristics of transition M_xO_y are described, as well as their electrochemical application. This is followed by a brief literature review of graphene@M_xO_y-based biosensors for the determination of glucose and polyphenols. Electrochemical methods are further described with special review to cyclic voltammetry and chronoamperometry, followed by the basic characteristics of electrochemical sensors, with an emphasis on the SPCE. Then follows a brief description of the principles of X-ray powder diffraction (XRPD) and field emission scanning electron microscopy (FE-SEM) techniques, as a method for defining the crystal structure of nanocomposites. The next section is dedicated to biosensors and enzyme immobilization methods, with special reference to glucose and polyphenolic index biosensors.

The ***EXPERIMENTAL PART*** lists nanomaterials, chemicals, solutions and reagents used in different experimental steps, instrumentation and synthesis procedures of nanocomposites, as well as procedures for the preparation of corresponding biosensors.

In ***RESULTS AND DISCUSSION***, the results obtained during the development of amperometric methods for the detection of glucose and caffeic acid (as a model compound for determining polyphenols content) with graphene@M_xO_y-based biosensors, are presented and discussed. Obtained electroanalytical parameters such as linear concentration range, limit of detection (LOD) and sensitivity of corresponding biosensors were compared with graphene@M_xO_y-based biosensor reported in literature in order to evaluated developed biosensors and proposed amperometric methods. As a final part of this chapter, the results obtained after the application of the developed biosensors in real samples are presented.

In ***CONCLUSION*** is a summarized scientific contribution of this doctoral dissertation in the field of electrochemical biosensors based on graphene nanomaterials and M_xO_y nanoparticles. Also, the main part of this chapter includes the final results and conclusions related to each segment of optimization and development of amperometric methods for the detection of glucose and caffeic acid with glucose and polyphenolic index biosensor, respectively.

2. General part

2.1. Graphene

2.1.1. Brief history of graphene

Before considering the history of graphene, the term "*graphite*" must be defined. Graphite is actually consisting of stacked layers of graphene. The first evidence of the use of graphite dates back 6000 years, but in the last 500 years the concept of graphite has been clearly defined. Already in the 16th century, graphite ore was found, which was originally thought to be lead ore. However, in 1779 the scientific Scheele proved that the mineral in chemical composition was carbon, not lead. This mineral was used by people to mark livestock. Based on this, in 1789, scientist Werner mineral named graphite (in Greek means "*writing*") *(Sharon & Sharon, 2015)*.

In the 19th century, the reduced graphite oxide was synthetized in the reaction of graphite and mixture of $KClO_4$ and HNO_3 *(Brodie, 1859)*, and in the early 1900's it was widely used in paper production. During the 20th century, an important step in discovering the structure of graphite was the first transmission electron microscopy (TEM) image of graphite layers *(Ruess & Vogt, 1948)*, while in 1960 Oxford scientists proved that graphite layers consist of a network of hexagonal rings of *C* atoms *(Ubbelohde et al., 1961)*.

In 1987, Mouras et al. introduced the term "*graphene*" and stated that graphene represent individual layers of graphite *(Mouras et al., 1987)*. Thereafter, the term "*graphite layers*" was replaced with the term "*graphene*" by the International Union of Pure and Applied Chemistry (IUPAC) commission and graphene becomes a generally accepted as two-dimensional layer of carbon atoms forming an integral part of graphite materials (graphite, carbon nanotubes (CNT), fullerene).

At the beginning of the 21st century, significant discoveries were appeared regarding the synthesis and application of graphene. Graphene was patented in 2002, and the patent was named "*Nano-scaled graphene plates*" *(Sharon & Sharon, 2015)*. The anisotropic properties of the C=C bond were discovered in 2003 *(Takai et al., 2003)*, which influenced the further development of procedures for the synthesis of graphene and a more detailed characterization of the material. In 2004, scientists at the University of Manchester utilized the *Scotch tape technique* in order to isolate layers of graphene out of graphite. After the successful isolation, the layers have been applied onto a thin SiO_2 film *(Novoselov, 2004)*, thus this year is considered the year of graphene discovery in many studies and publications. Soon after, graphene undergoes intense and detailed research, and in turn, many scientific papers about synthesis, properties, characterization, as well as potential application emerged from this field of chemistry.

2.1.2. Structure of graphene

Carbon (C) is one of the most represented elements on Earth. Accordingly, it is part of the largest number of compounds (usually as a major element). Carbon can build bonds in all types of hybridization (sp^3, sp^2 and *sp*). Different types of hybridization provide the packing of carbon atoms into different allotropic modifications. sp^2 hybridization allows carbon bonding to different structures (Figure 1) such as *0-D* (fullerene), *1-D* (CNT or single wall carbon nanotubes (SWCNT)), *2-D* (graphene) and *3-D* structure (graphite). Carbon atoms bound by sp^3 hybridization form a diamond (Figure 1. 3-D_b). This allotropic carbon modification is considered to be the most rigid material and occupies the highest position on the *Mohs* scale of mineral hardness (hardness level 10) *(Pumera et al., 2010)*.

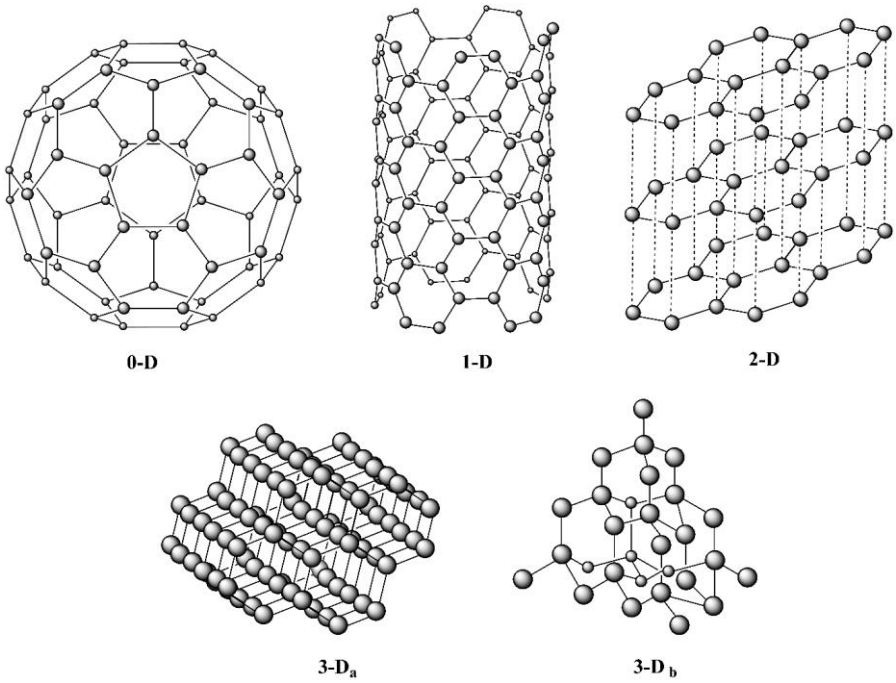

Figure 1. Schematic illustration of different carbon allotropic modifications. Forms of sp^2-bonded *C* atoms: *O-D* structure (fullerene), *1-D* structure (SWCNT), *2-D* structure (graphene) and *3-D$_a$* structure (graphite) and sp^3-bonded *C* atoms: *3-D$_b$* structure (diamond).

Graphene is a planar, two-dimensional (*2-D*), monolayer of graphite. The carbon atoms in graphene are sp^2 hybridized and linked by covalent bonds in a hexagonal configuration. The distance between graphene layers is 3.3 Å (Figure 2) and the layers are connected by weak van der Waals forces *(Sharon & Sharon, 2015)*. The *C=C* bond length in graphene is 1.42 Å (Figure 2). Due to sp^2 hybridization between carbon atoms *ie*. the existence of delocalized electron clouds above and below the ring (Figure 2), the electronic properties of graphene are particularly pronounced. The electrical conductivity and mobility of electrons is one of the main characteristics of graphene. Electron mobility is defined by the *charge-carrier mobilities* parameter *(Wang et al., 2018a; Yang et al., 2010a)*. The quality of the newly synthesized graphene is evaluated on the basis of this parameter (*see section 2.1.3. Fabrication of graphene). Charge-carrier mobilities* within and between graphene layers are summarized in *Table 1*. In addition to its excellent electronic properties, *Table 1*. gives other parameters that reflect the unique properties of graphene.

Table 1. Properties of graphene.

Parameters	Value	Reference
Charge-carrier mobilities $(cm^2 (V*s)^{-1})$	$1.5*10^4$ (between layers at 298 K) $2.0*10^5$ (inside layers at 298 K)	*(Adetayo & Runsewe, 2019; Krishnan et al., 2019; (Wang et al., 2018a)*
Surface area $(m^2 g^{-1})$	~ 2600 (*for com.**: graphite - 10; CNT - 1315)	*(Bahadır & Sezgintürk, 2016; Krishnan et al., 2019)*
Electrical conductivity $(mS\ cm^{-1})$	~ 65 (*for com.*: SWCNT - 1)	*(Bahadır & Sezgintürk, 2016)*
Thermal conductivity $(Wm\ K^{-1})$	~ 5300 (*for com.*: SWCNT - 3500; MWCNT - 3000)	*(Adetayo & Runsewe, 2019; Balandin et al., 2008)*
Mechanical strength *(GPa)*	130	*(Pugno, 2009)*
Optical transmittance *(%)*	~ 97 (at visible light)	*(Adetayo & Runsewe, 2019; Hu et al., 2010)*
Opacity *(%)*	~ 2 (at visible light)	*(Hu et al., 2010; Krishnan et al., 2019)*
Elasticity *(TPa)*	1.0 (*for com.*: steel - 0.1)	*(Hu et al., 2010; Krishnan et al., 2019)*

**for comparison*

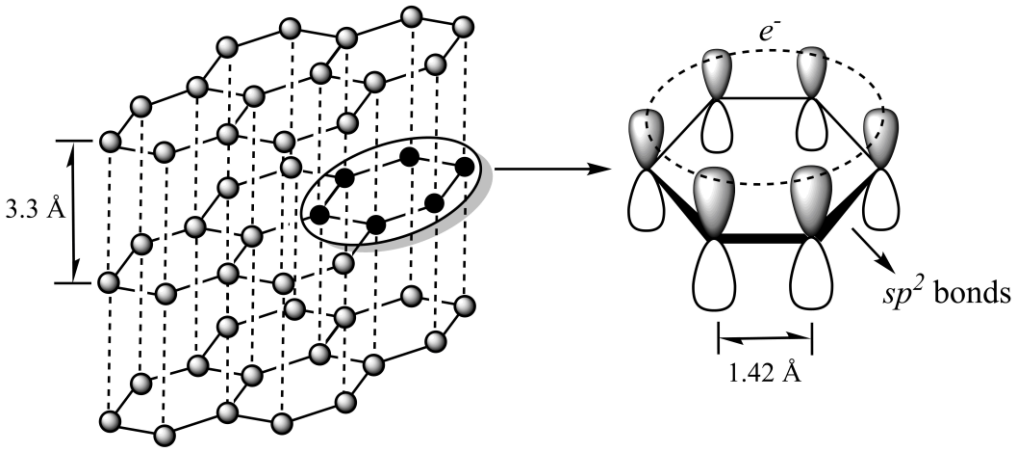

Figure 2. Schematic illustration of graphene layers structure (left). sp^2 hybridization within graphene structure with electron delocalization (right).

2.1.3. Fabrication of graphene

Techniques for the production of graphene can be broadly divided into two groups: "*Top down*" and "*bottom up*" techniques *(Wang et al., 2018a; Adetayo & Runsewe, 2019; Omkaram et al., 2018)*. The classification of these techniques by the appropriate methods is shown in *Scheme 1*.

Graphene obtained by "*Top down*" techniques is typically characterized by *charge-carrier mobilities* up to $1*10^3$ cm^2 $(V*s)^{-1}$. The dispersion of graphene layers in solvents (aqueous or organic depending on the method) is the main principle of graphene synthesis by these techniques. "*Bottom up*" techniques are based on epitaxial growth or evaporation of graphene layers from the surface of certain substrates. The graphene obtained by these methods is characterized by *charge-carrier mobilities* greater than $1*10^3$ cm^2 $(V*s)^{-1}$, indicating high quality graphene. The basic principles of all the above methods given in *Scheme 1.*, with a schematic illustration, will be explained in this doctoral dissertation.

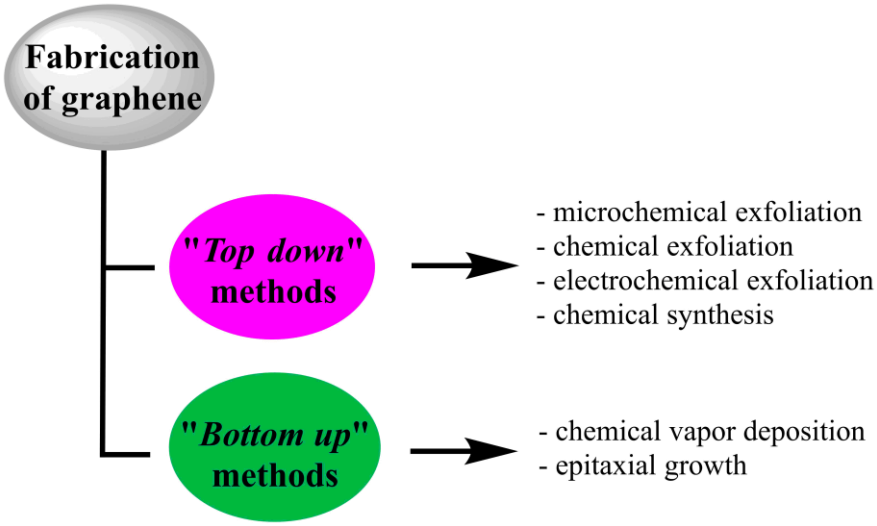

Scheme 1. Graphene fabrication methods.

2.1.3.1. "*Top down*" techniques

2.1.3.1.1. Mechanical exfoliation

In 2004, the first method for extracting graphene layers from graphite was introduced. The method was based on micromechanical peeling of graphite using a simple adhesive tape technique *(Novoselov & Castro Neto, 2012; Omkaram et al., 2018)*. The method is based on pressing the Scotch tape against the surface of the graphite, so few graphene layers are attached to the adhesive. Then, the tape with the graphene layers was pressed onto the surface of the corresponding substrate. Upon peeling off, the graphene monolayer is left on the substrate (Figure 3).

Highly oriented pyrolytic graphite (HOPG), microcrystalline graphite or natural graphite can be used as a raw material for graphene production. Mechanical exfoliation (cleaving, peeling) of graphite, in addition to adhesive tape technique, can be performed by electric field or ultrasonication. In order to obtain larger graphene fragments (up to several millimeters), mechanical cleavage can also be carried out by applying a suitable polymer on which the graphene layers are considerably better adhered *(Adetayo & Runsewe, 2019; Yang et al., 2010a)*.

This method is excellent for obtaining high quality single-layer, two-layer graphene and generally graphene nanomaterials. However, obtaining graphene by mechanical peeling is a lengthy

process. In addition, the yield of graphene is very small, so graphene obtained by this method is mainly used for research purposes *(Wang et al., 2018a; Yang et al., 2010a)*.

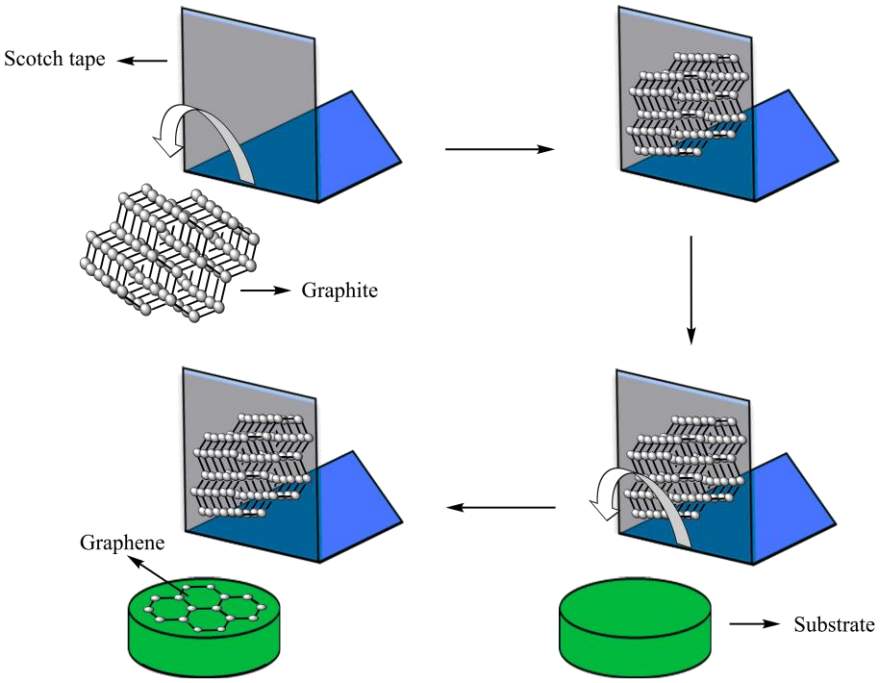

Figure 3. Schematic illustration of micromechanical exfoliation.

2.1.3.1.2. Chemical exfoliation

Method is based on intercalation of alkali metals or anions into graphite *(Adetayo & Runsewe, 2019; Rizwan & Fatima, 2018)*. Intercalation is performed at elevated temperatures, resulting in a chemical reaction between metals/anions and graphite. In session *2.1.4.1. Graphene nanomaterials* is given the principle of intercalation of ions (persulfate anions) into graphite, while the intercalation of alkali ions into graphite is described below.

Due to its small radius (1.52 Å) which allows it to facilitate intercalation within the graphene layers of graphite, potassium ion (K^+) is one of the frequently used alkali metals for chemical exfoliation *(Adetayo & Runsewe, 2019)*. In the first step, the graphite is melted with potassium at 200°C in an inert condition (Figure 4), producing potassium graphite (KC_8). Introducing K^+ results in layering within the graphite and the formation of a graphene units (*graphene-intercalated compounds*). The second step involves dispersing the obtained graphene units in ethanol by ultrasonication (*Reaction 1.*). Also, the resulting H_2 further stimulates the exfoliation of graphene units from graphite. In addition to ethanol, other organic solvents, such as tetrahydrofuran (THF) or *N*-methyl-2-pyrrolidone (NMP), can be used. At the end of the process, the organic solvents are removed by vacuum distillation and then the single-layer graphene sheets are left behind *(Adetayo & Runsewe, 2019; Saleem et al., 2018)*.

$$KC_8 + EtOH \longrightarrow 8C + EtOK + \frac{1}{2}H_2$$

Reaction 1. Dispersion of potassium graphite (KC_8) in aqueous ethanol (EtOH).

The advantages of this method are the high yield of the reaction and the production of high-quality graphene. In addition, the application of low temperatures during graphene synthesis has a positive effect on the cost-effectiveness of the method. Chemical exfoliation has proven to be excellent for obtaining nanomaterials such as graphene nanoplatelets whose properties and characteristics are described in session *2.1.4.1. Graphene nanomaterials*.

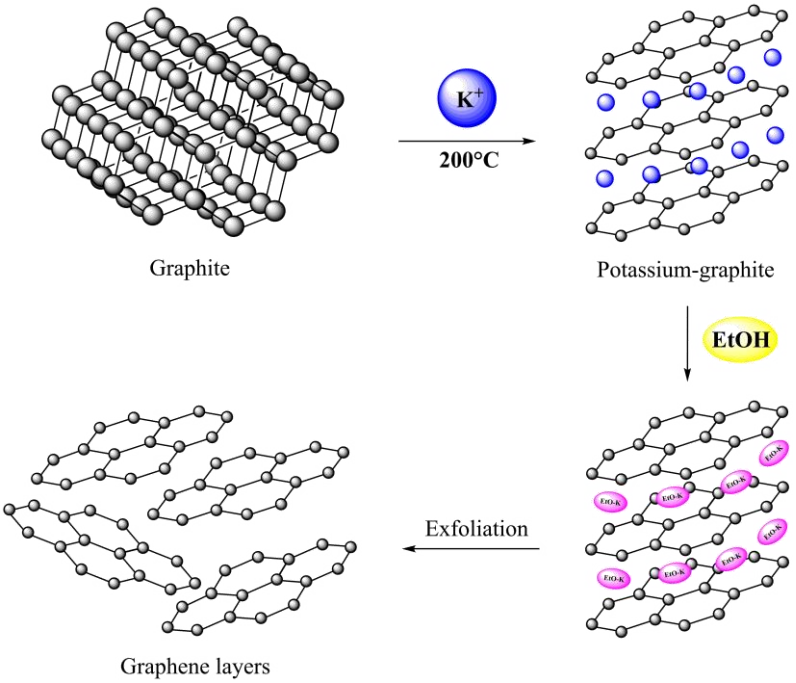

Figure 4. Schematic illustration of chemical exfoliation.

2.1.3.1.3. Electrochemical exfoliation

Graphite is used as a working electrode in this process of producing graphene. Electrochemical exfoliation is based on peeling of graphene layers from a graphite electrode using a direct current (Figure 5). Tetra-*n*-butylammonium bisulfite or ammonium-sulfate can be used as the supporting electrolyte, but acid solutions such as sulfuric, nitric, phosphoric or oxalic have also proven to be excellent supporting electrolytes in the electrochemical exfoliation of graphite *(Coroş et al., 2016; Liu et al., 2008; Wang et al., 2018a)*. The role of the supporting electrolyte during the production of graphene by this method is to insert it into the deeper graphite layers, which at a certain electrode potential leads to the peeling of graphene from the working electrode. In addition to the main exfoliation process, water electrolysis occurs due to the action of direct current. This secondary process leads to the production of radical species (most commonly $OH^{\cdot}$) that can damage the extracted graphene layers. This problem is solved by the addition of (2,2,6,6-tetramethylpiperidin-1-yl)oxyl (TEMPO) compound that acts as an oxidizing agent. The resulting graphene flakes can be collected by vacuum filtration, after which they are dispersed in an organic solvent (for example *N*,*N*-dimethylformamide (DMF)). The obtained suspension is stable for up to two months *(Wang et al., 2018a)*.

The graphene layers obtained by this method are up to 10 μm in size and are considered high quality. Also, due to the high yield of graphene flakes but also the speed, this method has found high application in the industry, in addition to laboratory research. In order to obtain a larger amount of graphene, it is possible to exfoliate graphite with two graphite electrodes by applying an alternating

current where one electrode acts as an anode and the other is a cathode. This production of graphene was only recorded under laboratory conditions *(Wang et al., 2018a; Liu et al., 2008)*.

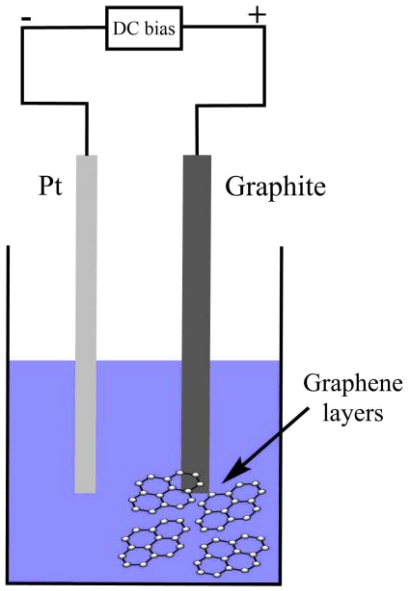

Figure 5. Schematic illustration of experimental setup for graphite electrochemical exfoliation.

2.1.3.1.4. Chemical synthesis

The method of chemical synthesis of graphene is one of the main methods for mass production of graphene. This method is based on the chemical reduction of graphite oxide (Figure 6). Three methods can be used to reduce graphite oxide: *Brodie* method, *Staudenmaier* method and *Hummer's* method. The basic principles of the *Hummer's* method will be further described, as the most applicable method for the synthesis of reduced graphite oxide *(Adetayo & Runsewe, 2019)*.

Hummer's method is based on the oxidation of graphite with a mixture of $NaNO_3$, H_2SO_4 and $KMnO_4$ *(Adetayo & Runsewe, 2019; Wang et al., 2018a)*. The structure of graphite during oxidation is altered due to the formation of functional groups (COO^-, OH^-) on graphite layers. The obtained graphene oxide (GO) shows significantly higher polarity than graphene. In GO, sp^3 hybridization between carbon atoms is mainly represented and graphene sp^2 hybridization is impaired. Also, the presence of functional groups increases the distance between graphene layers, so this phenomenon has been used to facilitate exfoliation of GO layers from unreacted graphite (Figure 6). Exfoliation is simplest by ultrasound in a mixture of organic solvent and water *(Yang et al., 2010a)*.

Functional groups on GO adversely affect the unique properties of graphene. Therefore, the reduction of GO must be carried out. Reduction is performed with hydrazine or thermal annealing. Graphene obtained by reduction is often called reduced graphene oxide (rGO) and has largely regained its properties, but still contains a significant number of functional groups. Therefore, further investigations are aimed at finding new processes for the complete, detailed reduction of GO and the synthesis of high-quality graphene *(Adetayo & Runsewe, 2019; Wang et al., 2018a; Yang et al., 2010a)*.

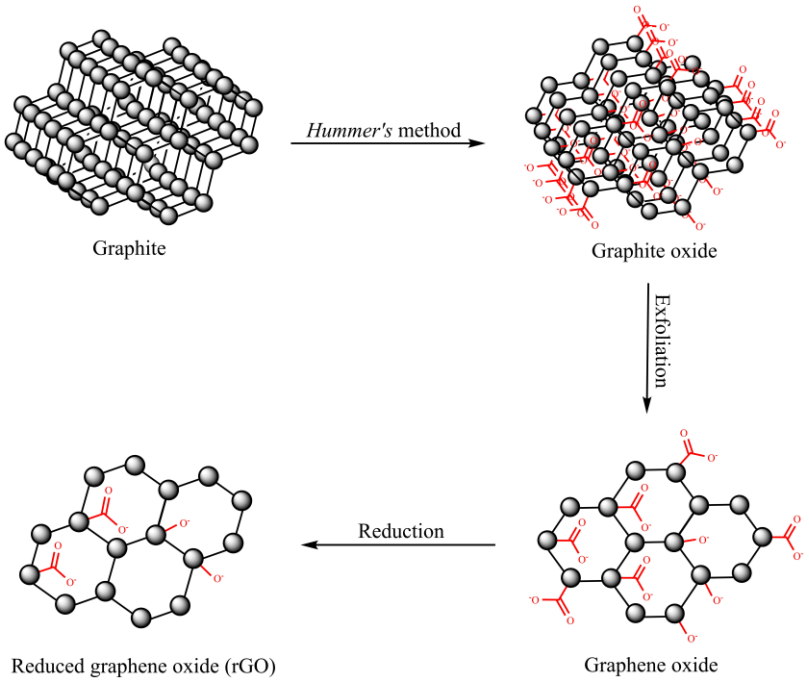

Figure 6. Schematic illustration of graphite oxide synthesis by *Hummer's* method. An additional method involves the exfoliation of graphite oxide. The resulting GO is usually chemically reduced to graphene, typically called rGO.

2.1.3.2. "*Bottom up*" techniques

2.1.3.2.1. Chemical vapor deposition

Chemical vapor deposition (CVD) is based on the thermal decomposition of hydrocarbons. Raw materials for the synthesis of graphene are gaseous hydrocarbons (methane, ethene, ethyne), aromatic hydrocarbons (benzene), but also complex organic compounds (camphor). The resulting gaseous phase is deposited on the substrate. Transition metals (copper, nickel, palladium, ruthenium) are used as a substrate due to its catalytic effect *(Adetayo & Runsewe, 2019; Wang et al., 2018a; Yang et al., 2010a)*.

The CVD principle is based on the flow of a mixture of gases (CH_4, H_2 and Ar) through a quartz tube heated at a temperature higher than 900°C. The quartz tube is equipped with a substrate most commonly made of copper due to the limited absorption of graphene layers in it. Due to the high temperatures, hydrocarbons decompose and the gaseous phase of the carbon atoms is deposited on the Cu substrate. During the process, the substrate is saturated with carbon atoms. After cooling the substrate, a thin film of graphene layer is coated on its surface (Figure 7). Deposition of graphene can be monolayer or multilayer, depending on pre-set conditions such as temperature, gas flow, pressure *(Adetayo & Runsewe, 2019; Wang et al., 2018a; Yang et al., 2010a; Liu et al., 2018)*.

After heat treatment, the Cu substrate with graphene layers is coated with a polymeric carrier. The first polymer was polymethylmethacrylate (PMMA). Graphene layers are glued to the polymer surface, followed by removal of Cu substrate with aqueous $FeCl_3$ solution or hot deionized water. After removal of the substrate, the polymer with graphene layers is transferred to the target substrate (typically Si/SiO_2). The final step of this method is the removal of the polymeric carrier by acetone, as well as the drying/annealing of the Si/SiO_2 substrate with graphene (Figure 7).

The graphene obtained by the CVD method shows high quality (*charge-carrier mobilities* is over $4*10^3$ cm^2 $(V*s)^{-1}$). Another major advantage of the method is mass production of graphene, so

its application has expanded significantly to industry. Also, the production of graphene at high temperatures is not economically profitable, so many facilities have switched to using plasma for CVD. Finally, it has been proven that CO_2 can replace H_2 in the synthesis process. This modification of the method also yields high-quality graphene (*charge-carrier mobilities* is $2*10^3$ cm^2 $(V*s)^{-1}$), which significantly increases the safety of the procedure *(Adetayo & Runsewe, 2019; Wang et al., 2018a; Yang et al., 2010a; Liu et al., 2018)*.

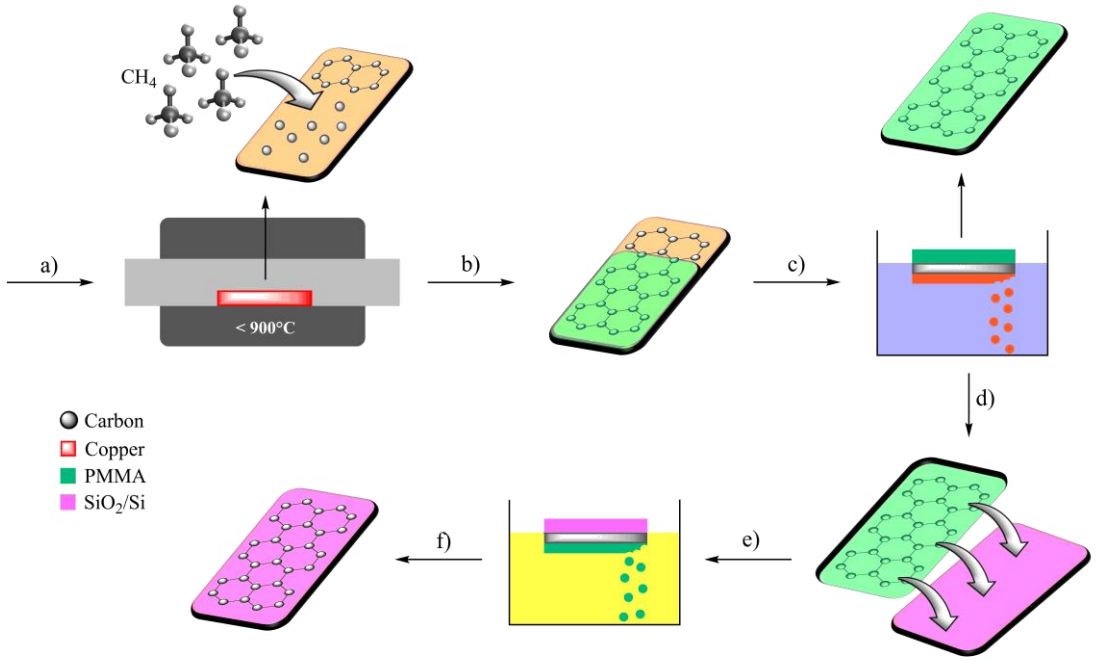

Figure 7. Schematic illustration of graphene synthesis by CVD. The process involves the following steps: ***a)*** CVD and growth process of graphene at Cu substrate; ***b)*** coating of Cu substrate with polymer (PMMA); ***c)*** washing the Cu substrate; ***d)*** transfer of graphene layers from the polymer carrier to the target substrate (SiO_2/Si); ***e)*** washing the PMMA; ***f)*** dry or annealing and finally graphene production.

2.1.3.2.2. Epitaxial growth of graphene

The epitaxial growth method is based on the formation of a single-crystalline layer (film) on a single-crystalline substrate at high temperatures, in an inert atmosphere. The epitaxial growth process can be homoepitaxial or heteroepitaxial, depending on the same or different chemical composition of the newly formed epitaxial film and substrate, respectively.

The epitaxial growth of graphene on a silicon carbide substrate (SiC) belongs to the heteroepitaxial mechanism of production. The method is based on heating the SiC-substrate at temperatures higher than 1000°C, at high pressure (Figure 8). During the process, Si sublimates from the substrate, leaving behind carbon on the substrate surface. Then, carbon atoms at high temperatures undergo a graphitization process, forming a film of monolayer or multilayer graphene. An aggravating step in this process is the transfer of graphene layers to other substrates. Therefore, SiC-substrates are coated with thin films of transition metals (nickel, copper) that act as catalysts, further facilitating the transfer of graphene *(Adetayo & Runsewe, 2019; Wang et al., 2018a; Yang et al., 2010a)*.

Graphene obtained by epitaxial growth shows high quality and excellent electronic properties. Growth of graphene on *Si*-terminus shows the *charge-carrier mobilities* up to $2*10^3$ cm^2 $(V*s)^{-1}$, while growth on the *C*-terminus even up to $3*10^4$ cm^2 $(V*s)^{-1}$. Although epitaxial growth produces high quality graphene, this method has not found application in the industry due to demanding

conditions such as high temperature and high pressure. Therefore, the application of graphene obtained in this way is largely limited to laboratory research *(Adetayo & Runsewe, 2019; Wang et al., 2018a)*.

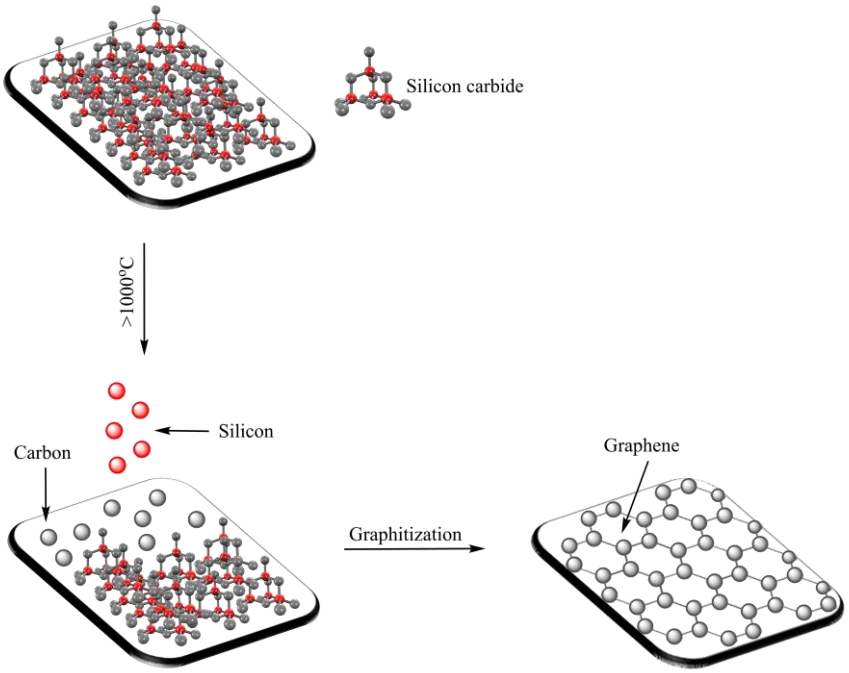

Figure 8. Schematic illustration of graphene epitaxial growth processes.

2.1.4. Nanomaterials

"*Nanomaterials*" or "*nanoscale materials*" is a term defined by the International Organization for Standardization (ISO). These terms refer to materials that have one dimension (*x*, *y* or *z*) less than 100 nm (Figure 9), *ie.* at least one dimension in the nanoscale domain (1-100 nm) *(Krishnan et al., 2019; Wang et al., 2018a)*. Accordingly, a special field of technology called nanotechnology has been developed and is focused on the production and synthesis of nanomaterials. Compared to their *bulk* materials, nanomaterials are characterized by unique chemical and physical properties such as large contact area and high conductivity. In addition, nanomaterials shows pronounced magnetic, optical and electric properties *(Krishnan et al., 2019; Malhotra & Ali, 2018*).

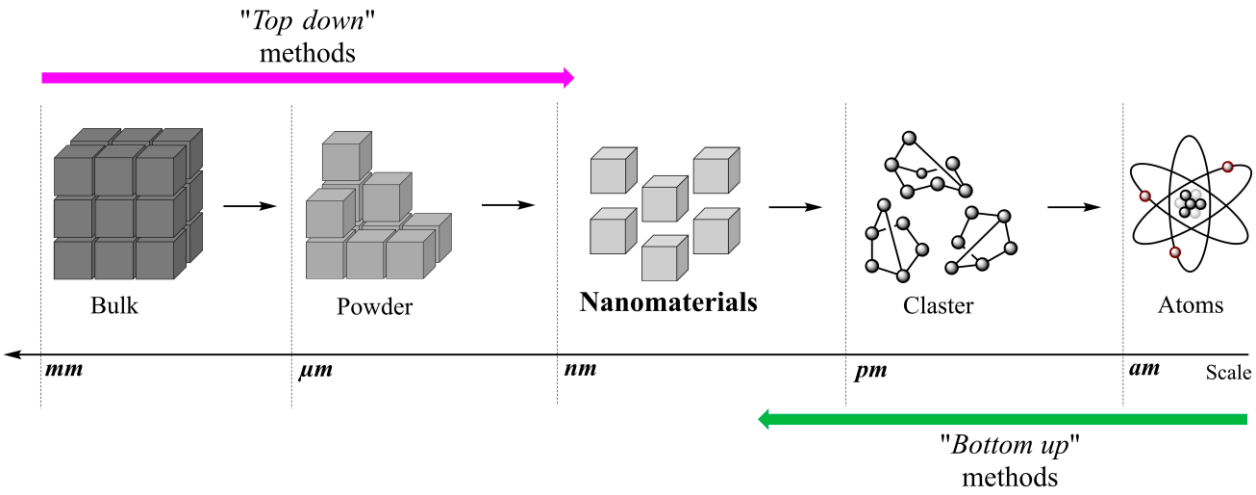

Figure 9. An overview of length scale for nanomaterials. Schematic illustration of a strategy for obtaining nanomaterials by "*top down*" and "*bottom up*" techniques.

Depending on the dimensions and size, nanomaterials can be divided into 3+1 categories *(Krishnan et al., 2019; Malhotra & Ali, 2018)* (Figure 10):

- ✓ 0-D nanomaterials - *x*, *y* and *z* dimensions are in the nanoscale domain. This group includes metallic (Ag, Pt, Au, Pd) and semiconducting (Mn, Zn) nanoparticles. The particle diameter is usually between 1 and 50 nm, and the particle shape is spherical;

- ✓ 1-D nanomaterials - one dimension, e.g., *z* in the nanoscale domain, while *x* and *y* are in the micro or macroscale domain. This group includes carbon nanomaterials (nanotubes, nanofibers, nanowires, nanorods), as well as M_xO_y nanoparticles (MnO_2, Bi_2O_3, ZnO, TiO_2);

- ✓ 2-D nanomaterials - two dimensions (e.g. *x* and *y*) in the nanoscale domain, while the *z* dimension is in the range of micro/macro scale. Graphene nanomaterials (graphene nanosheets, graphene nanoribbons, graphene nanoplatelets) are classic representatives of 2-D nanomaterials. Also, nanowalls and nano-thin films (single/multilayers) belong to this group. The thickness of 2-D nanomaterials is always in the nanoscale domain, while their surface can be in the micro/macroscale domain;

- ✓ 3-D nano/materials - this group of nanomaterials does not describe classical nanomaterials whose at least one of the dimensions is in the nanoscale domain. The dimensions of 3-D nanomaterials are in the micro/macroscale domain, but the individual blocks, of which 3-D materials are composed, are in the nanoscale domain. Polycrystals are the most faithful representatives of this group.

"*Top down*" and "*bottom up*" techniques are used for the synthesis of nanomaterials *(Wang et al., 2018a)*. The strategy of these methods is given in *Figure 9.*, while the principles are described in the previous section (*2.1.3. Fabrication of graphene*). The selection of the method depends on the desired size and category of nanomaterials. Today, nanomaterials are extremely popular in sciences such as chemistry, physics, biology. Although performance and properties have been defined, testing the structure and characteristics of nanomaterials still represent a challenge to world science. In addition to science, nanomaterials have found widespread application in other fields. Due to their unique properties, but also nano-sizes that provide easier manipulation, nanomaterials have found application in the production of primarily miniature devices. Also, due to their comparable size with biological species (enzymes, proteins, antibodies), nanomaterials are widely used in medicine for the production of devices for diagnosing diseases such as biosensors or medical (bio)imaging devices. Nanomaterials have a special application in the electronic (computer) industry for the production of nanoelectronics and semiconductor devices. Application of nanomaterials in energy technology are reflected in the development of fuel and solar cell, photocatalysts and gas sensors.

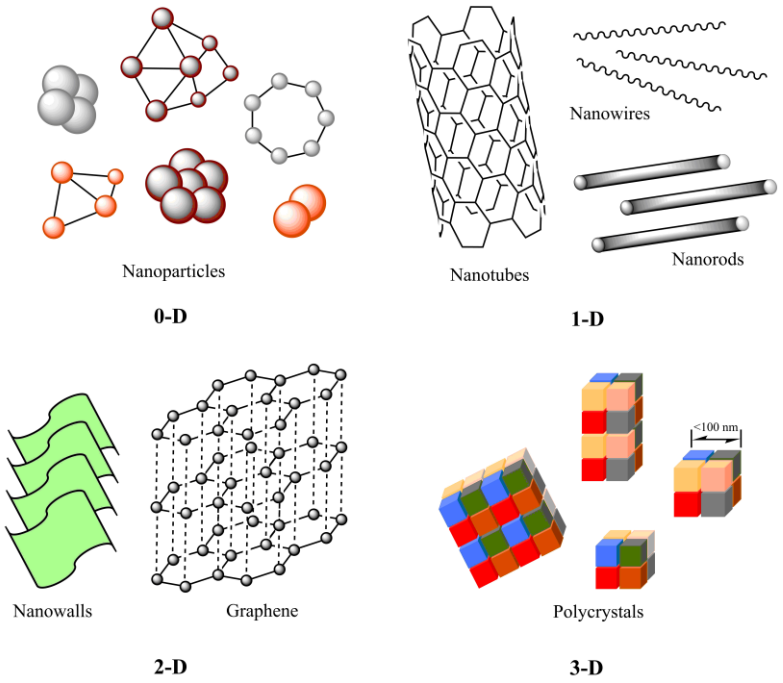

Figure 10. Nanomaterials categories.

2.1.4.1. Graphene nanomaterials

The term "*graphene sheets/nanosheets*" is generally used for graphene-based materials/nanomaterials, but this term does not define edge dimensions and material size. Graphene nanosheets include various nanomaterials such as graphene nanoribbons (GNR), graphene nanoplatelets (GNP), GO, rGO. In this doctoral dissertation, GNR and GNP were used to prepare glucose and polyphenolic index biosensors, respectively. Accordingly, description of their basic characteristics is given below. Also, a brief review of the literature which describing the synthesis of GNR and GNP is given, but in general, synthesis of graphene nanomaterials, which involving simpler precursors and cheaper experimental steps, still poses a challenge in world science.

Each graphene sheet is defined with two basic surfaces: an edge and a basal plane. These two surfaces are responsible for the excellent electronic and electrochemical properties of graphene. Categorization of graphene-based nanomaterials by dimensions can be performed according to *z*- and *x-y* axes. However, a key step during the synthesis of graphene-based nanomaterials is the growth of graphene sheets along the axis. Namely, the limitation of the sheets growth along different axes significantly affects the electronic and electrochemical properties of the obtained graphene *(Pumera, 2010)*.

Limitation on the growth of graphene sheets along the *z*-axis are given in *Figure 11*. Observing the *z*-axis (while the *x*- and *y*-axes are virtually infinite) the limitation of graphene growth can begin after the separation of a single layer, resulting in a *single-layer* of graphene (Figure 11a). Then, the growth of graphene sheets can be stopped after two separate layers (*double-layer* graphene), or after three to ten layers (*few-layer* graphene) (Figure 11b and 11c, respectively). Single-, double- and few-layers graphene are characterized by size of lateral dimensions greater than 10 nm. Finally, by growing graphene from 10 to 100 sheets (Figure 11d), GNP are obtained. The sheets inside the GNP have the shape of a rectangle whose sides are precisely defined. Sizes of platelets are usually 50 to 100 nm. GNPs are characterized by a thickness of 3-30 nm *(Pumera, 2010; Pumera, 2013)*.

GNP synthesis is most often performed using the chemical exfoliation method ("*top down*" method). Graphite is the simplest precursor for obtaining GNP. The principle of this method have been explained earlier, on the example of obtaining GNP, thickness 2-150 nm, by intercalation of alkali metals (K^+) within graphite (*Viculis et al., 2005*). Also, *Truong et al., (2012)* report GNP synthesis by intercalation of Li^+ ions into graphite. In addition to alkali metals, a mixture of persulfate anions, sulfuric acid and oleum (sulfuric acid saturated with SO_3) can be used for GNP synthesis. This type of chemical exfoliation is known as the oxidative exfoliation process and is based on intercalation of persulfate anions within graphite, which results in the separation of graphene layers. Finally, ultrasound treatment results in pilling of GNP from graphite. Using intercalation of the persulfate anion into graphite, *Melezhyk & Tkachev, (2014)* synthesized GNP with a thickness of 5-10 nm. Also, using the same method, *Dimiev et al., (2016)* and *La et al., (2016)* describe the synthesis of GNP with a thickness of 10-35 nm and 10-20 nm, respectively, with a yield over 95%. Since this method gives a high yield, it is used for mass production of GNP *(Dimiev et al., 2016; La et al., 2016)*. However, as sulfuric acid is used in the process, the presence of sulfur (up to 2%) was confirmed in the GNP structure using the X-ray diffraction method *(Dimiev et al., 2016)*. The sulfur content adversely affects its properties, so it can be expected that the graphene obtained by intercalation of alkali metals provides more dominant electrical and electrochemical properties.

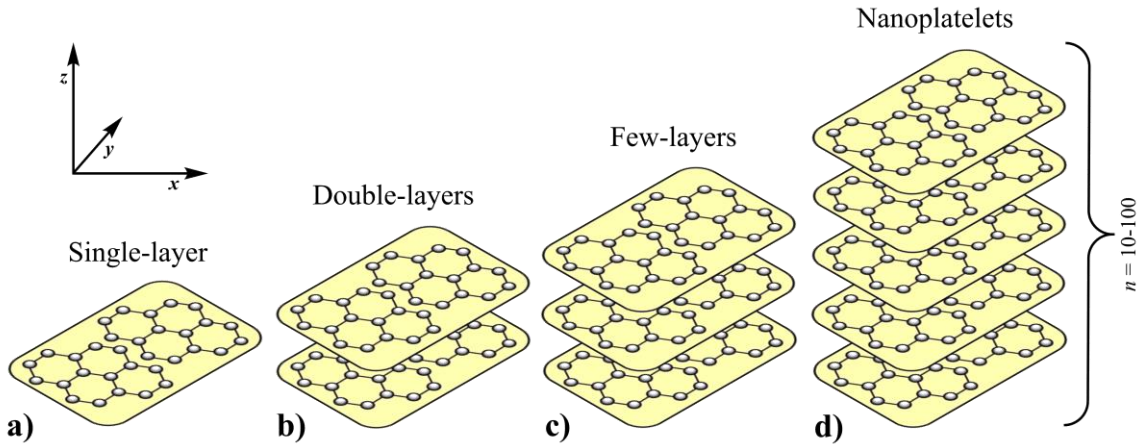

Figure 11. Graphene nanomaterials. Limiting the growth of graphene sheets along the *z*-axis in order to obtain ***a)*** single layer, ***b)*** double-layers, ***c)*** few-layers and ***d)*** nanoplatelets with different electronic and electrochemical performances.

Further, by observing the *x*- and *y*- axes, it was noticed a different orientation of the sheet edges along the axes. The orientation of the edges along the *x*-axis is defined as "*zig-zag*", while along the *y*-axis as "*armchair*" orientation (Figure 12a). The different orientation of the edges significantly affects the electronic and electrochemical properties of graphene *(Pumera, 2010)*. Electrochemistry of graphene is based on fast heterogeneous electron transfer (HET) which takes place at the edges of the sheets. Accordingly, it can be concluded that HET would play an appropriate mechanism on the "*zig-zag*" edges, and with different mechanism on the "*armchair*" edges. Well-defined graphene narrow stripes along the *x*- and *y*-axes (while sheets growth along the *z*-axis is set to single-layer) are called graphene nanoribbons (GNR) *(Pumera, 2013)*. GNR is characterized by a strip width of ~50 nm, while strip length is determined by limiting sheets growth during synthesis. Synthesized "*zig-zag*" GNRs are characterized by electronic properties of metallic conductors, while GNRs with edges in "*armchair*" orientation shows mainly semiconductor properties. This is clear evidence of how different edge orientations affect electronic properties differently. If sheets growth increased to several layers along the *z*-axis, a few-layer GNR would be obtained. This type of GNR reflects the typical properties of metallic conductors. Then, if the growth of the sheets continued along the *z*-axis (in that case the *z*-axis would be larger than the *x*- and *y*- axes), the *platelet graphite nanofibers* are obtained. This type of graphene nanomaterials is characterized by highly represented edges, which makes its electrical and electrochemical performances more dominant than graphite or other carbon nanomaterials *(Pumera, 2010)*.

GNR are most commonly synthesized using "*bottom up*" techniques *(Cai et al., 2010)*. Organic synthesis of GNR is based on the oxidative cyclodehydrogenation of precursors such as oligophenylene and polyphenylene compounds with halogen substituents (Figure 12b) *(Wang et al., 2018a)*. The most widely used "*bottom up*" method for GNR synthesis is the growth of GNR on Au (111) single crystal surfaces. This method is based on the precipitation of precursors on Au (111) crystal. The crystal is then annealed to 250^{o}C in order to activate the polymer surface. Annealing continues at 350^{o}C causing a cyclodehydrogenation process, which is followed by the formation of GNR. Using this method, *Narita et al., (2019)* and *Ruffieux et al., (2016)* report the synthesis of "*zig-zag*" GNR with a width of 6 and 12 carbon atoms (*6-zGNR* and *12-zGNR*), respectively. In contrast, using the same method, *Han et al., (2020)* and *Talirz et al., (2017)* explain the synthesis of GNR in the "*armchair*" conformation with a width of 9 carbon atoms (*9-aGNR*), while *Chen et al., (2013b)* reported the synthesis of "*armchair*" GNR with a width of 13 carbon atoms (*13-aGNR*).

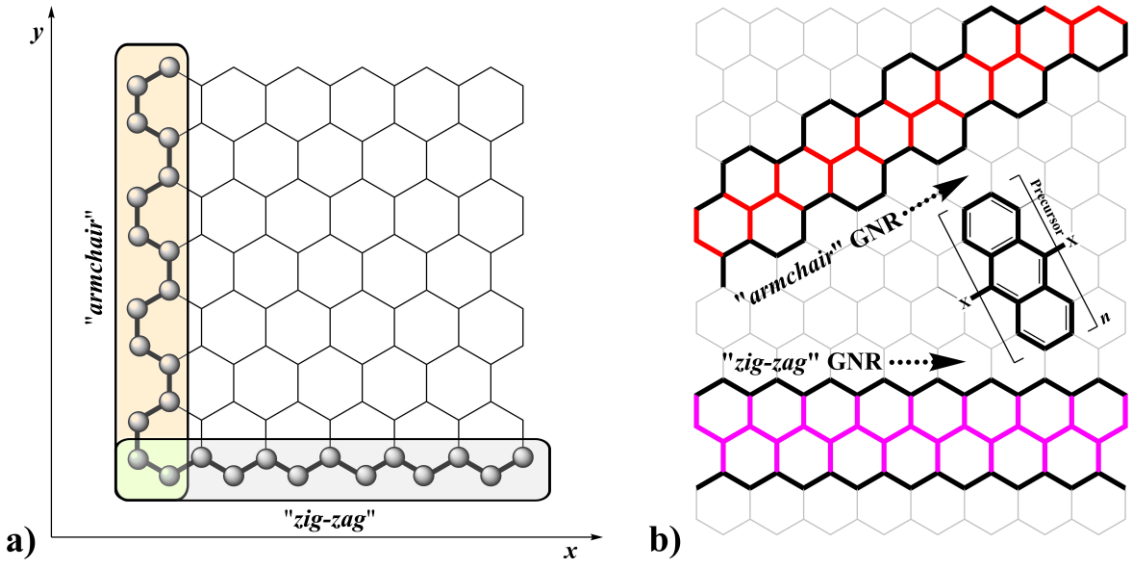

Figure 12. a) Different orientations of edges of graphene sheets along the *x*- and *y*- axes. ***b)*** Synthesis of "*zig-zag*" or "*armchair*" GNR with appropriate halogen-based precursor.

2.1.5. Application of graphene (nano)materials

After the discovery of graphene and forthcoming justification of its unique electronic, magnetic and mechanical characteristics, the application of graphene is experiencing expansion. Graphene, as a new material, is used in many industrial, technological and scientific fields. Due to its exceptional properties such as high conductivity, elasticity, strength, porosity and high surface area, graphene has found enormous applications in energy storage and conversion. In this regard, graphene is an indispensable part of fuel and solar cells, batteries (a significant application in the production of Li^+ battery) and supercapacitators *(Shao et al., 2010)*. Furthermore, the high conductivity of graphene, as one of the main characteristics, has been used in the manufacture of electronic devices. Namely, graphene electrodes are an integral part of field-effect transistors and memory devices. In addition, the production of optical devices today is unthinkable without graphene materials. Graphene transparent films have found great application in touch screen technology. Also, transparent graphene films are used in the production of liquid crystal displays (LCDs) and light-emitting diodes (LEDs) *(Adetayo & Runsewe, 2019; Chabot et al., 2014; Choi et al., 2010; Jo et al., 2012)*.

In addition to industrial and technological, graphene has great application in science. Chemistry is at the forefront of this. Superhydrophobicity, elasticity, flexibility and high strength are the main properties of graphene that have been used to produce flexible and conductive polymer composites. Then, the high adsorption capacity of graphene towards organic solvents (up to 700 g g^{-1} adsorbent), dyes (up to 200 g g^{-1} adsorbent) and oil (up to 130 g g^{-1} adsorbent) was used to produce adsorbents for these molecules. This application, in addition to the scientific aspect, is significantly accepted in green technology. Finally, graphene materials in particular are used in electrochemistry. Its properties have been used to produce sensors (working electrodes) in order to quantify a wide range of compounds. Today, almost every developed gas sensor, biosensor or immunosensor is based on graphene materials *(Adetayo & Runsewe, 2019; Chabot et al., 2014; Choi et al., 2010; Jo et al., 2012)*. Graphene is expanding its application to various fields of technology, energy and electronics on a daily basis and is frequently finding irreplaceable application in medicine and pharmacy. The main areas of graphene application are summarized in *Scheme 2*.

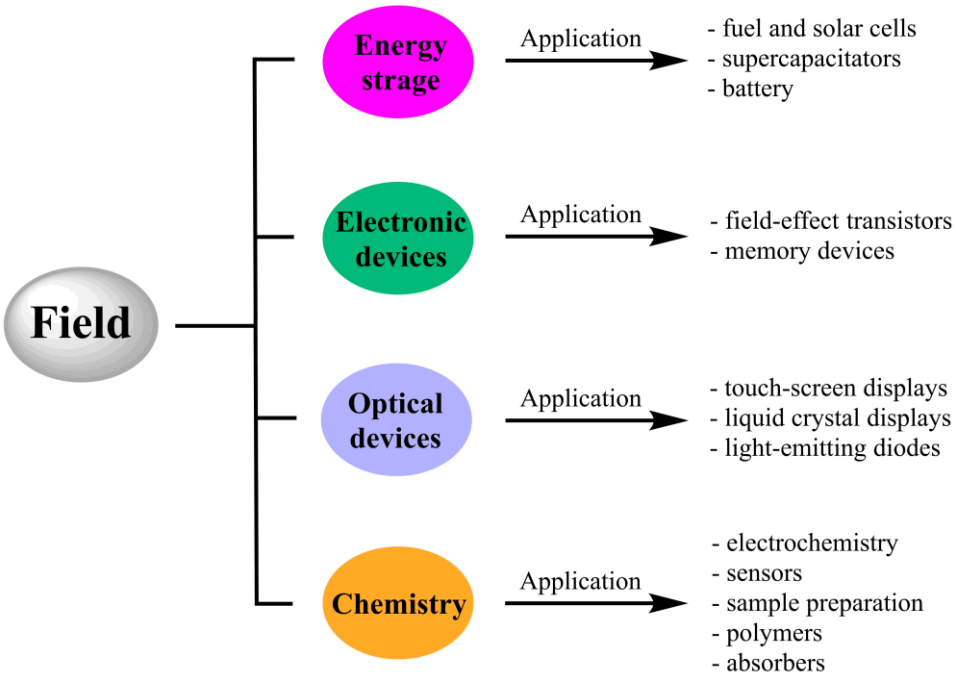

Scheme 2. The main fields of graphene application.

2.1.5.1. Graphene in electrochemistry

Carbon is one of the most commonly used material in electrochemistry. Today, almost every working electrode, especially after the introduction of graphene materials, is based on carbon materials. Due to its unique characteristics, graphene has found great application in electrochemistry. As mentioned earlier, electrochemistry of graphene is based on the fast HET. This process takes place between graphene sheets and target analyte from supporting electrolyte. Studies have shown that the HET in graphene is higher than in other carbon materials, for example CNT or SWCNT *(Pumera et al., 2010)*. *M. Pumera* states in his studies on graphene that the planar structure of graphene is responsible for faster electron transfer *(Pumera et al., 2010; Pumera, 2010)*. Therefore, working electrodes in electrochemistry are increasingly based on graphene materials, or standard electrochemical sensors (glassy carbon electrode (GCE), carbon paste electrode (CPE), SPCEs) modified with graphene materials in order to improve their electrochemical performance.

After the introduction of graphene into electrochemistry, it was necessary to examine electrochemical parameters such as working potential range, the system reversibility and the electron transfer rate. *Zhou et al., (2009)* reported that the working potential range of graphene is similar to other working carbon electrodes such as GCE, boron doped diamond (BDD) electrode or graphite electrode (-1 to 1.5 V in 0.1 mol L^{-1} phosphate buffer solution). On the other hand, the alternating current impedance method proved that the *charge-transfer resistance* on graphene layers is significantly lower compared to these electrodes *(Zhou et al., 2009)*. This confirmed the high electrocatalytic effect of graphene.

During the system reversibility test of the redox couple $[Fe(CN)_6]^{3-/4-}$ by cyclic voltammetry, the graphene-based working electrode (reduced graphene sheets) showed a well-defined oxidation and reduction peak of the mentioned couple. Also, it was observed that with increasing scan rate, the intensity of the peak currents increases linearly with the square root of the scan rate. This indicates that the processes that take place on the surface of graphene-based electrodes are controlled by the diffusion process *(Lin et al., 2009)*. *Peak-to-peak potential separation* (ΔEp) for the $[Fe(CN)_6]^{3-/4-}$

couple, where 1 electron is exchanged, was very close to the ideal, 0.059 V *(Tang et al., 2009)*, while in the case of GCE, for the same redox couple, ΔEp was 0.229 V *(McCreery, 2008)*. ΔEp close to ideal indicates fast electron transfer on graphene for electrochemical reaction in which 1 electron was exchanged *(Shang et al., 2008)*.

In order to examine the electron transfer rate on the surface of graphene materials, *Tang et al., (2009)* observed the behavior of the graphene electrode by cyclic voltammetry (scan rate of 0.1 V s^{-1}) in three different redox couples: $Fe^{3+/2+}$, $[Ru(NH_3)_6]^{3+/2+}$ and $[Fe(CN)_6]^{3-/4-}$. As supporting electrolyte was used 1 mol L^{-1} KCl. An *electron-transfer rate constant* (k^o, *cm* s^{-1}) was calculated from the cyclic voltammograms for each redox couple. The obtained k^o values were compared with the corresponding k^o obtained with a GCE, under the same conditions. In $[Ru(NH_3)_6]^{3+/2+}$, the k^o obtained with the graphene electrode was 3.5 times higher than the k^o obtained with GCE, while in $Fe^{3+/2+}$ was 10 times higher than GCE. Finally, graphene showed a 17 times higher electron-transfer rate in $[Fe(CN)_6]^{3-/4-}$ redox couple, compared to GCE. This shows that the unique structure of graphene directly affects the extremely fast electron transfer, which makes graphene ideal in electrochemical studies. Also, this research has shown that $[Fe(CN)_6]^{3-/4-}$ is the most ideal analyte for testing the system reversibility with graphene-based working electrodes.

After testing the performance of graphene as working electrode, a significant development of electrochemical sensors based on graphene materials for the quantification of, among other things, biologically important compounds (metabolites, enzyme cofactors, neurotransmitters, hormones) begins. For example, *Zhou et al., (2009)* state that performance of graphene-based working electrode [rGO] was significantly better than GCE performance during H_2O_2 quantification (Figure 13a; Figure13b). H_2O_2 is one of the main mediators in food, clinical and industrial analysis, which makes its detection very important. Further, *Zhou et al., (2009)* also shows that rGO-based electrode showed better performance than GCE during quantification of nicotinamide adenine dinucleotide (NADH) (Figure 13c; Figure13d). NADH (and its reduced form NAD^+) are present in all living cells and represent a cofactor of almost all dehydrogenases. Electrochemical quantification of these cofactors provides very sensitive and selective determination, especially when graphene-based working electrodes were used *(Tang et al., 2009)*. The authors, again, explained that the unique structure of graphene is responsible for the higher electron transfer rate, which directly affects the increase in the selectivity and sensitivity of quantification methods *(Tang et al., 2009; Zhou et al., 2009)*. It is important to note that during the development of the method for NADH detection, using standard electrochemical sensors, the problem of large overvoltage for NADH oxidation occurs, as well as the adsorption of oxidation products on the electrode surface. In this case, graphene has proven to be a good material that offers promising results in solving this problem *(Banks & Compton, 2005; Liu et al., 2009; Tang et al., 2009)*.

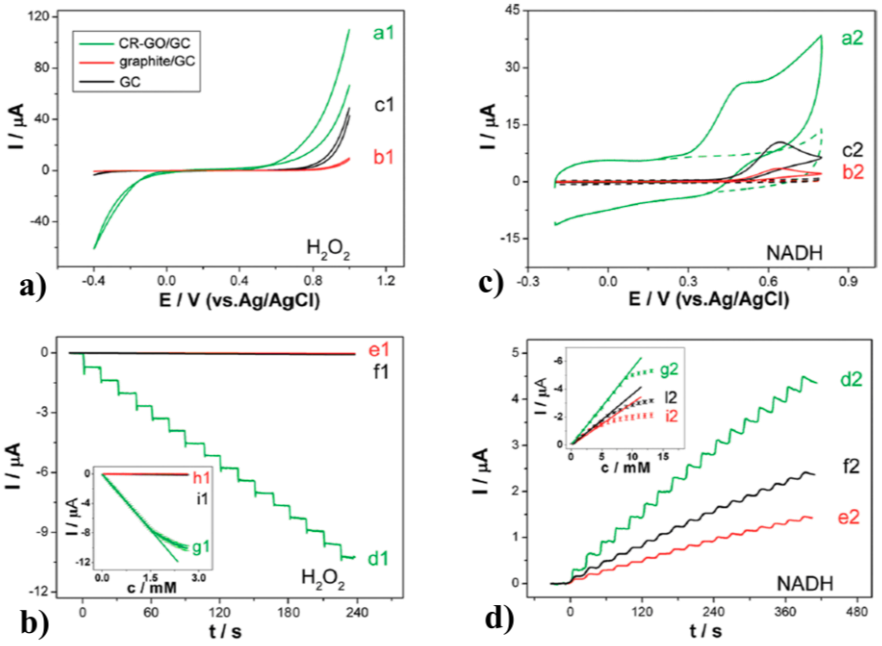

Figure 13.

a) *"Cyclic voltammograms for 4 mmol L^{-1} H_2O_2 at chemically reduced graphene oxide modified glassy carbon electrode, CR-GO/GC (a1), graphite/GC (b1) and GC electrodes (c1). Electrolyte: 0.1 mol L^{-1} PBS (pH=7.0). Scan rate: 50 mV s^{-1}".*

b) *"Current-time curves for CR-GO/GC (d1), graphite/GC (e1) and GC electrodes (f1) at -0.20 V with successive addition of 0.1 mmol L^{-1} H_2O_2. Inset: calibration curves for H_2O_2 at CR-GO/GC (g1), graphite/GC (h1) and GC electrodes (i1). Electrolyte: magnetically stirred 0.1 mol L^{-1} PBS (pH=7.0)".*

c) *"Cyclic voltammograms for 2 mmol L^{-1} NADH at CR-GO/GC (a2), graphite/GC (b2) and GC electrodes (c2). Electrolyte: 0.1 mol L^{-1} PBS (pH=7.0). Scan rate: 50 mV s^{-1}".*

d) *"Current-time curves for CR-GO/GC (at +0.45 V, d2), graphite/GC (at +0.65 V, e2) and GC electrodes (at +0.65 V, f2) with successive addition of 0.1 mmol L^{-1} NADH. Inset: calibration curves for NADH at CR-GO/GC (g2), graphite/GC (h2) and GC electrodes (i2).*

Electrolyte: magnetically stirred 0.1 mol L^{-1} 1 PBS (pH=7.0)" ***(Zhou et al., 2009)***.

The characteristics of graphene were significantly expressed in the quantification of dopamine. Standard electrochemical sensors do not have the ability to separate voltammetric signals of dopamine, ascorbic acid and uric acid (peaks overlap), which is very important in the detection of dopamine in clinical samples. *Yang et al., (2014a)* used graphene-based electrode [electrochemically reduced graphene oxide (ERGO)] to separate signals of dopamine, ascorbic acid and uric acid (Figure 14) and successfully quantified these metabolites in urine samples. Research has shown that the use of graphene-based electrodes or modification of GCE with graphene materials leads to the separation of dopamine signals from interferences such as ascorbic and uric acid. The authors explained that the large active surface area as well as the high electron-transfer rate were responsible for the significantly higher selectivity and sensitivity of the graphene-based electrochemical sensor during the quantification of this hormone *(Shang et al., 2008; Wang et al., 2009)*.

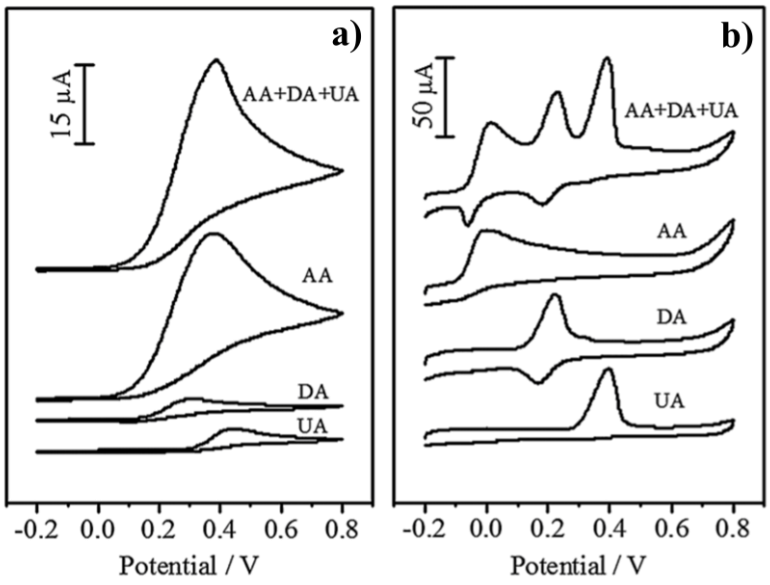

Figure 14.
*"Cyclic voltammograms at **a)** GCE and **b)** GCE modified with ERGO (ERGO/GCE) in 0.1 mol L^{-1} PBS (pH=7.0) with 5 mmol L^{-1} ascorbic acid (AA), 0.5 mmol L^{-1} dopamine (DA) 0.5 mmol L^{-1} uric acid (UA) and their mixture. Scan rate: 50 mV s^{-1}" **(Yang et al., 2014a)**.*

The properties of graphene were especially prominent in the quantification of catechol (CT) and hydroquinone (HQ). CT (1,2-dihydroxybenzene) and HQ (1,4-dihydroxybenzene) are two isomers of dihydroxybenzene. These compounds are used in the industries of paints, cosmetics, antioxidants, plastics, pharmaceutical products and pesticides and, after being released into the environment, exhibit toxic properties. Due to their very similar structure, these compounds are difficult to separate electrochemically. Chromatographic methods or mass spectrometry can be used for their detection, but these methods, in contrast to electrochemical ones, are expensive and require complex sample preparation. Standard electrochemical sensors did not show high selectivity in determining these two isomers, so the signals overlapped. After the introduction of graphene into electrochemistry, many studies relate precisely to the use of graphene-based working electrodes in the quantification of CT and HQ. For example, *Si et al.,(2012)* showed that using graphene-based electrode [poly(3,4-ethylenedioxy-thiophene)/GO (PGE)] it is possible electrochemical separation of CT and HQ, as well as their mixture (Figure 15). *Erogul et al., 2015, Huang et al., 2015b, Ognjanović et al., 2018, Si et al., 2012, Yin et al., 2011* and *Zhang et al., 2015a* are part of scientific reports related to successful electrochemical separation, as well as simultaneous quantification of CT and HQ by modification of GCE with different graphene materials. All of the above studies state that the use of graphene materials significantly improves the characteristics of GCE as well as significantly increases the selectivity and sensitivity during the quantification of these two isomers using graphene-based electrodes.

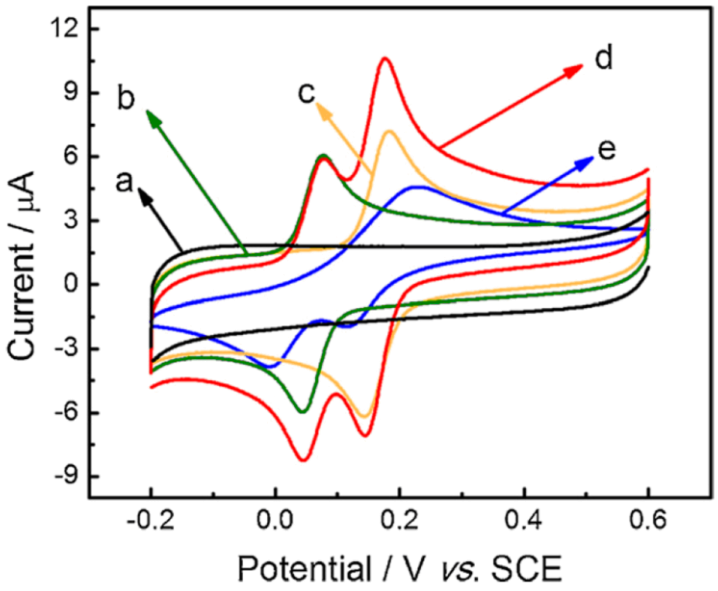

Figure 15.
"Cyclic voltammograms in PBS containing 0 mmol L^{-1} (a), 0.1 mmol L^{-1} HQ (b), 0.1 mmol L^{-1} CT (c), the mixture of 0.1 mmol L^{-1} HQ + 0.1 mmol L^{-1} CT (d) at PGE; CVs in PBS containing the mixture of 0.1 mmol L^{-1} HQ + 0.1 mmol L^{-1} CT at GCE (e). Scan rate: 50 mV s^{-1}" ***(Si et al., 2012)***.

Unique characteristics of graphene have been demonstrated in the detection of free nucleotides, a specific deoxyribonucleic acid (DNA) sequence or a mutated gene. *Zhou et al., (2009)* compared electrochemical responses for all four nucleotides of DNA [adenine (A), thymine (T), guanine (G) and cytosine (C)] using GCE, GCE modified with graphite (GCE/graphite) and GCE modified with graphene materials [chemical-reduced graphene oxide (CR-GO/GCE)]. *Figure 16a.* and *Figure 16b.* shows that GCE and GCE/graphite do not have the ability to completely separate the signals. In contrast, CR-GO/GC provides complete separation of all four free nucleotides, A, T, G and C (Figure 16c). In addition, extremely intense signals are observed for free nucleotides from graphene-based electrode relative to other working electrodes. Accordingly, it can be concluded that electrochemical DNA sensors based on graphene materials provide high sensitivity and high selectivity during the detection of free DNA nucleotides. *Figure 16e.* shows that graphene-based electrode can separate all four nucleotides in single-stranded DNA (ssDNA). Also, complete separation of nucleotide signals in double-stranded DNA (dsDNA) is possible with a graphene-based electrode (Figure 16f), although nucleotide oxidation in dsDNA is significantly hampered, compared to free nucleotides. The authors explain that the unique physic-chemical properties of graphene (fast electron transfer, large surface area, high conductivity) are responsible for the complete separation of free nucleotides, as well as nucleotides within DNA. *Benvidi et al., (2015), Fan et al., (2011), Han et al., (2013), Huang et al., (2011), Lin et al., (2011), Rasheed & Sandhyarani, (2014), Zheng et al., (2015)* report the construction of an electrochemical DNA sensor based on graphene materials. The authors state that in addition to high selectivity and sensitivity, graphene-based DNA sensors provide a wide linear range as well as a low LOD during simultaneous detection of nucleotides, a specific sequence in the DNA strand or a specific target gene.

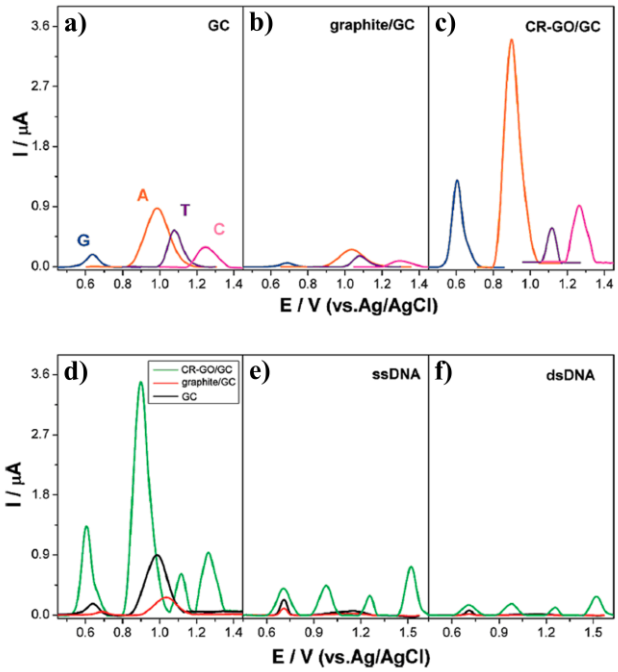

Figure 16.
a) *"Differential pulse voltammograms (DPVs) at the GCE for G (blue), A (orange), T (violet) and C (magenta), respectively.*
b) *DPVs at the graphite/GCE for G (blue), A (orange), T (violet) and C (magenta), respectively.*
c) *DPVs at the CR-GO/GCE for G (blue), A (orange), T (violet) and C (magenta), respectively.*
d) *DPVs for a mixture of G, A, T and C at CR-GO/GCE (green), graphite/GCE (red), and GCE (black).*
e) *DPVs for ssDNA at CR-GO/GCE (green), graphite/GCE (red) and GCE (black).*
f) *DPVs for dsDNA at CR-GO/GCE (green), graphite/GCE (red) and GCE (black).*
Concentrations for different species (A-F): G, A, T, C, ssDNA or dsDNA: 10 µg mL^{-1}. Electrolyte: 0.1 mol L^{-1} PBS (pH=7.0)" ***(Zhou et al., 2009)***.

HET, as well as the large specific contact surface of graphene, have proved particularly useful in the production of electrochemical biosensors. Namely, graphene provides excellent electron transport between the active center of the biological species and the graphene-based electrode. Increasing the electron transfer rate directly affects the sensitivity of the determination, which leads to a decrease in the detection limit of the biosensor toward analyzed species *(Bahadır & Sezgintürk, 2016; Pumera et al., 2010; Shao et al., 2010; Zhu, 2017)*. Large contact surface of graphene provides a large number of electroactive sites, which further contributes to the transfer of electrons between the biological species and the electrode. Therefore, graphene is immobilized with various types of biological compounds such as enzymes, DNA or antibodies. Studies show that graphene is actively involved in the preparation of enzyme biosensors, DNA biosensors and immunosensors *(Vukojević et al., 2018a; Vukojević et al., 2018b; Stanković et al., 2020b; Chen et al., 2013a; Hu et al., 2011; Zhang & Jiang, 2012)*. This indicates that its application today is significantly expanded to medical and pharmaceutical research, precisely because of the possibility of successful immobilization of various biological species.

2.2. Nano-structured transition metal oxides

Nano-structured transition M_xO_y, in the last few decades, have been widely studied. Interest in their study grew after the discovery of their excellent magnetic, electronic, mechanical, photochemical, catalytical, thermal and optical properties. In transition M_xO_y, the *s*-shells of metal ions are completely filled, while the *d*-shells are mostly half-filled by electrons. Consequently, the electrons in the *d*-shells have the possibility of different electronic transitions within the *d*-orbitals (d_{xy}, $d_{x^2y^2}$, d_{xz}, d_{yz}, d_{z^2}), which affects their electronic properties. For example, *Figure 17.* represent schematic illustration of half-filled *d*-orbitals of Mn in MnO_2. In fact, the electronic structure of transition M_xO_y defines the characteristics of materials such as metallic, semiconductor or insulating. Their unique and adaptable structure is defined by a large contact surface, high dielectric constants and wide bandgaps. Transition M_xO_y can occur in different oxidation states which can also define the conductive or semiconductor properties of the material *(Ashik et al., 2018; Guo et al., 2015; Mallakpour & Madani, 2015; Nunes et al., 2019; Rastogi et al., 2017)*.

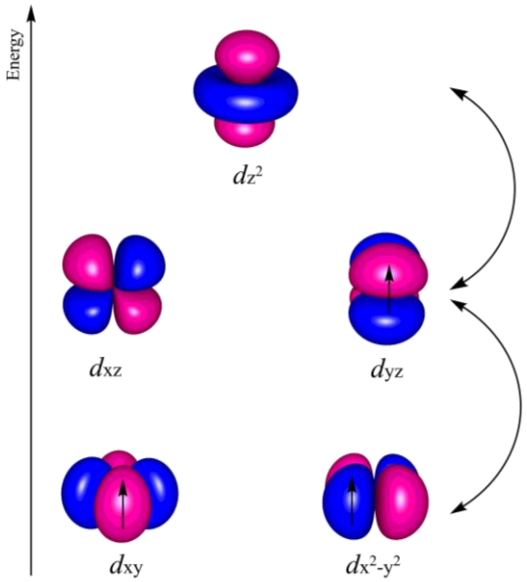

Figure 17. Schematic illustration of half-filled *d*-shells of Mn in MnO_2.

As a result of their unique properties, transition M_xO_y have found wide application in the production of solar and fuel cells, alkaline ion batteries, ceramic and polymeric substrates, supercapacitors, infrared adsorbers, lasers, as well as in petrochemical processing, piezoelectrical, pyroelectrical, ferroelectrics and corrosion programs *(Ashik et al., 2018; Joo & Zhao, 2017; Mallakpour & Madani, 2015)*. Transition M_xO_y have a special application in electrochemistry for the preparation of various sensors and biosensors. Transition M_xO_y are used in the water treatment, cosmetics and pharmaceutical industries *(Joo & Zhao, 2017)*. Their application in medicine is interesting and significant. Namely, M_xO_y are used in the diagnosis of diseases, as well as the drugs delivery and biomaterials. Their solubility in various agents is examined in order to prepare the carrier of a particular drug to the tumor site during cancer treatment. Nano-structure transition M_xO_y are used in optical devices to map cancer cells, but it is also an integral part of probes for diagnosing various diseases *(Malhotra & Ali, 2018)*. According to a brief overview of properties and applications, transition M_xO_y are considered to be one of the most fascinating functional materials/mediators, which explains the fact that they are still an active research topic in world science.

In this doctoral dissection, nano-structured oxides of bismuth (post-transition metal) and manganese (transition metal) were used to modify graphene nanomaterials during the preparation of glucose and polyphenolic index biosensors, respectively. Accordingly, further in the text, a description of their properties, synthesis procedures as well as their wide application in electrochemical measurements are given.

2.2.1. Nano-structured transition metal oxides in electrochemistry

In electrochemical measurements, nano-structured transition and post-transition M_xO_y act as catalysts in redox processes of target analyte at electrode surface. This results in the multiplication of the current signal and the increase in the sensitivity of electrochemical methods. A large number of scientific papers refer to the modification of standard electrochemical sensors (GCE, CPE, SPCE, Pt electrode) with nano-structured *T*-MO and *pT*-MO in order to achieve low concentration levels (μmol L^{-1}, nmol L^{-1}) during the quantification of various analytes. In addition to the electrocatalytic effect, a large surface area of this M_xO_y has shown high biocompatibility towards biological species (enzymes, DNA, antibodies), which has extended their application to the construction of electrochemical biosensors/immunosensors. Electrocatalytic effect in the case of biosensors is reflected in the accelerating electron transfer between the active site of species and the electrode surface.

Transition metals and their M_xO_y such as cooper [CuO or Cu_2O] *(Devaraj et al., 2016; Karimi-Maleh et al., 2019)*, iron [Fe_2O_3 or Fe_3O_4] *(Radhakrishnan et al., 2014; Wang et al., 2008)*, nickel [NiO] *(Noorbakhsh & Salimi, 2011; Salimi et al., 2007)*, silver [Ag_2O or Ag_2O_3] *(Wang et al., 2016a; Wang et al., 2020)*, cobalt [CoO or Co_3O_4] *(Razmi & Habibi, 2010; Shahid et al., 2015)*, titanium [TiO_2] *(Yan et al., 2015; Zhang et al., 2004)*, tungsten [WO_3] *(Anithaa et al., 2015; Yang et al., 2012)*, vanadium [V_2O_5] *(Sun et al., 2010; Suresh et al., 2014)*, zinc [ZnO] *(Freire et al., 2016; Umar et al., 2009)*, zirconium [ZrO_2] *(Qiao & Hu, 2009; Zhao et al., 2005)* and post-transition metals and their oxides like gallium [Ga_2O_3] *(Kim et al., 2017; Yan et al., 2010)*, indium [In_2O_3] *(Wang et al., 2011; Wei et al., 2012)*, lead [PbO or PbO_2] *(Bateni et al., 2020; Kurt Urhan et al., 2019)*, tin [SnO_2] *(Ansari et al., 2009; Zhou et al., 2013)* are examples of highly used mediators in photo/electrocatalysis, as well as sensing and biosensing of a large number of chemical compounds (ions, molecules), pharmaceuticals and biologically important compounds. In addition to these M_xO_y, oxides of manganese and bismuth are widely used *(Li et al., 2010; Ping et al., 2012; Pauliukaite et al., 2002; Staiti & Lufrano, 2009*; *Taufik et al., 2011; Veeralingam & Badhulika, 2020; Zhang & Zheng, 2016)*. Since nano-structured Bi_2O_3 and MnO_2 were used to construct glucose and polyphenolic index biosensors, respectively, a description of their properties and structure is given below, as well as a brief overview of synthetic methods and electrochemical applications.

2.2.1.1. Nano-structured Bi_2O_3 nanoparticles

Bismuth and bismuth(III)-oxide (Bi_2O_3) represent one of the most studied semiconductor mediators and materials in electrochemistry and photo/electrocatalysis. Its wide application as a mediator in photovoltaic cells *(Hussain et al., 2010)*, optical coating *(Li et al., 2006)*, supercapacitor technology *(Gujar et al., 2006)* as well as in photocatalysis of organic pollutants *(Chen et al., 2018)* derives from its unique characteristics. The properties of Bi_2O_3 are reflected in a high band gap, large contact area, high refractive index, high photocatalytic activity, high photoconductivity, as well as high dielectric permittivity *(Gujar et al., 2006; Oudghiri-Hassani et al., 2018b); Weber et al., 2017)*.

In addition to the listed properties, Bi_2O_3, during electrochemical sensing and biosensing, shows a very stable signal current. Standard electrochemical sensors are often modified with Bi_2O_3

nanoparticles in order to improve performances of electrochemical methods. Modification of CPE with Bi_2O_3 nanoparticles was reported by *Pauliukaite et al., (2002)* and *Ping et al., (2012)* for quantification of toxic metals in drinking water and milk, respectively. *Teradal & Seetharamappa, (2015)*, using a similar CPE@Bi_2O_3 modification, explains the quantification of drug nevirapine in serum and urine samples. Modification of GCE with Bi_2O_3 particles has been reported by *Zidan et al., (2011a)* and *Zidan et al., (2011b)* in order to develop new sensors for the quantification of pharmaceuticals such as ascorbic acid and paracetamol, respectively. Bi_2O_3 has proven to be very suitable for the development of gas sensors *(Park et al., 2015; Takeda et al., 2015)*, especially for nitrogen-oxides since the Bi_2O_3 shows high selectivity during the determination of these gases *(Bang et al., 2018; Cabot et al., 2004)*. As already mentioned, the large surface area of Bi_2O_3 nanoparticles has been shown to be suitable for immobilizing biological species *(Mani et al., 2013)*. *Wang et al., (2019)* reported Bi_2O_3-based immunosensor for the detection of N^6-methyladenosine, while *Taufik et al., (2011)* and *Veeralingam & Badhulika, (2020)* explain the construction of a Bi_2O_3-based biosensors for the quantification of DNA and hormones, respectively. On another hand, the difficult electronic transport inside the Bi_2O_3 crystal lattice reduces the electrical conductivity of this oxide. However, the combination of Bi_2O_3 nanoparticles with high promising nanomaterials (for example graphene) achieves excellent electrochemical performance, which is explained in this doctoral dissertation during the development of a glucose biosensor based on GNR@Bi_2O_3 nanocomposite.

The crystal structure of Bi_2O_3 can be defined through five main polymorphic modifications: α-B_2O_3 (monoclinic), β-B_2O_3 (tetragonal), γ-B_2O_3 (cubic, body-centered), δ-B_2O_3 (cubic, face-centered) (Figure 18) and ε-B_2O_3 (orthorhombic) *(Oudghiri-Hassani et al., 2018a; Tien & Peng, 2019)*. By annealing α-B_2O_3, different Bi_2O_3 polymorphisms are obtained (except ε-B_2O_3). Namely, annealing α-B_2O_3 at 730°C produces δ-B_2O_3. α-B_2O_3 and δ-B_2O_3 are defined as room and high temperature stable polymorphic modifications, respectively. Metastable modifications β-B_2O_3 and γ-B_2O_3 are obtained by cooling δ-B_2O_3 to 650°C and 640°C, respectively. By cooling β-B_2O_3, already at 300°C the polymorphic structure of Bi_2O_3 returns to the basic (α). On the other hand, γ-B_2O_3 can maintain its structure at room temperature, if extremely slow cooling from 640°C is performed. A hydrothermal method based on heating $Bi(NO_3)_3$ with a different Mn-based compound (in order to stabilize the obtained ε-B_2O_3) at 240°C was reported for obtaining ε-B_2O_3. Although ε-B_2O_3 cannot be obtained directly from α-B_2O_3, progressive heating of ε-B_2O_3 can produce α-Bi_2O_3 (characterized by the typical properties of α-Bi_2O_3 *(Drache et al., 2007)*.

The synthesis of Bi_2O_3 nanoparticles can be performed using various methods. *Tien & Peng, (2019)* explained the synthesis of α-Bi_2O_3 and β-B_2O_3 nanowires using the thermal evaporation method. Using the sol-gel method, *Pan et al., (2008)* and *Xiaohong et al., (2007)* reported the synthesis of α-Bi_2O_3 (average particle size of 40 nm) and β-B_2O_3, respectively. Obtaining α-Bi_2O_3 and β-B_2O_3 nanowires (diameters - 100 nm, length - 300 nm) were reported by *Sirota et al., (2012)* using the magnetron sputtering deposition method. Hydrothermal method was used by *Chen et al., (2011)* in order to obtain *mesh-like* α-Bi_2O_3 and β-B_2O_3 (thickness - 100 nm). On the other hand, the precipitation method is the simplest method for obtaining Bi_2O_3 nanoparticles. This method is mostly based on mixing of $Bi(NO_3)_3$ with HNO_3 or HCL (in order to prevent hydrolysis of Bi^{3+}). This is followed by the addition of NaOH resulting in the formation of yellow Bi_2O_3 precipitates. Using precipitation method, *Liu et al., (2016a)* reported the synthesis of α-Bi_2O_3 and γ -Bi_2O_3, while *Yang et al., (2014b)* explained the preparation of α-Bi_2O_3 nanorods, with a particle size of 80 nm. In this doctoral dissertation, the precipitation method was used to obtain Bi_2O_3 nanoparticles. The synthetic monoclinic Bi_2O_3 was determined by X-ray diffraction method.

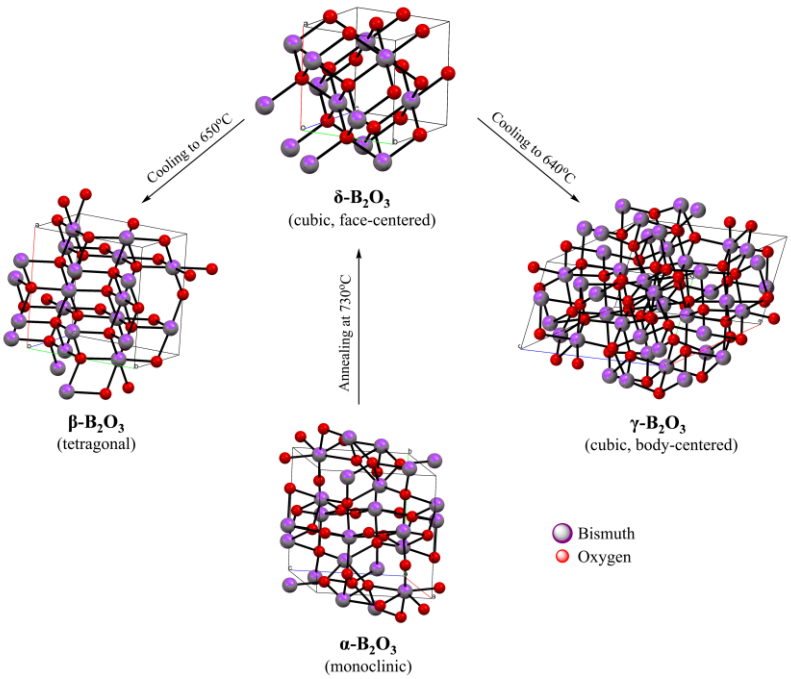

Figure 18. Polymorphic modifications of Bi_2O_3 and different temperature programs for their production.

2.2.1.2. Nano-structured MnO_2 nanoparticles

Manganese(IV)-oxide (MnO_2) reflects excellent electrochemical and electrocatalytic properties such as high catalytic effect, high activity in alkaline medium, soft magnetism, high energy density, high specific capacitance, as well as high adsorption capacity. In addition, MnO_2 is characterized by long cycle life, easy availability, low cost, non-toxicity and a positive environmental aspect *(Chen et al., 2012; George et al., 2018; Huang et al., 2015a; Xiao et al., 2010)*. Accordingly, MnO_2 is one of the most studied electrode materials in electrochemistry. Also, MnO_2, as an electrode material, plays an important role in electrical energy storage systems (battery, supercapacitors) *(Gnana Sundara Raj et al., 2014; Shin et al., 2020; Su et al., 2013)*. Due to its high adsorption ability, MnO_2 has found significant application in wastewater treatment *(Eslami et al., 2018; Gao et al., 2018; Song et al., 2019)*.

The structure of MnO_2 can be defined through several crystallographic polymorphic modifications. The basic structural unit of each polymorphic modification is the [MnO_6] octahedron (Figure 19) *(Dong et al., 2014; Shin et al., 2020)*. Different packaging of [MnO_6] units results in polymorphic modifications such as α-MnO_2 (corresponds to MnO_2 packaging within the mineral hollandite), β-MnO_2 (mineral pyrolusite), γ-MnO_2 (mineral nsutite) (Figure 19), δ-MnO_2 (mineral birnessite) and λ-MnO_2 (3D-spinel) *(Galliez et al., 2013; Yuan et al., 2019)*. Each of these MnO_2 modifications contains different large-size tunnels that define different electrochemical and electrical properties. This tunnels structure is important for the insertion or extraction of different ions or small molecules (ions and H_2O molecules can be inserted into the α-MnO_2 and δ-MnO_2 structure, while λ-MnO_2 may contain Li^+ or H^+) *(Galliez et al., 2013)*. Energy storage technology, *ie*. battery technology, was developed on this phenomenon. Namely, MnO_2 is used as an active cathode material with high specific storage capacitance (F g^{-1}) in Li- or Na-ion batteries, as well as in supercapacitors *(Gnana Sundara Raj et al., 2014; Su et al., 2013)*.

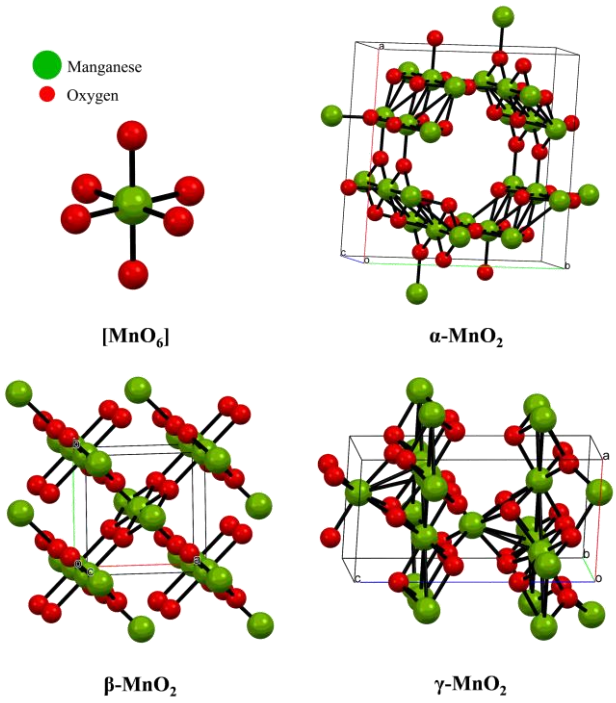

Figure 19. Crystal structure of [MnO_6] octahedron unit and crystal structures of MnO_2 polymorphic modifications.

As in the case of Bi_2O_3, standard electrochemical sensors are modified with MnO_2 nanoparticles in order to improve their electrochemical performances. The authors often modify the CPE with MnO_2 in order to develop a sensitive electrochemical sensor for H_2O_2, explaining that MnO_2 showed a high catalytic effect during the determination of this compound *(Schachl et al., 1997; Schachl et al., 2006; Zheng & Guo, 2000)*. *Li et al., (2010)* and *Zhang & Zheng, (2016)* developed an electrochemical method to quantify H_2O_2 in toothpaste using GCE modified with MnO_2 nanoparticles and α-MnO_2 nanotubes, respectively. Various modifications of electrochemical sensors with MnO_2 nanoparticles have been developed for ions sensing. *Dai et al., (2019)* and *Rahman et al., (2013)* report α-MnO_2-based sensors for micromolar quantification of NO_2^- and Cl^- anions, respectively. Also, *Teixeira et al., (2001)* explain the modification of CPE with MnO_2 nanoparticles for the determination of Li^+ ion in pharmaceuticals. On the other hand, *Xie et al., (2010)* explain the modification of the ZnO-based gas sensor with MnO_2 nanoparticles in order to improve the electrochemical performance during the quantification of gas formaldehyde. Modification of graphene materials with MnO_2 nanoparticles is widely present in electrochemical determination in order to improve the performance of electrochemical sensors/biosensors. For example, *Boopathy et al., (2018)* report the development of a GO-based sensor decorated with MnO_2 nanosheets for picomolar detection of guanine in calf thymus DNA. *Wang et al., (2015b)* and *Zaidi & Shin, (2015)* report the development of GO-based decorated with MnO_2 nanoparticles for nanomolar quantification of *L*-cysteine and *p*-nitrophenol, respectively. *Said et al., (2018)* explain the development of an electrochemical method using a pencil graphite electrode (previously treated with chitosan) modified with γ-MnO_2 nanoparticles for nanomolar quantification of diuretic furosemide in pharmaceutical and urine samples. Electrochemical sensors based on graphene nanomaterials modified, among other mediators, with MnO_2 nanoparticles have been reported by *Rao et al., (2016)* and *Wang et al., (2016b)* for the determination of dopamine and glucose (non-enzymatic sensor) in human blood serum samples, respectively. *Tian et al., (2020)* proposed a modification of GCE with rGO@MnO_2 nanowires for nanomolar quantification of bisphenol A. *Çakıroğlu et al., (2019)*, *Dontsova et al., (2011)*, *Norouzi et al., (2010)* and *Xu et al., (2005)* describe the development of electrochemical methods based on MnO_2@graphene-based biosensors for determination of

biologically important compounds such as glucose/lactose, choline, cholesterol and lactate, respectively, while *Zhuang et al., (2017)*, using similar biosensor construction, report electrochemical method for quantification of theophylline (pharmaceutical) in drug tablet. Finally, *Beyene et al., (2004)* explain the catalytic redox cycle of MnO_2 during the oxidation of H_2O_2, ascorbic acid and uric acid at the MnO_2-based sensor. Authors state that during the oxidation of noted biologically important compounds (depending on the applied potential), MnO_2 is reduced to its lower oxidation states: Mn^{2+} (MnO) and Mn^{3+} (Mn_2O_3). This is followed by re-oxidation of MnO and Mn_2O_3 to MnO_2 (in this way the electrode surface is restored), which results in the appearance of a current signal. Similar mechanism of reduction and re-oxidation of MnO_2 is reported by *Turkusić et al., (2001, 2005)* during the determination of glucose at MnO_2-based biosensor.

Various methods have been reported for the synthesis of MnO_2 nanoparticles. The hydrothermal method is one of the most commonly used method. Using this method, *Su et al., (2013)* synthesized α-MnO_2 and β-MnO_2 nanorods with a specific capacitance of ~300 F g^{-1} for both modifications. Also, by the hydrothermal method, *Dong et al., (2014)* reported the synthesis of α-MnO_2, β-MnO_2 and γ-MnO_2 using different molar ratios of $MnCl_2$ and $KMnO_4$, while *Xu et al., (2007)* synthesized α-MnO_2 hollow spheres and α-MnO_2 hollow urchins. In addition to the hydrothermal method, the authors report the synthesis of MnO_2 nanoparticles using sonochemical, micro-emulsion, sol-gel and electrochemical methods. Applying sonochemical reduction of $KMnO_4$, *Gnana Sundara Raj et al., (2014)* and *Nam et al., (2010)* explain the synthesis of δ-MnO_2 nanoparticles (specific capacitance ~280 F g^{-1}) and MnO_2 nanowires (specific capacitance ~300 F g^{-1}), respectively. On the other hand, *Chen et al., (2007)* and *Reddy & Reddy, (2004)* explained the synthesis of MnO_2 nanoparticles using micro-emulsion and sol-gel methods, respectively. Electrochemical methods for MnO_2 synthesis are based on the electrochemical deposition of MnO_2 at a specific substrate surface. *Hu & Tsou, (2002)* explain the anodic deposition of α-MnO_2 nanoparticles (specific capacitance ~320 F g^{-1}) from $MnSO_4$ aqueous solution at graphite substrate, while *Pang et al., (2000)* report anodic deposition of MnO_2 thin film at Ni foils. In addition to the above methods, the authors noted the precipitation method (reduction of $KMnO_4$ with Mn^{2+} salts), as the simplest method, for the synthesis of MnO_2. Using this method, *Hu et al., (2016)* and *Staiti & Lufrano, (2009)* reported the synthesis of ultrafine MnO_2 (particle size 3 nm) and α-MnO_2 nanoparticles, respectively. In this doctoral dissertation, MnO_2 was synthesized using the precipitation method. The X-ray diffraction method proved that α-MnO_2 nanoparticles were synthesized.

2.3. Graphene@M_xO_y nanocomposites for glucose and polyphenol biosensing - *literature review*

The combination of graphene nanomaterials and M_xO_y nanoparticles, as two very promising materials, has proven to be very applicable in electrochemistry. As already mentioned, the large surface area and HET of graphene and the pronounced catalytic effect of M_xO_y nanoparticles provide a new platform for the development of highly sensitive sensors/biosensors for the detection of a wide range of compounds (organic/inorganic compounds, biological important compounds, metabolites, supplements, pesticides) in different real samples (drink, food, environmental, clinical samples).

Table 2. provides a literature review of electrochemical enzymatic glucose biosensors based on graphene nanomaterials decorated with M_xO_y nanoparticles. In the table can be found electroanalytical parameters of these biosensors such as working linear range, sensitivity of developed method and LOD. The second part of *Table 2.* provides an overview of enzymatic polyphenolic biosensors based on graphene@M_xO_y nanocomposites, but also graphene-based and M_xO_y-based polyphenolic biosensors. As in the case of the glucose biosensor, the mentioned electroanalytical parameters are defined. After developing analytical methods for the detection of glucose and caffeic acid, with the appropriate biosensor, the obtained electroanalytical parameters were compared with the same parameters of selected literature biosensors in order to evaluate the proposed analytical methods and developed biosensors.

Finally, the review shows that standard electrochemical sensors have been modified with graphene@M_xO_y nanocomposites in order to improve the performance of biosensors and to develop highly sensitive analytical methods for quantification of metabolites such as glucose and polyphenols.

Table 2. Literature review of enzymatic glucose and polyphenolic biosensors.

Glucose biosensors				
Electrode	**Linear range (mmol L^{-1})**	**Sensitivity μA (μmol L^{-1})$^{-1}$**	**LOD (mmol L^{-1})**	**References**
GCE/**rGO@TiO_2**/GO_x/CS	0.032 - 1.67	not given	$4.8*10^{-3}$	*Luo et al., (2013)*
GCE/**rGO@ZnO**/GO_x	0.2 - 6.6	13.7	$2\cdot10^{-4}$	*Dey & Raj, (2013)*
GCE/**rGO@ZrO_2**/GO_x	0.29 - 14	11.65	0.13	*Vilian et al., (2014a)*
GCE/**rGO@Fe_3O_4**/GO_x	0.5 - 12	not given	0.05	*Teymourian et al., (2014)*
GCE/**rGO@MnO_2**/PLL/GO_x	0.04 - 10	46.36	0.02	*Vilian et al., (2014b)*
GCE/CNT-**GR@ZnO**/GO_x	0.01 - 6.5	5.36	$4.5*10^{-3}$	*Hwa & Subramani, (2014)*
CS-**GR@Fe_3O_4**/GO_x	up to 26	5658	0.016	*Zhang et al., (2015b)*
Au/**rGO@SnO_2**/PANI/GO_x	$5*10^{-7}$ - 0.03	96.1	$2.6*10^{-7}$	*Wu et al., (2017)*
GCE/**GR@MnO_2**/GO_x	0.04 - 2	3.3	0.01	*Liu et al., (2016b)*
MSPE/**rGO@Fe_3O_4**/GO_x	0.05 - 1	5.9	$1*10^{-4}$	*Pakapongpan & Poo-Arporn, (2017)*
GCE/**rGO@Fe_3O_4**/GO_x	0.5 - 10	2.645	0.106	*Wang et al., (2018b)*
SPCE/**GNR@MnO_2**/GO_x	0.1 - 1.4	56.32	0.05	*Vukojević et al., (2018b)*
GCE/**GNS@ZnO**/GO_x	$1\cdot10^{-4}$ - 0.02	not given	$2*10^{-5}$	*Norouzi et al., (2011)*
GCE/**rGO@ZnO**/GO_x	0.02 - 6.24	18.97	0.02	*Palanisamy et al., (2012)*
SPCE/GNR@Bi_2O_3/GO_x/Naf	**0.28 - 1.70**	**520**	**0.07**	***This work***
Polyphenolic biosensors				
Electrode	**Linear range (μmol L^{-1})**	**Sensitivity μA (μmol L^{-1})$^{-1}$**	**LOD (μmol L^{-1})**	**References**
GCE/PED/**rGO@Fe_2O_3**/PPO	0.04 - 620*	not given	$7*10^{-3}$	*Sethuraman et al., (2016)*
GCE/**GR@Co_3O_4**/CS-Tyr	1 - 30*	1856.8	0.03	*Liang et al., (2016)*
GCE/**rGO@Fe_2O_3**/PANI/Lac	0.4 - 337.2♣	36.39	2.94	*Lou et al., (2020)*
MGCE/**Fe_2O_3**/CS-Tyr	2.64 - 84*	14.72	0.79	*Zhou et al., (2018)*
SPCE/**GR**/CMF/Lac	0.2 - 209.7*	0.932	0.085	*Palanisamy et al., (2017)*
GCE/**GO**/GA/Tyr	0.05 - 50*	0.34	0.03	*Wang et al., (2018c)*
GCE/**rGO**-GC/Lac	0.2 - 15*	93	0.076	*Boujakhrout et al., (2016)*
GCE/**ZnO**/CS/Lac	1 - 100*	not given	0.29	*Qu et al., (2015)*
CPE/**Fe_3O_4**/PANI/CS/Lac	0.5 - 80*	126	0.4	*Sadeghi et al., (2015)*
SPCE/GNP@MnO_2/Lac/Naf	**5 - 320♠**	**720**	**1.9**	***This work***

model compounds: *for CT, ♣for HQ, ♠for caffeic acid

Abbreviations: CS - chitosan; PLL - poly-*L*-lysine; PANI - polyaniline; MSPE - magnetic screen printed electrode; GNS - graphene nanosheets; PED - poly(3,4-ethylenedioxythiophene); PPO – polyphenol oxidase; GR - graphene; Tyr - tyrosinase; MGCE - magnetic GCE, CMF - cellulose microfibers; GA - glutaraldehyde; GC - glycol chitosan

2.4. Methods

2.4.1. Electrochemical methods

Electrochemical methods are analytical techniques that, based on the measured potential, charge or current, enable the determination of an unknown concentration of the target analyte or the characterization of analyte's chemical reactivity. The electrode is a key component in electrochemical methods. Electrochemical methods are divided into non-faradaic (conductometric, potentiometry) and faradaic methods (electrogravimetry, voltammetry/amperometry). Faradaic methods are based on the direct exchange of electrons, due to redox processes, between the electrode surface and the analyte. Electrodes that participate in redox processes are called working electrodes. The analyte can reach the electrode surface by diffusion (it is based on the formation of a concentration gradient due to ox/red analyte on the electrode surface), convection (mixing) and migration processes (due to the application of an electric field). Redox processes take place due to the application of a certain potential value (potential range) to the electrode. As a result of the process on the electrode surface, a current is recorded (defined by its intensity). The total current passing through the working electrode represents the sum of faradaic and capacitive currents (Figure 20). Faradaic current is a current of interest and occurs due to the *direct electron transfer* (DET) between the analyte and the electrode surface. Capacitive current occurs due to the discharge of the electrochemical double layer on the electrode surface. This type of current is undesirable and has been developed through electrochemical methods to minimize it. In general, the advantages of electrochemical methods are reflected through high selectivity and sensitivity, simplicity, time saving, low cost, easy sample preparation and low consumption of reagents, when compared to other analytical methods.

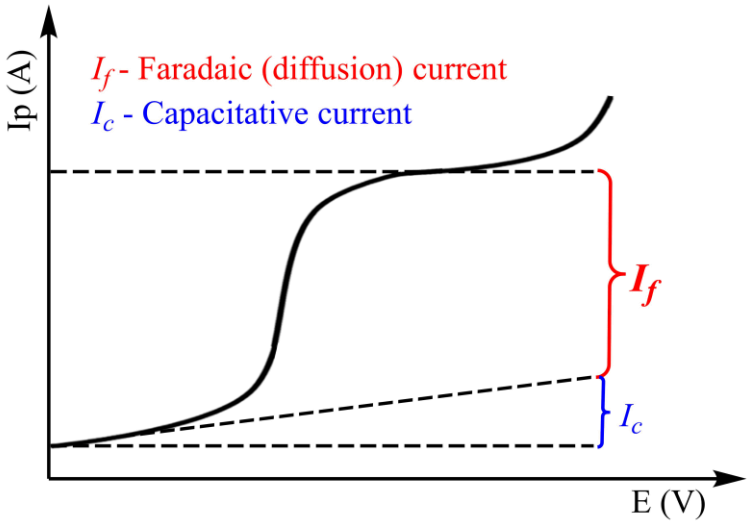

Figure 20. Peak current intensity (*Ip*) *vs.* potential (*E*) for certain analyte at the appropriate electrode. Relationship of Faradaic and capacitive current.

Voltammetry and amperometry are electrochemical methods most commonly used in the analysis of the target substance. Voltammetry is based on monitoring the behavior of analyte depending on the applied potential range. As a result of voltammetric measurements, a curve of the dependence of the current intensity on the applied potential was obtained, the so-called voltammogram. A very important parameter can be read from the voltammogram - the value of the potential at which, in a certain supporting electrolyte, the target analyte is oxidized or reduced. Further, quantification of the analyte can be performed on this potential. In this case we are talking

about amperometry. Amperometry is a method that originated from voltammetry and is based on monitoring the analyte at a constant potential *ie.* potential that allows oxidation or reduction of the analyzed substance. Voltammetric/amperometric measurements are performed in a three-electrode electrochemical cell. The three-electrode system consists of a working (WE), reference (RE) and auxiliary/counter (CE) electrode, immersed in a supporting electrolyte with an analyte (Figure 21). Depending on the applied potential, the analyte is oxidized or reduced at the WE. The RE has a constant potential and the potential of the WE is measured in relation to it. All current in the cell passes between the WE and CE (Figure 21). An inert gas (N_2, Ar, He) can be flow through the cell to remove dissolved O_2 from the analyte, because oxygen negatively affects the detection/quantification of the analyte. The electrochemical cell is connected to the potentiostat and this instrument controls the potential given to the WE.

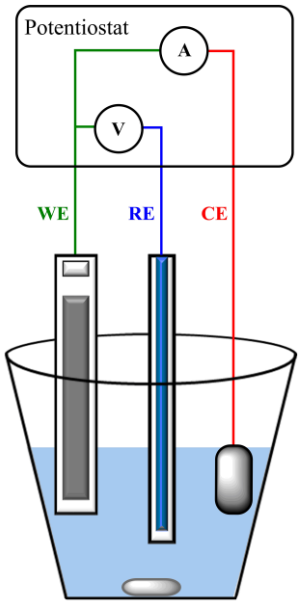

Figure 21. Three-electrode electrochemical cell. *WE* - working electrode, *RE* - reference electrode, *CE* - counter electrode.

Voltammetric methods, depending on the technique, are divided into polarography (dropping mercury electrode is used as the WE), cyclic voltammetry, square wave voltammetry (SWV). Then, normal pulse and differential pulse polarography, as well as polarography with rectangular waves, are methods developed in order to minimize the capacitive current, which results in improved sensitivity and selectivity of analytical methods. Amperometric methods are also, depending on the technique, divided into chronoamperometry, hydrodynamic chronoamperometry, multistep amperometry, differential pulse amperometry and double differential pulse amperometry. Voltammetric and amperometric methods provide the quantification of organic/inorganic substances at very low levels (μmol L^{-1}, nmol L^{-1}). In addition to high sensitivity, these methods can be used to simultaneous determination of several different analytes, without prior separation and preparation.

Cyclic voltammetry and hydrodynamic chronoamperometry are electroanalytical methods used in this doctoral dissertation. Accordingly, a basic principle and brief concepts of the above methods are given below.

2.4.1.1. Cyclic voltammetry

Cyclic voltammetry is based on the linear application of the WE potential from the value of E_1 to the value of E_2, and then again to the value of E_1, in a unit of time (Figure 22a). The model of cyclic voltammogram is shown in *Figure 22b*. For the determination of oxidation process, the potential ranging from negative to positive values is applied. Obtained oxidation peak is named the anodic peak (p_a). In contrast, for the reduction of analyte during the analysis, the potentials are applied from positive to negative value. The peak formed due to the reduction of the electroactive species is called the cathodic peak (p_k) *(Bard & Faulkner, 2011; Manojlović et al., 2011; Scholz, 2010)*. Important parameters such as potential of anodic peak (Ep_a) and potential of cathodic peak (Ep_k) (potential values at which the analyzed species is oxidized/reduced), as well as intensity of anodic peak (Ip_a) and intensity of cathodic peak (Ip_k) can be obtained from the cyclic voltammogram (Figure 22b).

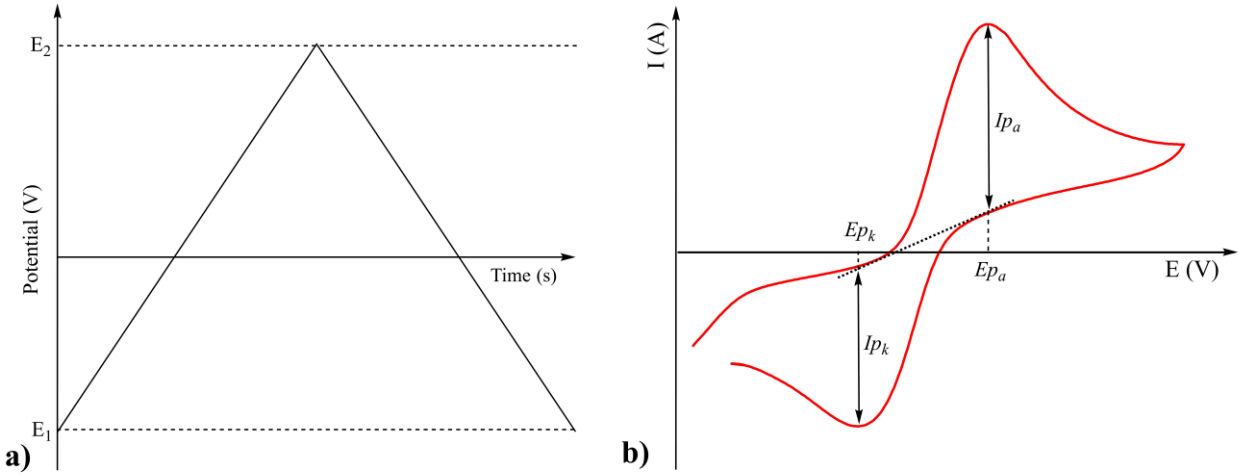

Figure 22. a) Potential change profile over time. ***b)*** Appropriate cyclic voltammogram. Look of a cyclic voltammogram of a reversible process.

In the case of reversible reactions, both peaks (p_a and p_k) are observed on the cyclic voltammogram (Figure 22b). The basic criterion of reversibility is the difference between the potentials of the anodic and cathodic peak (ΔEp). *Peak-to-peak potential separation* (ΔEp), at a temperature of 25ºC, is explained by *Equation 1.*, where: *n* - the number of exchanged electrons in the half-reaction. In the case of irreversible processes, ΔEp is greater than 0.059/n, due to the slow kinetic electron transfer. However, very often, in irreversible processes, the absence of oxidation or reduction peak is observed *(Bard & Faulkner, 2011; Manojlović et al., 2011; Scholz, 2010)*.

$$\Delta Ep = | Epa - Epk | = 0.059/n \qquad \textit{Equation 1.}$$

Ip_a and Ip_k, in reversible processes, are approximately equal in absolute value, but are of the opposite sign. The peak current intensity can be explained by the *Randles-Sevcik's* equation, which at 25ºC has the form given by *Equation 2.*, where is: *Ip* - peak current (A); *n* - number of exchanged electrons; *A* - electrode surface (cm^2); *D* - diffusion coefficient ($cm^2\ s^{-1}$); *C* - concentration of analyte ($mol\ L^{-1}$), *V* - scan rate ($V\ s^{-1}$). It can be seen from the equation that the peak current intensity is directly proportional to the analyte concentration *(Bard & Faulkner, 2011; Manojlović et al., 2011; Scholz, 2010)*.

$$Ip = 2.69 * 10^5 \cdot A \cdot n^{3/2} \cdot D^{1/2} \cdot V^{1/2} \cdot C$$ *Equation 2.*

An important operating parameter during substance analyzing by cyclic voltammetry is the scan rate. The scan rate is the rate of change of potential *ie.* the rate of polarization of the WE. Most often, the scan rate is applied in the range of 10-200 mV s^{-1}. A change in the scan rate causes an increase in the current signal, at a constant analyte concentration (Figure 23). By considering the relationship between the current intensity and the applied scan rate, the mechanism of transport of the analyte from the solution to the electrode surface can be understood. If the current increases linearly with the square root of the scan rate (r=0.9-0.9999), the diffusion-controlled process is responsible for transporting the analyte molecules to the electrode. On the other hand, the adsorption-controlled process is proved with a linear relationship between current intensity and scan rate *(Bard & Faulkner, 2011; Manojlović et al., 2011; Scholz, 2010)*.

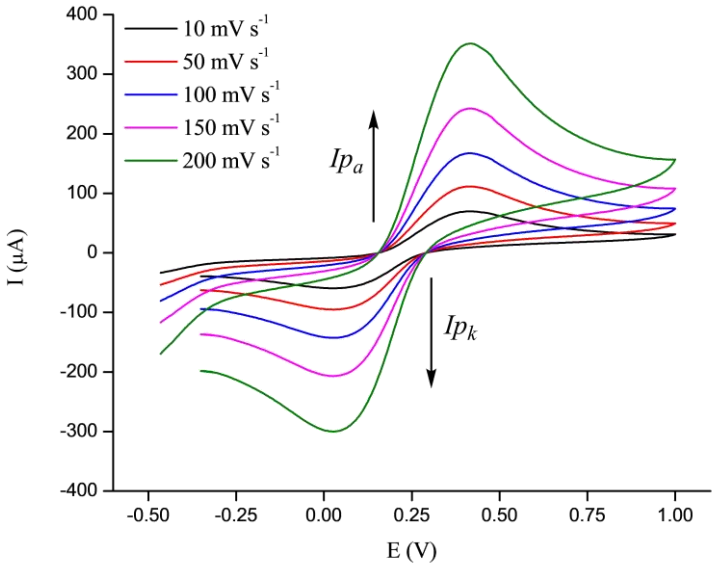

Figure 23. Change in intensities of anodic (Ip_a) and cathodic (Ip_c) peak with scan rate (10-200 mV s^{-1}).

Cyclic voltammetry is one of the most applied electrochemical techniques. It is especially pronounced in the analysis of compounds about which there is not much literature information on electrochemical redox processes or structure. This method has wide application in all fields of chemistry (organic, inorganic, analytical, biochemistry). The efficiency of cyclic voltammetry is reflected in obtaining information about the ox/red behavior of the target analyte, system reversibility, kinetics of electrochemical reactions, the nature of the process that takes place on the electrode surface, the thermodynamics of the redox process. Also, this method is very effective for examining the mechanisms of the electrode process, especially for the identification of intermediates. In addition, with high scan rates, it is possible to identify short-lived intermediates *(Bard & Faulkner, 2011; Manojlović et al., 2011; Scholz, 2010)*.

In this doctoral dissertation, during the development of methods for glucose and polyphenolic index biosensors, cyclic voltammetry was used for electrochemical characterization of the obtained WEs, testing of system reversibility, as well as for selection and optimization of pH of appropriate supporting electrolyte.

2.4.1.2. Chronoamperometry. Hydrodynamic chronoamperometry

Chronoamperometry is a type of amperometric method that is based on monitoring the change in current intensity over time, at a constant potential. The potential is set to the value at which the analyte is electroactive. However, it is very common that other substances (interferences) are electroactive at the set potential, which affects the selectivity of the method. Therefore, it is necessary to optimize the potential of the chronoamperometric method, which will later be used for quantification of analyte.

Chronomaperometric measurements can be performed in unstirred (calm) and stirred solution. The type of chronoamperometry in which the solution is constantly stirred is called hydrodynamic chronoamperometry. The current response of the WE, at constant potential, in stirred and unstirred solution after the addition of the analyte is similar (Figure 24). Due to the redox process on the electrode surface, the current intensity increases. However, the current signal, in both solutions, changes significantly over time. In the stirred solution, the current stabilizes at a constant value after a short time. In unstirred solution, the current intensity increases in proportion to $t^{1/2}$. This difference in the response of the electrode after the addition of the analyte, in the stirred and unstirred solution is a consequence of different mechanisms for the transport of the analyte molecules to the electrode surface. In the stirred solution, the analyte reaches the electrode surface by the convection mechanism, while in the unstirred solution the current intensity increases due to the diffusion of the analyte. In hydrodynamic chronoamperometry, the reading of current intensity is considerably facilitated. In addition, due to the rapid reaction on the electrode surface, due to convection, this method is significantly faster than chronoamperometry in unstirred solution *(Bard & Faulkner, 2011; Guy & Walker, 2016; Scholz, 2010)*.

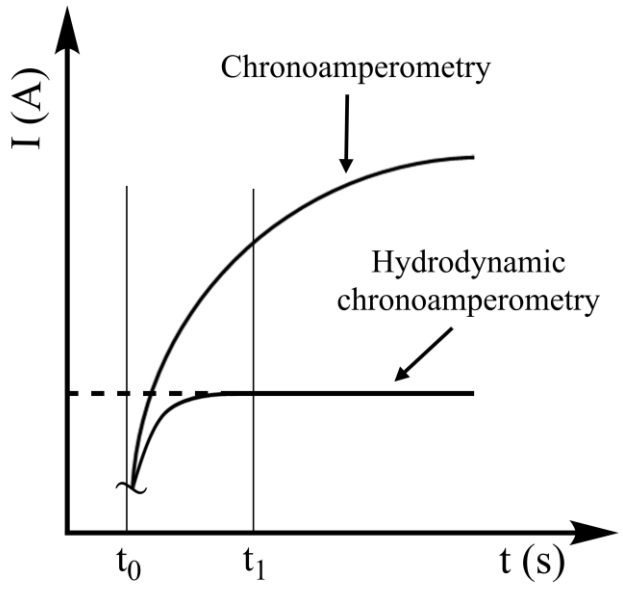

Figure 24. Electrode current response in a unit of time at a constant potential in stirred (hydrodynamic chronoamperometry) and unstirred (chronoamperometry) solution.

In this doctoral dissertation, hydrodynamic chronoamperometry is a method used for quantification of glucose and caffeic acid with a glucose and polyphenolic index biosensors, respectively. Prior to quantification, the working potential of WEs (biosensors) was optimized.

2.4.1.2.1. Optimization of working potential

Determining the optimal working potential of a sensor/biosensor plays an important role in amperometric determinations. Namely, it is known that an increase in the working potential of the electrode leads to an increase in the current intensity of the target electroactive species. Increased current intensity has a positive effect on analytical parameters such as LOD and limit of quantification (LOQ). However, at higher potentials, other electroactive substances (interfering substances) may react at the electrode surface, which negatively affects the analytical signal of the analyte. Accordingly, the potential of the electrode should be applied as low as possible. Based on this, it can be concluded that there must be a compromise between the selection of electrode working potential and the influence of interfering substances on the determination of the analyte. This problem is usually solved by using a mediator. In the last decade, the use of nanomaterials significantly reduced the influence of interfering substances at higher potentials during amperometric determinations. Nanomaterials, especially graphene nanomaterials and nano-structured M_xO_y, have found a great application in the production and design of sensors/biosensors *(Bilgi & Ayranci, 2016; Xu et al., 2004)*.

2.4.1.3. Sensors (WEs) in voltammetry/amperometry

As already mentioned, the WE represent the place where the redox process takes place. WEs can be classified as electrochemical sensors, because they show selectivity according to a tested analyte, at a certain potential. However, the selectivity mainly depends on the electrode modification, where specific functional groups from the electrode surface react only with the desired analyte *(Lubert & Kalcher, 2010)*.

The first amperometric sensor was developed in 1956 by Clark (Clark's oxygen sensor) and was widely used to detect soluble oxygen in blood and other body fluids *(Clark, 1956)*. The operation of the voltammetric/amperometric sensors mostly depends on the selection of the electrode material. Mercury, precious metals and carbon materials are the main components of these sensors. Nowadays, special attention is paid to nanomaterials as excellent materials for the production of electrochemical sensors in general, because they have a positive impact on the electrochemical characteristics of sensors *(Stradiotto et al., 2003)*.

Voltammetric techniques have been developed on the dropping mercury electrode (DME) and its various techniques (static mercury drop electrode (SMDE) and hanging mercury drop electrode (HMDE)). The main advantage of the DME is its wide application in the negative potential field (up to -2.5 V). In addition, the constant renewal of the electrode surface due to mercury dropping, as well as the possibility of forming amalgams with metals also gives DME an advantage over other sensors. However, this electrode can be applied in the positive potential range up to 0.4 V *(Manojlović et al., 2011; Vyskočil & Barek, 2009)*. Since most chemical compounds show their electrochemical activity in the positive potential range, as well as due to mercury toxicity, this electrode is replaced by other electrode materials. Electrodes based on Bi or Sb films, as well as different types of amalgam electrodes, have proven to be suitable alternatives *(Kapturski & Bobrowski, 2008; Królicka & Bobrowski, 2004; Tesarova et al., 2009)*.

Precious metal electrodes are mainly based on Pt, Au, Pd, Ir. Precious metals act as catalysts in redox reactions and accelerate HET between the electrode surface and the analyte. Their main advantage is reflected in the wide application in the positive (anodic) potential range, while the application in the cathodic range is limited (they are applied in the range from -0.2 V to -0.5 V). The main disadvantage of this type of sensor is the high background current that occurs due to the formation of oxides on the electrode surface *(Wang, 2000)*.

Carbon-based electrodes are widely used electrochemical sensors. The most commonly used carbon-based sensors are graphite electrode, GCE and BDD electrode. Modern electrode materials are based on nanomaterials such graphene (rGO, GNR, GNP) or CNT and SWCNT. The diversity of carbon as an electrode material originate from its unique structural properties.The advantage of these electrode materials is reflected in the application in a wide potential window, large contact area, electrocatalytic activity, as well as low cost *(Lubert & Kalcher, 2010; McCreery, 2008)*.

In addition to the above carbon-based electrodes, CPE and SPCEs (heterogeneous carbon electrodes) have been developed. With the introduction of these electrodes in the field of electrochemistry, many methods have been developed for the quantification of a large number of compounds/metabolites while achieving low LODs, which has significantly expanded the application of these electrodes, especially in medicine.

In this doctoral dissertation, modified SPCEs were used as WEs. Accordingly, the basic principles of "*screen printing*" technology and the characteristics of SPCEs are given below.

2.4.1.3.1. Screen-printed carbon electrodes

2.4.1.3.1.1. "*Screen printing*" process

"*Screen printing*" technology is based on applying *layer-by-layer* of conductive or non-conductive ink/paste to the appropriate substrate. This technology is used for mass production of disposable electrochemical sensors. Depending on the desired sensor, the electrode production process is based on the selection and preparation of ink/paste, the selection of the substrate and the method of electrode drying *(Alonso-Lomillo et al., 2010; Fanjul-Bolado et al., 2008; Fletcher, 2015; Honeychurch & Hart, 2003; Mistry et al., 2014; Thiyagarajan et al., 2014; Li et al., 2012)*.

For the production of electrochemical sensors, carbon inks are most commonly used. Commercially available carbon-based inks consist of an electroactive component, a polymeric binder and a solvent. The electroactive component in the ink is graphite (graphite particles). In addition to graphite, activated carbon and carbon black are used, but today much attention is paid to other forms of carbon such as graphene nanomaterials and CNTs. A polymeric binder (vinyl or epoxy polymer) increases the mechanical strength of the ink as well as the adhesive properties between the ink and the substrate. The solvent serves to increase the viscosity of the ink, which facilitates the process of printing electrodes. Also, solvent must be non-electroactive in a wide range of potentials (*Fanjul-Bolado et al., 2008; Fletcher, 2015;*). In addition to carbon, SPCE can also be produced from Ag or Pt inks.

The manufacturing process of SPCEs is simple and fast. It consists of *i)* applying ink to the substrate using a screen and *ii)* pulling the applicator along the screen under pressure (Figure 25). Substrates can be made of ceramic, plastic, glass, aluminum, nylon (*Li et al., 2012; Mistry et al., 2014; Wang, 2000*). The thickness of the electrode layer can be in the range from 1 μm to 100 μm (*thick-film electrodes*) and is controlled by the thickness of the screen *(Kalcher et al., 2009; Metters et al., 2011)*. The dimensions of the produced electrodes depend on the dimensions of the screen, but electrodes with dimensions of 40x10x1 mm are usually produced. An important parameter during the production of SPCEs is drying. The drying temperature affects the electrochemical properties of carbon ink. Drying the electrode at 80ºC leads to the formation of active edges of graphite, while a temperature of 120ºC leads to an increase in the active surface due to the formation of cracks within the carbon ink. Such physical changes in ink directly affect the improvement of electrochemical characteristics of SPCEs (*Patris & Kauffmann, 2015*).

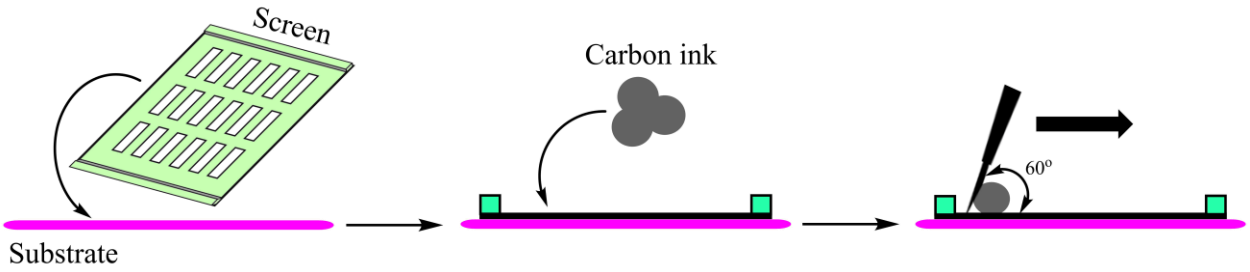

Figure 25. "*Screen printing*" technology. The process consists of applying carbon ink to the screen and evenly distributing the ink to the substrate.

An illustration of the standard type of SPCE is given in *Figure 26b*. The final preparation step refers to the covering of a larger part of the electrode, leaving the active surface which is further used for measurements and/or modification. At the top of the electrode, a metal ink (usually Ag) is applied in order to make contact with the instrument. Also, "*screen printing*" technology allows the application of a single strip three-electrode system to the substrate (Figure 26a). The production process of these electrodes consists of applying a WE, RE and CE electrode using appropriate screen and printing technology. The first step involves applying Ag paste in order to print lines which connect the electrode active surface and wire connection. After drying the silver lines, carbon ink is applied using a suitable screen, while the working and counter electrodes are printed. This is followed by printing of the reference electrode, which is most often Ag/AgCl. After drying the RE, the final step requires coating the electrode with an inactive material, except for the active surface of WE, RE and CE *(Li et al., 2012; Mistry et al., 2014; Thiyagarajan et al., 2014)*.

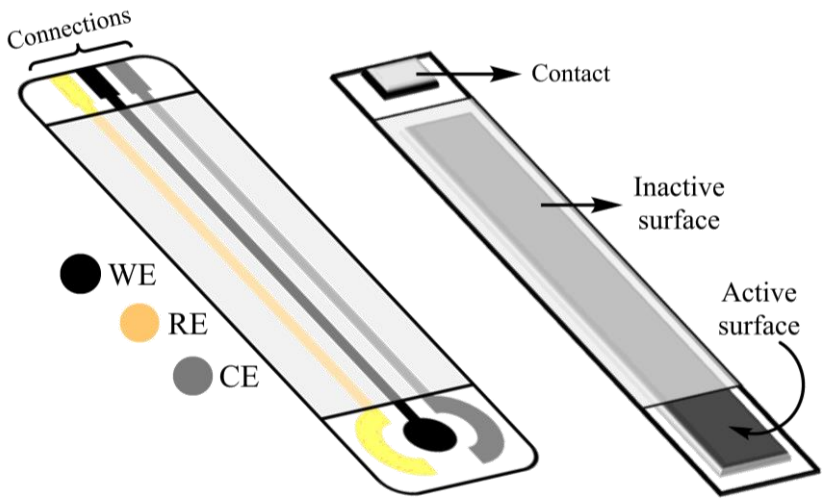

Figure 26. Illustration of SPCEs. Three-electrode system (left) and standard type (right).

The advantages of SPCEs are reflected in the application in a wide potential range, fast response, as well as high sensitivity. However, SPCEs give a moderately background current originating from adsorbed or dissolved oxygen in the ink. This effect can be partially, not completely, eliminated by "*precathodization*" (*negative pretreatment potentials*) *(Kalcher et al., 2009)*. SPCEs are made of a heterogeneous carbon material which very often exhibits slower electron transfer than homogeneous carbon electrodes (*e.g.* GCE). Moreover, SPCEs have higher resistance depending on

composition of printed layer and its thickness. These electrodes, like classic solid electrodes, are characterized by a memory effect and a tedious cleaning process. Polymeric binder can block the active centers of carbon ink, which leads to the limitation of DET and affects the reversibility of reactions that take place on the SPCEs. Usually these reactions are quasi-reversible or irreversible *(Alonso-Lomillo et al., 2010; Li et al., 2012; Nawaz et al., 2016; Navarreto-Lugo et al., 2018)*.

SPCE, since they are portable sensors, can be used for *in situ* analyzes. SPCEs belong to the group of disposable sensors, whose production is massive and cheap. Although disposable, SPCEs have shown adequate stability and can be used several times, with adequate storage *(Thiyagarajan et al., 2014; Li et al., 2012; Stanković et al., 2020b; Vukojević et al., 2018a)*. These electrodes have found wide application in the determination of electroactive organic compounds, as well as metal ions (Al^{3+}, Cd^{2+}, Cu^{2+}, Fe^{2+}, Hg^{2+}, Pb^{2+}) in industry, environmental, biomedical analysis. Today, it is popular to print microelectrodes as well as electrode arrays that allow the analysis of several different analytes simultaneously (*Honeychurch & Hart, 2003; Li et al., 2012*). Since screen printing technology is limited to flat surfaces, it is a great challenge to print electrodes on uneven surfaces (e.g. textiles) (*Yang et al., 2010b*).

2.4.1.3.1.2. Modification of SPCEs

A great advantage of SPCEs is their simple modification due to the composite nature of the electrode material. Modifications of SPCEs are performed in order to improve their electrochemical performance such as reducing the LOD for a particular analyte, generating and/or increasing electrochemical signals, as well as separating overlapping signals. Also, in the case when the HET of a certain reaction on an unmodified electrode is slow and accelerates only at significantly higher potentials (in addition to its thermodynamic redox potential), then the modification of the electrode in most cases facilitates HET between analyte and electrode surface, and allows reaction at lower potentials. In addition, the play of reactions at lower potentials in many cases prevents the occurrence of interference signals *(Kalcher et al., 2009; Wang, 2000)*.

The modifier is added to the SPCE in a form of several drops (~ 1 µL). SPCEs can be modified by the principle of covalent bonding, where a covalent bond is formed between specific functional groups on the electrode surface and the corresponding modifier. Then, the polymerization method of modification is based on electro-polymerization of conductive polymer on the electrode surface. This procedure is suitable for indentation of enzyme within polymer when developing biosensors. The electrodeposition method is based on the electrochemical coating of the electrode surface with a thin film of metal (Au, Hg, Bi, Sb, Cu). In this procedure the advantage of SPCE is that it is not necessary to polish the surface before coating the film. The formation of heterogeneous layers is the simplest and most commonly used procedure for the modification of SPCE, and is the reason why SPCE has found great popularity in electrochemical testing. This procedure is based on mixing a solid modifier or a certain volume of modifier (*volume modification*) with carbon ink. Also, the modification of SPCE can be based on adsorption/hemisorption, covering the electrode surface with a membrane, as well as on non-covalent binding (interactions) *(Beyene et al., 2004; Kalcher et al., 2009)*.

Various chemical elements/compounds can be used as modifiers. M_xO_y, as well as pure metals, are the most widely used modifiers of SPCEs, but also electrochemical sensors in general. Metal/M_xO_y act as electrocatalysts and accelerate HET between the analyte and the electrode surface. The most commonly used transition metals are Mn, Cu, Fe, Sn, Ti, as well as their oxides (MnO_2, CuO, Fe_3O_4, SnO_2, TiO_2) *(Švancara & Kalcher, 2015; Turkušić et al., 2001; Turkušić et al., 2005)*. Pure precious metals and their oxides (IrO_2, RuO_2, PdO, OsO_2, PtO_2, RhO_2) also have a significant application in electrochemical determination *(Kotzian et al., 2005; Kotzian et al., 2006; Kotzian et al., 2007)*. Also, surfactants (improve the surface characteristics of the electrode), ion exchangers (facilitate the accumulation of ions), as well as sorbents (ion adsorption based on ion exchange or

particle size) are used as modifiers *(Kalcher et al., 2009)*. In addition to the listed chemical modifiers, SPCE can be modified with biological compounds (enzymes, DNA, antibodies). In this case we are talking about biosensors.

Nanomaterials are modifiers that today enjoy special attention and whose application is significantly represented in electrochemical determinations. Graphene nanomaterials decorated with transition M_xO_y nanoparticles significantly affect the performance of SPCE.

2.4.2. Methods for structural characterization of nanomaterials

2.4.2.1. X-ray diffraction method

To obtain information on the crystal structure of a substance by diffraction methods, radiations whose wavelengths correspond to the interatomic distances in the crystal lattice are used. Diffraction methods can be based on three types of radiation: neutron, electron and X-rays. Neutrons are scattered on atomic nuclei and unpaired electrons, while electron radiation is scattered in the electrostatic field of atoms (ions). X-rays are scattered on the electrons surrounding the nucleus, so this type of diffraction is suitable for studying electron densities *(Drago, 1992)*. In this doctoral dissertation, the crystal structure of all nanomaterials and synthesized nanocomposites was determined using the X-ray diffraction (XRD) method. Therefore, the basic principles and concepts of this method are described below.

The XRD method is based on *constructive interferences* between the crystal sample and monochromatic X-rays. The diffraction patterns can be analyzed by applying *Bragg*'s law (*Equation 3.*), where is: where n - order of reflection (an integer), λ - the wavelength of the X-rays, d - the interplanar spacing (so-called d-spacing) in the crystal grids generating the diffraction, θ - diffraction angle. The formation of *constructive interferences* occurs when *Bragg*'s low is satisfied.

$$\mathbf{2 \cdot d \cdot sin\theta = n \cdot \lambda} \qquad \textit{Equation 3.}$$

A typical X-ray diffractometer consists of an X-ray cathode tube, a goniometer, a sample holder and an X-ray detector (Figure 27). The principle of X-ray formation in a cathode tube is as follows: the filament inside the cathode tube, after heating, produces electrons. The released electrons are accelerated under a magnetic field. After acceleration, electrons fall on the desired material (Cu, Mo, Cr, Fe), whereby electrons are ejected from the inner shell of the material. As a consequence of the ejection of electrons from the shell of the material, characteristic X-ray spectra are formed (wavelengths within the spectrum are usually mark as K_α and K_β). Specific wavelengths within the spectrum are characteristic of the material used. For single crystal diffraction, Cu is the most commonly used material for X-ray production (CuK_α, λ=1.5418 Å). Then, the spectra are directed to crystalline monochromators which have the role of extracting the X-rays required for diffraction. The isolated collimated X-rays are directed to the sample. The sample rotates in the path of the collimated X-ray beam at an angle θ. After satisfying *Bragg*'s low, *constructive interference* occurs between the incident rays and the sample (diffraction rays are created). At the same time, during the rotation of the sample, the detector is rotated at an angle of 2θ and collects diffracted X-rays from the sample. The goniometer is part of the XRD system used to rotate the sample and maintain the angle. As a consequence of rotation, diffraction peaks of certain intensities appear. By converting the diffraction peaks into d-spacings, information about the analyzed sample is obtained. Identification of compound is enabled because each compound has its own unique d-spacings. Then, the crystal structure of the

sample is determined by comparing the obtained diffraction peaks with the diffraction peaks of the reference standards *(Bunaciu et al., 2015; Drago, 1992)*.

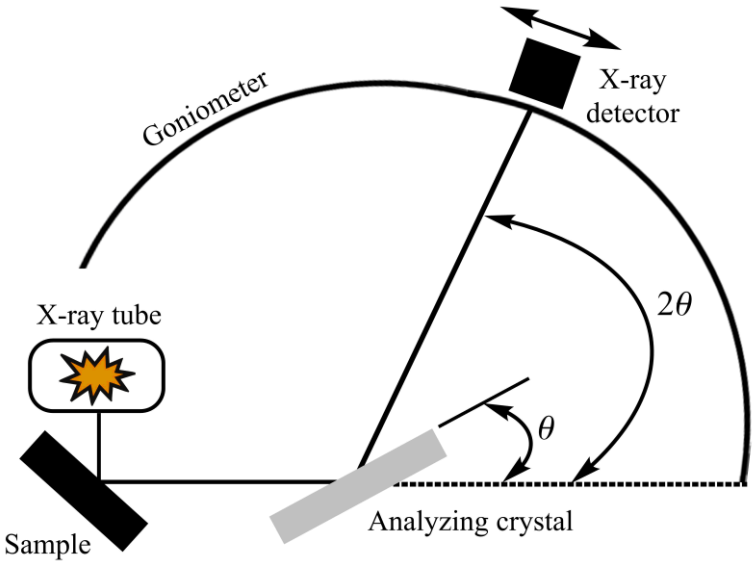

Figure 27. Schematic illustration of a diffractometer system.

Based on the width of the diffraction peaks, the degree of crystallinity of the sample can be determined. Namely, the width of the diffraction line (peak) is measured at half the maximum of peak and is defined as width at half-maximum. The sample is considered to be highly crystallized if the width at half-maximum is less than 0.1 (2θ). The width of the diffraction peak depends on the size of the crystallite. Diffraction peaks are considered sharp when the crystallite size is above $1*10^4$ Å, while the peaks become wide if the crystallite size is below 200 Å. Small crystallites (below 50 Å) are extremely wide, so it is very possible that they will not be seen on the diffractogram. The size of the crystallite can be calculated via *Scherrer*'s equation (*Equation 4.*), where is: D_{xrd} - mean size of the crystalline domains, K - dimensionless shape factor, λ - X-ray wavelength, β - line broadening at half the maximum intensity, θ - *Bragg*'s angle *(Drago, 1992)*.

$$\boldsymbol{Dxrd = {K \cdot \lambda}/{\beta \cdot cos\theta}} \qquad \textit{Equation 4.}$$

XRD methods can be divided into two different classes, whereby the first is based on the examination of the single crystal, and the second utilizes the polycrystalline powder. Methods for testing single crystals require the existence of single crystals of certain dimensions (it is not always possible to provide). XRPD methods have found wide application for determining the crystal structure of solid materials (minerals), especially in environmental, geology and metallurgy. The XRPD method enables the characterization of thin films, fine-grained minerals (clay), as well as the orientation of grains in minerals. The advantages of the XRPD method are reflected in the simple preparation of samples, rapid analysis and unambiguous identification of the analyzed mineral, as well as the relatively simple presentation of data. On the other hand, access to reference standards, as well as inhomogeneity of materials (homogeneous and single-phase material is most ideal for analysis) are limitations of this method *(Bunaciu et al., 2015; Drago, 1992)*.

The XRD/XRPD, as a non-destructive technique, are used to analyze a wide range of materials (fluids, minerals, polymer catalysts, drugs, plastics, ceramics, solar cells). Accordingly, this method finds wide application in many fields of industry. In addition to determining the crystal structure of the material and the size of the crystallite, this method can detect damage within the crystal, textures, as well as the resistance level to stress *(Bunaciu et al., 2015)*.

2.4.2.2. Scanning electron microscopic method

Electron microscopy is a method of examining the morphology (topography) of the surfaces of solid materials. Surface topographies can be analyzed by direct observation or study of photographic images of the object. An electron microscope is used to form an enlarged image of an object by diffraction of high-energy electrons. For comparison, the magnification of the optical microscope is 10^3, while electron microscope is 10^8. If the determination of the topography of the sample surface is based on the programmed scanning of the electron beam, then we are talking about the scanning electron microscopic (SEM) method. In order to achieve high resolution and obtain sharper images of the sample surface, a field emission gun (see below) is used as the electron beam source. The SEM method that uses the field emission gun as an electron source is called field emission scanning electron microscopy *(Jusman et al., 2014; Reimer, 1998)*. Since in this doctoral dissertation FE-SEM was used to determine the morphology of all nanomaterials and synthesized nanocomposites, the basic principles of this method are further described.

The FE-SEM instrument consists of an electron beam source, an anode, magnetic lens, scanning coils and detectors. All parts of the instrument are placed in a vacuum atmosphere. The electron beam is generated in a field emission gun equipped with a tungsten filament cathode (diameter 100 nm). Tungsten is the most commonly used element for generating an electron beam, because it has the highest melting point, as well as the lowest vapor pressure compared to other elements, and it is cheap. By heating the tungsten to 2700°C, an electron beam is released, which then reaches the anode. A voltage of 2-6 kV was applied to the anode, which resulted in the creation of an electromagnetic field (~ 10^{10} V m^{-1}). Due to the presence of a magnetic field, the emitted electrons are accelerated, which facilitates their passage through the vacuum. The electron beam passes through a magnetic lens which has the role of focusing the beam towards the sample (Figure 28). After that, the electron beam passes through scanning coils that turn the beam in the direction of the *X* and *Y* axes, which allows scanning in a rectangular area of the sample surface *(Goldstein, 2003; Jusman et al., 2014; Reimer, 1998)*.

After the electron beam reaches the sample surface, the electrons lose energy by absorption or random scattering within a *teardrop-shaped volume* of the sample (Figure 28) known as the interaction volume (depending on the electron beam energy, sample density, and atonic sample number). The exchange of energy between the incident electron beam and the sample leads to the emission of low energy secondary electrons (up to 50 eV) from the sample surface. Due to the low energy, these electrons were emitted from the first few nanometers of the sample surface. A secondary electronic detector is installed in the path of the secondary electron beam. Secondary electrons are attracted to the detector by an electric field, after which the obtained signal is multiplied by electronic amplifiers. The number of detected electrons depends on the variations of the surface. The magnification of the image of the sample surface can be below 1 nm, because the signal of the secondary electrons has the ability to be highly localized at the point of impact of the incident electron beam. By programming the electron beam along the sample, an image of the sample surface is formed. Based on the obtained image, the morphology of the sample surface is defined *(Goldstein, 2003; Reimer, 1998)*.

In addition to the emission of secondary electrons responsible for characterization of topography of the sample surface, other signals are generated between the incident radiation and the

sample. Namely, when the incident electron beam penetrates deeper into the sample, the reflection of the backscattered electrons occurs. The image of backscattered electrons is smaller compared to the image of secondary electrons because it originates from the deeper locations of the sample. These electrons are detected by a backscattered detector. Finally, X-rays occur when an incident electron beam removes one electron from the inner shell of a sample. Characteristic X-rays are detected by an appropriate detector and used for quantitative sample analysis (determination of the elemental composition of the sample). The signal of backscattered electrons is closely related to the atomic number of the sample. Therefore, the image of backscattered electrons is often used in combination with the spectra of X-rays. However, the backscattered electrons cannot provide information on the composition of the sample, but only on the distribution of components in the sample *(Goldstein, 2003; Reimer, 1998*).

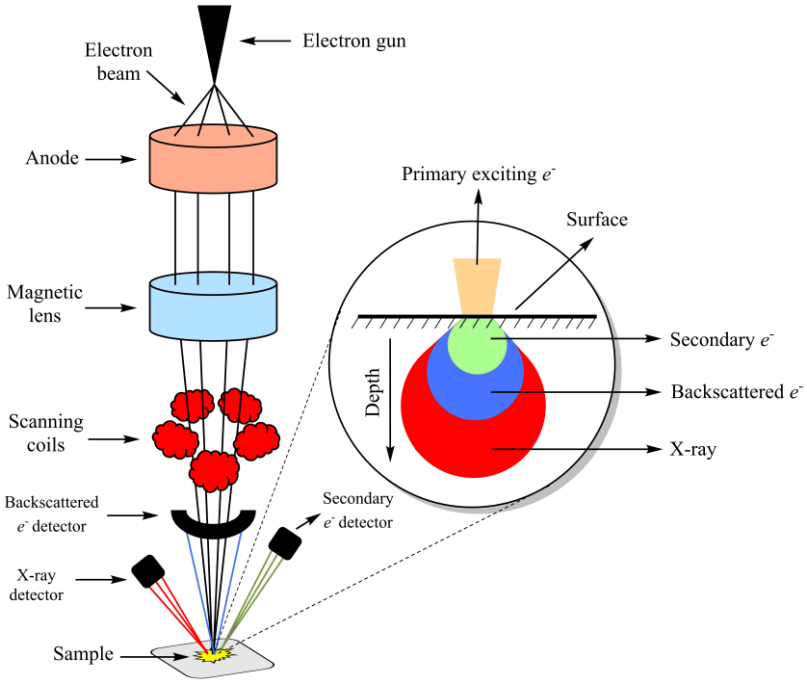

Figure 28. Schematic illustration of FE-SEM system. Obtained signals when the incident electron beam reaches the sample surface.

The FE-SEM technique enables the examination of the morphology of surfaces of a large number of samples, conductive as well as non-conductive, without prior preparation. For scientific purposes, today it is mainly used for detailed imaging of morphology of newly synthesized materials, as well as nanomaterials (mostly carbon/graphene). High-resolution imaging avoids damage to the beam of secondary electrons, which extends the application of this method to the analysis of sensitive materials with low beam energy. Also, elemental analysis of sample can be done thanks to X-ray mode. In addition, from the aspect of industry, this method is a significant application in metallurgy (characterization of inclusions), environmental/geology (examination of morphology and elemental composition of minerals and ores), polymer and ceramics industry (testing of surface porosity of ceramic and polymer products), as well as electronic industry (nanochip damage testing) *(Jiang et al., 2012; Lopes et al., 2019; Manekkathodi et al., 2010; Shao et al., 2007)*.

2.4.3. Method of standard addition

The standard addition method is one of the methods for quantification of analytes in the sample. This method is used when the influence of the matrix is dominant *ie.* when different components of the matrix significantly interact with the analyte and thus affect the final result of the analysis. Accordingly, the preparation of the standard series and sample is different. Namely, the analyzed sample is divided into several equal parts - subsample (for example 7). After that, an accurately known amount of corresponding standard is added to each subsample, increased at regular intervals, except in the first subsample. Eventually all subsamples are diluted to the same volume. In this case, the influence of the matrix is minimized, compared to the classical calibration method based on the use of standard solutions that may differ in composition from the sample itself. Finally, the instrument reads the appropriate magnitude (absorbance, intensity) in all subsamples, after which the calibration curve of the signal intensity *vs.* added amount of standard are constructed. Then, by extrapolating to the value *Y=0*, the value of the unknown concentration in the analyzed sample C_x is determined (Figure 29), *ie*. *Equation 5.* is applied (*a* and *b* - intercept and slope, respectively, obtained from the calibration curve) *(Miller, 1991)*.

$$C = {}^{a}/_{b} \qquad \textit{Equation 5.}$$

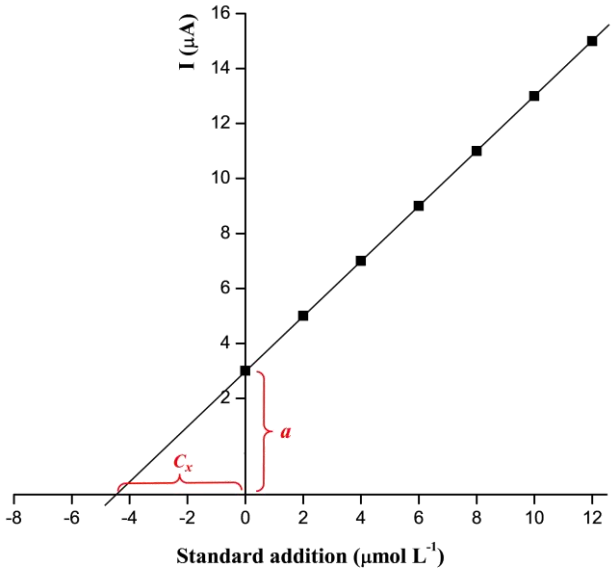

Figure 29. Plot of intensity (*I*) *vs.* addition (*C*) for standard addition method; *a* - intercept, C_x - concentration of analyte obtained by extrapolation.

2.5. Biosensors - general terms

A biosensor is defined as an analytical device that has a built-in biologically active component in close contact with a physico-chemical converter and an electronic signal processor. The biosensor consists of two components - a bioreceptor and a transducer. A bioreceptor is a biological molecule that recognizes the target analyte and specifically interacts with it. Enzymes, antibodies, membranes, organelles, cells or tissues can be used as biological components during biosensor preparation. The transducer converts the observed physical or chemical change into a measured signal. Transducers can be electrochemical, optical, piezoelectric, thermal or acoustic. Therefore, the classification of biosensors is mainly based on the nature of the biocomponent or the type of transducer. Biosensors can be applied to different types of samples such as food, beverages, cell cultures, clinical samples (blood serum and urine samples) as well as for the analysis of samples from the environment *(Bahadır & Sezgintürk, 2016; Cho et al., 2020; Krishnan et al., 2019; Pumera et al., 2010; Korotkaya, 2014)*. The structure of the general biosensor is given in *Figure 30*.

Electrochemical biosensors are a type of biosensor based on electrochemical transducers. The electrode is used as a solid support for immobilization of a biological species (enzyme, antibody or DNA). The biological species recognizes the target analyte (substrate), which can lead to an interaction or chemical reaction between the species and the analyte. Then, the resulting change is detected by the electrode, and the corresponding physico-chemical signal is converted into an electrochemical signal. The electrochemical signal can be expressed via current, voltage or impedance, so voltammetric/amperometric, potentiometric or electrochemical impedance spectroscopy (EIS) methods can be used to detect the analyzed species. Depending on the type and construction of the biosensor, the intensity of the generated signal is directly or inversely proportional to the analyte concentration *(Cho et al., 2020)*. Electrochemical biosensors can be classified into three categories *(Krishnan et al., 2019; Castrovilli et al., 2019; delle Noci et al., 2008)*:

- ✓ first generation - the electroactivity of the enzyme product,
- ✓ second generation - application of redox mediators (small electrochemical compounds that have the role of accelerating electron conduction in the electrochemical cell. Mediators act as an electron shuttle between enzyme active center and the electrode surface) *(Francke & Little, 2014; Mani et al., 2018)*,
- ✓ third generation - the DET between the active site of the enzyme and the electrode surface.

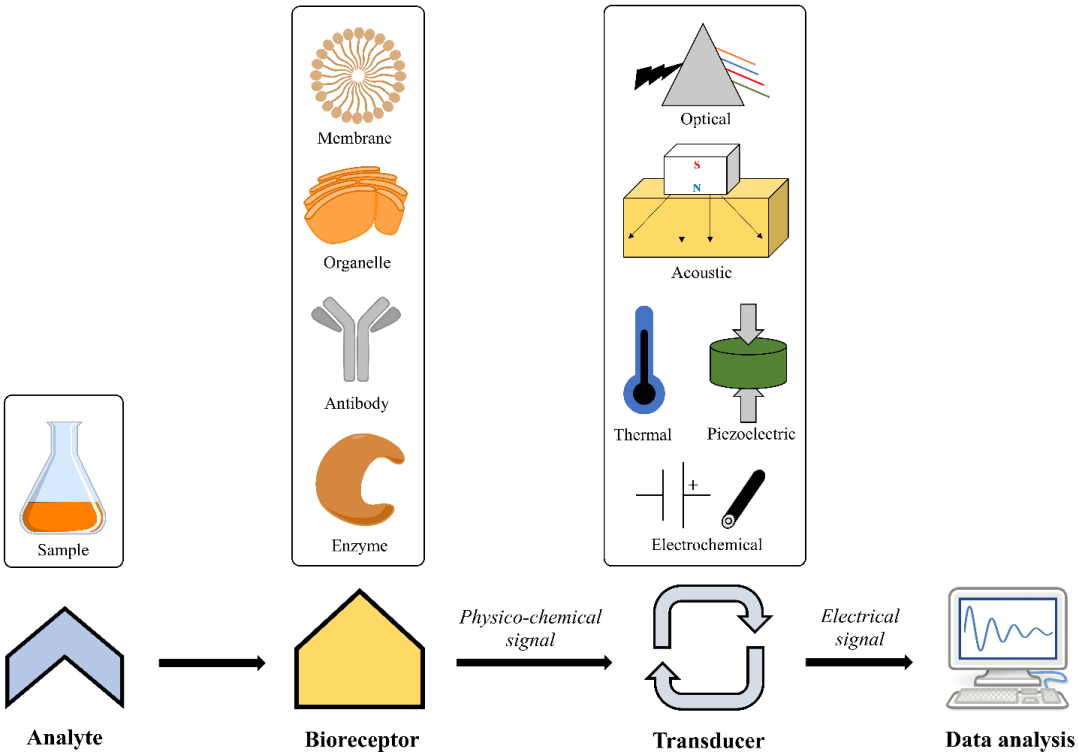

Figure 30. Typical components of a biosensor.

The most commonly used biological components are enzymes. They can be used in pure form or can be applied without prior isolation from microorganisms or plant material. Oxidoreductases, transferases, hydrolases, lyases, isomerases are classes of enzymes that can be used in the production of enzyme biosensors. The advantages of the enzyme are reflected in high selectivity, easy binding to the substrate, high catalytic activity and rapid activation. On the other hand, enzymes may lose their activity during immobilization, so special attention must be paid to this step during biosensor production. In addition, although immobilization is successful, biosensor activity may be lost after a relatively short period of analysis *(Gerard, 2002; Korotkaya, 2014; Sassolas et al., 2012)*.

Immobilization of the species, *ie*. modification of the electrode with the appropriate biological species, is a key step during the production of electrochemical biosensors. The activity of immobilized molecules depends on the size of the contact surface, porosity, hydrophilic character of the immobilization matrix, reaction conditions, but also on the immobilization method itself. Biological species immobilization can be based on covalent (chemical), non-covalent (interactions), adsorption, cross-linking, bioaffinity or capture strategies *(Bahadır & Sezgintürk, 2016; Castrovilli et al., 2019; Homaei et al., 2013; Sassolas et al., 2012)*. Chemical strategy involves a chemical reaction between an electrode and a biological species. Preparation of electrochemical immunosensor is one of the examples of chemical modification of electrodes with biological species *(Chen et al., 2013a; Stanković et al., 2020b)*. Immunosensors are analytical devices used to detect the binding between antibody and antigen with formation of a stable complex. For example, in order to construct an immunosensor for the detection of antigen such as human serum albumin (HSA), it is necessary to modify (immobilize) the electrode surface with a biological species that is selective for that analyte - anti-HSA (antibody). Electrode modification with anti-HSA is based on establishing an amide bond (covalent bond) between the antibody and the carboxyl group (COOH) from the electrode. This requires the presence of COOH on the electrode surface. For this purpose, standard electrochemical sensors are pre-modified with carboxylated composites. Carboxylated graphene composites decorated with metal or M_xO_y nanoparticles have been shown to be a very good support for antibody immobilization, while later providing high sensitivity and selectivity *(Chen et al., 2013a; Stanković et al., 2020b)*. COOH group

on the electrode surface is activated with 1-ethyl-3-(3-dimethylamino- propyl) carbodiimide hydrochloride (EDS) and N-hydroxysulfosuccinimide sodium salt (NHS), followed by the establishment of an amide bond with the antibody (Figure 31). In this way, the antibody is chemically immobilized on the electrode surface.

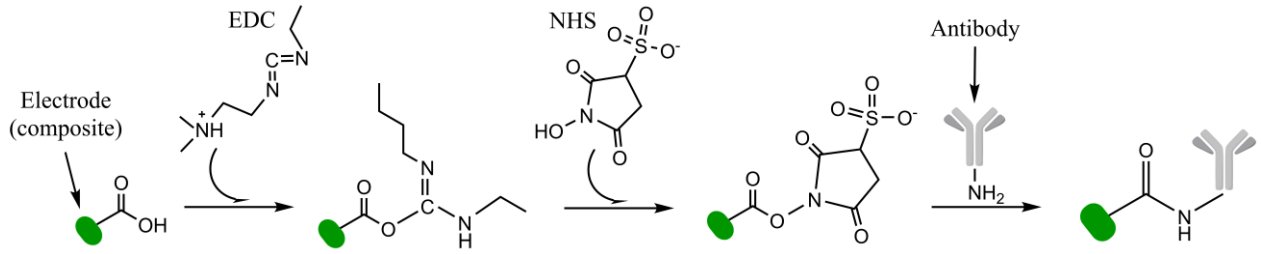

Figure 31. Chemical immobilization of antibody on the electrode surface. Establishing an amide bond (covalent bond) between COOH from the electrode surface and the NH_2 group from the antibody.

During the preparation of an enzyme electrochemical biosensor, the enzyme is most often immobilized using a non-covalent strategy. This immobilization method is performed in order to save the native structure of the enzyme and its full activity, which directly affects the sensitivity of the developed biosensor. Non-covalent binding involves the immobilization of enzymes by non-covalent interactions such as hydrogen bonding, van der Waals forces, coordination bands or electrostatic interactions. The "*drop coating*" technique is one of the methods of non-covalent enzyme immobilization *(Prashanth et al., 2012; Stanković et al., 2020b; Vukojević et al., 2018a; Vukojević et al., 2018b)*. It is based on the application of a certain amount of enzyme solution to the electrode surface (Figure 32). During drying, the enzyme binds by noncovalent interactions to the electrode surface. Since non-covalent interactions are weak, very often enzyme is flushed from the electrode surface during the electrochemical measurements. Therefore, after drying the enzyme, a certain amount of diluted Nafion solution is applied to the electrode surface by the same technique (Figure 32). This polymer covers the enzyme and does not allow washing during the experiment *(Vukojević et al., 2018a; Vukojević et al., 2018b)*. Also, Nafion does not disrupt the native structure of the enzyme. After drying of Nafion, the prepared biosensor is ready for analysis.

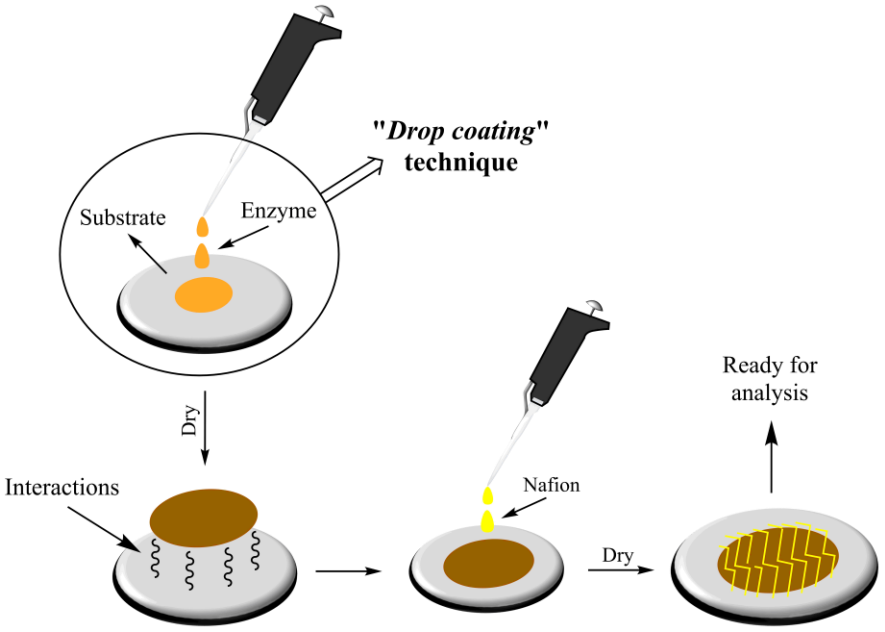

Figure 32. Schematic illustration of "*drop coating*" technique.

In this doctoral dissertation, depending on the preparation of the glucose or polyphenolic index biosensor, the "*drop coating*" technique is used for the modification of the SPCE with a corresponding nanocomposite, as well as for the immobilization of the appropriate enzyme on the surface of the nanocomposite.

2.5.1. Glucose oxidase. Glucose biosensors

Glucose oxidase (GO_x) belongs to the enzyme class of oxido-reductases. This enzyme catalyzes the oxidation of glucose, via oxygen, to the corresponding lactone and hydrogen-peroxide (*Reaction 2.*). GO_x belongs to the group of flavoproteins, which means that the presence of coenzyme flavin adenine dinucleotide (FAD^+) is required for the manifestation of activity. GO_x consists of two subunits and the molecular weight of each is $8*10^4$ Da. FAD^+ is bound by noncovalent interactions to the active site of each subunit and plays the role of a redox carrier in redox reactions (*Ferri et al. 2011; Leskovac et al., 2005*).

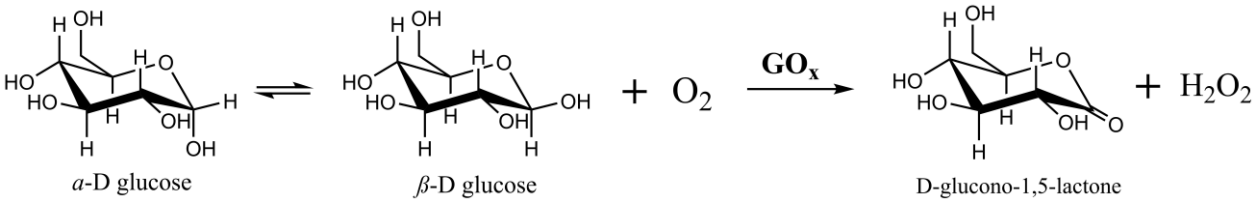

Reaction 2. Oxidation of glucose by GO_x.

GO_x can be isolated from fungi, bacteria or yeast. The largest source of GO_x is fungus *Aspergillus niger*. GO_x obtained from this fungus shows the highest activity as well as the highest selectivity toward glucose. In contrast, GO_x isolated from bacteria and yeast is not completely

selective for glucose and oxidizes other sugars such as maltose. GO_x shows its greatest activity at neutral or slightly basic medium, while it can most often be inhibited by a large amount of lactone or H_2O_2 (feedback inhibition) *(Ferri et al. 2011; Leskovac et al., 2005)*.

Since diabetes has become one of the most common diseases in the world, the goal has been to develop a rapid, selective and sensitive method for detecting glucose in blood and monitoring the clinical picture of diabetes. Electrochemical methods have been used for this purpose. The first glucose biosensor was developed in 1962 by Clark and Lyons *(Clark & Lyons, 1962)*. The biosensor was based on an oxygen electrode, and GO_x was immobilized on the electrode surface using a semipermeable dialysis membrane. This was a pure example of a first-generation biosensor and glucose concentration in blood was monitored through a decrease in oxygen concentration.

As mentioned, electrochemical glucose biosensors can be classified into three categories – first, second and third generation (Figure 33). First generation of glucose biosensors is based on indirect measurement of glucose concentration. Namely, as observed from *Reaction 2.*, GO_x oxidizes glucose to corresponding lactone. The released electron accepts coenzyme FAD^+ and transforms into its reduced form $FADH_2$. In order to regenerate the coenzyme, $FADH_2$ is oxidized and the released two electrons are converted to O_2 from the water (environment), and then the O_2 is reduced to H_2O_2. The formed H_2O_2 is oxidized on the electrode surface to the water, and only then the signal is recorded (Figure 33a). The amount of generated H_2O_2 is directly proportional to the amount of glucose (Reaction 2). This method of measuring glucose concentration is extremely convenient, because measuring H_2O_2 is simple, especially if miniaturized devices are used. On the other hand, amperometric determination of H_2O_2 using standard electrochemical sensors requires determination at high potential, which opens the possibility of oxidation of other compounds. Since glucose is most often determined in the blood, ascorbic acid and uric acid, as accompanying components of the blood, are very often oxidized together with H_2O_2. This significantly reduces the selectivity of first-generation glucose biosensors *(Krishnan et al., 2019; Wang, 2008)*.

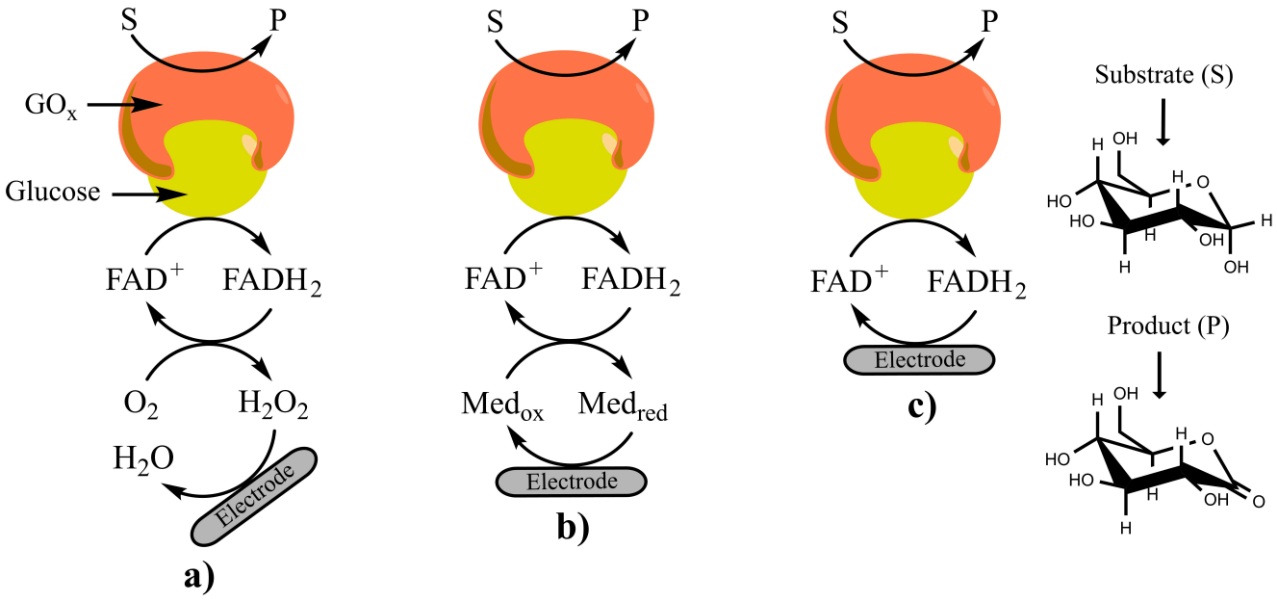

Figure 33. Schematic illustration of three level of electrochemical glucose biosensors; ***a)*** First generation is based on the application of oxygen cofactor; ***b)*** second generation on the application of artificial mediator; ***c)*** third generation is based on DET between active site of enzyme (FAD^+) and electrode surface.

The second generation of glucose biosensors is based on the replacement of O_2 with a synthetic electron acceptor. Such acceptors are called redox mediators. The role of the redox mediator

is reflected in facilitating electron transfer between the FAD^+ in the enzyme and the electrode surface. This type of transfer is called *mediated electron transfer* (MET). As before, GO_x oxidizes glucose to the lactone, and the redox mediator accepts the electron and goes into a reduced state. In order to regenerate, the mediator is oxidized on the electrode and an amperometric signal is recorded (Figure 33b). The signal intensity is directly proportional to the glucose concentration. *(Krishnan et al., 2019; Wang, 2008)*. Ferrocene-monocarboxylic acid (FCMA), 1,1-ferrocene-dicarboxylic acid (FCDA), ferrocene-carboxaldehyde (FCCA) are some examples of commercial redox mediators used to interfere between enzyme active site and the electrode surface *(delle Noci et al., 2008; Tan et al., 2009)*.

The third generation of glucose biosensors is based on DET between FAD^+ in the active center of enzyme and the electrode surface (Figure 33c). The absence of mediators ensures the operation of the system at lower potentials, which significantly increases the selectivity of biosensors. Accordingly, an electrode surface should be developed that ensures that $FADH_2$ is directly regenerated on it. For this purpose, various nanostructured materials for the production of glucose biosensors have been employed (CNT, SWCNT). Due to its unique properties, graphene stood out in particular. Graphene significantly increased the DET between the active center of GO_x and the electrode surface, which directly affected the sensitivity of the biosensor. In addition, graphene has proven to be an excellent material for enzyme immobilization, without disturbing the native structure of the enzyme *(Krishnan et al., 2019; Wang, 2008)*. *Table 2.* provides a literature review of electrochemical enzymatic graphene-based glucose biosensors.

2.5.2. Polyphenols. Polyphenolic index

Polyphenols are considered to be one of the most dominant antioxidants in nature. These compounds are synthesized as secondary metabolites in important biochemical processes in plants. Their role is reflected in the removal of free radicals formed in the oxidative processes of the organism, as well as in the inhibition of oxidation of lipoproteins and enzymes. Polyphenolic antioxidant activity has an impact on the prevention of certain human diseases such as diabetes, stroke and cancer. In addition to pronounced antioxidant activity, these compounds show antibacterial, antiviral and anti-inflammatory activities *(Di Fusco et al., 2010; Gil & Rebelo, 2010; Jakobek, 2015; Lorrain et al., 2013)*. Food such as fruits (oranges, lemons, grapes, apples, black currants), vegetables (onions, tomatoes, cabbage) and spices (sage, rosemary), as well as beverages (tea, juice, coffee, wine) are significant sources of polyphenols *(Bordonaba & Terry, 2012; (Chawla et al., 2012b); Cieślik et al., 2006; Georgé et al., 2005; Li et al., 2017; Scalbert & Williamson, 2000)*. When it comes to polyphenolic content, wines represent the most frequently tested real sample due to the high content of soluble polyphenols (~3000 mg L^{-1} in red wines and ~100 mg L^{-1} in white wines), as well as high absorption ratio and bioavailability *(Arribas et al., 2013; Brenna & Pagliarini, 2001; García-Guzmán et al., 2015; Lino et al., 2014; Makhotkina & Kilmartin, 2010; Šeruga et al., 2011; Viñas et al., 2009; Chawla et al., 2012a)*. Consumption of polyphenol-rich food and beverages contributes to a daily average polyphenol intake of 1 g, for the average consumer (body weight of 70 kg) *(Scalbert & Williamson, 2000).*

Gallic acid, caffeic acid, catechol, *p*-coumaric acid, catechin, guaiacol, pyrogallol, ferulic acid can be used as standards (model compound) for the determination of polyphenolic content. The structural formulas of the most frequently used model compounds are given in *Figure 34*. Depending on the standard, the polyphenolic content is expressed as *mg* of the standard equivalents per *L* or *g* of analyzed sample *(Chawla et al., 2012b; Di Fusco et al., 2010; Gil & Rebelo, 2010; Roy et al., 2005; Arribas et al., 2013; Chawla et al., 2012b; Chawla et al., 2012a)*.

The *Folin-Ciocalteu* method is the reference method for determination of total phenolic content (TPC) *(Arribas et al., 2013)*. This spectrophotometric method is based on mixing the analyzed sample with *Folin-Ciocalteu* reagent (phosphomolybdate and phosphotungstate). Then, Na_2CO_3

(7.5%) was added to the resulting mixture, and after 2 hours absorbance was measured at 765 nm. Gallic acid is used as model compound in this method. *(Arribas et al., 2013; Vasić et al., 2019)*. In addition to this widely used method, analytical methods such as high-performance liquid chromatography, gas chromatography or capillary electrophoresis (with ultra violet or mass detection) are used to determine the polyphenolic content as well as the separation of different polyphenolic compounds (species). However, although these methods provide high sensitivity and selectivity during determination, they require expensive equipment, long sample preparation, as well as trained personnel *(Chawla et al., 2012b; Di Fusco et al., 2010)*.

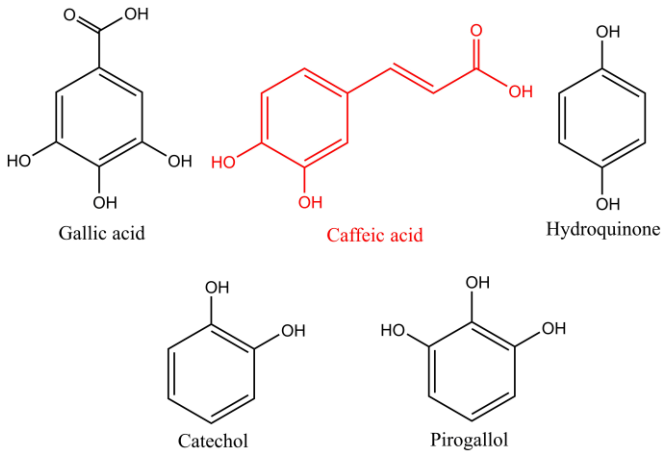

Figure 34. Structural formulas of model compound for the determination of polyphenolic content.

As already mentioned, electrochemical methods allow simpler sample preparation and equipment, while providing high sensitivity. Therefore, electrochemical sensors (GCE, BDD, CPE) in combination with voltammetric/amperometric methods have found wide application in the determination of polyphenolic content in various real samples. A sensor such as the GCE stood out in particular. According to the literature data, the GCE was significantly used to determine the polyphenolic composition *(Brasanac-Vukanovic et al., 2018; Đorđević et al., 2017; Kilmartin et al., 2001; Petković et al., 2015; Šeruga et al., 2011; Vasić et al., 2019)*. Therefore, GCE is considered the standard for electrochemical determination of polyphenolic composition. On the other hand, GCE shows a tendency to adsorb polyphenolic compounds onto the electrode surface, which significantly affects the LOD of electroanalytical methods. Therefore, there is a constant need to develop new electrochemical systems and new sensors/biosensors, in order to improve the sensitivity and selectivity of developed electrochemical methods.

The polyphenolic content determined by the electrochemical method using a specific electrochemical sensor is expressed as the electrochemical polyphenolic index (EPI). In addition, electrochemical determination of polyphenols can be performed with electrochemical biosensors. In that case, the polyphenolic content is expressed as the bioelectrochemical polyphenolic index (BPI). The already mentioned compound model can be used as standards for developing electrochemical/bioelectrochemical quantification methods. As in the case of TPC, EPI and BPI is expressed as *mg* of standard per *L* or *g* of sample.

In this doctoral dissertation, caffeic acid was used as a model compound in developing a method for quantification of polyphenols in real samples with a produce polyphenolic index biosensor. The proposed amperometric method was validated with a GCE, determining the polyphenolic content in the same samples under the same experimental and instrumental conditions.

2.5.2.1. Laccase. Polyphenolic biosensors

The enzymes tyrosinase, peroxidase and laccase can be used to prepare electrochemical polyphenolic biosensors. Although tyrosinase and peroxidase have been used to determine polyphenolic content, they have shown some disadvantages. Namely, tyrosinase is characterized by low stability and the possibility of inhibition with reaction products, while peroxidase activity requires the cofactor H_2O_2. On the other hand, laccase has been shown to be a suitable enzyme for the production of electrochemical polyphenolic biosensors. This enzyme shows high stability during amperometric determinations, and does not require the presence of co-substrate or any cofactors to exhibit its activity *(Gamella et al., 2006; Rawal et al., 2011; Fernandes & Rebelo, 2009; Rodríguez-Delgado et al., 2015)*.

Like GO_x, laccase belongs to the group of oxidoreductases. By structure, laccase is a glycoprotein. Most isolated laccases consist of a mono subunit, but this enzyme can also occur in multimeric structures. The molecular mass of mono subunits ranges from 60 to 70 kDa, while the masses of multimeric forms, depending on the number of subunits, can be from 50 to 140 kDa. Laccase can be extracted mainly from mushrooms (*Trametes versicolor*, *Trametes hirsuta*, *Agaricus bisporus*), but can also be found in higher plants, prokaryotes and bacteria *(Riva, 2006; Rodríguez-Delgado et al., 2015; Arregui et al., 2019)*.

Laccase catalyzes the one-electron oxidation of aromatics phenols/polyphenols and aniline, with simultaneous reduction of oxygen to water (*Reaction 3.*). Laccase belongs to the group of so-called *blue-copper family of oxidases* because it contains four copper ions in the active site. The copper cluster in the active site consists of three types of Cu (Figure 35). Type 1 (Cu^{I}) is responsible for the oxidation of the substrate, while type 2 (Cu^{II}) and type 3 (Cu^{III}) form a three-nuclear cluster where oxygen is reduced to water *(Riva, 2006; Roy et al., 2005)*.

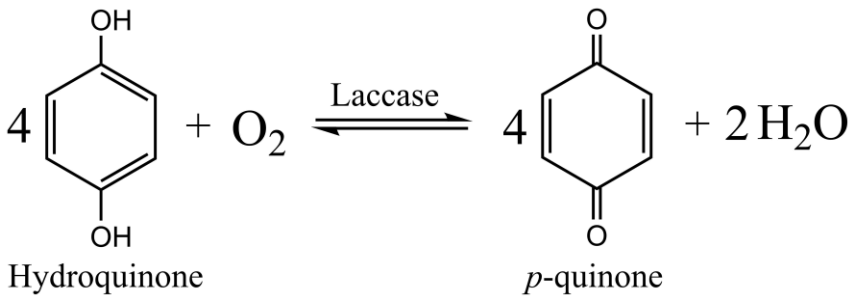

Reaction 3. Oxidation of phenols by laccase.

Laccase is a widely used enzyme. It is used in the food, pulp, paper, textile, dye, medicine and cosmetics industries. Also, laccase has found application in wastewater treatment, oxidation of organic pollutants and environmental bioremediation. The application of laccase in electrochemistry is particularly pronounced. Namely, this enzyme has found application in electrocatalytic reduction of oxygen, as well as in the preparation of micro-fuel cells as a cathode for oxygen reduction. Laccase has found a special application in the production of biosensors for the detection of polyphenolic content in various real samples *(Roy et al., 2005; Arregui et al., 2019; Tan et al., 2009; Rodríguez-Delgado et al., 2015; García-Guzmán et al., 2015; Chawla et al., 2012b; Gupta et al., 2003)*.

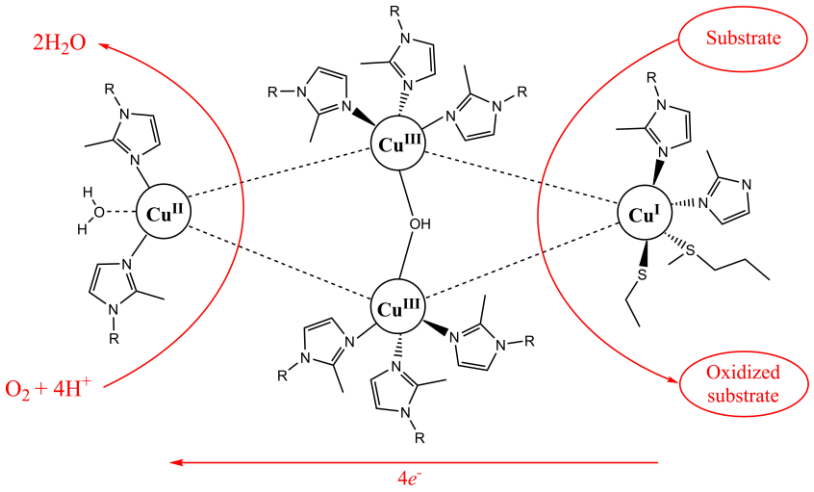

Figure 35. Schematic illustration of laccase active site. Simplified oxidation mechanism of substrate by laccase.

As mentioned, electrochemical biosensors can be categorized into three generations. The basic principles of each generation of polyphenolic biosensors are explained on the example of a laccase-based biosensor. HQ was used as model compound.

The first generation of polyphenolic biosensor is based on the indirect measurement of HQ. Namely, laccase oxidizes HQ to the corresponding *p*-quinone, while Cu^{2+} in the active site accepts electrons and is reduced to Cu^{+}. Then, Cu^{+} is oxidized to Cu^{2+}, while oxygen from the medium is reduced to water. In this way, the active site of the enzyme is regenerated. Finally, the resulting *p*-quinone is reduced at the electrode surface, recording the current signal (Figure 36a). The amount of obtained *p*-quinone is directly proportional to the amount of HQ. In this generation, a series of electrochemical polyphenolic biosensors was developed for the determination of EPI or antioxidant activity in various real samples *(Gil & Rebelo, 2010; Roy et al., 2005; Fernandes & Rebelo, 2009; Šeruga et al., 2011; Vasić et al., 2019; Lugonja et al., 2014)*.

In the second generation of polyphenolic biosensors, laccase, as in the previous case, oxidize HQ to *p*-quinone and Cu^{2+} is reduced to Cu^{+}, while during oxidation of Cu^{+} to Cu^{2+} the released electrons are taken over by an artificial redox mediator. Then, the mediator is reduced to the electrodes, recording the signal (Figure 36b). The current signal is proportional to the amount of HQ. The first mediator used in laccase-based biosensors was ABTS (2,2'-azino-bis (3-ethylbenzothiazoline-6-sulfonic acid)) *(Riva, 2006; Odaci et al., 2006)*. Although the use of mediators generally requires operation at high potential, this generation of biosensors has been significantly applied to the determination of polyphenolic content and pharmaceuticals in real samples *(Tan et al., 2009; Mousty et al., 2007; Odaci et al., 2006; Diaconu et al., 2010; Rodríguez-Delgado et al., 2015)*.

Laccase has proven to be an ideal enzyme in the construction of third-generation polyphenolic biosensors. Namely, in addition to the above advantages, the authors state that this enzyme has capabilities of DET between the active site and the electrode surface (Figure 36c), allowing the construction of electrodes without mediators *(Castrovilli et al., 2019; Favero et al., 2015; Gutierrez-Sanchez et al., 2015; Hou et al., 2016)*. This allows a cheaper design of the biosensor, as well as the possibility of operating the biosensor at potentials closer to the potential of the substrate. As mentioned with the glucose biosensor, the third generation of biosensors is based on the application of graphene materials. Also, graphene materials decorated with metal nanoparticles and nanostructured oxides of transition metals replace redox mediators and provide DET, which directly increases the sensitivity and selectivity of biosensors. Therefore, special attention has been paid to these materials in the last few years and many combinations of graphene materials and nanoparticles

have been made in order to improve the electrochemical properties of polyphenolic biosensor *(Castrovilli et al., 2019; Della Pelle & Compagnone, 2018; Favero et al., 2015; Hou et al., 2016; Palanisamy et al., 2017)*. *Table 2.* provides an overview of the literature related to the application of graphene nanomaterials and M_xO_y nanoparticles, as well as their combinations, in the production of enzymatic polyphenolic biosensors.

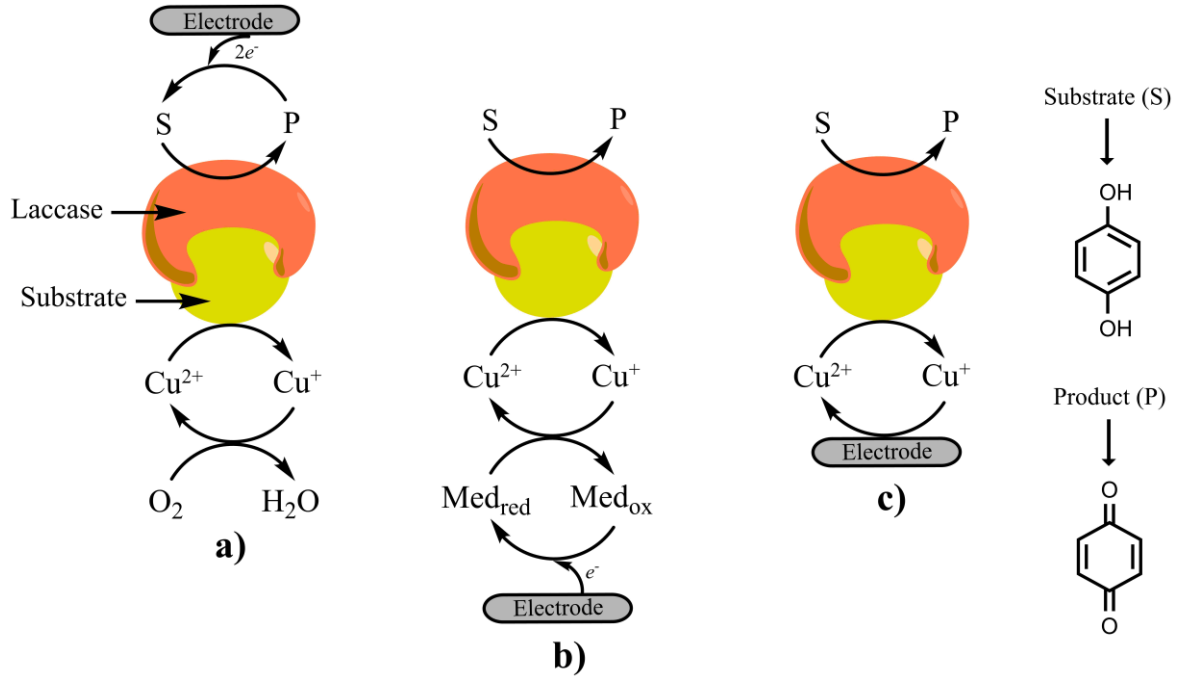

Figure 36. Three generations of polyphenolic biosensors. ***a)*** first - based on electroactivity of reaction product; ***b)*** second - based on reduction of redox mediator at electrode surface; ***c)*** third - DET between laccase active site (Cu^{2+}) and electrode surface.

2.6. Subject and goals of research

The subject of research of this doctoral dissertation was the development of new amperometric biosensors for the detection of glucose and polyphenols in real samples. The new glucose and polyphenolic index biosensors were based on graphene nanomaterials (GNR, GNP) decorated with M_xO_y nanoparticles (Bi_2O_3, MnO_2) in order to improve the electroanalytical parameters during the development of appropriate amperometric methods. Also, within this dissertation, the possibilities of application of the developed biosensors in food samples were investigated.

The object of this doctoral dissertation included the synthesis of the mentioned graphene@M_xO_y nanocomposites, as well as their characterization using XRPD and FE-SEM methods. After confirming the crystal structure of the nanocomposites, the goal was to modify the SPCE with appropriate nanocomposites, which was followed by electrochemical characterization of the obtained WEs by cyclic voltammetry. After the construction of the biosensors, the aim was to develop an electroanalytical method for quantification of glucose and polyphenols using the hydrodynamic chronoamperometry method and to define electroanalytical parameters such as linear concentration range, LOQ, LOD, reproducibility, repeatability, accuracy and precision. Finally, the application of developed glucose biosensor in honey samples and polyphenolic index biosensor in wine samples, as well as the validation of the proposed methods, was the main point of this doctoral dissertation.

Finally, the glucose biosensor was based on the modification of SPCE with GNR@Bi_2O_3, followed by GO_x immobilization. On the other hand, SPCE was modified with GNP@MnO_2 nanocomposite, and then laccase immobilization was performed in order to construct a polyphenolic index biosensor.

3. Experimental part

3.1. Materials, reagents, chemicals and solutions

All chemicals used in these studies were of analytical grade. All aqueous solutions were prepared with ultra-pure water (*Millipore Simplicity 185 System*). $K_3[Fe(CN)_6]$ and $K_4[Fe(CN)_6]$, used for investigation of system reversibility and characterization of synthetized nanocomposite, were supplied by Merck (Germany). DMF, used for the preparation of nanocomposite suspensions, was supplied by Alfa Aesar (Germany).

Carbon ink (No. C50905DI) and ceramic supports (thickness 100 mm, electrode printing area 105 mm^2, No. CLS 641000396R), used for preparation of SPCEs, were supplied by Gwent (Pontypool, UK) and Coors Ceramics GmbH (Chattanooga, TN, USA), respectively. Ag nanoparticle conductive ink (<150 nm particle size (DLS), 20 wt. % dispersion in organic solvents), used to improve the contact between the electrode and the instrument, was supplied by Sigma Aldrich (USA).

"*Zig-zag*" GNR and GNP were supplied by Merck (Germany) and ACS Material (Pasadena, California), respectively. Specification of graphene nanomaterials are given in *Table 3.* Further in the text, "*zig-zag*" GNR will be marked as GNR.

Table 3. Specification of graphene nanomaterials used for preparation of glucose and polyphenolic index biosensors.

Graphene nanomaterials	Specification	Surface area (m^2/g)
GNR "*zig-zag*"	length: 2-15 μm width: 40-250 nm	48-58
GNP	thickness: 2-10 nm diameter: 2-7 μm	20-40

For preparation of Bi_2O_3 nanoparticles were used $Bi(NO_3)_3$, polyethylene glycol, PEG-1500 (used as a dispersant), HNO_3 and NaOH, while for preparation of MnO_2 nanoparticles were used $Mn(NO_3)_2*4H_2O$ and $KMnO_4$. All noted substances were supplied by Merck (Germany).

H_2O_2 (8.8 mol L^{-1}) and glucose monohydrate are used for optimization of working parameters and examination of electrochemical performances of glucose biosensor, respectively. Caffeic acid was used as model analyte during the investigation of electrochemical characteristics of polyphenolic index biosensor. Also, these chemicals were supplied by Merck (Germany).

Enzyme GO_x from *Aspergillus niger* (Type X-S, lyophilized powder, 100.000-250.000 units/g solid, without added oxygen) was used for preparation of glucose biosensor, while fungal laccase enzyme from *Trametes Versicolor* (TvL) (benzenediol: oxygen-oxidoreductase EC1.10.3.2, activity provided on the bottle >10 U/mg) was used for construction of polyphenolic index biosensor. Both enzymes were supplied by Sigma Aldrich (USA) and storied at -18°C. Enzymes solutions were prepared by dissolving of 100 mg of corresponding enzyme in 10 mL of 0.1 mol L^{-1} phosphate buffer solution (pH=7.40). Final concentrations of GO_x and TvL solution were 10 mg/L. Enzyme solutions were stored in the refrigerator at 4°C.

Nafion solution (tetrafluoroethylene-perfluoro-3,6-dioxa-4-methyl-7-octenesulfonic acid copolymer) was supplied by Merck (Germany). A 5% solution of Nafion (Naf) in ethanol was used in the final step of biosensor production.

As supporting electrolytes in these studies were used 0.1 mol L^{-1} phosphate buffer solution (PBS), 0.1 mol L^{-1} acetate buffer solution (ABS) and 0.1 mol L^{-1} Britton-Robinson buffer solution

(BRBS). Na_2HPO_4 and NaH_2PO_4 were used for preparation of PBS, while CH_3COONa and glacial CH_3COOH (17 mol L^{-1}) used to prepared the 0.1 mol L^{-1} ABS. BRBS (1 L) was prepared by dissolving 2.80 mL of H_3PO_4 (16 mol L^{-1}), 2.40 mL of CH_3COOH (17 mol L^{-1}) and 2.48 g of H_3BO_3. All these substances were supplied by Alfa Aeser (Germany).

Honey sample (*PT* scheme with declared glucose content of 32.6 %) was obtained from colleagues from the Department of Analytical Chemistry (Faculty of Chemistry, University of Belgrade). Wine samples were purchased at a nearby market.

3.2. Instrumentation

3.2.1. Characterization of nanocomposites crystal structures

The crystallographic structure of graphene nanomaterials (GNR and GNP) and nanoparticles (Bi_2O_3 and MnO_2), as well as corresponding nanocomposites (GNR@Bi_2O_3 and GNP@MnO_2) were identified by XRPD method. XRPD analysis were performed on high-resolution Smart Lab® X-ray diffractometer (Rigaku, Japan), based on *Cu Kα* radiation (λ=1.542 Å). Samples were prepared by flattening dried powders with a zero-background silicon wafer. In the case of GNR, Bi_2O_3 and GNR@Bi_2O_3 samples, the diffraction data were collected in the 2θ range from 20° to 50° in steps on 0.04°/min, with divergent slit of 0.5 mm, operated at accelerating voltage of 40 kV and current of 30 mA. The diffraction patterns of GNP, MnO_2, GNP@MnO_2 samples were collected within 2θ range of 10-70° in a scan rate of 0.02° with the exposition of 2 sec/step, operated at 40 kV and 30 mA, too. The size of the nanocrystals of the analyzed samples was determined by applying the *Scherrer*'s equation (*Equation 4.*).

Morphology of the all nanocomposites was determined by FE-SEM method. FE-SEM analysis were performed at FE-SEM MIRA3 microscope (Tescan, Czech Republic), coupled with EDS analyzer (Oxford, UK). The all nanocomposite samples were prepared by dispersing the corresponding powder in water. Then, diluted dispersions were dropped on a carbon-coated copper grid and left to dry at room temperature for FE-SEM observations. *Image J* software was used for manually analysis of micrographs. The largest internal dimension of 100 nanoparticles were measured in the order to evaluated the mean particle size and distribution. Obtained data were fitted to a log-normal function *(Ognjanović et al., 2020; Stanković et al., 2020a)*. According to the log-normal function, mean diameter size of all samples and index of polydispersity (PdI) were obtained.

3.2.2. Electrochemical measurements

The cyclic voltammetry and chronoamperometry measurements, in the case of glucose biosensor, were performed at potentiostat/galvanostat *Autolab PGSTAT 302 N* (MetrohmAutolab B.V., The Netherlands). The internal system of this instrument was controlled by *Nova 2.0* software. All electrochemical measurements, in the case of polyphenolic index biosensor, were carried out at *PalmSens 3* (PalmSens BV, The Netherlands), controlled by *PST Trace 5* software. Real look of these instruments is given at *Figure 37*.

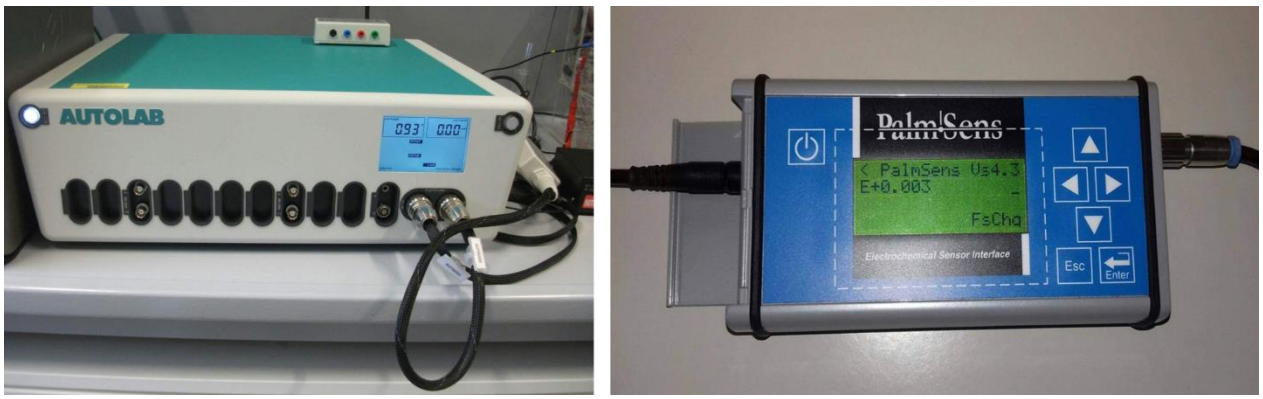

Figure 37. Real look of potentiostat/galvanostat *Autolab PGSTAT 302 N* (left) and *PalmSens 3* (right).

Conventional three electrode cell (total volume of 25 mL) were used in these studies. As RE and CE were used silver/silver chloride electrode (Ag/AgCl/in 3 mol L^{-1} KCl) and platinum wire (diameter 0.5 mm), respectively. As WEs were used SPCEs. Depending on the research objective, the experimental step and the applied method, the WEs were replaced. The following is a list of all WEs used in these studies:

For glucose biosensor

- ✓ unmodified SPCE
- ✓ SPCE modified with GNR
- ✓ SPCE modified with Bi_2O_3
- ✓ SPCE modified with GNR@Bi_2O_3
- ✓ biosensor

For polyphenolic index biosensor

- ✓ unmodified SPCE
- ✓ SPCE modified with GNP
- ✓ SPCE modified with MnO_2
- ✓ SPCE modified with GNP@MnO_2
- ✓ biosensor

The adjustment of pH value of supporting electrolytes was performed with 0.1 mol L^{-1} NaOH and a pH meter (Orion 1230) equipped with a combined glass electrode (Orion 9165BNWP) was used.

3.3. Preparation procedures

3.3.1. Preparation of SPCEs

SPCEs were prepared using a ceramic support and carbon ink. The electrode template was pre-engraved on the ceramic supports. Carbon ink was applied on ceramic support and ink was evenly distributed using manual screen-printed device. Ceramic supports with a thin layer of carbon ink were allowed to dry for 24 hours at room temperature (Figure 38).

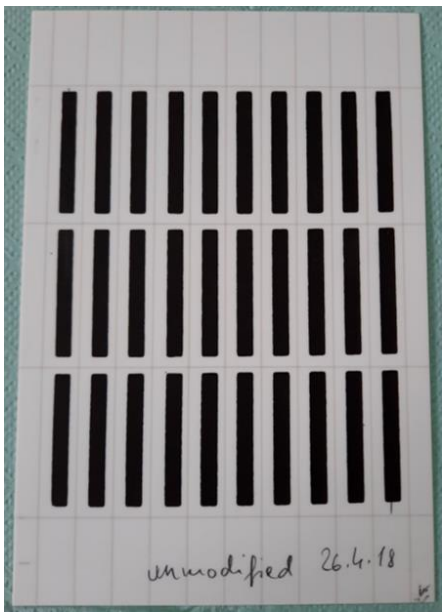

Figure 38. Real look of SPCEs after "*screen-printing*" process.

The dried SPCEs were coated with nail polish, providing the same active surface of carbon ink on each electrode (0.5 cm x 0.5 cm). Then, the tip of each SPCEs was coated with an Ag nanoparticle conductive ink in order to improve contact between the electrode and the instrument. After drying the Ag ink, the SPCEs were modified. Depending on the preparation of the glucose or polyphenolic index biosensor, the active area of SPCEs were modified with corresponding nanocomposite and/or enzyme by a "*drop coating*" technique (Figure 39), depending on the study objective, the experimental step and applied method. Also, this technique was used for the immobilization of the appropriate enzyme on the surface of the corresponding nanocomposite.

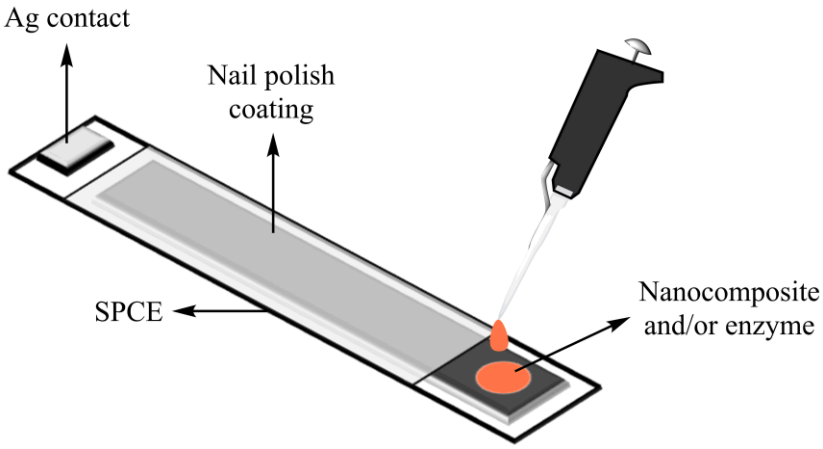

Figure 39. Schematic diagram of SPCE ready for electrochemical application. SPCE modification by "*drop coating*" technique.

3.3.2. Procedures for glucose biosensor

3.3.2.1. Preparation of Bi_2O_3 nanoparticles

Bi_2O_3 nanoparticles were prepared following a synthetized procedure from the literature *(Periasamy et al., 2011)*. The first step involved the preparation of 30 mL of an aqueous solution of $Bi(NO_3)_3$ at a concentration of 1.67 mol L^{-1}. Then, 108 µL of HNO_3 (14 mol L^{-1}) and 20 mL of polyethylene glycol (PEG-1500) were added to the Bi^{3+} solution. In the second step, 50 mL of 4 mol L^{-1} NaOH was added to this solution with constant stirring. Addition of base immediately causes the formation of a yellowish precipitate. Thereafter, the whole reaction mixture was heated to 90°C for 2 hours. After cooling, the mixture was centrifuged and the precipitate was washed three times with ultra-pure water and three times with ethanol. In the third step, the yellow precipitate was dried at 60°C. Then, yellow precipitate was suspended in DMF and final concentration of Bi_2O_3 nanoparticles was 1 mg ml^{-1}. Finally, the SPCE was modified with 10 µL of Bi_2O_3 nanoparticles suspension. In this way, the SPCE/Bi_2O_3 was prepared as a WE.

3.3.2.2. Preparation of GNR@Bi_2O_3 nanocomposite

GNR were also suspended in DMF (5 mg in 5 mL). Thereafter, the Bi_2O_3 nanoparticles were added to the GNR suspension and the whole mixture was ultrasonicated for 2 hours, causing the nanoparticles to be incorporated into the GNR structure. The final concentration of GNR@Bi_2O_3 nanocomposite was 1 mg ml^{-1}. In addition, 1 mg of GNR was suspended in 1 mL of DMF (final concentration 1 mg ml^{-1}). Finally, the SPCEs were modified with 10 µL of GNR suspension and 10 µL of GNR@Bi_2O_3 nanocomposite suspension in order to obtain WEs such as SPCE/GNR and SPCE/GNR@Bi_2O_3, respectively.

3.3.2.3. Preparation of glucose biosensor

SPCE/GNR@Bi_2O_3 electrode was modified with 5 µL of GO_x solution in the order to produce biosensor (SPCE/GNR@Bi_2O_3/GO_x). Then, the biosensor was left in the refrigerator at 4°C. After drying for 24 hours, 2.5 µL of 5 % Naf solution was applied to the SPCE/GNR@Bi_2O_3/GO_x electrode. The obtained electrode was dried for 1 hour at 4°C. The biosensor thus prepared was ready for electrochemical determinations. Further on, the glucose biosensor is labeled SPCE/GNR@Bi_2O_3/GO_x/Naf.

3.3.2.4. Preparation of honey sample

Honey sample was dissolved in 25 mL of 0.1 mol L^{-1} PBS (pH=7.40) and final concentration of glucose in this solution was 0.015 mol L^{-1}. Different aliquots of the sample solution were analyzed directly using the developed SPCE/GNR@Bi_2O_3/GO_x/Naf biosensor.

3.3.3. Procedures for polyphenolic index biosensor

3.3.3.1. Preparation of MnO_2 nanoparticles

MnO_2 nanoparticles were prepared following a synthetized procedure from the literature *(Vukojević et al., 2018b; Hu et al., 2016)*. $Mn(NO_3)_2*4H_2O$ (21.8 mg) and $KMnO_4$ (45.7 mg) were dissolved in 45 mL of ultra-pure water. During 6 hours of magnetic stirring, a uniform brown dispersion was formed. Suspension was centrifuged and brown precipitate was washed three times with ultra-pure water and, then, three times with ethanol. Brown precipitate was dried at room temperature at overnight. Thereafter, the composite was suspended in 2 mL DMF and final concentration of MnO_2 nanoparticles was 2 mg ml^{-1}. Finally, SPCE was modified with 5 µL of MnO_2 nanoparticles suspension in the order to produce a SPCE/MnO_2 electrode.

3.3.3.2. Preparation of GNP@MnO_2 nanocomposite

GNP@MnO_2 nanocomposite was synthesized using a procedure reported in the literature *(Vukojević et al., 2018b)*. GNP (10 mg) was added in of ultra-pure water (5 mL) and subjected ultrasonication for 1 hour. Final concentration of GNP was 2 mg ml^{-1}. Then, a 0.005 mol L^{-1} solution of $Mn(NO_3)_2$ was prepared using $Mn(NO_3)_2*4H_2O$ and ultra-pure water. In GNP suspension was added 20 mL of 0.005 mol L^{-1} $Mn(NO_3)_2$ solution and the whole mixture was placed on ultrasonication. After 2 hours, 25 mL of 0.012 mol L^{-1} $KMnO_4$ solution was added to the GNP-$Mn(NO_3)_2$ suspension and placed under magnetic stirring to obtain the GNP@MnO_2 nanocomposite. After 6 hours, GNP@MnO_2 nanocomposite was centrifugated and washed three times with ultra-pure water and three times with ethanol. After 24 hours of drying at room temperature, GNP@MnO_2 nanocomposite (10 mg) was suspended in DMF (5 mL) with final concentration of 2 mg ml^{-1}. SPCE/GNP@MnO_2 working electrode was obtained by modification of SPCE with 5 µL of GNP@MnO_2 suspension. Also, 2 mg of GNP was suspended in 1 mL of DMF and 5 µL of this suspension was applied at SPCE in order to produce SPCE/GNP electrode.

3.3.3.3. Preparation of polyphenolic index biosensor

SPCE/GNP@MnO_2 electrode was modified with 5 µL of TvL solution in the order to produce the biosensor (SPCE/GNP@MnO_2/TvL). Electrode was left 24 hours in 4 °C. The final step of preparing the biosensor involved adding 2.5 µL of 5 % Naf solution to the surface of SPCE/GNP@MnO_2/TvL electrode. After 2 hours of drying, the biosensor was ready for electrochemical applications. The polyphenolic index biosensor thus prepared is further labeled SPCE/GNP@MnO_2/TvL/Naf.

3.3.3.4. Preparation of wine samples

Since the wine samples were directly analyzed, no sample preparation was required. BPI in wine samples was determined by the standard addition method.

3.3.4. Storage stability of glucose and polyphenolic index biosensor

Storage conditions significantly affect the performance of biosensors. Keeping the biosensor at inadequate temperature and humidity leads to a change in the active sites of the enzyme, which can result in complete denaturation. The practice of storing enzymes (enzyme solutions) at a temperature of 4°C is well known. At this temperature it has been proven that the activity of the enzyme changes the least (*Burtis et al., 2013*). Accordingly, after the preparation of the glucose and polyphenolic index biosensors, as well as after each use, the biosensors were stored in the refrigerator at 4°C. Similar storage conditions of glucose and polyphenolic biosensors are reported in the literature *(Ahmad et al., 2010; Salimi et al., 2004; Wu et al., 2009; Di Fusco et al., 2010; ElKaoutit et al., 2007; Haghighi et al., 2003; Portaccio et al., 2006)*.

3.4. Optimization of experimental and instrumental conditions

3.4.1. Optimization of amount of nanocomposite, enzyme and Naf added to SPCEs

The first experiments, in both biosensors, were to optimize the amount of the corresponding nanocomposites added to SPCEs, in order to obtain the best electrochemical performances of WEs. According to the preparation procedures reported in the literature *(Arvand et al., 2016; Bergamini et al., 2010; Chaiyo et al., 2016; Cao et al., 2017; Gan et al., 2010; Huang et al., 2010; Jampasa et al., 2014; Oliveira et al., 2012; Xin et al., 2013; Yang et al., 2014c; Ye & Ju, 2005; Yu et al., 2004)*, volumes of the corresponding nanocomposites from 1 µL to 10 µL were tested. Also, a larger amount of 10 µL was attempted, but nanocomposites spilled beyond the active surface of the SPCEs. Consequently, volumes greater than 10 µL were not taken into account.

During the preparation of glucose biosensors, the amount of GO_x added to the modified SPCEs was examined. According to the glucose biosensor procedures described in the literature *(Kuek Lawrence et al., 2014; Devasenathipathy et al., 2015; ; Anusha et al., 2015; Wu & Yin, 2011; Wang et al., 2015a; Li et al., 2008; Wu et al., 2009; Zhao et al., 2007)*, the volume range of the 10 mg L^{-1} GO_x solution added to the electrodes was from 5 µL to 20 µL. A slight spillage of the enzyme outside the active electrode surface was observed at the additional volume of 15 µL, while with the addition of 20 µL this spill was significantly more pronounced. Despite this problem, biosensors prepared with 15 µL and 20 µL were also analyzed in order to observe the behavior of such SPCEs.

The final step in the preparation of the glucose biosensor was to optimize the amount of 5% Naf solution added to the corresponding SPCEs. In accordance with procedures published in the literature, a 5% Naf solution was applied in the range of 1.5 µL to 5.5 µL *(Li et al., 2008; ; Zhao et al., 2007; Wu et al., 2009)*.

The polyphenolic index biosensor was prepared based on the experience gained during the preparation of the glucose biosensor. The optimized amount of 10 mg L^{-1} GO_x was 5 µL. Accordingly, a polyphenolic index biosensor was prepared by adding 5 µL of 10 mg L^{-1} TvL to the modified SPCE. Also, the optimal amount of 5 % Naf solution, during the preparation of the glucose biosensor, was 2.5 µL. Finally, the last step in the preparation of the polyphenolic index biosensor involved the addition of 2.5 µL of 5% Naf solution to the electrode. Literature data show that 5 µL of laccase enzyme is one of the optimal amounts for preparation of polyphenolic biosensors *(Eremia et al., 2013; Ibarra-Escutia et al., 2010; Liu et al., 2006; Vasilescu et al., 2016)*.

The previous chapter (*Section 2.3.*) which describes the detailed preparations of SPCEs, the noted volumes of nanocomposites were actually optimized. In the case of the glucose biosensor, the stated volumes of 10 mg L^{-1} GO_x solution and 5% Naf solution were also optimized.

3.4.2. Selection of supporting electrolyte

During the optimization of all experimental parameters and development of the amperometric method for glucose biosensor, 0.1 mol L^{-1} PBS was selected as a supporting electrolyte. PBS is one of the most commonly used buffer solutions in the development of glucose biosensors. Also, PBS is most commonly used at pH values from 6.50 to 8.00. The reason is because the enzyme GO_x exhibits its highest activity in neutral (pH=7.00) or slightly basic medium (pH=7.20 or physiological conditions pH=7.40) *(Crouch et al., 2005)(Vukojević et al., 2018b; Uang & Chou, 2003; Mano et al., 2007; ; Wu et al., 2004; Liu & Lin, 2006; Salimi et al., 2004; Wang et al., 2003; Rakhi et al., 2016; Lamas-Ardisana et al., 2018)*. Accordingly, in the case of our glucose biosensor, different pH values of the 0.1 mol L^{-1} PBS (pH=6.80-7.60) were applied in order to obtain the best electrochemical performance of the biosensor. In addition, this pH range was selected due to the potential application of glucose biosensor in in food and drink samples.

In the case of the polyphenolic index biosensor, 0.1 mol L^{-1} ABS was used as the supporting electrolyte. Literature data show that this buffer solution is most often used in developing electrochemical methods for the quantification of polyphenols if the laccase enzyme is used to construct a biosensor *(Fu et al., 2014; Ibarra-Escutia et al., 2010; Moccelini et al., 2011; Mousty et al., 2007; Patel et al., 2018; Roy et al., 2005; Vasilescu et al., 2016; Xu et al., 2009)*. ABS was applied in the pH range from 4.00 to 5.30. This pH range was chosen because the enzyme laccase exhibits its highest activity between pH 4.00 and 5.00 *(Freire et al., 2002; Gomes et al., 2004)*. In addition to ABS, the electrochemical performance of biosensors in the presence of 0.1 mol L^{-1} BRBS as a supporting electrolyte was examined. BRBS was applied in the same pH range as ABS. This was done to investigate the electrochemical behavior of the polyphenolic index biosensor in another acidic supporting electrolyte.

Also, 0.1 mol L^{-1} PBS was used as supporting electrolyte during the investigation of system reversibility using SPCEs modified with corresponding nanocomposites. In the case of glucose biosensor, pH of 0.1 mol L^{-1} PBS was 6.80, while, in the case of polyphenolic index biosensor, pH was 6.50.

3.4.3. Optimization of working potential of amperometric method

Hydrodynamic chronoamperometric method was used for quantification of glucose and polyphenolic index (caffeic acid as model compound) with glucose and polyphenolic index biosensors, respectively. Before testing the analytical parameters (working linear range, LOQ, LOD), it is necessary to find the optimal working potential at which the electrode (biosensor) provides the best electrochemical performances.

Since GO_x and TvL are oxidizing enzymes, positive potential values have been applied. Accordingly, during the development of amperometric methods for glucose and polyphenolic index biosensors, the potential range from 0.2 to 0.7 V and 0.3 to 0.5 V was applied, respectively.

4. Results and discussion

4.1. Glucose biosensor

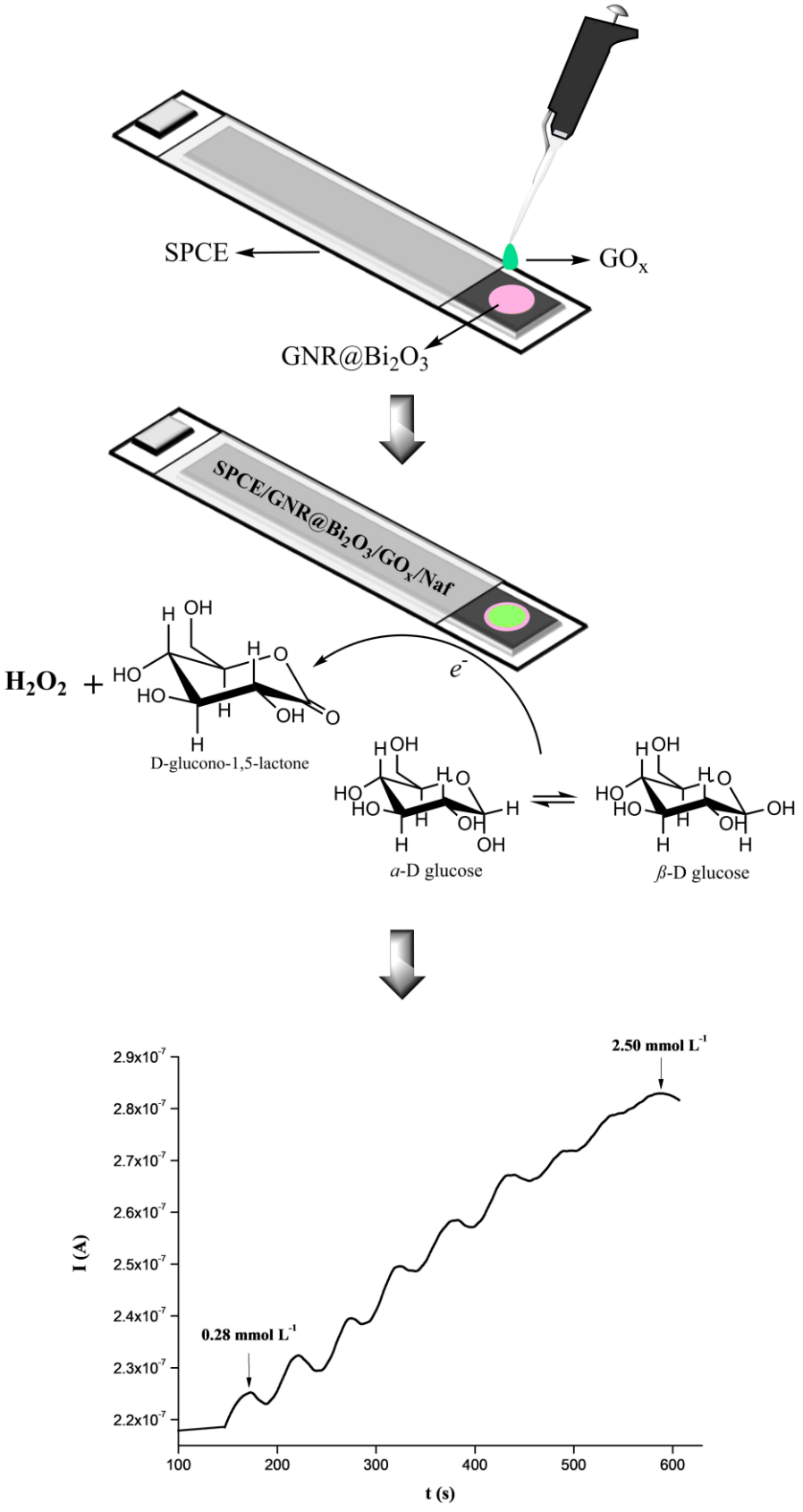

Figure 40. Main experimental points in glucose biosensor preparation and amperometic response of developed biosensor to target analyte.

The first aim of the doctoral dissertation was to develop the glucose biosensor. Therefore, the first part of chapter *RESULTS AND DISCUSSION* refers to the results and discussion obtained during the development of the glucose biosensor. Summarized experimental steps of glucose biosensor preparation and corresponding amperometric response of developed biosensor towards glucose are given at *Figure 40*.

Research was based on modification of SPCE with GNR@Bi_2O_3. Obtained SPCE/GNR@Bi_2O_3 electrode was used for optimization and development of method that would be applied for glucose quantification with a biosensor. H_2O_2, as a final product of enzymatic glucose oxidation, was used for electrochemical testing and optimization of all operating conditions. The final step was to modify the SPCE/GNR@Bi_2O_3 electrode with GO_x in order to produce the biosensor. Then, the aim was to examine the electrochemical characteristics of the developed biosensor and compare it with the biosensors reported in the literature. Finally, application of the developed biosensor in real samples was done.

Primarily, synthesis of Bi_2O_3 nanoparticles and GNR@Bi_2O_3 nanocomposite was performed. Characterization of the synthesized nanocomposites was performed using XRPD and FE-SEM methods. XRPD analysis was applied to obtain the crystal structure of nanomaterials, while FE-SEM method provided information about size and shape of nanomaterial particles.

After confirmation of the nanocomposite structure, electrochemical tests were performed.

The first part of the electrochemical results involves the examination of the electrochemical characteristics of SPCE/GNR@Bi_2O_3 electrode by cyclic voltammetry. The tests included optimization of the amount of modifier added to the SPCE, system reversibility testing, selection of pH of 0.1 mol L^{-1} PBS and the effect of scan rate on the electrochemical response of the target electrode.

The second part of the results represent amperometric measurements related to optimization of working potential, as well as testing of the linear range of H_2O_2 at SPCE/GNR@Bi_2O_3 electrode. Also, the stability, reproducibility and repeatability of the electrode were examined.

The third, major, part of the results relates to the examination of the electrochemical characteristics of the developed glucose biosensor. Under optimized experimental and instrumental conditions, the linear working range of glucose biosensors was examined. Important analytical parameters (precision, LOD, LOQ, reproducibility and repeatability) were determined. In addition, the effects of different interfering substances on the electrochemical response of the glucose biosensor were examined.

The final part covers the application of glucose biosensors in real samples and validation of the proposed and developed method.

4.1.1. Characterization of nanocomposites by XRPD and FE-SEM methods

The diffractions patterns of Bi_2O_3 nanoparticles, GNR and GNR@Bi_2O_3 nanocomposite, obtained by XRPD method, are given at *Figure 41*. All obtained peaks of the Bi_2O_3 were compared with peaks of α-Bi_2O_3 crystal planes (JCPDS card #41-1449). Based on the matched peaks, it is concluded that the synthesized oxide is of the α-Bi_2O_3 type (Figure 41a), and crystallizes in a monoclinic system. Applying the *Scherrer's* equation (*Equation 4.*) to peak 020 (peak of least intensity) and peak 120 (the most intense peak), values of 63.1 nm and 67.5 nm, respectively, were obtained. These values indicate the high crystallinity of the analyzed sample. In addition to the peaks that characterize monocrystalline Bi_2O_3, diffraction peaks of 24.8°, 27.9°, 33.1° and 41.7° at 2Θ are observed (in Figure 41a marked with *****). These peaks belong to $BiONO_3$, which indicates that Bi_2O_3 is contaminated with this compound. The presence of the impurity can be addressed to insufficient [NaOH]/[Bi] ratio used during the synthesis of the Bi_2O_3 nanoparticles *(Yang et al., 2014b)*. The XRPD pattern of GNR (*green line*) shows a maximum diffraction at about 26° (Figure 41b), which corresponds to an interlayer distance of 3.4 Å within graphene *(Liu et al., 2015)*. The XRPD profile of GNR@Bi_2O_3 nanocomposite (*gray line*) showed all peaks found in previous samples, which confirmed incorporation of Bi2O3 into GNR structures (Figure 41b).

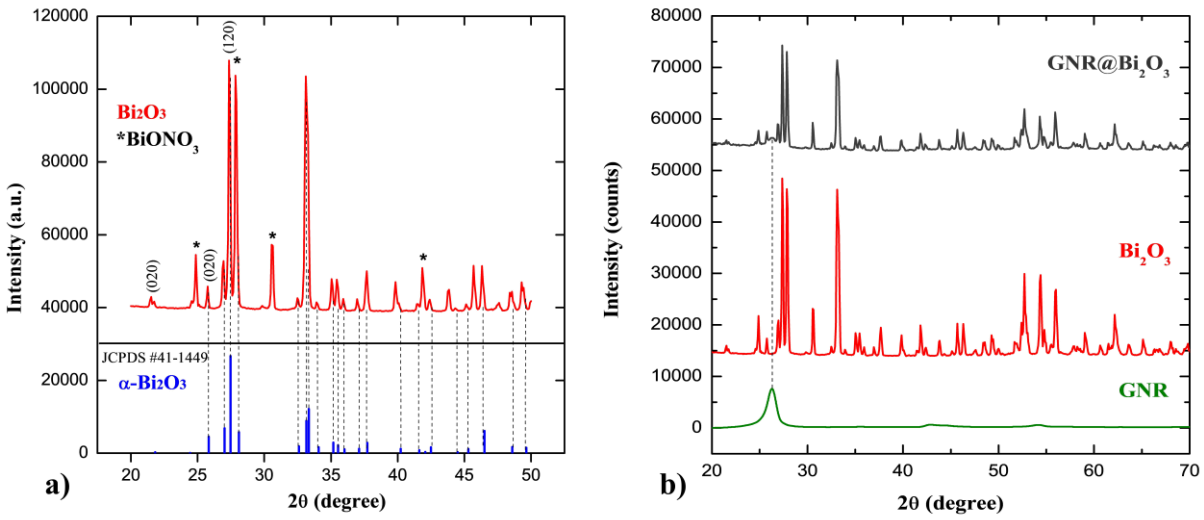

Figure 41. a) XRPD profile of synthesized Bi_2O_3 nanoparticles. JCPDS card #41-1449 represent the standard for α-Bi_2O_3 phase. ***b)*** XRPD patterns of GNR (*green line*), Bi_2O_3 nanoparticles (*red line*) and GNR@Bi_2O_3 nanocomposite (*grey line*).

Particle size and shape of mentioned nanocomposite was further observed using FE-SEM method. *Figure 42.* shows morphology of GNR, where a long curved rod-like structures of GNR was observed. The average length and width of the GNR was a few micrometers and ~100 nm, respectively. Bi_2O_3 nanopowder shows irregular morphology, where thin sheet-like particles packed in aggregates (Figure 43). *Figure 44.* shows the clear formation of nanocomposites between Bi_2O_3 and GNR. In addition, Bi_2O_3 nanoparticles have been observed to associate GNRs with long curved nanotubes or nanorods. This has a significant effect on increasing the surface area and conductivity.

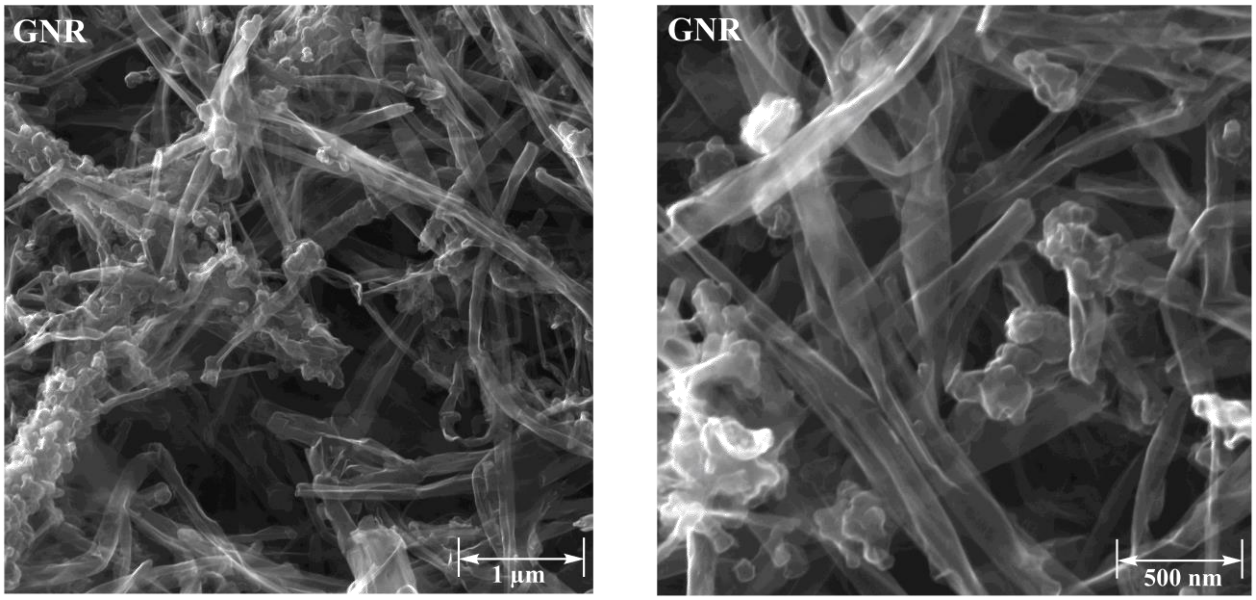

Figure 42. FE-SEM micrographs of GNR. Magnified $50*10^3$ times (left) and $100*10^3$ times (right).

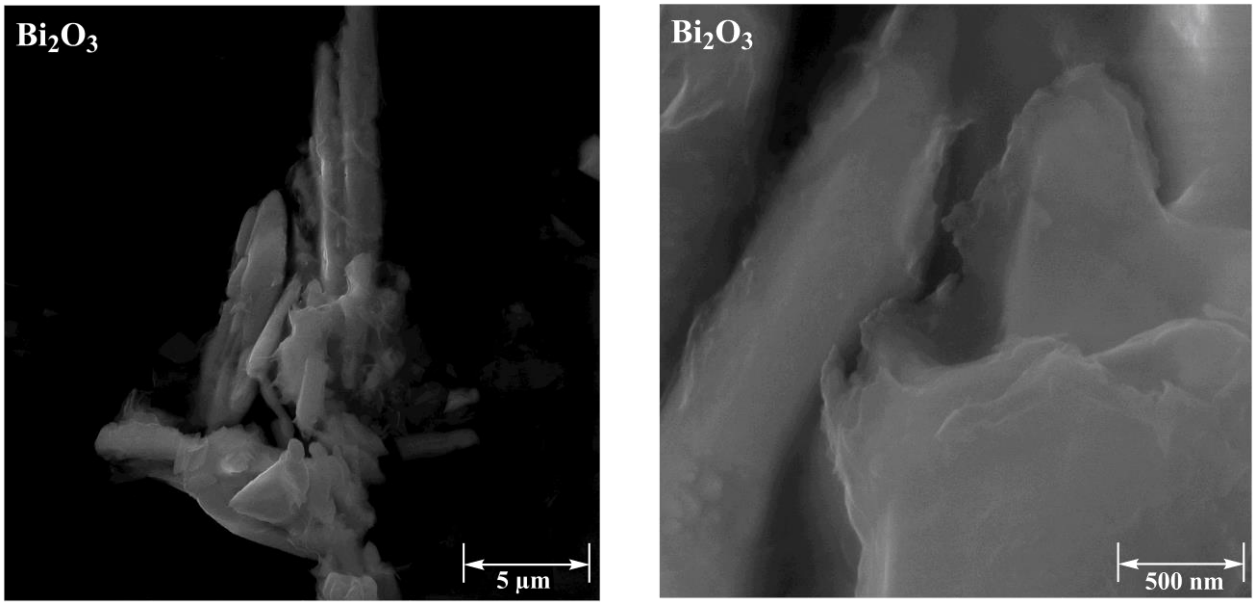

Figure 43. FE-SEM micrographs of pure Bi_2O_3 nanopowder. Magnified $10*10^3$ times (left) and $100*10^3$ times (right).

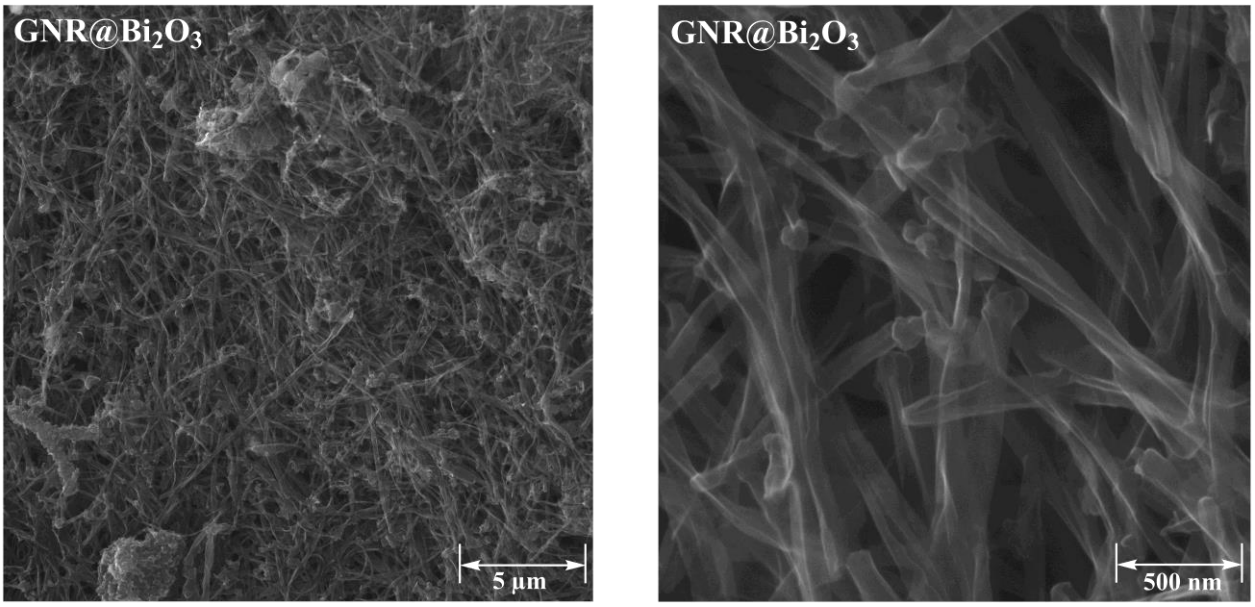

Figure 44. FE-SEM micrographs of GNR@Bi_2O_3 nanocomposite. Magnified $10*10^3$ times (left) and $100*10^3$ times (right).

4.1.2. Cyclic voltammetry study

4.1.2.1. Optimization of nanocomposite amount added to SPCE

Optimization of the amount of nanocomposite added to the SPCE was performed by cyclic voltammetry. In this experiment, the electrochemical response of SPCEs modified with 1 µL, 5 µL and 10 µL of 1 mg ml^{-1} of GNR@Bi_2O_3 nanocomposites was monitored. As analyte was used 5 mmol L^{-1} $[Fe(CN)_6]^{4-}$/$[Fe(CN)_6]^{3-}$ in 0.1 mol L^{-1} PBS (pH=6.80). Following the electrochemical response of SPCE/GNR@Bi_2O_3 electrodes, the absence of an oxidation peak was observed. On the other hand, a reduction peak was expressed in the case of all three amounts of nanocomposites added to the SPCEs. *Figure 45a.* shows that with the increase in the amount of nanocomposites, the cathodic current increases. A SPCE modified with 10 µL of 1 mg mL^{-1} of GNR@Bi_2O_3 produces the most intense current of the reduction peak. As explained in the section *2.4.1. Optimization of amount of nanocomposite, enzyme and Naf added to SPCEs*, 15 µL and 20 µL were added to the SPCE but spillage of the nanocomposite beyond the active electrode surface was observed, so these amounts were not further considered.

In addition, the electrochemical behavior of SPCEs modified with the same amounts of 1 mg mL^{-1} of GNR@Bi_2O_3 nanocomposites (1 µL, 5 µL and 10 µL) in the presence of a mean analyte was investigated. Electrochemical responses of modified SPCEs were monitored in the presence of 0.5 mmol L^{-1} H_2O_2 in 0.1 mol L^{-1} PBS (pH=6.80) by cyclic voltammetry. Oxidation of H_2O_2 was observed with all three SPCE/GNR@Bi_2O_3 electrodes. *Figure 45b.* shows the intensities of the oxidation peaks depending on the amounts of nanocomposite on the SPCE. As in the previous experiment, the highest current intensity was recorded with SPCE modified with 10 µL of GNR@Bi_2O_3 nanocomposite.

Based on the obtained results, the optimal amount of 1 mg mL^{-1} of GNR@Bi_2O_3 nanocomposite added to the SPCE was 10 µL. Also, for all further experiments, SPCEs were modified with 10 µL of GNR and Bi_2O_3 nanocomposites in order to obtain corresponding WEs.

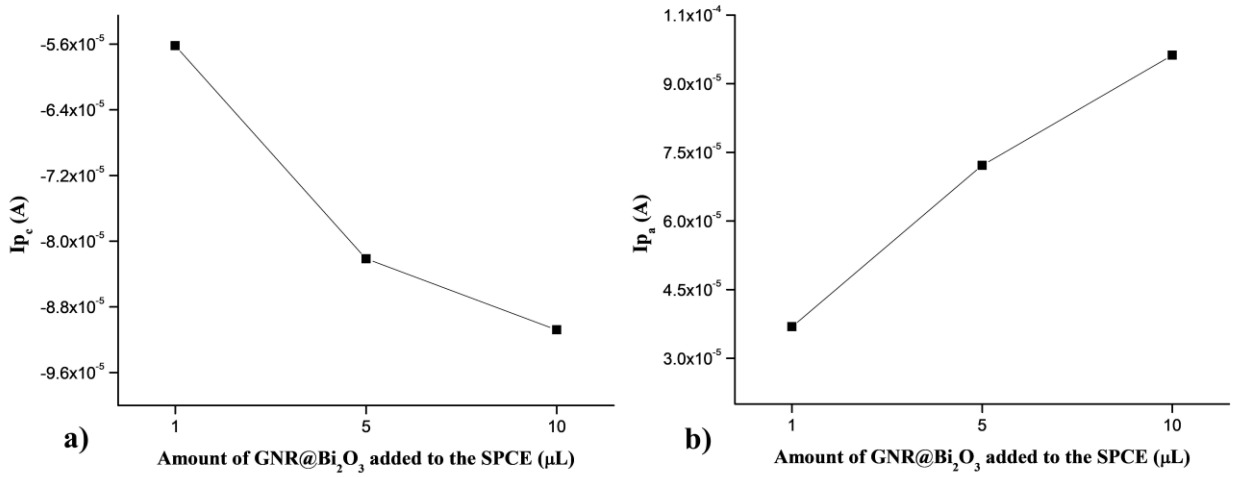

Figure 45. Optimization of amount of GNR@Bi_2O_3 nanocomposite to the SPCEs. ***a)*** Cathodic peak current (Ip_c) *vs.* amount of nanocomposite obtained for 5 mmol L^{-1} $[Fe(CN)_6]^{4-}$/$[Fe(CN)_6]^{3-}$ in 0.1 mol L^{-1} PBS (pH=6.80). ***b)*** Anodic peak current (Ip_a) vs. amount of nanocomposite obtained for 0.5 mmol L^{-1} H_2O_2 in 0.1 mol L^{-1} PBS (pH=6.80).

4.1.2.2. Electrochemical behavior of modified SPCEs

This chapter describes the impact of a different modification step (GNR, Bi_2O_3 and GNR@Bi_2O_3) on the electrochemical performance of SPCEs. Electrochemical performance/characteristics involve analyzing the shape of oxidation/reduction peaks as well as defining their currents level. The electrochemical response of each SPCE was monitored in $[Fe(CN)_6]^{4-}$/$[Fe(CN)_6]^{3-}$ solution (in order to test the system reversibility), but more importantly in the H_2O_2 solution as the analyte.

Electrochemical characteristics of WEs such as unmodified SPCE, SPCE/GNR, SPCE/Bi_2O_3 and SPCE/GNR@Bi_2O_3 were investigated by cyclic voltammetry. As supporting electrolyte was used 0.1 mol L^{-1} PBS (pH=6.80). Electrochemical responses of WEs were followed in 5 mmol L^{-1} $[Fe(CN)_6]^{4-}$/$[Fe(CN)_6]^{3-}$. Applied potential was from -1.0 V to +1.0 V, while the scan rate was 50 mV s^{-1}. Cyclic voltammograms clearly show the presence of an oxidation and reduction peaks in the case of all four WEs (Figure 46). Depending on the WEs, the oxidation peak occurs in the potential range from 0.29 to 0.36 V, while the reduction peak is between 0 and -0.04 V. SPCE/Bi_2O_3 shows a lower redox peaks current compared to the unmodified SPCE. In addition, SPCE/Bi_2O_3 gives a current intensity significant lower compared to other WEs. This can be explained by the low electrical conductivity of bismuth which results in a decrease in the conductivity of the diffusion layer. This phenomenon is further reflected through the appearance of peaks and their intensities. On the other hand, the SPCE/GNR provides well defined redox peaks with high current intensities. This confirms that graphene nanomaterials improve the electrochemical characteristics by increasing the electrode active surface area and expanding the electrode diffusion layer. In the case of the SPCE/GNR@Bi_2O_3 electrode, the best electrochemical characteristics are observed, compared to the other WEs. The best-defined shape of the redox peaks with highest current intensities, as well as the lowest value of ΔE (best reversibility of system), is the result of the synergetic effect of GNR and Bi_2O_3. In addition to the definition of redox peaks and the currents level, the synergetic effect of graphene nanomaterials and nano-structured M_xO_y increases the diffusion layer, electrical conductivity, as well as number of electrode active sites *(Wang et al., 2010)*.

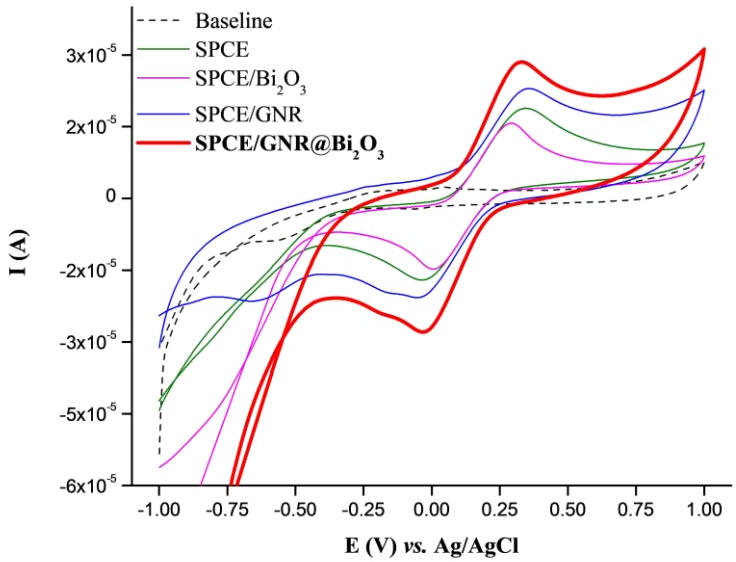

Figure 46. Cyclic voltammograms of modified SPCEs in 0.1 mol L^{-1} PBS (pH=6.80) containing 5 mmol L^{-1} $[Fe(CN)_6]^{4-}/[Fe(CN)_6]^{3-}$ at scan rate 50 mV s^{-1}.

4.1.2.2.1. Active surface area of unmodified SPCE and SPCE/GNR@Bi_2O_3

Active surface area of unmodified SPCE and SPCE modified with GNR@Bi_2O_3 nanocomposite were calculated after testing the scan rate on the electrochemical response of the mentioned WEs. The *Figure 47.* shows cyclic voltammograms recorded with unmodified SPCE and SPCE/GNR@Bi_2O_3 at different scan rates (10-200 mV s^{-1}) in 0.1 mol L-1 PBS (pH=6.80) containing 5 mmol L^{-1} $[Fe(CN)_6]^{4-}/[Fe(CN)_6]^{3-}$. *Figure 47.* also shows, in the case of both WEs, that increasing the scan rate leads to an increase in the intensity of the anodic (I_{pa}) and cathodic (I_{pc}) peaks, with a linear shift of the anodic peak to more positive potentials, i.e. a linear shift of the cathodic peak to more negative potential values. This phenomenon is accompanied by a constant value ΔE (around 0.25 V). Such results indicate a rather irreversible type of process on the electrode surfaces.

The active surface areas of unmodified SPCE and SPCE/GNR@Bi_2O_3 were calculated via *Equation 2.* using the values of the intensity of anodic peak (I_{pa}) with the corresponding scan rates. Average value of active surface area of unmodified SPCE and SPCE/GNR@Bi_2O_3 were 215 mm^2 and 785 mm^2, respectively. This difference in the active surface area is directly related to the synergistic effect of graphene nanomaterials with M_xO_y nanoparticles.

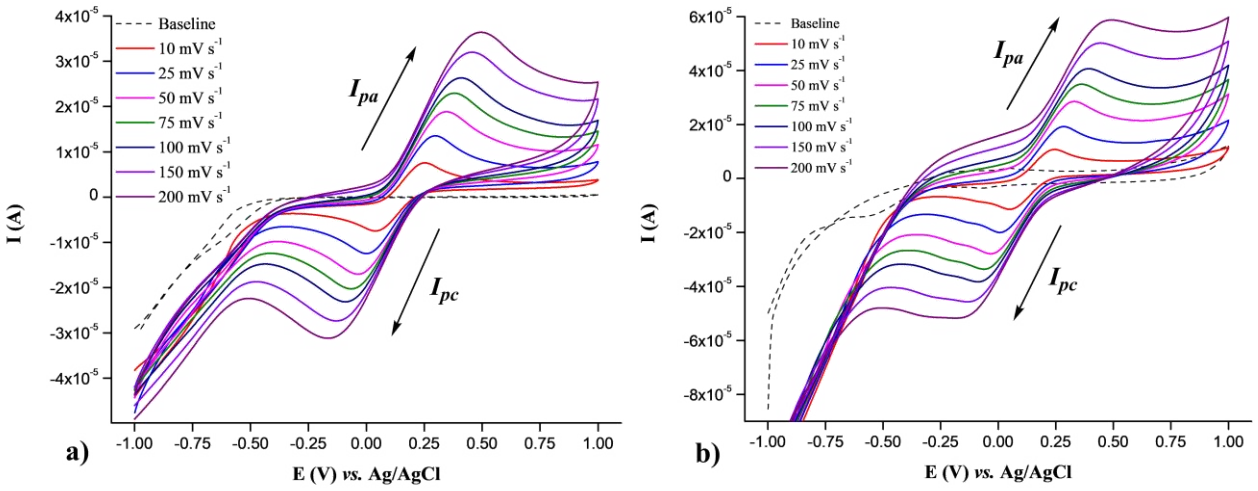

Figure 47. Cyclic voltammograms recorder with ***a)*** unmodified SPCE and ***b)*** SPCE/GNR@Bi_2O_3 in 5 mmol L^{-1} $[Fe(CN)_6]^{4-}/[Fe(CN)_6]^{3-}$ at different scan rates (10-200 mV s^{-1}). Supporting electrolyte was 0.1 mol L^{-1} PBS (pH=6.80).

4.1.2.2.2. Electrochemical behavior of modified SPCEs in presence of H_2O_2

The electrochemical responses of the modified SPCEs were also monitored in the presence of 80 µmol L^{-1} H_2O_2. Cyclic voltammetry was done in 0.1 mol L^{-1} PBS (pH=6.80), as supporting electrolyte, with a scan rate of 100 mV s^{-1}. *Figure 48a.* clearly shows the difference in current intensities by stepwise introducing the modifier into the experiment, although no peak occurrence is defined. Also, in this case, when the analyte was analyzed, the synergetic effect of GNR and Bi_2O_3 is dominant, which is observed in the highest current of the oxidation peak given by the SPCE/GNR@Bi_2O_3. Based on the appearance of cyclic voltammograms (Figure 48a), we suggest that H_2O_2 oxidation is best at potentials greater than 0.4 V, which is in line with the most active studies reported in the literature *(Kosto et al., 2019; Zbiljić et al., 2015)*.

In addition, the response of the SPCE/GNR@Bi_2O_3 to the stepwise addition of H_2O_2 was examined by cyclic voltammetry. As supporting electrolyte was used 0.1 mol L^{-1} PBS (pH=6.80) and scan rate was 100 mV s^{-1}. *Figure 48b.* shows the cyclic voltammograms obtained for different concentrations of H_2O_2 with SPCE/GNR@Bi_2O_3. It has been observed from the *Figure 48b.* that the current intensity of the oxidation peak increases with increasing H_2O_2 concentration. This can be explained by a decrease in the oxidation overvoltage of H_2O_2 at the SPCE/GNR@Bi_2O_3 resulting in an increase in the oxidation peak current. Based on the results obtained for system reversibility testing, as well as after analyzing H_2O_2 as an analyte, we have selected the SPCE/GNR@Bi_2O_3 for further testing and application in this study.

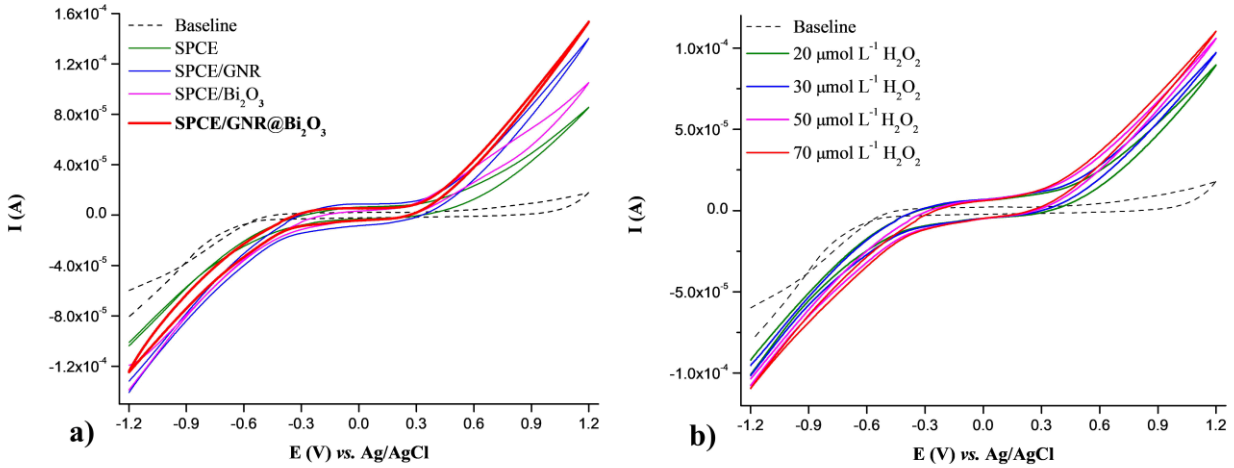

Figure 48. a) Comparison of cyclic voltammograms obtained with unmodified SPCE, SPCE/GNR, SPCE/Bi_2O_3 and SPCE/GNR@Bi_2O_3 in the presence of 80 μmol L^{-1} H_2O_2 in 0.1 mol L^{-1} PBS (pH=6.80). Scan rate of 100 mV s^{-1}. ***b)*** Cyclic voltammograms obtained with SPCE/GNR@Bi_2O_3 for different concentration of H_2O_2 in 0.1 mol L^{-1} PBS (pH=6.80). Scan rate of 100 mV s^{-1}.

4.1.2.3. Effect of pH of supporting electrolyte on the SPCE/GNR@Bi_2O_3 performances

The influence of different pH of 0.1 mol L^{-1} PBS on the electrochemical response of the SPCE/GNR@Bi_2O_3 was followed by cyclic voltammetry. The pH of 0.1 mol L^{-1} PBS was applied in the range from 6.80 to 7.60. *Figure 49a.* shows the cyclic voltammograms obtained for different pH of 0.1 mol L^{-1} PBS in the presence of 80 μmol L^{-1} H_2O_2, with a scan rate of 100 mV s^{-1}. Again, although there is no occurrence of a defined oxidation peak, a slight difference in peak currents is clearly seen using different pHs (inset Figure 49a). In addition, the dependence of the peak current intensity of anodic peak on the applied pH was monitored. *Figure 49b.* clearly indicates that pH=7.40 provides the highest peak current for 80 μmol L^{-1} H_2O_2 using a SPCE/GNR@Bi_2O_3. Accordingly, pH of 7.40, which simulates physiological conditions, was selected as optimal and used in further experiments.

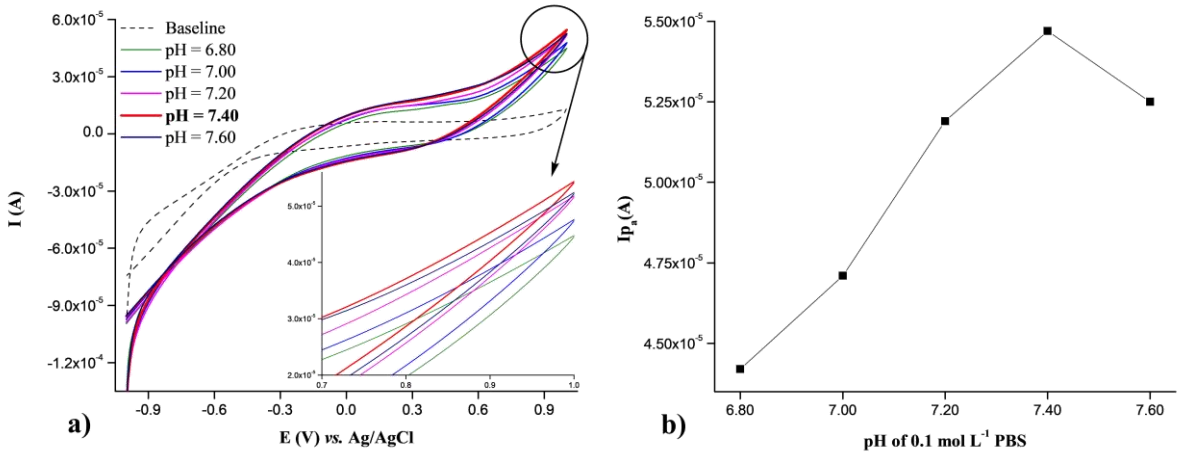

Figure 49. a) Cyclic voltammograms obtained at different pHs of 0.1 mol L^{-1} PBS in presence of 80 μmol L^{-1} H_2O_2 using a SPCE/GNR@Bi_2O_3. ***b)*** Anodic peak current (Ip_a) *vs.* applied pHs.

4.1.2.4. Effect of scan rate on the SPCE/GNR@Bi_2O_3 performances

In order to investigate the process responsible for the oxidation of H_2O_2 at the electrode surface, the effect of scan rate on the electrochemical response of the SPCE/GNR@Bi_2O_3 was examined. Influence of scan rate was investigated by cyclic voltammetry in 0.1 mol L^{-1} PBS (pH=7.40). *Figure 50a.* represent cyclic voltammograms obtained for 80 µmol L^{-1} H_2O_2 at SPCE/GNR@Bi_2O_3. Scan rate was applied in the range from 10 to 200 mV s^{-1}. The *Figure 50a.* shows that scan rate variation yields the obvious increase in oxidation peak currents. The *Figure 50b.* shows the linear dependence of the current intensity of anodic peak and the square root of the scan rate. This dependence is described by equation: $I\ (A) = 4.47*10^{-5} + 6.76*10^{-7}\ V^{1/2}\ (mV/s)^{1/2}$, with the *Pearson correlation coefficient* (*r*) of 0.9997. Excellent linearity indicates that oxidation of H_2O_2 on the surface of SPCE/GNR@Bi_2O_3 was caused by the diffusion-controlled process *(Li et al., 2015; Jia et al., 2014; Zhang et al., 2013)*.

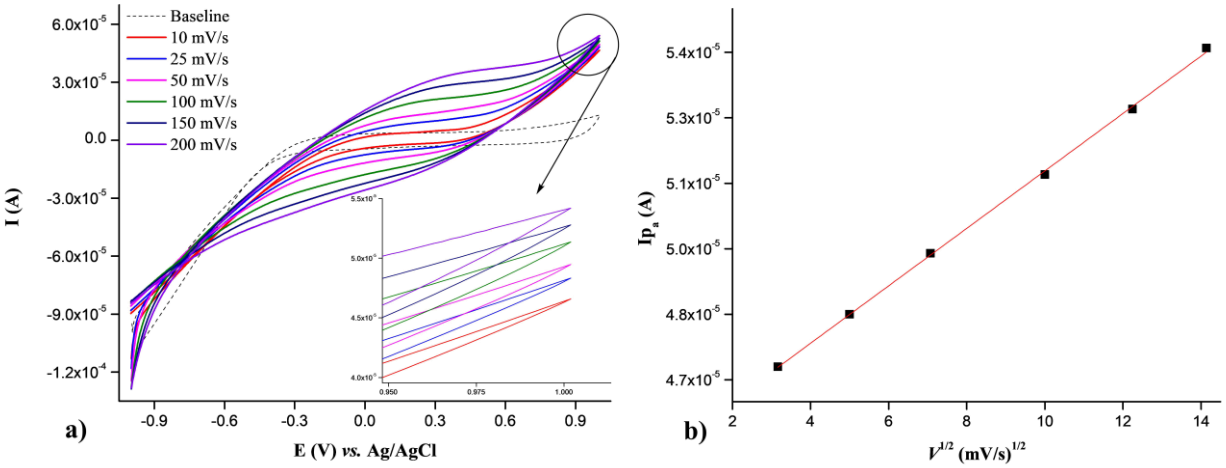

Figure 50. a) Cyclic voltammograms of 80 µmol L^{-1} H_2O_2 in 0.1 mol L^{-1} PBS (pH=7.40) at different scan rates obtained with SPCE/GNR@Bi_2O_3. ***b)*** Linearity of anodic peak current (Ip_a) *vs.* the square root of the scan rate ($V^{1/2}$).

4.1.3. Hydrodynamic chronoamperometric studies

4.1.3.1. Optimization of working potential

This parameter was optimized by monitoring the amperometric response of the SPCE/GNR@Bi_2O_3 to the successive addition of 0.01 mol L^{-1} H_2O_2 to 0.1 mol L^{-1} PBS (pH=7.40), under stirring conditions. *Figure 51a.* shows chronoamperometric response of SPCE/GNR@Bi_2O_3 for different concentration of H_2O_2 (10-90 µmol L^{-1}) at different working potential (0.2 to 0.7 V). As observed from chronoamperograms, higher potential contributes to higher current intensity. In order to determine the optimal working potential, the dependence of the current intensity and H_2O_2 concentrations at different potentials (0.4 to 0.7 V) was constructed (Figure 51b). Due to low current intensities, as well as low slope of calibration curves, amperometric responses of SPCE/GNR@Bi_2O_3 at potentials 0.2 V and 0.3 V were not considered in *Figure 51b*. Although the potential 0.7 V gives the highest current, the value of the *r* was the smallest (r=0.9907). In contrast, the 0.6 V potential provides excellent linearity between current and concentrations (r=0.9992). Also, SPCE/GNR@Bi_2O_3 shows a very stable electrochemical signal in the applied concentration range at potential of 0.6 V. Accordingly, the potential 0.6 V was selected as optimal.

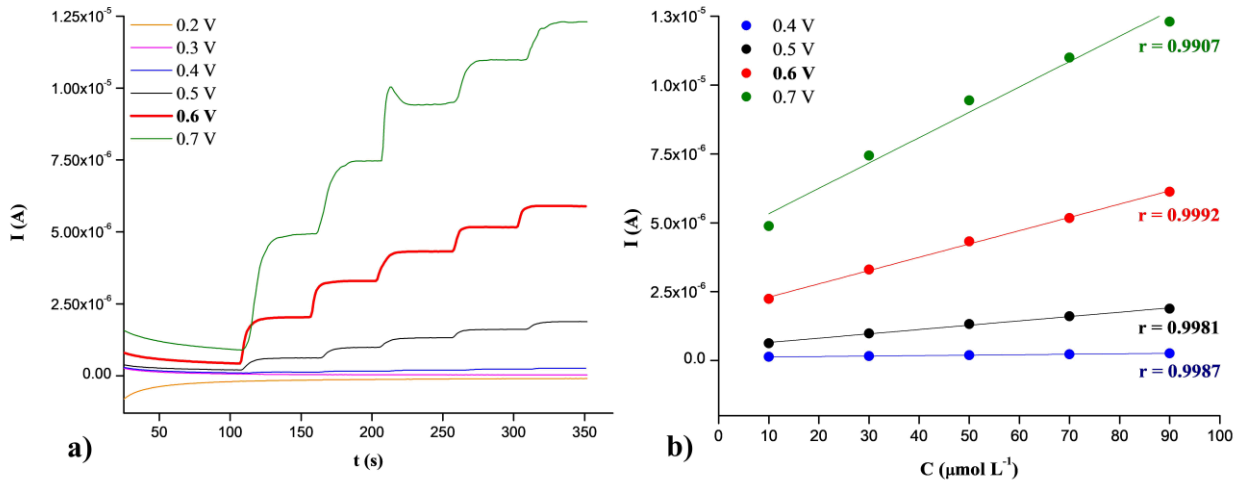

Figure 51. a) Chronoamperograms obtained with SPCE/GNR@Bi_2O_3 for different concentrations of H_2O_2 in 0.1 mol L^{-1} PBS (pH=7.40) at different working potentials (0.2 to 0.7 V), under stirring conditions. ***b)*** Plots of the current intensity *vs.* the concentration of H_2O_2 for working potentials 0.4 V, 0.5 V, 0.6 V and 0.7 V.

4.1.3.2. Analytical performances of the proposed method

Working linear range of H_2O_2 at SPCE/GNR@Bi_2O_3 was monitored by hydrodynamic chronoamperometry. The amperometric response of SPCE/GNR@Bi_2O_3 was monitored after each successive addition of a different aliquots of 0.0100 mol L^{-1} H_2O_2 standard solution in 0.1 mol L^{-1} PBS (pH=7.40), with intensive stirring (Figure 52a). The electrode working potential was set to optimum (0.6 V). The working linear range of H_2O_2 at SPCE/GNR@Bi_2O_3 was from 4 µmol L^{-1} to 550 µmol L^{-1}. *Figure 52b.* shows the constructed calibration curve of a given determination. There are two segments of linearity in the graph. One type of linearity (one slope value) was recorded in the concentration range from 4 µmol L^{-1} to 90 µmol L^{-1}, while the other slope value was recorded in the concentration range from 90 µmol L^{-1} to 550 µmol L^{-1}. All electroanalytical parameters of the corresponding linearity are summarized in *Table 4.* LOQ and LOD were calculated according to the *Equation 6.* and *Equation 7.*, respectively, where is: *S* - standard model error and *b* - slope of the regression line:

$$LOQ = {10 \cdot S}/{b} \qquad \textit{Equation 6.}$$

$$LOD = {3 \cdot S}/{b} \qquad \textit{Equation 7.}$$

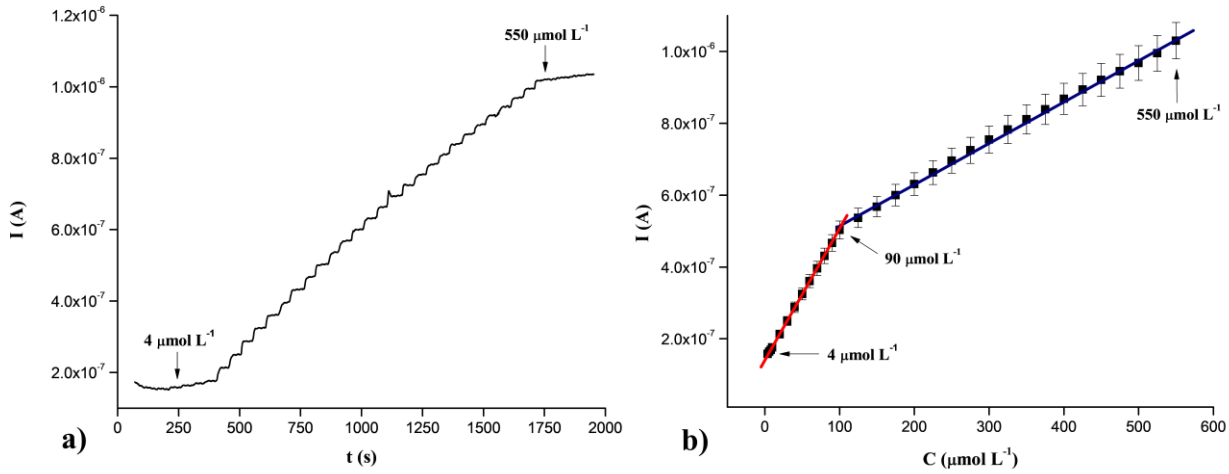

Figure 52. a) Amperometric response of SPCE/GNR@Bi_2O_3 for serial addition of different aliquots 0.0100 mol L^{-1} H_2O_2 to a stirred 0.1 mol L^{-1} PBS (pH=7.40) at potential of 0.6 V. ***b)*** Calibration graphs with corresponding error bars.

Table 4. Electroanalytical parameters obtained for SPCE/GNR@Bi_2O_3.

***C* range (μmol L^{-1})**	**Calibration curve equation**	***r***	**LOQ (μmol L^{-1})**	**LOD (μmol L^{-1})**
4 - 90	$I\ (A) = 1.42*10^{-7} + 3.63*10^{-9}\ C\ (\mu mol\ L^{-1})$	0.9999	1.97	0.60
90 - 550	$I\ (A) = 4.03*10^{-7} + 1.14*10^{-9}\ C\ (\mu mol\ L^{-1})$	0.9985	/	/

The occurrence of two linear calibration curves in electrochemistry, during the development of electroanalytical quantification methods, is relatively common, but has not been fully explained *(Mehmeti et al., 2017; Petković et al., 2015; Stanković et al., 2017; Stanković et al., 2020c)*. It is assumed that the presence of two linearity types is conditioned by the conditions and processes that are responsible for the redox analyte on the electrode surface. In fact, it is assumed that the electrodes processes are directly influenced by the concentration of the analyte. Namely, in the first segment of linearity, where the calibration curve is constructed from the values of lower concentrations, the diffusion-controlled process is dominant. On the other hand, in the second segment of linearity, where the values of higher analyte concentrations participate in the construction of the curve, the so-called adsorption process would be responsible for the redox behavior of analyte on the electrode surface. It is then assumed that adsorption of reaction products on the electrode surface occurs causing a trapping effect. In this case, further ox/red of analyte take place via the adsorbed layer. This equilibrium-based phenomenon results in a change in the slope value when constructing the calibration line.

If the obtained results were adjusted to this assumption, it is concluded that the diffusion-controlled process, in the region of lower concentrations (up to 90 μmol L^{-1}), was responsible for the oxidation of H_2O_2 on the surface of SPCE/GNR@Bi_2O_3. The next conclusion would be that the adsorption process is responsible for the oxidation of H_2O_2 at concentrations higher than 90 μmol L^{-1}.

4.1.3.2.1. Life-time, reproducibility and repeatability of SPCE/GNR@Bi_2O_3

The life-time of the SPCE/GNR@Bi_2O_3 was analyzed by hydrodynamic chronoamperometry. The experiment lasted 6 days. The amperometric response of the same SPCE/GNR@Bi_2O_3 was monitored daily after successive addition of three different aliquots of 0.0100 mol L^{-1} H_2O_2 standard solution in stirred 0.1 mol L^{-1} PBS (pH = 7.40). *Figure 53.* gives % of SPCE/GNR@Bi_2O_3 life-time depending on the day of analysis for corresponding H_2O_2 concentrations (80 µmol L^{-1}, 150 µmol L^{-1} and 400 µmol L^{-1}). The graph shows that the life-time of the SPCE/GNR@Bi_2O_3, within 6 days, was not below 93%.

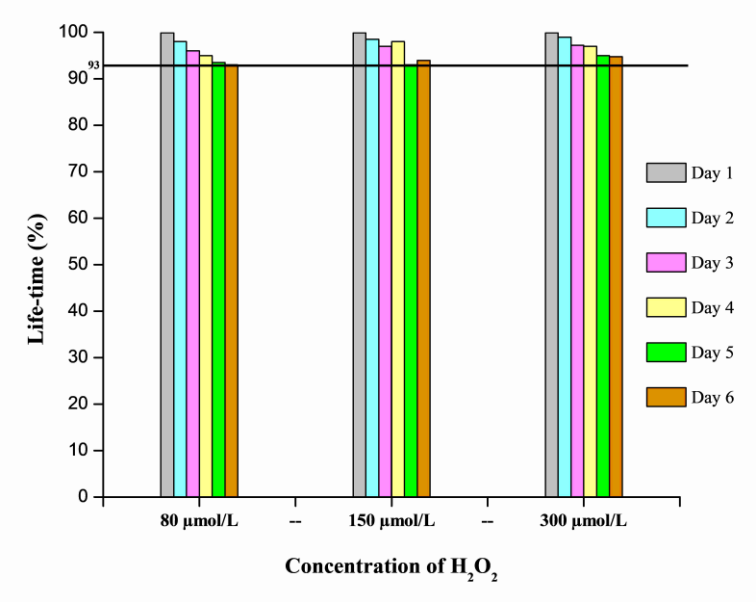

Figure 53. Life-time of the SPCE/GNR@Bi_2O_3 at different concentrations of H_2O_2 depending on the day of analysis.

The reproducibility of the SPCE/GNR@Bi_2O_3 was also determined by hydrodynamic chronoamperometry. The graph (Figure 54) shows the amperometric response of 10 independent SPCE/GNR@Bi_2O_3 after the addition of an aliquot of 500 µL of 0.0100 mol L^{-1} H_2O_2 standard solution in stirred 0.1 mol L^{-1} PBS (pH=7.40). Based on the obtained current intensities, the relative standard deviation (RSD) of the measurements was calculated. RSD was calculated according to *Equation 8*, where is: *S* - standard deviation of the measurement and *X* - average of the current intensity. RSD for the H_2O_2 concentration of 200 µmol L^{-1} measured with 10 independent SPCE/GNR@Bi_2O_3 was 1.33%.

$$\boldsymbol{RSD = {}^{S}/_{\chi} \cdot 100} \qquad \textit{Equation 8.}$$

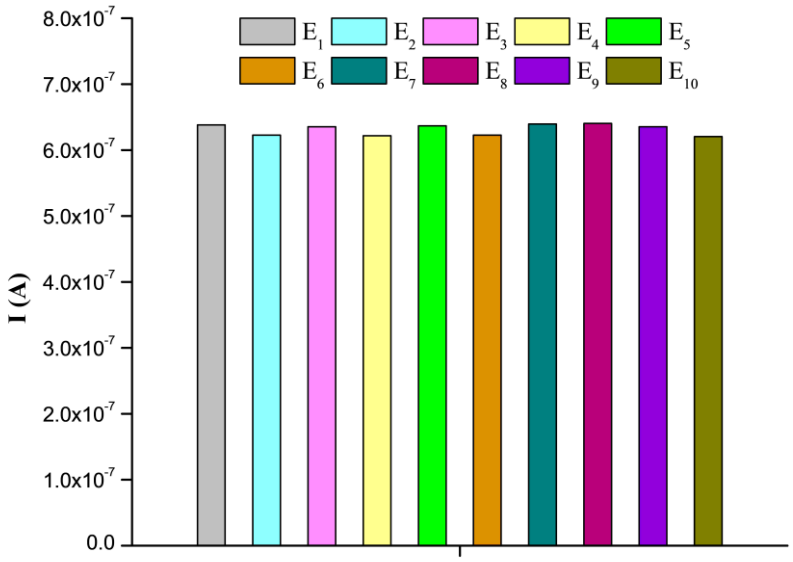

Figure 54. Amperometric response of 10 independent SPCE/GNR@Bi_2O_3 (E_1-E_{10}) for 200 µmol L^{-1} of H_2O_2 to determine reproducibility.

In order to determine the repeatability of SPCE/GNR@Bi_2O_3, three concentrations of H_2O_2 were monitored in 5 consecutive measurements (Figure 55). Also, the hydrodynamic chronoamperometric method was used and stirred 0.1 mol L^{-1} PBS (pH=7.40) was used as supporting electrolyte. Based on the obtained current intensities, RSD was calculated according to *Equation 8*. RSDs for H_2O_2 concentrations of 8 µmol L^{-1}, 200 µmol L^{-1} and 500 µmol L^{-1} were 4.33%, 2.84% and 1.98%, respectively.

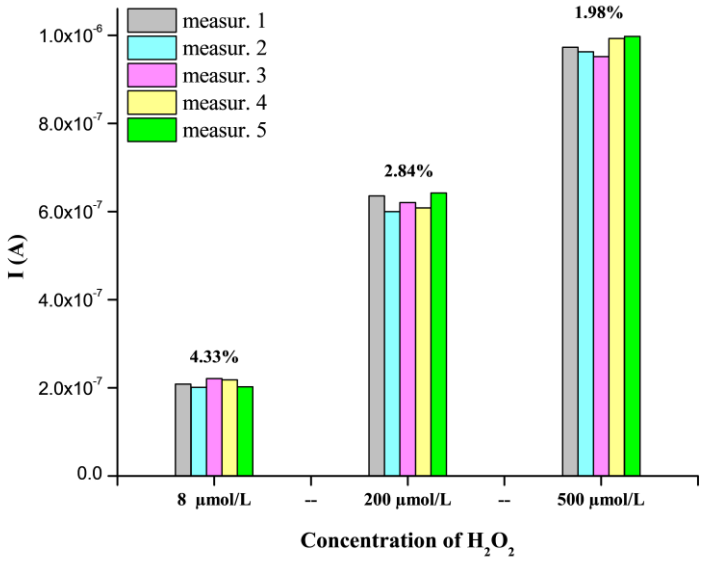

Figure 55. Repeatability of SPCE/GNR@Bi_2O_3 for three different concentration of H_2O_2 (n=5 for each concentration) with corresponding RSDs.

Based on the results obtained, it can be concluded that the electrode exhibits high activity, excellent reproducibility as well as very good precision and repeatability during H_2O_2 quantification.

4.1.3.2.2. Interferences study

Selectivity of SPCE/GNR@Bi_2O_3 was determined by an optimized chronoamperometric method. This experiment was performed to obtain preliminary results in order to partially predict the selectivity of SPCE/GNR@Bi_2O_3/GO_x/Naf biosensor. Considering the potential application of biosensor in food and clinical samples, the effects of sugars, vitamins and hormones on electrochemical performance, first SPCE/GNR@Bi_2O_3 and then biosensor, were examined. Fructose (*Fru*), maltose (*Mal*), ascorbic acid (*Asc*) and dopamine (*Dop*) were used as interfering substances. The potential of electrode was adjusted to 0.6 V. The amperometric response of the SPCE/GNR@Bi_2O_3 was monitored after successive addition of 50 µL of 0.0100 mol L^{-1} H_2O_2 standard solution in 25 mL of stirred 0.1 mol L^{-1} PBS (pH=7.40). Then, the amperometric signal of the H_2O_2 was monitored after the addition of the interfering substances (Figure 56). *Fru* and *Mal* were applied at a concentration of 10 µmol L^{-1}, while 5 times lower concentrations of *Asc* and *Dop* were used (2 µmol L^{-1}). *Figure 56.* shows that the presence of *Fru* and *Mal* does not affect the determination of H_2O_2 by the SPCE/GNR@Bi_2O_3 (changes in the current signals were negligible). On the other hand, addition of *Asc* increases the current signal by 30%. Also, *Dop* was similarly affected during H_2O_2 quantification by SPCE/GNR@Bi_2O_3 (current signal increased by 26%). In summary, amperometric quantification of the H_2O_2 by SPCE/GNR@Bi_2O_3, using an optimized method, can be carried out in the presence of sugars (monosaccharides). On the contrary, in order to quantify the H_2O_2 with the SPCE/GNR@Bi_2O_3 in the presence of ascorbic acid and dopamine, more detailed tests must be carried out. Further analyzes should involve examination of the effect of different concentration levels of these substances on the electrochemical signal of H_2O_2 with SPCE/GNR@Bi_2O_3. Finally, based on these results, similar behavior of SPCE/GNR@Bi_2O_3/GO_x/Naf biosensor, in the presence of interfering substances, was expected.

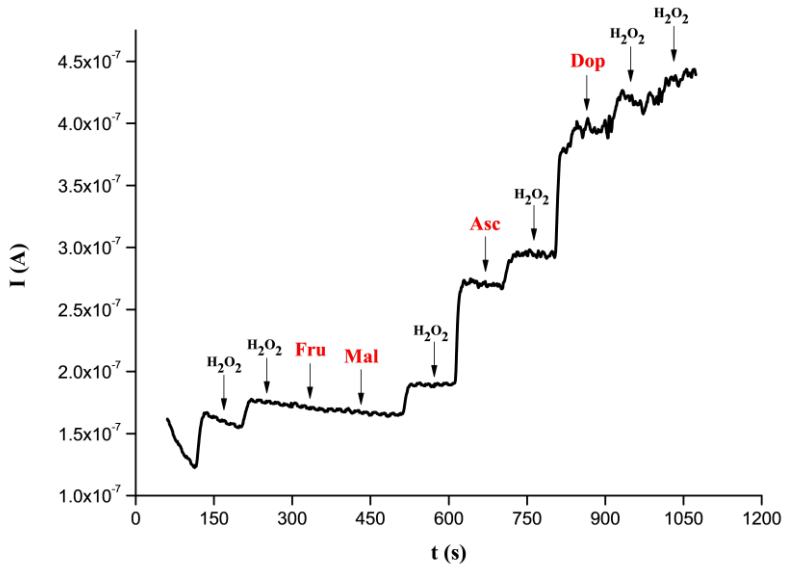

Figure 56. Amperometric response of SPCE/GNR/Bi_2O_3 for successive addition of H_2O_2 in presence of interfering compounds (*Fru* - fructose, *Mal* - maltose, *Asc* - ascorbic acid, *Dop* - dopamine).

4.1.4. SPCE/GNR@Bi_2O_3/GO_x/Naf biosensor performance

In this section, the electrochemical characteristics of the SPCE/GNR@Bi_2O_3/GO_x/Naf by hydrodynamic chronoamperometric method were investigated under optimized experimental and operating conditions (supporting electrolyte was 0.1 mol L^{-1} PBS (pH=7.40); working potential of electrode (biosensor) was adjusted at 0.6 V). After optimizing the amount of GO_x added to the SPCE/GNR@Bi_2O_3, it was optimized the amount of 0.5 % Naf. Then, the working range of the glucose biosensor was examined. The influence of interference on the electrochemical response of the SPCE/GNR@Bi_2O_3/GO_x/Naf was also examined.

4.1.4.1. Optimization of amount of enzyme and Naf added to SPCEs

In order to improve the electrochemical performance, the influence of the amount of enzyme on the amperometric response of the developed biosensor was examined. Volume range of the 10 mg L^{-1} GO_x solution added to the SPCE/GNR@Bi_2O_3 was from 5 µL to 20 µL. In this experiment, 1.5 µL of 5% Naf was used to cover the enzyme. The electrochemical response of the prepared SPCE/GNR@Bi_2O_3/GO_x/Naf was monitored after the addition of 125 µL of 0.1000 mol L^{-1} glucose standard solution in stirred 0.1 mol L^{-1} PBS (pH=7.40), at a potential of 0.6 V. The graph shows that the highest current intensity for 0.5 mmol L^{-1} glucose was obtained with 5 µl of enzyme on the electrode (Figure 57a). Further, the significant decrease in current for the volumes of 15 µL and 20 µL can be explained by the problem encountered during the preparation of the biosensor. Again, as described previously, during the addition of 15 µL and 20 µL of the enzyme, a spillage of the enzyme past the active surface of the SPCE/GNR@Bi_2O_3 was observed. Based on these results, 5 µL was determined as the optimal enzyme amount. Further, all biosensors were prepared with 5 µL of 10 mg L^{-1} GO_x.

After optimizing the amount of enzyme applied to the electrode, the amount of added 5% Naf to the biosensor was optimized. In preparing the biosensor for this experiment, an optimized amount of GO_x (5µL) was added to the SPCE/GNR@Bi_2O_3. A 5% Naf was applied in the range of 1.5 µL to 5.5 µL. As in the previous experimental step, the amperometric responses of the biosensors in 0.5 mmol L^{-1} glucose solution were monitored, at a potential of 0.6 V. The graph shows that the biosensor covered with 2.5 µL of 5% Naf provides the highest current value (Figure 57b). Further increase in the amount of 5% Naf on the biosensor does not lead to a significant change in current. Conversely, a lower value of current was observed at 1.5 µL of 5% Naf. This can be explained by the fact that the amount of 1.5 µL was insufficient to cover the enzyme which led to the enzyme being washed off the electrode. Accordingly, 2.5 µL was determined as the optimum amount of 5 % Naf applied to the electrode.

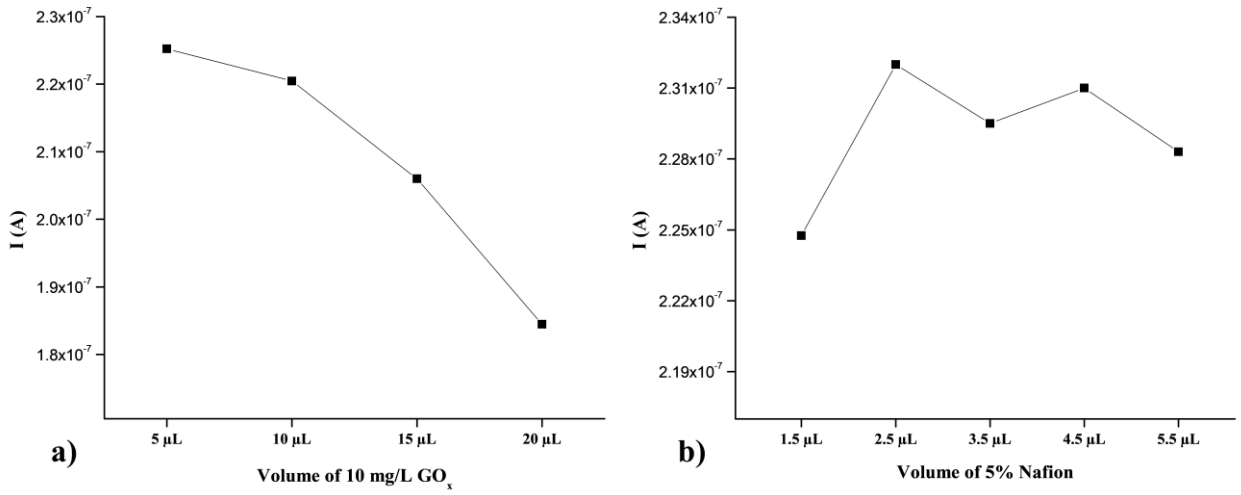

Figure 57. a) Optimization of the amount of 10 mg L^{-1} GOx solution and ***b)*** 5% Naf applied on SPCE/GNR@Bi_2O_3 for the final preparation of glucose biosensor.

4.1.4.2. Amperometric detection of glucose by SPCE/GNR@Bi_2O_3/GO_x/Naf

This chapter describes the development of a method for glucose quantification with a SPCE/GNR@Bi_2O_3/GO_x/Naf under previously optimized experimental and instrumental conditions. A hydrodynamic chronoamperometry method was used for glucose determination. The potential of SPCE/GNR@Bi_2O_3/GO_x/Naf was adjusted to the optimum, 0.6 V. After each 50 seconds, successive aliquots of 0.1000 mol L^{-1} glucose standard solution were added to stirred 0.1 mol L^{-1} PBS (pH=7.40). The amperometric response of the SPCE/GNR@Bi_2O_3/GO_x/Naf was monitored as a function of time (Figure 58a). Based on the obtained current intensity and the applied glucose concentrations, a calibration curve was constructed (Figure 58b). Working range of biosensor to glucose was from 0.28 mmol L^{-1} to 2.50 mmol L^{-1}. However, the working linear range of the SPCE/GNR@Bi_2O_3/GO_x/Naf was from 0.28 mmol L^{-1} to 1.70 mmol L^{-1}. Further increase in glucose concentrations (above 1.70 mmol L^{-1}) results in a deviation of current from linearity. This curve flattening indicates that the active sites on the enzyme were saturated. Further glucose concentration increase causes the current intensity to enter (reach) the flattened part of the curve (*Michaelis-Menten kinetics*). All analytical parameters obtained from the linear part of the calibration curve are summarized in *Table 6.* LOQ and LOD are calculated according to *Equation 6.* and *Equation 7.*, respectively. Sensitivity of developed amperometric method was calculated according to *Equation 9.*, where is: *b* - slope of the regression line and a^2 - active surface area of WE.

$$\boldsymbol{Sensitivity} = {}^{\boldsymbol{b}}/_{\boldsymbol{a^2}} \qquad \textit{Equation 9.}$$

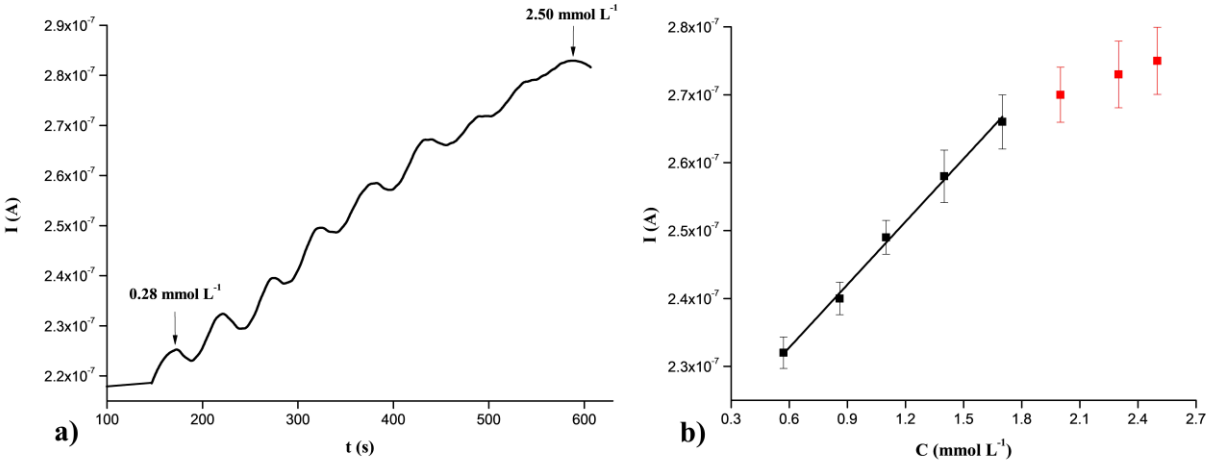

Figure 58. a) Amperometric response at SPCE/GNR@Bi_2O_3/GO_x/Naf at 0.6 V in 0.1 mol L^{-1} PBS (pH=7.40) for successive addition of 0.1000 mol L^{-1} glucose standard solution. ***b)*** Plot of chronoamperometric currents *vs.* glucose concentrations.

Table 6. Summarized electroanalytical parameters for SPCE/GNR@Bi_2O_3/GO_x/Naf.

***C* range (mmol L^{-1})**	**Calibration curve equation**	**LOQ (mmol L^{-1})**	**LOD (mmol L^{-1})**	**Sensitivity (μA (μmol L^{-1}*cm^2)$^{-1}$)**
0.28 - 1.70	$I\ (A) = 2.14*10^{-7} + 3.12*10^{-8}\ C\ (mmol\ L^{-1})$ r=0.9990	0.25	0.07	520

The obtained results were compared with the electrochemical characteristics of graphene@M_xO_y-based enzymatic glucose biosensors reported in the literature. From *Table 2.* it can be seen that the developed SPCE/GNR@Bi_2O_3/GO_x/Naf and the proposed amperometric method provide high sensitivity during determination of glucose. Also, the developed glucose biosensor generally provides similar electroanalytical characteristics such as LOD and concentration linear range compared to given biosensors.

4.1.4.2.1. Activity, reproducibility and repeatability of SPCE/GNR@Bi_2O_3/GO_x/Naf biosensor

An optimized hydrodynamic chronoamperometric method was used to define physico-chemical (activity) and analytical parameters (reproducibility and repeatability) of developed SPCE/GNR@Bi_2O_3/GO_x/Naf. As supporting electrolyte was used 0.1 mol L^{-1} PBS (pH=7.40). The potential of the SPCE/GNR@Bi_2O_3/GO_x/Naf during all amperometric determinations was adjusted to the optimum, 0.6 V.

The activity of the SPCE/GNR@Bi_2O_3/GO_x/Naf were monitored for 7 days. A glucose concentration of 0.86 mmol L^{-1} was used to analyze these parameters. On the first day, at the beginning of the experiment, the current intensity of listed glucose concentration was measured using a single SPCE/GNR@Bi_2O_3/GO_x/Naf electrode. Then, the same electrode was used to determine repeatability where 15 measurements were done. Subsequently, a glucose concentration of 0.86 mmol L^{-1} was re-determined. The current intensity, after 15 measurements, was not below 92% (Figure 59). An activity loss of 8% after 15 measurements indicates excellent activity of SPCE/GNR@Bi_2O_3/GO_x/Naf. After that, storage mode on biosensor activity was monitored daily.

The SPCE/GNR@Bi_2O_3/GO_x/Naf was stored in the refrigerator at 4°C, and a glucose concentration of 0.86 mmol L^{-1} was measured daily under the same conditions (Figure 59). After day 7, biosensor activity was not below 68%.

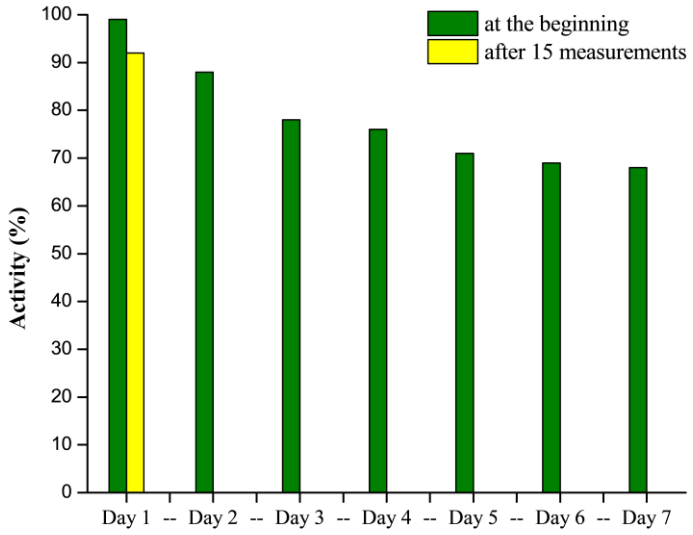

Figure 59. Glucose biosensor activity after 15 measurements with single SPCE/GNR@Bi_2O_3/GO_x/Naf electrode (day 1), as well as activity of SPCE/GNR@Bi_2O_3/GO_x/Naf for 7 days.

Repeatability of the biosensor was determined by measuring three different glucose concentrations with single SPCE/GNR@Bi_2O_3/GO_x/Naf electrode. Glucose concentrations were 0.45 mmol L^{-1}, 0.95 mmol L^{-1} and 1.50 mmol L^{-1}. *Figure 60.* shows the amperometric responses of SPCE/GNR@Bi_2O_3/GO_x/Naf for different glucose concentrations measured in five consecutive measurements. Based on the obtained current intensities, RSDs were calculated for each concentration using *Equation 8.* RSDs for concentrations of 0.95 mmol L^{-1}, 1.90 mmol L^{-1} and 2.40 mmol L^{-1} were 3.61%, 3.12% and 2.63%, respectively.

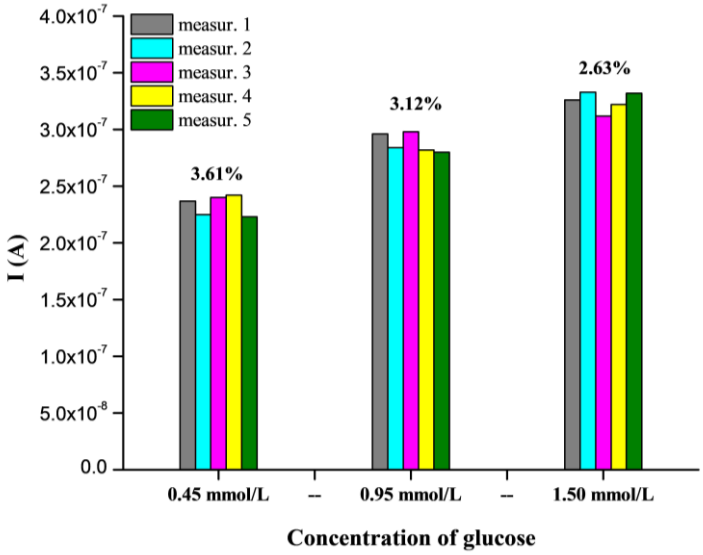

Figure 60. Repeatability of SPCE/GNR@Bi_2O_3/GO_x/Naf obtained for three different glucose concentration measured in five consecutive measurements.

The reproducibility of biosensor was also examined. Amperometric responses of 10 independent SPCE/GNR@Bi_2O_3/GO_x/Naf electrodes were monitored at a glucose concentration of 1.4 mmol L^{-1}. After each finished amperometric measurement, the current intensity was recorded (Figure 61). Based on the current intensity, the RSD of all measurements was calculated over *Equation 8*. RSD was 4.14%.

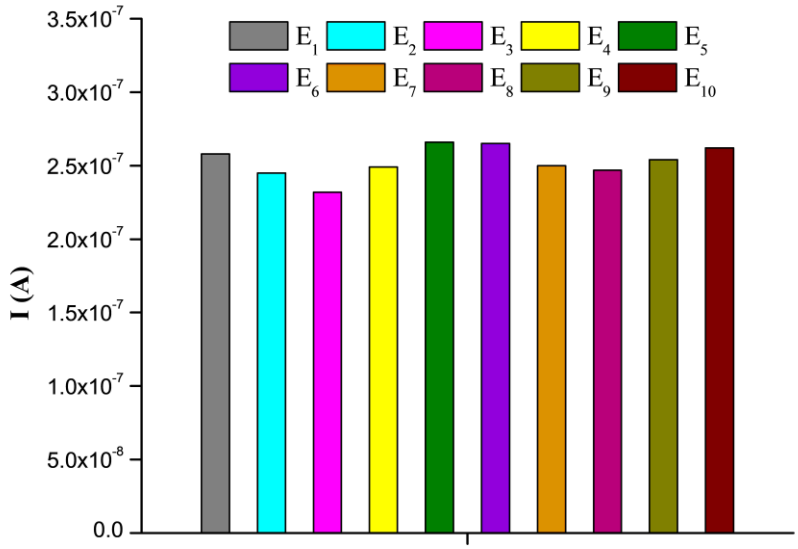

Figure 61. Amperometric responses of ten SPCE/GNR@Bi_2O_3/GO_x/Naf independent electrodes (E_1-E_{10}) for 1.40 mmol L^{-1} glucose concentration in order to determine a reproducibility.

Based on the summarized results, it can be concluded that the SPCE/GNR@Bi_2O_3/GO_x/Naf provide high activity and stability. In addition, the biosensor showed excellent analytical parameters such as precision, reproducibility and repeatability during glucose quantification by optimized amperometric method.

4.1.4.2.2. Selectivity of SPCE/GNR@Bi_2O_3/GO_x/Naf biosensor

The selectivity of the SPCE/GNR@Bi_2O_3/GO_x/Naf was determined similarly to the SPCE/GNR@Bi_2O_3. As mentioned, the electrochemical performance of glucose biosensor in the presence of sugars, vitamins and hormones were examined due to potential application of developed biosensor in real samples. The amperometric response of SPCE/GNR@Bi_2O_3/GO_x/Naf was monitored after successive addition of 250 µL of 0.0100 mol L^{-1} glucose standard solution in 25 mL of stirred 0.1 mol L^{-1} PBS (pH=7.40). This was followed by additions of the interference (Figure 62). *Fru* and *Mal* were applied at a concentration of 10 µmol L^{-1}, while *Asc* and *Dop* were used at a concentration of 2 µmol L^{-1}. Similar to the SPCE/GNR@Bi_2O_3, *Fru* and *Mal* do not affect the quantification of glucose by the developed SPCE/GNR@Bi_2O_3/GO_x/Naf. Contrary to the SPCE/GNR@Bi_2O_3, the SPCE/GNR@Bi_2O_3/GO_x/Naf was selective to glucose in the presence of *Asc*. Changes in glucose current signal with biosensor after addition of *Asc* were negligible (current signal increased by 3%). However, as predicted, dopamine has a negative impact on glucose quantification. The glucose current signal after addition of dopamine increased by 70%. This *Dop* behavior was expected since this compound is oxidized at positive potential values *(Shahrokhian & Bozorgzadeh, 2006; Shahrokhian & Zare-Mehrjardi, 2007; Shahrokhian & Zare-Mehrjardi, 2007)*. In

summary, the developed biosensor and the proposed method could potentially be applied for the quantification of glucose in clinical samples (for example blood and urine samples), since the pH of the supporting electrolyte was selected at 7.40, which simulates physiological conditions. However, in this case, the level of dopamine in the clinical samples should be strictly known, which requires further detailed testing and analysis. On the other hand, since the SPCE/GNR@Bi_2O_3/GO_x/Naf showed selectivity to glucose in the presence of sugars and vitamins, it could be, with an optimized amperometric method, applied in food and beverage samples.

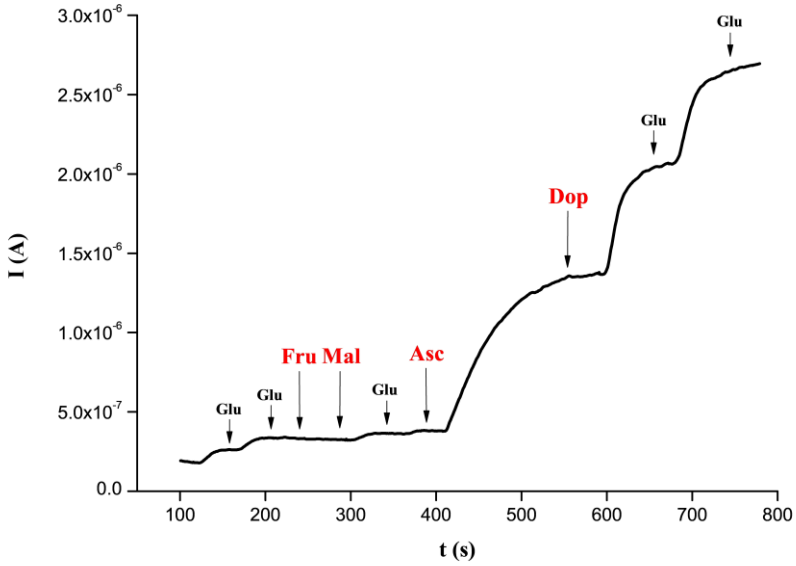

Figure 62. Selectivity of SPCE/GNR@Bi_2O_3/GO_x/Naf at glucose in the presence of *Fru*, *Mal*, *Asc* and *Dop*.

4.1.4.3. Application of SPCE/GNR@Bi_2O_3/GO_x/Naf biosensor in honey sample

In order to validate the developed SPCE/GNR@Bi_2O_3/GO_x/Naf and the optimized amperometric method, glucose content of a honey sample, which represents the *PT* scheme, was determined. As noted, the declared glucose content in the honey sample was 32.6%. The sample was prepared by dissolving 201.9 mg of honey in 25 mL of 0.1 mol L^{-1} PBS (pH=7.40). The glucose concentration in the solution thus prepared was 0.015 mol L^{-1} (*solution A*). Then, aliquots of 1 mL and 2 mL of solution *A* were added to 24 mL and 23 mL of 0.1 mol L^{-1} PBS (pH=7.40), respectively, and directly analyzed by SPCE/GNR@Bi_2O_3/GO_x/Naf. Glucose concentrations of 0.6 mmol L^{-1} and 1.2 mmol L^{-1} were analyzed in this way, respectively. Then, *solution A* was diluted twice and a glucose concentration of 0.0075 mol L^{-1} (*solution B*) was obtained. Aliquots of 3 mL, 4 mL and 5 mL of solution *B* were analyzed in the same way as aliquots of solution *A*. In this case, glucose concentrations of 0.9 mmol L^{-1}, 1.2 mmol L^{-1} and 1.5 mmol L^{-1} were analyzed, respectively. This analysis of the honey sample was carried out in order to determine the accuracy and precision of the developed method. *Figure 63.* shows a comparison of the calculated glucose content with the declared value. Corresponding recovery values were calculated in relation to the declared value. Recovery (95.0-99.4%) shows that the developed SPCE/GNR@Bi_2O_3/GO_x/Naf and the proposed amperometric method provide high accuracy and precision during glucose quantification, with minimal impact of the matrix effect.

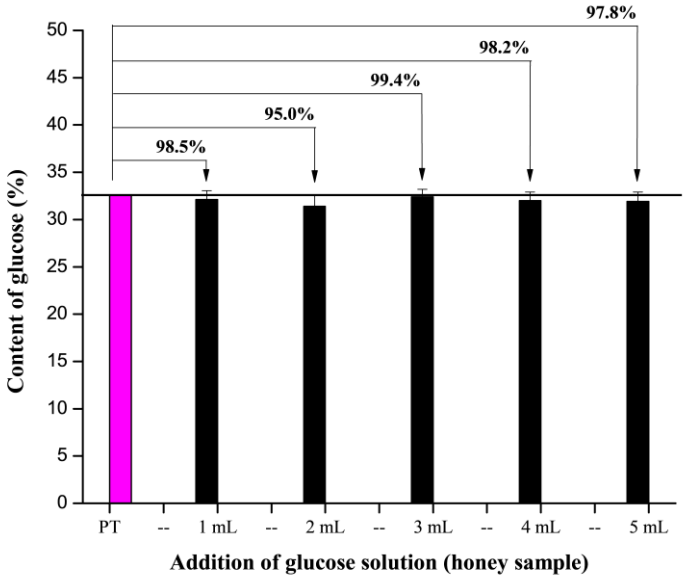

Figure 63. Comparison of glucose content (%) of *PT* scheme with calculated glucose content (%) obtained with SPCE/GNR@Bi_2O_3/GO_x/Naf for different aliquots of honey sample. Recovery was calculated in relation to the declared value (32.6%).

4.2. Polyphenolic index biosensor

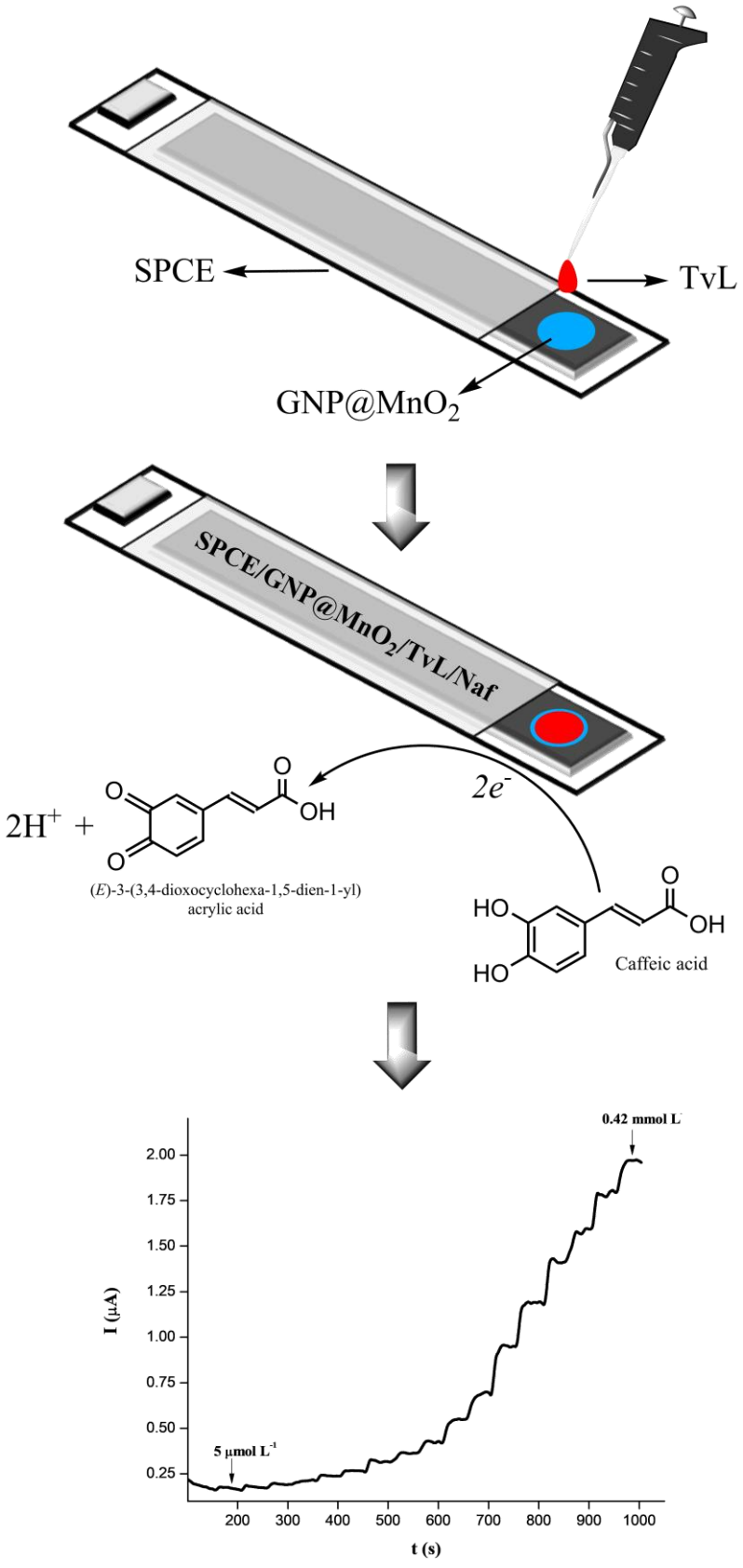

Figure 64. An overview of the main experimental steps related to the preparation of polyphenolic index biosensor followed by amperometric response of the developed biosensor toward caffeic acid.

The second part of the chapter *RESULTS AND DISCUSSION* refers to the results obtained during the development of the of polyphenolic index biosensor. *Figure 64.* represent mean experimental steps during preparation of polyphenolic index biosensor, as well as amperometric response of developed biosensor toward caffeic acid as mean analyte.

This study was based on the modification of SPCE with GNP@MnO_2 nanocomposite and the examination of the electrochemical characteristics of the obtained WE. SPCE/GNP@MnO_2 was then modified with enzyme laccase in the order to produce a polyphenolic index biosensor. Caffeic acid, as model compound, was used for optimization of all experimental and instrumental parameters. The aim of the study was to examine the working linear range of biosensor toward caffeic acid and compare the obtained results with the performances of polyphenolic biosensors reported in the literature, in order to evaluated developed biosensors and proposed method. The final step involved the application of developed biosensor in real samples.

The synthesis of MnO_2 and GNP@MnO_2 nanocomposites was performed primarily. Therefore, the first part of the results includes the characterization of nanomaterials and synthesized nanocomposites. The crystal structure and the shape and particle size of all samples were determined by XRPD and FE-SEM methods, respectively.

After confirmation of the nanomaterials and nanocomposite structures, electrochemical measurements followed.

Cyclic voltammetry is the first method used in electrochemical testing. The first experiments were related to the optimization of the amount of nanocomposites added to the SPCE, as well as the examination of system reversibility using modified SPCEs. Also, a comparison of the electrochemical performances of modified SPCEs in caffeic acid as the main analyte was done. After that, the laccase form *Trametes Versicolor* (TvL) was immobilized on the modified SPCE and the appropriate supporting electrolyte was selected using the obtained biosensor.

The next part of the results includes amperometric measurements using the developed polyphenolic index biosensor. After the optimization of the working potential, the working linear range of the biosensor toward caffeic acid was examined by the hydrodynamic chronoamperometry method. Important electroanalytical parameters such as LOD, LOQ, sensitivity, precision, reproducibility and repeatability were determined. Also, the activity of developed biosensor was monitored for a week. In addition, the effect of different interfering substances was examined on the amperometric response of the polyphenolic index biosensor to caffeic acid.

The final part of the electrochemical results was based on the application of polyphenolic index biosensor in wine samples and the determination of polyphenolic content in them. After that, under optimized experimental and instrumental conditions, the polyphenolic content in the same wine samples was determined by GCE. This experiment was done in order to validate the proposed amperometric method and the developed polyphenolic index biosensor.

4.2.1. Characterization of nanocomposites by XRPD and FE-SEM methods

The XRPD profiles of MnO_2, GNP and GNP@MnO_2 nanocomposite were presented at *Figure 65*. The XRDP profile of MnO_2 (*pink line*) was defined by diffraction peaks at 12.8°, 18.2°, 28.8°, 37.7°, 42.4°, 50.0° 56.4° and 60.2° at 2θ. The mentioned peaks are in accordance with (110), (200), (310), (211), (301), (411), (600) and (521) crystal planes of α-MnO_2, respectively (JCPDS card#44-0141) *(Yang et al., 2017)*. The GNP diffraction profile shows a very sharp peak at 25.9° at 2θ (*green line*). According to Bragg's law, the sharp peak of GNP corresponds to a distance between graphene layers of 3.3 Å, as well as a high crystallinity (002) of GNP. The diffraction peaks of GNP at 42.2°, 44.0°, and 53.7° are consistent with the reflection of (100), (101) and (004) planes. This indicates that GNP were not fully exfoliated *(Parveen et al., 2016)*. Finally, the XPDR profile of GNP@MnO_2 (*grey line*) shows the presence of individual diffraction profiles of GNP and MnO_2 indicating successful GNP@MnO_2 nanocomposite synthesis.

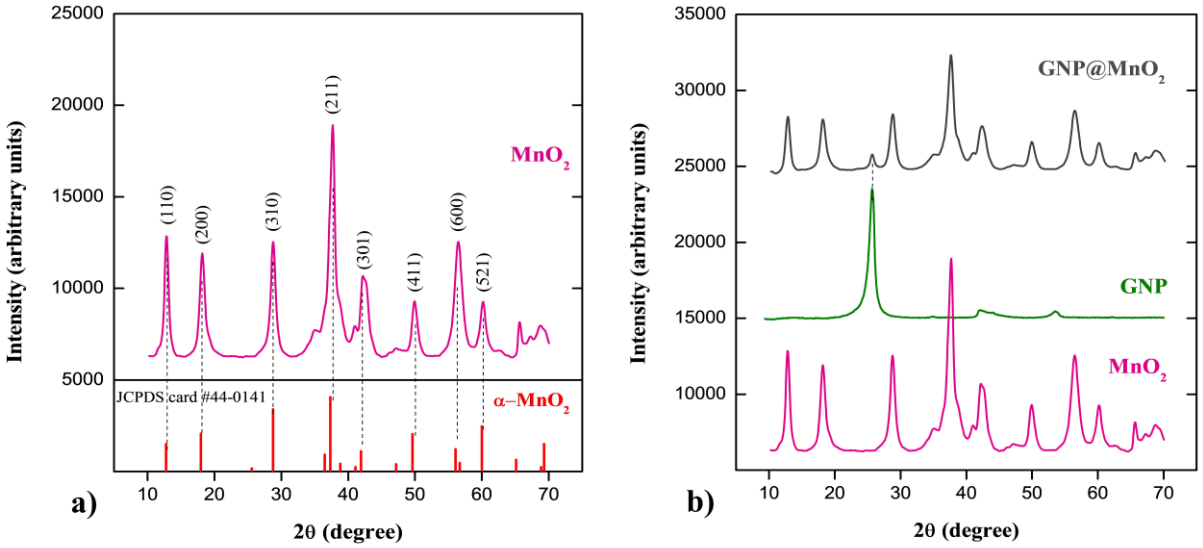

Figure 65. a) XRPD profiles of MnO_2 compared with standard data of α-MnO_2 (JCPDS card #44-0141). ***b)*** Diffraction patterns of MnO_2 nanoparticles (*pink line*), GNP (*green line*) and GNP@MnO_2 nanocomposite (*grey line*).

Morphology of MnO_2 nanoparticles, GNP and GNP@MnO_2 nanocomposite was observed by FE-SEM method. Considering the FE-SEM micrographs given in *Figure 66*, it is observed that the GNP sheets are flat, thin, transparent and free of other impurities on a smooth surface. In addition, a partial grouping of wavy GNP sheets was observed. The diameter of the GNP sheets was between 2 and 4 nm. FE-SEM micrographs of pure MnO_2 nanopowder are given in *Figure 67*. MnO_2 nanoparticles were spherical in shape and packed on top of each other. The average diameter of MnO_2 nanoparticles was 153±2 nm. Finally, FE-SEM micrographs of GNP@MnO_2 nanocomposite shown that MnO_2 nanoparticles were randomly distributed and strongly bound to the surface of GNP nanomaterials (Figure 68). Also, MnO_2 nanoparticles were observed to be inserted between graphene sheets, resulting in the separation of closely packed GNP sheets. This unique nanocomposite morphology significantly increases the active surface of the electrode, as well as the conductivity and electron transfer rate. Also, successful GNP@MnO_2 nanocomposite synthesis was confirmed by EDS mapping method (Figure 69).

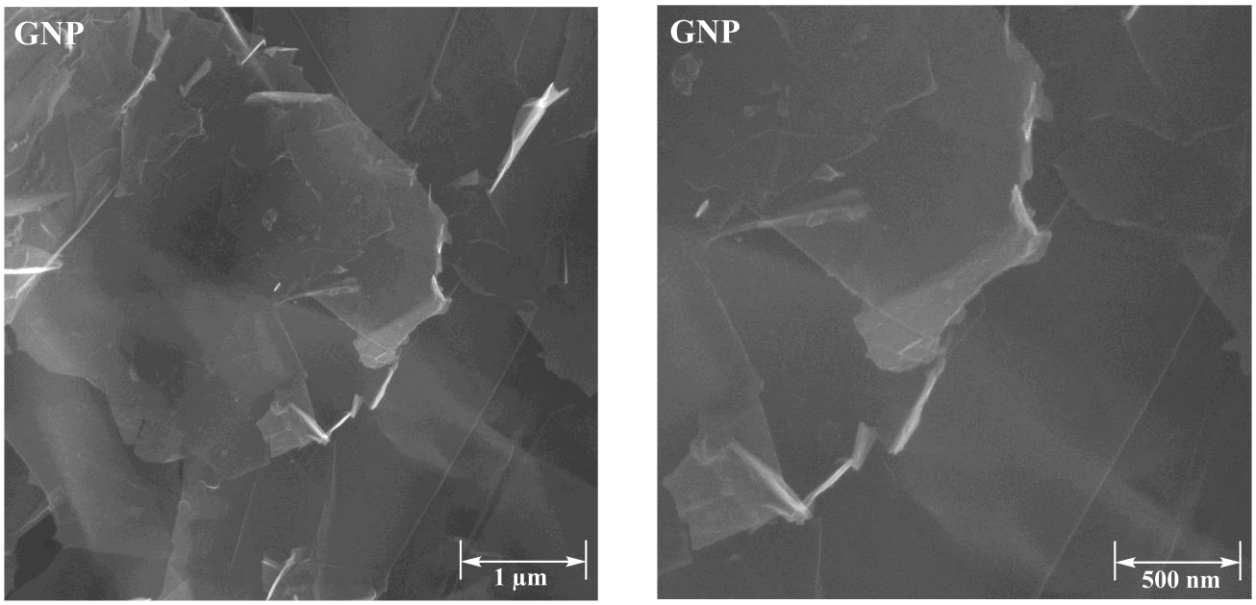

Figure 66. FE-SEM micrographs of pure GNP nanocomposite. Magnified $50*10^3$ times (left) and $100*10^3$ times (right).

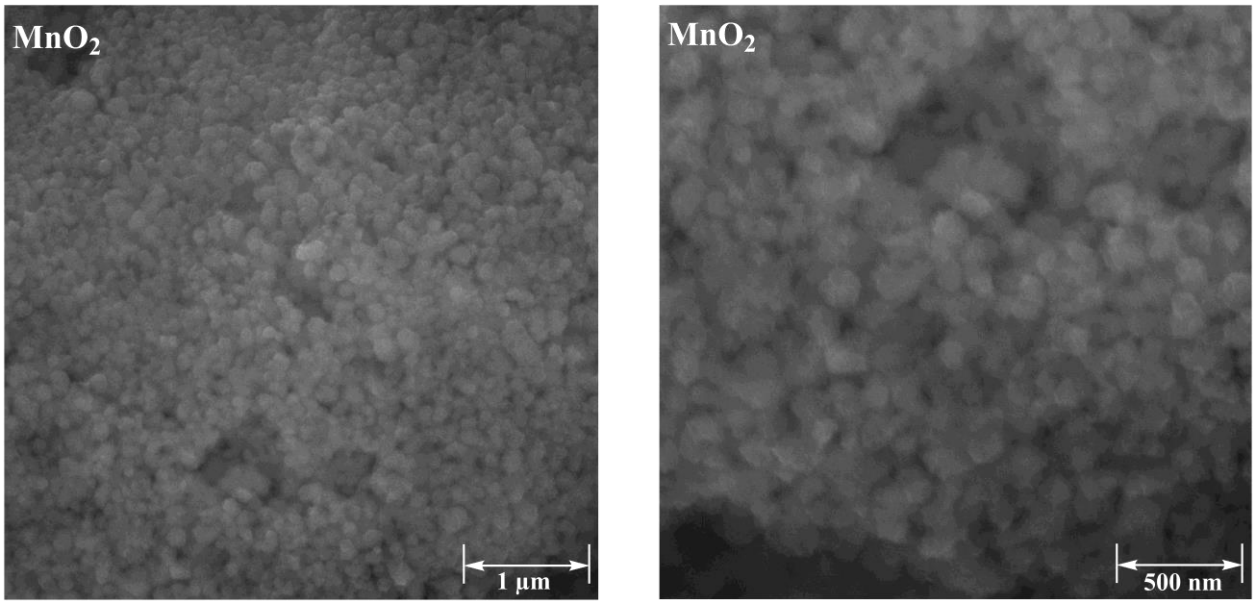

Figure 67. FE-SEM micrographs of pure MnO_2 nanopowder. Magnified $50*10^3$ times (left) and $100*10^3$ times (right).

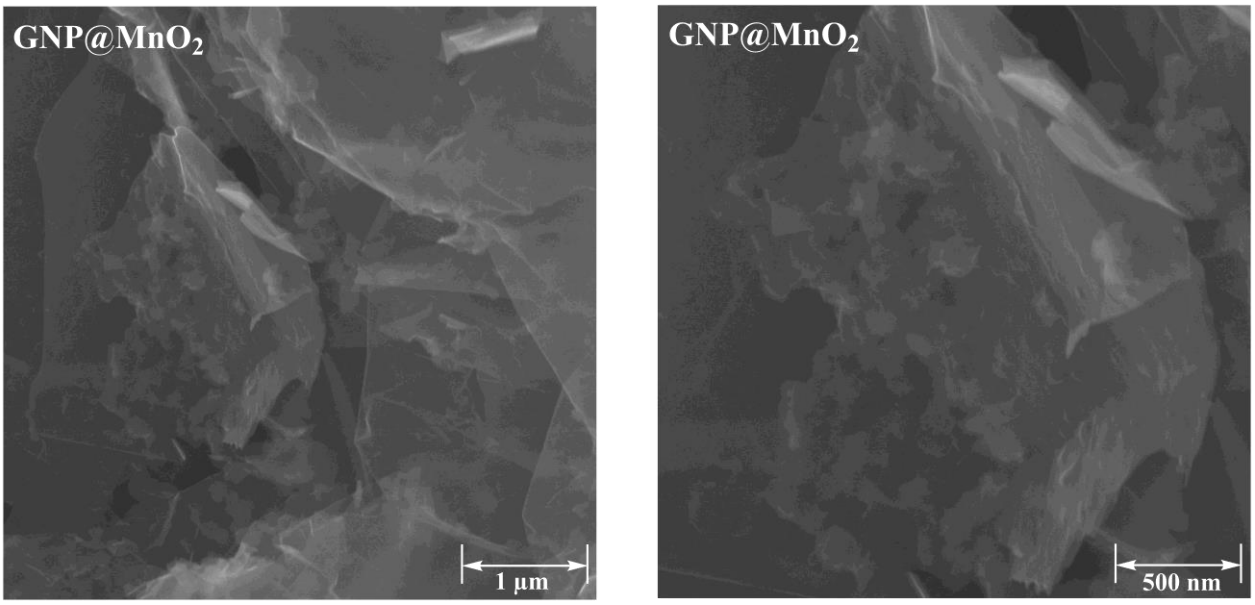

Figure 68. FE-SEM micrographs of GNP@MnO_2 nanocomposite. Magnified $50*10^3$ times (left) and $100*10^3$ times (right).

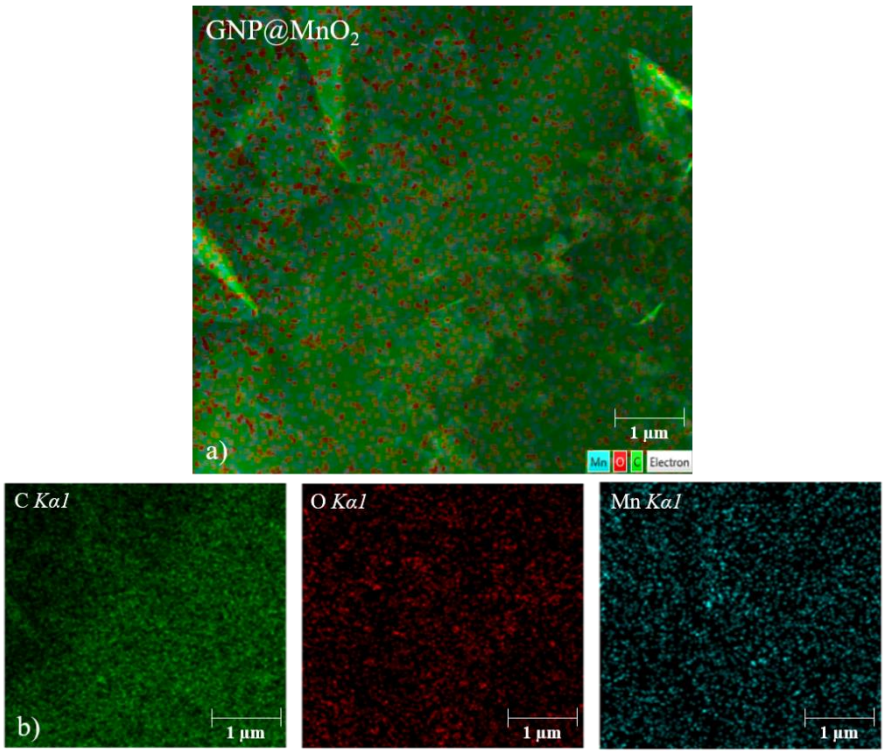

Figure 69. a) EDS mapping of GNP@MnO_2 nanocomposite. ***b)*** EDS mapping of carbon (*C*), oxygen (*O*) and manganese (*Mn*) atom. Magnification of $50*10^3$ times.

4.2.2. Cyclic voltammetry

4.2.2.1. Optimization of amount of nanocomposite added to SPCEs

The amount of the solution of 2 mg mL^{-1} GNP@MnO_2 nanocomposite applied to the SPCE was optimized by cyclic voltammetry. The influence of 1 µL, 5 µL and 10 µL of nanocomposite on the electrochemical behavior of the SPCEs was monitored. In the first part of this experiment, the electrochemical responses of the SPCEs were followed in presence of 5 mmol L^{-1} $[Fe(CN)_6]^{4-}$ /$[Fe(CN)_6]^{3-}$ in 0.1 mol L^{-1} PBS (pH=6.50). Scan rate was 50 mV s^{-1}. Modified SPCEs gave oxidation and reduction peaks of the given analyte. *Figure 70a.* shows the current intensity of oxidation and reduction peak depending on the amount of nanocomposite added to the SPCE. It is observed that the current intensity of redox peaks increases with increasing amount of nanocomposite. There is a possibility that larger amounts of GNP@MnO_2 nanocomposite would give better electrochemical performance, but as mentioned earlier, 15 µL and 20 µL of nanocomposite were attempted to be applied to the SPCEs, but spillage of nanocomposite beyond the active electrode surface was observed. Therefore, amounts greater than 10 µL were not considered.

The second part of the experiment involved monitoring the behavior of SPCEs modified with 1 µL, 5 µL and 10 µL of 2 mg mL^{-1} GNP@MnO_2 nanocomposite in the presence of caffeic acid as the main analyte. Electrochemical responses of modified SPCEs were followed in 0.1 mol L^{-1} PBS (pH=6.50) containing 0.1 mmol L^{-1} caffeic acid by cyclic voltammetry. Scan rate was 50 mV s^{-1}. All three SPCEs showed oxidation and reduction of caffeic acid. In this experiment, too, the current intensities were monitored depending on the added amount of nanocomposite. As can be seen in *Figure 70b.*, the amount of 5 µL of nanocomposite gives a higher current intensity compared to 1 µL for both peaks. On the other hand, minimal differences were observed between amounts of 5 µL and 10 µL, especially in the intensity of oxidation peak of caffeic acid (the difference in the current signal was up to 1%). The current intensities of the reduction peaks for the nanocomposite amounts of 5 µL and 10 µL differ by 9%. However, in this experiment, emphasis was placed on the oxidation of caffeic acid. The SPCE modified with the GNP@MnO_2 nanocomposite will be further modified with laccase in order to prepare the polyphenolic index biosensor. Since laccase is an oxidative enzyme that oxidizes caffeic acid, the oxidation peak of caffeic acid will be monitored in all further experiments.

Comparing the results obtained in both analytes, differences in electrochemical performance of modified SPCEs were observed. Since caffeic acid is the main analyte in this experiment, priority was given to the results obtained during the study of electrochemical behaviors of modified SPCEs in this analyte. Furthermore, as mentioned, there is no significant difference in current between the nanocomposite amounts of 5 µL and 10 µL at the oxidation peak of caffeic acid. Accordingly, 5 µL was selected as the optimal amount applied to the SPCE. In summary, for all further tests, SPCEs were modified with 5 µL of GNP@MnO_2 nanocomposite. In addition, in order to prepare all WEs, the SPCEs were modified with 5 µL of GNP and MnO_2 nanocomposites.

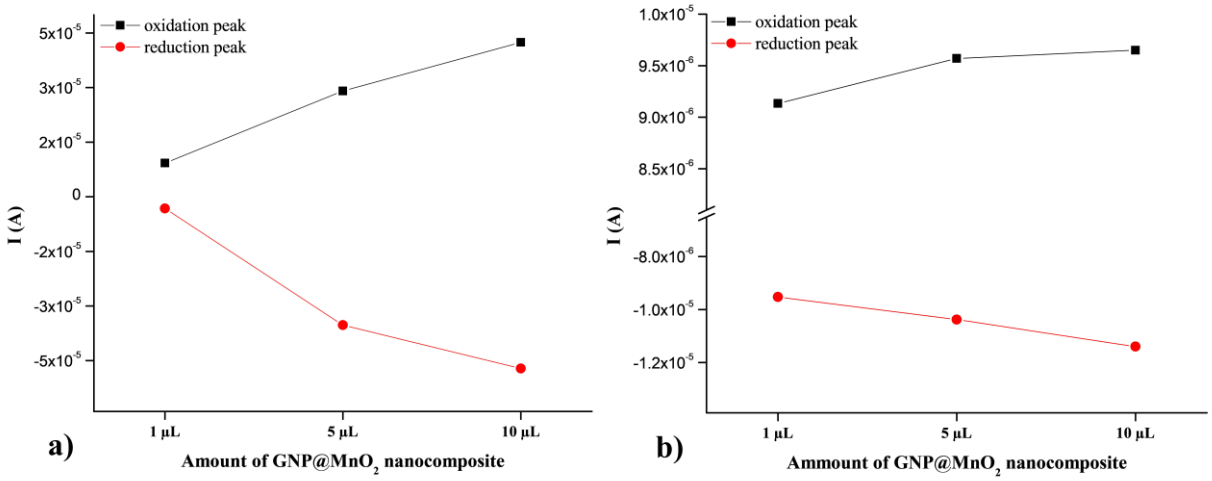

Figure 70. Plot of current intensity of redox peaks (*I*) *vs.* amount of GNP@MnO_2 nanocomposite added to the SPCEs obtained for ***a)*** 5 mmol L^{-1} $[Fe(CN)_6]^{4-}/[Fe(CN)_6]^{3-}$ and ***b)*** 0.1 mmol L^{-1} caffeic acid. Supporting electrolyte, in both cases, was 0.1 mol L^{-1} PBS (pH=6.50). Scan rate was 50 mV/s.

4.2.2.2. Electrochemical behavior of SPCEs

Electrochemical responses of SPCEs (unmodified SPCE, SPCE/GNP, SPCE/MnO_2 and SPCE/GNP@MnO_2) were investigated by cyclic voltammetry. As analyte was used 5 mmol L^{-1} $[Fe(CN)_6]^{4-}/[Fe(CN)_6]^{3-}$ in 0.1 mol L^{-1} PBS (pH=6.50). Scan rate was 50 mV s^{-1}. Applied potential was from -0.5 V to 1.0 V. Cyclic voltammograms indicate that all WEs provide an oxidation and reduction peaks of tested system (Figure 71). The SPCE/MnO_2 electrode gives the lowest current of the oxidation peak, while the intensity of the reduction peak was slightly higher. Unmodified SPCE and SPCE/GNP electrode gives similar electrochemical responses to the tested system, but significantly better than SPCE/MnO_2. Contrary to the mentioned WEs, SPCE/GNP@MnO_2 provide the best electrochemical characteristics. The performances were reflected in the highest current intensities, but also in the best-defined shape of the oxidation and reduction peak compared to other WEs. Such results indicate that the synergistic effect of GNR and MnO_2 nanoparticles influence on the increase of electrical conductivity, the active surface of electrode, as well as the diffusion layer expansion. This confirms, as mentioned in the glucose biosensor, that the combination of graphene nanomaterials and M_xO_y nanoparticles significantly improves the electrochemical performance of WEs.

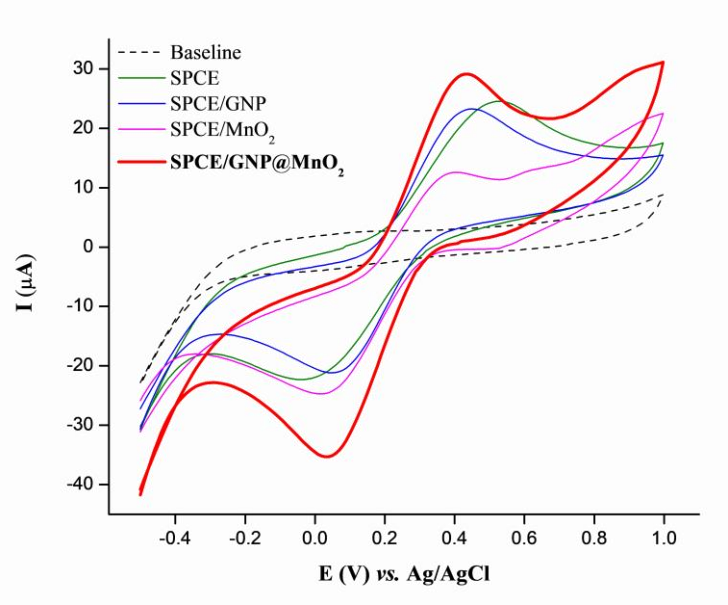

Figure 71. Cyclic voltammograms obtained with unmodified SPCE, SPCE/GNP, SPCE/MnO_2 and SPCE/GNP@MnO_2 in 0.1 mol L^{-1} PBS (pH=6.50) containing 5 mmol L^{-1} $[Fe(CN)_6]^{4-}$/$[Fe(CN)_6]^{3-}$. Scan rate was 50 mV s^{-1}.

4.2.2.2.1. Effect of scan rate at unmodified SPCE and SPCE/GNP@MnO_2

The effect of scan rate at electrochemical response of unmodified SPCE and SPCE modified with GNP@MnO_2 nanocomposite was examined in 0.1 mol L^{-1} PBS (pH=6.50) containing 5 mmol L^{-1} $[Fe(CN)_6]^{4-}$/$[Fe(CN)_6]^{3-}$. Scan rate was applied in the range from 10 to 200 mV s^{-1}. *Figure 72.* shows, in the case of both WEs, there is an increase in the current intensity of the anodic and cathodic peaks with increasing scan rates. There is also a linear shift of the anodic (I_{pa}) and cathodic (I_{pc}) peaks towards more positive and more negative potential values, respectively, providing a constant value of ΔE (Figure 72). Such measurements and high values of ΔE (around 0.3 V) indicates that the reactions on the surface of WEs were rather irreversible.

Using data obtained after scan rate measurements, the active surface area of unmodified SPCE and SPCE/GNP@MnO_2 was calculated using *Equation 2*. Active surface area of unmodified SPCE was 182 mm^2, while the SPCE/GNP@MnO_2 was characterized by an active surface area of 400 mm^2, showing that the active surface area of SPCE was significantly increased after modification with GNP@MnO_2 nanocomposite. The stated values of the active surface area of the WEs represent the average values obtained after calculating the active surface area from intensity of anodic peak (I_{pa}) for each applied scan rate.

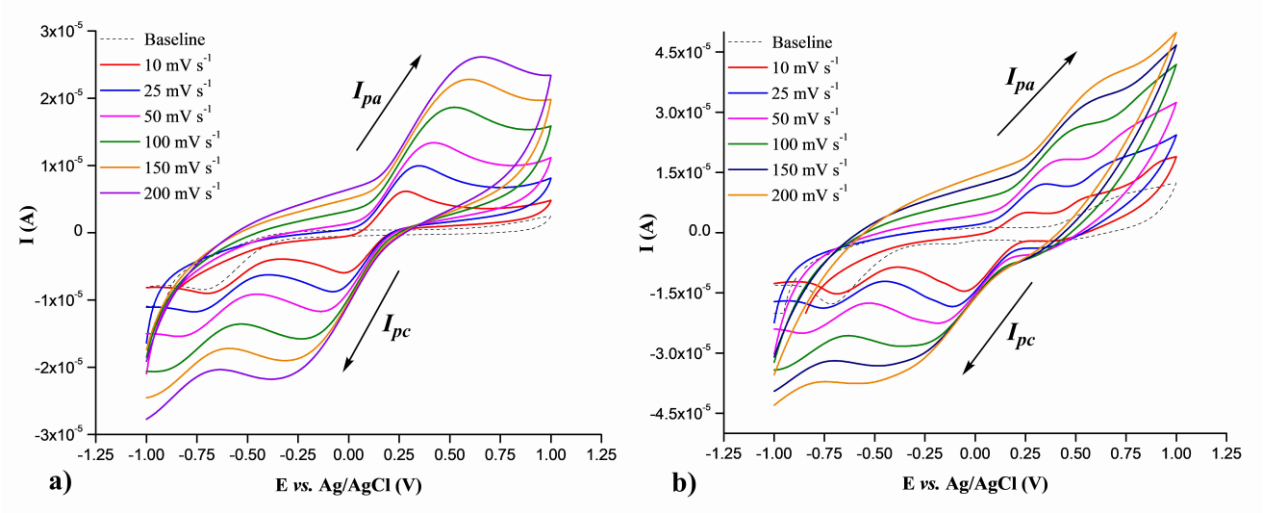

Figure 72. Cyclic voltammograms for 5 mmol L^{-1} $K_3[Fe(CN)_6]/K_4[Fe(CN)_6]$ in 0.1 mol L^{-1} PBS (pH=6.50) at different scan rates (10-200 mV s^{-1}) recorded with ***a)*** unmodified SPCE and ***b)*** SPCE/GNP@MnO_2.

4.2.2.2.2. Electrochemical behavior of SPCEs in presence of caffeic acid

Comparison of the WEs was performed in the main analyte by cyclic voltammetry. Electrochemical responses of SPCEs were monitored in the presence of 0.1 mmol L^{-1} caffeic acid in 0.1 mol L^{-1} PBS (pH=6.50). Cyclic voltammograms showed that caffeic acid was oxidized and reduced at the electrode surfaces (Figure 73). As in the previous case, the SPCE/GNP@MnO_2 electrode gives the highest intensity of the anodic and cathodic peaks, as well as the best-defined shapes of these peaks. Again, the same conclusion was reached - combination of these two promising modification materials (GNP and MnO_2) significantly improves the electrochemical performance of SPCEs.

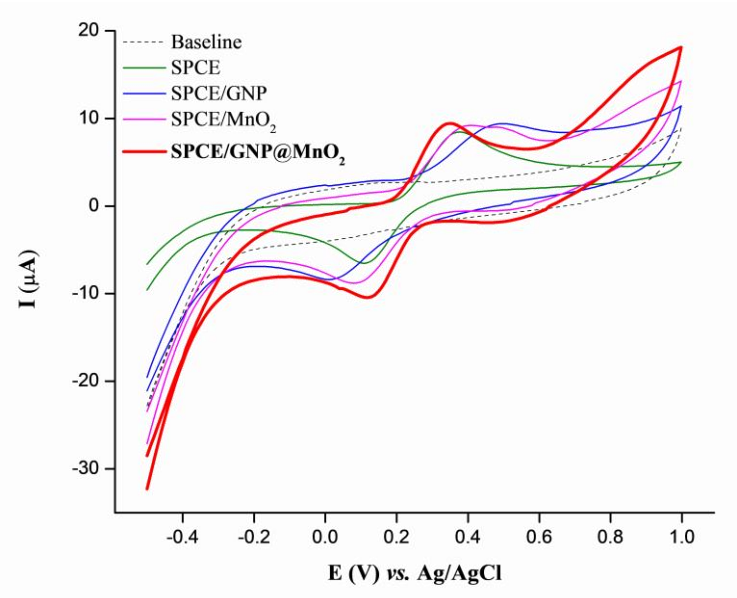

Figure 73. Cyclic voltammograms obtained with unmodified SPCE, SPCE/GNP, SPCE/MnO_2 and SPCE/GNP@MnO_2 working electrodes in presence of 0.1 mmol L^{-1} caffeic acid. Supporting electrolyte was 0.1 mol L^{-1} PBS (pH=6.50). Scan rate was 50 mV s^{-1}.

After electrochemical characterization of SPCEs modified with appropriate nanocomposites and definition of their electrochemical performances in $[Fe(CN)_6]^{4-}/[Fe(CN)_6]^{3-}$ redox system, as well as mean analyte, preparation of polyphenolic index biosensor followed. As mentioned earlier, TvL, and then Naf, were immobilized on the SPCE/GNP@MnO_2 surface by "*drop coating*" technique in order to prepare SPCE/GNP@MnO_2/TvL/Naf polyphenolic index biosensor. Accordingly, all further electrochemical measurements related to the optimization of experimental and instrumental steps were carried out with the developed SPCE/GNP@MnO_2/TvL/Naf.

4.2.2.3. Selection of supporting electrolyte. Effect of pH in the biosensor performances

Electrochemical performances of SPCE/GNP@MnO_2/TvL/Naf were investigated in two supporting electrolytes. Electrochemical responses of developed biosensor in 0.1 mol L^{-1} ABS and 0.1 mol L^{-1} BRBS were monitored by cyclic voltammetry. As analyte was used 0.3 mmol L^{-1} caffeic acid. Potential window was from -0.5 V to 1.0 V, while scan rate was 50 mV S^{-1}. Applied pH of 0.1 mol L^{-1} ABS and 0.1 mol L^{-1} BRBS was from 4.00 to 5.30, because laccase enzyme shows its highest activity in this range. Cyclic voltammograms in the *Figure 74*. show the presence of an anodic (oxidation) and cathodic (reduction) peaks. The anodic peak originates from the oxidation of caffeic acid by enzyme (biosensor), while the reduction peak occurs as a result of the reduction of O_2 from water at the electrode. Namely, during the oxidation of caffeic acid, Cu^{2+} from the active site of laccase is reduced to Cu^{+}. In order to regenerate the laccase active site, Cu^{+} is oxidized to Cu^{2+} by oxygen from medium, while the oxygen itself is reduced to H_2O, creating a reduction peak. Voltammograms show a clear difference in anodic peaks in 0.1 mol L^{-1} ABS (Figure 74a) and 0.1 mol L^{-1} BRBS (Figure 74b) depending on the applied pH. Also, it can be seen that 0.1 mol L^{-1} ABS give a better-defined anodic peak of caffeic acid, compared to the same peak in 0.1 mol L^{-1} BRBS. In addition, the current intensity of caffeic acid in 0.1 mol L^{-1} ABS was slightly higher than in 0.1 mol L^{-1} BRBS. *Figure 74a.* shows that the highest intensities of anodic peaks were obtained with pH 4.40 and 4.60. Applying pH=5.00 and higher, a decrease in the anodic peak of caffeic acid was observed, which clearly indicates a decrease in enzyme activity. Comparing the electrochemical performance of the anodic peak at pH=4.40 and pH=4.60, it is noted that pH=4.60 gives a sharper and better-defined shape of peak. Based on these results, 0.1 mol L^{-1} ABS (pH=4.60) was selected as the optimal supporting electrolyte for all further experiments and tests.

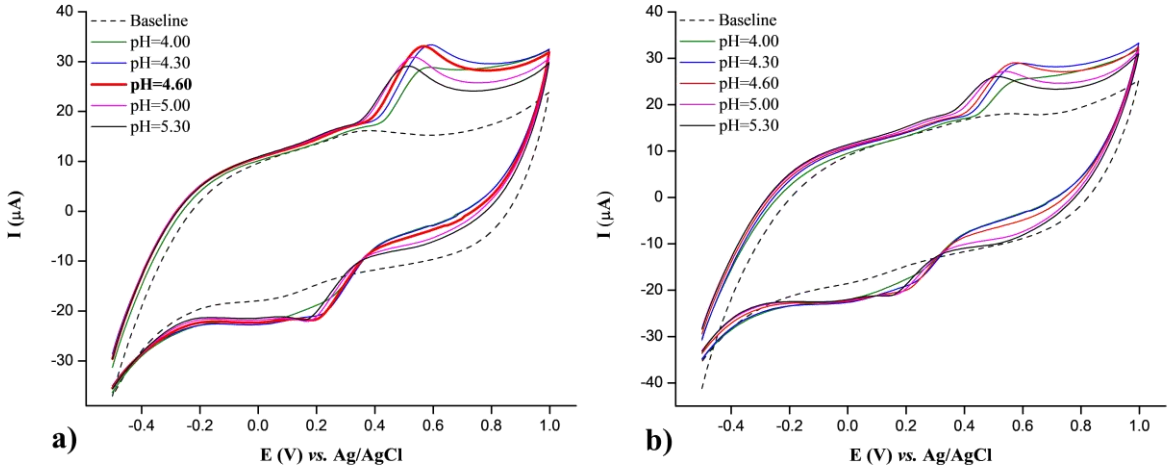

Figure 74. Electrochemical responses of SPCE/GNP@MnO_2/TvL/Naf for 0.3 mmol L^{-1} caffeic acid obtained in ***a)*** 0.1 mol L^{-1} ABS and ***b)*** 0.1 mol L^{-1} BRBS at different pHs.

4.2.3. Hydrodynamic chronoamperometry studies

4.2.3.1. Selecting the optimal working potential for biosensor operation

The amperometric response of the SPCE/GNP@MnO_2/TvL/Naf was monitored after each successive addition of 0.0100 mol L^{-1} caffeic acid standard solution in 25 mL of 0.1 mol L^{-1} ABS (pH=4.60). The caffeic acid concentration range in this experiment was from 0.04 mmol L^{-1} to 0.20 mmol L^{-1}, and was monitored at different working potentials (0.3 to 0.5 V). The amperograms given in the *Figure 75.* shows that increasing the potential from 0.3 to 0.4 V results in an increase in current intensity. On the contrary, at potentials higher than 0.4 V there is no significant change in the current signal. In addition, the biosensor at a potential of 0.4 V gives the most stable current signal toward caffeic acid. Therefore, 0.4 V was chosen as the optimal working potential of the chronoamperometric method, and further SPCE/GNP@MnO_2/TvL/Naf analyzes were conducted at this potential.

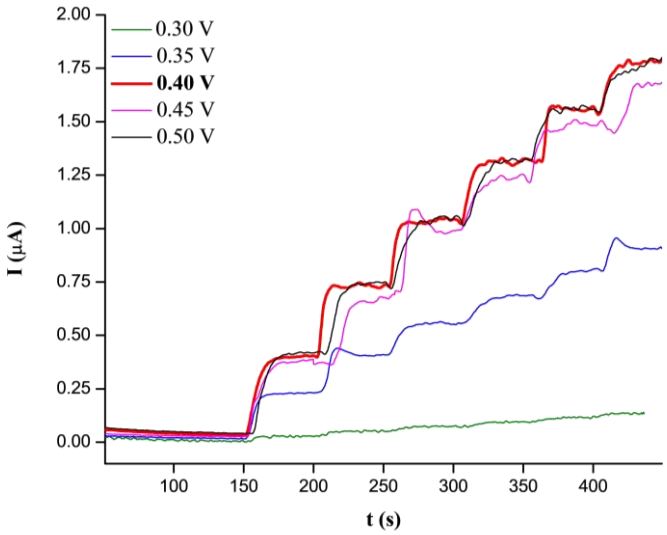

Figure 75. Amperometric responses of SPCE/GNP@MnO_2/TvL/Naf toward caffeic acid in 0.1 mol L^{-1} ABS (pH=4.60) at different working potentials.

Since that very good electrochemical characteristics of SPCEs, especially SPCE/GNP@MnO_2 electrode, were observed toward caffeic acid (Figure 73), a comparison of the electrochemical performance of SPCEs and the developed biosensor was done. This experiment was also done by chronoamperometric method. The amperometric responses of SPCEs (SPCE, SPCE/GNR, SPCE/MnO_2 and SPCE/GNP@MnO_2) and SPCE/GNP@MnO_2/TvL/Naf were monitored after each successive addition of 0.0100 mol L^{-1} caffeic acid standard solution in 0.1 mol L^{-1} ABS (pH=4.60). The working potential of all electrodes was adjusted to the optimum, 0.4 V. Applied concentration of caffeic acid were 0.04 mmol L^{-1}, 0.08 mmol L^{-1}, 1.00 mmol L^{-1} and 1.50 mmol L^{-1}. *Figure 76.* clearly shows that the developed biosensor is most sensitive to caffeic acid due to highest intensity of the current signal. In addition, it is clearly observed that the biosensor provides the most stable current signal compared to other SPCEs. This experiment explained why a SPCE/GNP@MnO_2/TvL/Naf was selected for further quantification of caffeic acid (polyphenols).

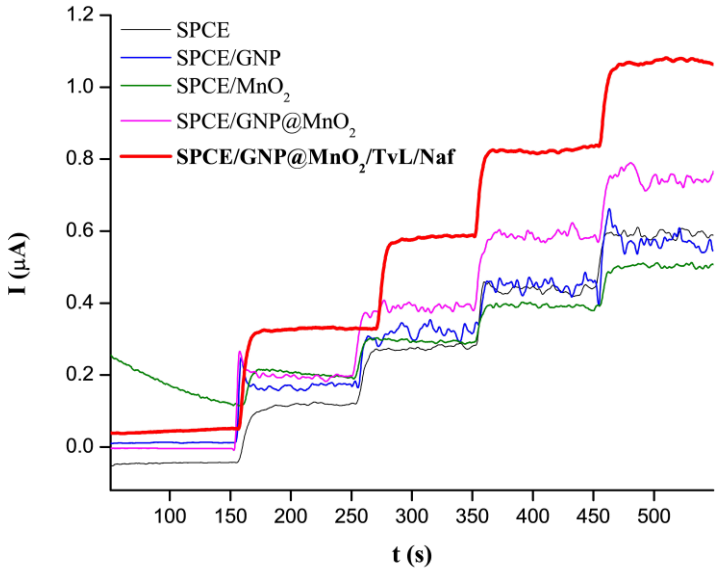

Figure 76. Amperometric responses of bare SPCE, modified SPCEs and SPCE/GNP@MnO_2/TvL/Naf at 0.4 V upon successive addition of caffeic acid in 0.1 mol L^{-1} ABS (pH=4.60).

4.2.3.2. Analytical characterization of the SPCE/GNP@MnO_2/TvL/Naf biosensor

Analytical performances of SPCE/GNP@MnO_2/TvL/Naf were examined by hydrodynamic chronoamperometry. Working linear range of biosensor was tested by successive addition of 0.0100 mol L^{-1} caffeic acid standard solution in 25 mL of 0.1 mol L^{-1} ABS (pH=4.60). The potential of electrode (biosensor) was set to optimal, 0.4 V. *Figure 77a.* shows the electrochemical response of the biosensor as a function of the time. Working linear range of biosensor toward caffeic acid was from 5 μmol L^{-1} to 0.32 mmol L^{-1}. The calibration curve was constructed as the dependence of the current intensity to applied concentration of caffeic acid (Figure 77b). LOQ, LOD and sensitivity were calculated from calibration curve according to the *Equation 6., Equation 7. and Equation 9.*, respectively. All calculated electroanalytical parameters are summarized in *Table 7.*

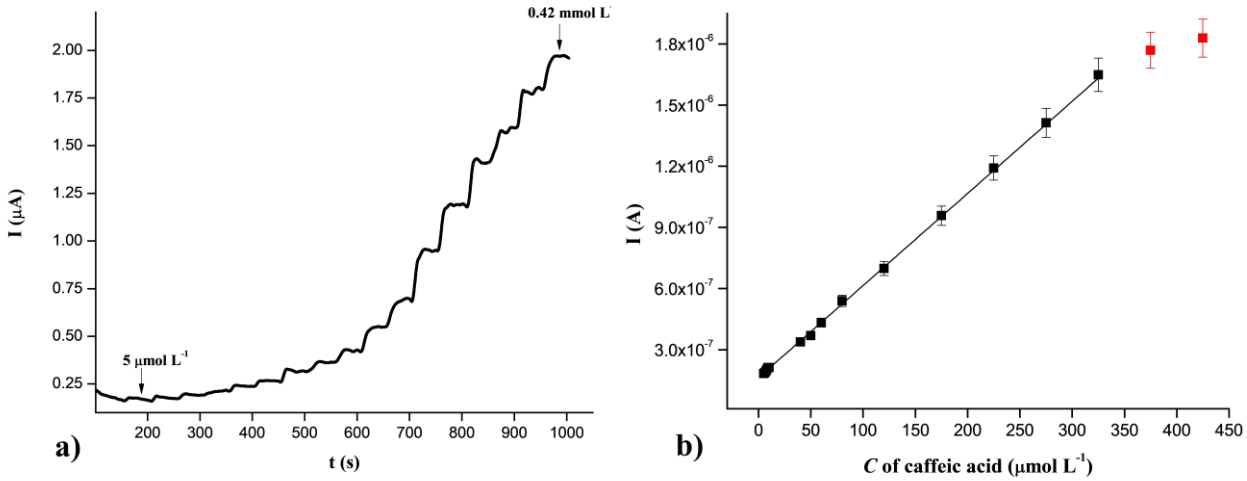

Figure 77. a) Amperometric response of SPCE/GNP@MnO_2/TvL/Naf after successive addition of 0.0100 mol L^{-1} of caffeic acid standard solution in 0.1 mol L^{-1} ABS (pH=4.60). ***b)*** Plot of current intensity *vs.* concentration of caffeic acid with corresponding error bars.

Table 7. Summarized electroanalytical parameters for SPCE/GNP@MnO_2/TvL/Naf.

***C* range (µmol L^{-1})**	**Calibration curve equation**	**LOQ (µmol L^{-1})**	**LOD (µmol L^{-1})**	**Sensitivity (µA (µmol L^{-1}*cm^2)$^{-1}$)**
5 - 320	*I (A)=1.63*10^{-7} + 4.52*10^{-9} C (µmol L^{-1})* *r*=0.9997	1.9	5.8	720

As in the case of the glucose biosensor, the essential analytical parameters (working linear range, LOD and sensitivity) of the developed biosensor were compared with amperometric enzymatic graphene@M_xO_y-based, as well as graphene- and M_xO_y-based, polyphenolic biosensors reported in the literature. As can be seen from *Table 2.*, the developed SPCE/GNP@MnO_2/TvL/Naf and the proposed amperometric method provide a very wide concentration linear range, extremely high sensitivity and low LOD during quantification of caffeic acid, compared to the listed biosensors.

4.2.3.2.1. Activity, reproducibility and repeatability of SPCE/GNP@MnO_2/TvL/Naf biosensor

Activity, reproducibility and repeatability of SPCE/GNP@MnO_2/TvL/Naf were examined by hydrodynamic chronoamperometry. The potential of electrode (biosensor) was set at optimal, 0.4 V. As supporting electrolyte was used 0.1 mol L^{-1} ABS (pH=4.60).

Activity of SPCE/GNP@MnO_2/TvL/Naf was monitored daily. The experiment lasted 7 days. For the activity test, a caffeic acid concentration of 80 µmol L^{-1} was monitored. On the first day, a current signal was recorded for the mentioned concentration of caffeic acid. Thereafter, the repeatability of the biosensor was tested with the same electrode, where 15 measurements were performed (*see next paragraph*). After repeatability testing, the caffeic acid concentration of 80 µmol L^{-1} was measured again with the same electrode. The current intensity in that case was lower by 7% (Figure 78). After completing the mentioned experiments, the biosensor was stored in the refrigerator at 4°C. From the second day until the end of the study period, the concentration of caffeic acid of 80 µmol L^{-1} was measured with the same electrode (biosensor), under the same experimental,

instrumental and storage conditions. After 7 days, activity of SPCE/GNP@MnO_2/TvL/Naf, was not below 77.1% (Figure 78).

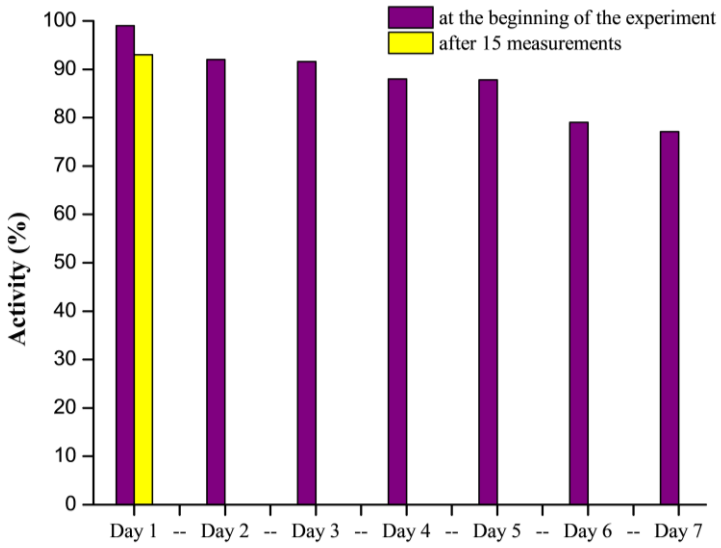

Figure 78. Activity of SPCE/GNP@MnO_2/TvL/Naf at the beginning of experiment and after 15 measurements (Day 1). Day 2 to day 7 represent an activity of biosensor toward 80 μmol L^{-1} of caffeic acid using the same electrode.

In order to examine repeatability, three different concentrations of caffeic acid were measured with the same SPCE/GNP@MnO_2/TvL/Naf (electrode) in five consecutive measurements. Concentrations of 7 μmol L^{-1}, 50 μmol L^{-1}, and 210 μmol L^{-1} were monitored in this experiment. The amperometric responses of the biosensor were monitored for the mentioned concentrations, where the current intensities were recorded (Figure 79). Using current intensities, RSD values were calculated for each concentration according to *Equation 8*. RSDs for concentrations 7 μmol L^{-1}, 50 μmol L^{-1}, and 210 μmol L^{-1} were 3.01%, 2.08% and 1.83%, respectively.

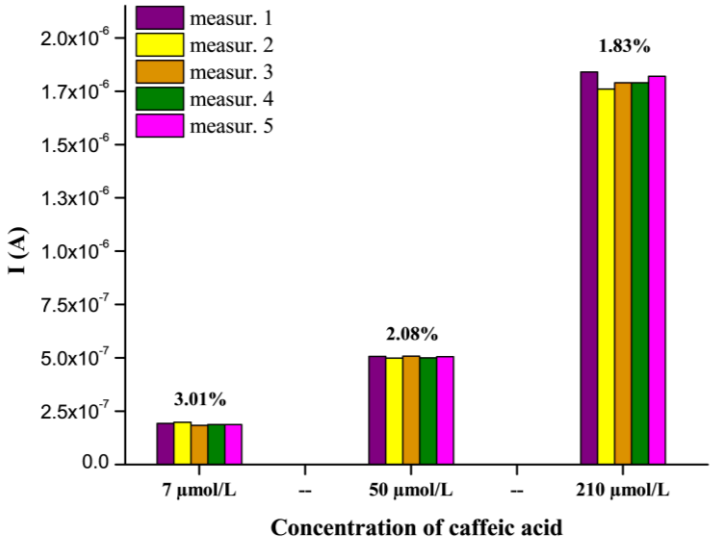

Figure 79. Repeatability of SPCE/GNP@MnO_2/TvL/Naf for three different concentration of caffeic acid (n=5 for each concentration) with corresponding RSDs.

Reproducibility of SPCE/GNP@MnO_2/TvL/Naf was examined independently prepared electrodes. In this experiment, a caffeic acid concentration of 70 μmol L^{-1} was monitored. Amperometric current intensities were recorded with each electrode (Figure 80). RSD of all measurements was calculated according to *Equation 8*. RSD was 3.90%.

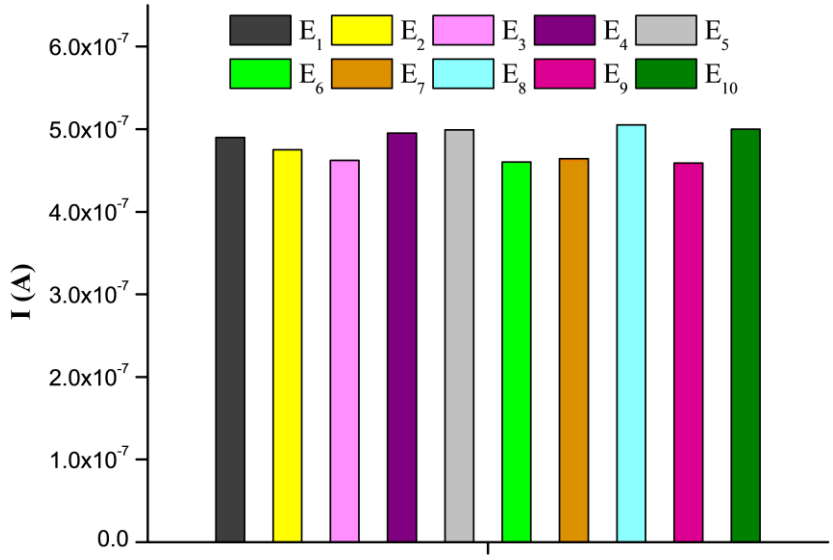

Figure 80. Current intensities obtained with ten independent SPCE/GNP@MnO_2/TvL/Naf electrodes for 70 μmol L^{-1} of caffeic acid in the order to test a reproducibility.

Summarizing all the results obtained from the experiments mentioned in this *Section*, we conclude that the developed SPCE/GNP@MnO_2/TvL/Naf shows high activity toward caffeic acid during amperometric measurements. In addition, the biosensor provides very good repeatability and reproducibility, as well as precision during quantification of caffeic acid by optimized hydrodynamic chronoamperometric method.

4.2.3.2.2. Selectivity of SPCE/GNP@MnO_2/TvL/Naf biosensor

Selectivity of SPCE/GNP@MnO_2/TvL/Naf was examined in the presence of different interfering substances. Due to the potential application of the developed biosensor in food and beverages samples, the effects of glucose (*Glu*) and *Fru* (sugars), *Asc* (vitamins) and tartaric acid (*Tart*) on the amperometric response of the biosensor were examined. *Uric* (metabolites), pharmaceutical products such as paracetamol (*Par*) and *p*-nitrophenol (*p-nPh*) and *Dop* as hormone, have also been used as interfering substances due to the potential use of biosensors in clinical samples. Substance *p-nPh* is used in the manufacture of drugs *(Eichenbaum et al., 2009)*. In addition, *p-nPh* was chosen as an interference due to its structure, in order to test the selectivity of biosensors in the presence of other phenolic compounds. Selectivity of biosensor was determined by optimized hydrodynamic chronoamperometric method. Current response of biosensor was followed after addition of 100 μL of 5 mmol L^{-1} caffeic acid (*CA*), and then addition of listed interferences in 23 mL of 0.1 mol L^{-1} ABS (pH=4.60). *Glu* and *Fru* were applied at the concentration of 20 μmol L^{-1}, while 10 μmol L^{-1} was concentration of other substances. In *Figure 81*. it is observed that after the addition of *Dop* there is an increase in current intensity up to 30%. As mentioned in the case of the glucose biosensor, *Dop* is oxidized in a positive potential window. The effect of other interfering substances was negligible. Based on the given results, it can be concluded that the

SPCE/GNP@MnO_2/TvL/Naf shows high selectivity in the presence of sugars, vitamins, metabolites and pharmaceutical product during the quantification of caffeic acid by the proposed ampermetric method. Accordingly, a biosensor can be found as a potential application for determination of polyphenolic index in food and beverages. Further studies are needed to extend the application of biosensor to clinical samples. More detailed analyzes would, above all, include testing dopamine levels on electrochemical behavior of biosensor.

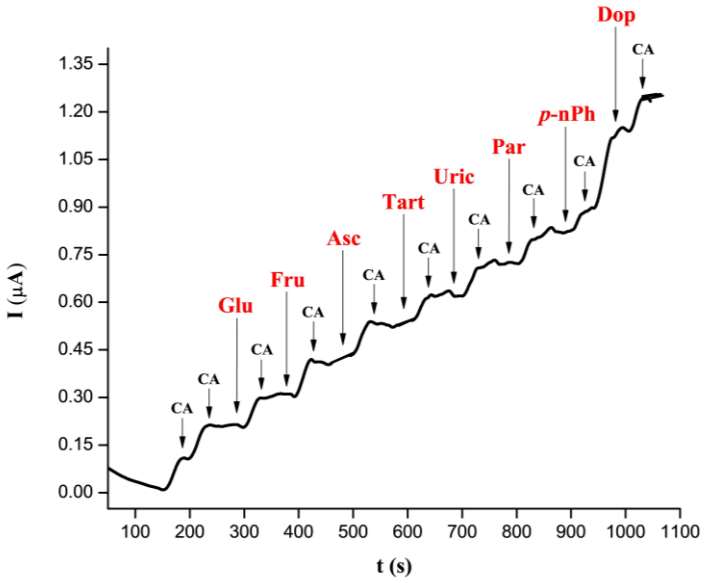

Figure 81. Amperometric response of SPCE/GNP@MnO_2/TvL/Naf after addition of 100 µL of 5 mmol L^{-1} *CA* and different interfering compounds.

4.2.3.3. Application on real samples

4.2.3.3.1. Determination of BPI in wine samples by SPCE/GNP@MnO_2/TvL/Naf

As mentioned in section *3.3.3.4. Preparation of wine samples*, wine samples were analyzed directly. A volume of 100 µL of red wine was added to 23.5 mL of 0.1 mol L^{-1} ABS (pH=4.60). Then, under optimized conditions, the amperometric response of the SPCE/GNP@MnO_2/TvL/Naf was monitored. After 250 s of analysis, the sample was spiked five times with 100 µL of 5 mmol L^{-1} caffeic acid solution. In the same way, 150 µL and 200 µL of red wine were analyzed, *ie.* spiked five times with 150 µL and 200 µL of 5 mmol L^{-1} caffeic acid, respectively. The amperometric responses of the SPCE/GNP@MnO_2/TvL/Naf for analyzed aliquots of red wine and different standard additions are given in *Figure 82a*. The polyphenolic content in white wines was determined in the same way as in red wine. The amperometric responses of the SPCE/GNP@MnO_2/TvL/Naf for aliquots of white wine of 100 µL, 150 µL and 200 µL and standard additions are given in *Figure 82b*. For each aliquot of red/white wine, a calibration curve of the dependence of current intensity on the standard addition of caffeic acid was constructed. The polyphenolic content in red and white wine was determined from the corresponding graphs shown in *Figure 83a-c.* and *Figure 83d-f.*, respectively. BPI was calculated for each aliquot of red/white wine and is given in *Table 8*.

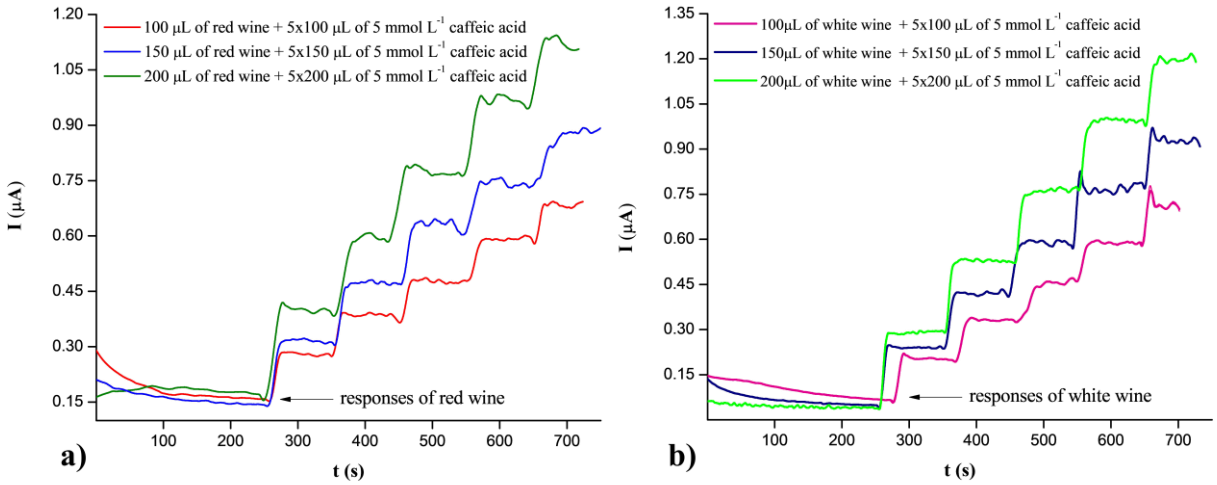

Figure 82. Amperometric responses of SPCE/GNP@MnO_2/TvL/Naf obtained for 100 µL, 150 µL and 200 µL of wine samples (***a)*** red wine; ***b)*** white wine, spiked with different standard additions of 5mmol L^{-1} caffeic acid.

Table 8. BPI in red and white wines obtained with SPCE/GNP@MnO_2/TvL/Naf.

Wine samples	**Standard addition*** **(µL)**	**$^a/_b$ from calibration curve (mmol L^{-1})**	***m* of caffeic acid**** **(mg)**	**BPI***** **(mg/L)**
Red	100	0.026	110.0	1100
	150	0.027	114.2	1142
	200	0.027	114.2	1142
White	100	0.012	51.0	510
	150	0.012	50.3	203
	200	0.012	50.8	508

*5 mmol L^{-1} caffeic acid
** calculated in relation to $^a/_b$
***mg of caffeic acid per L of wine

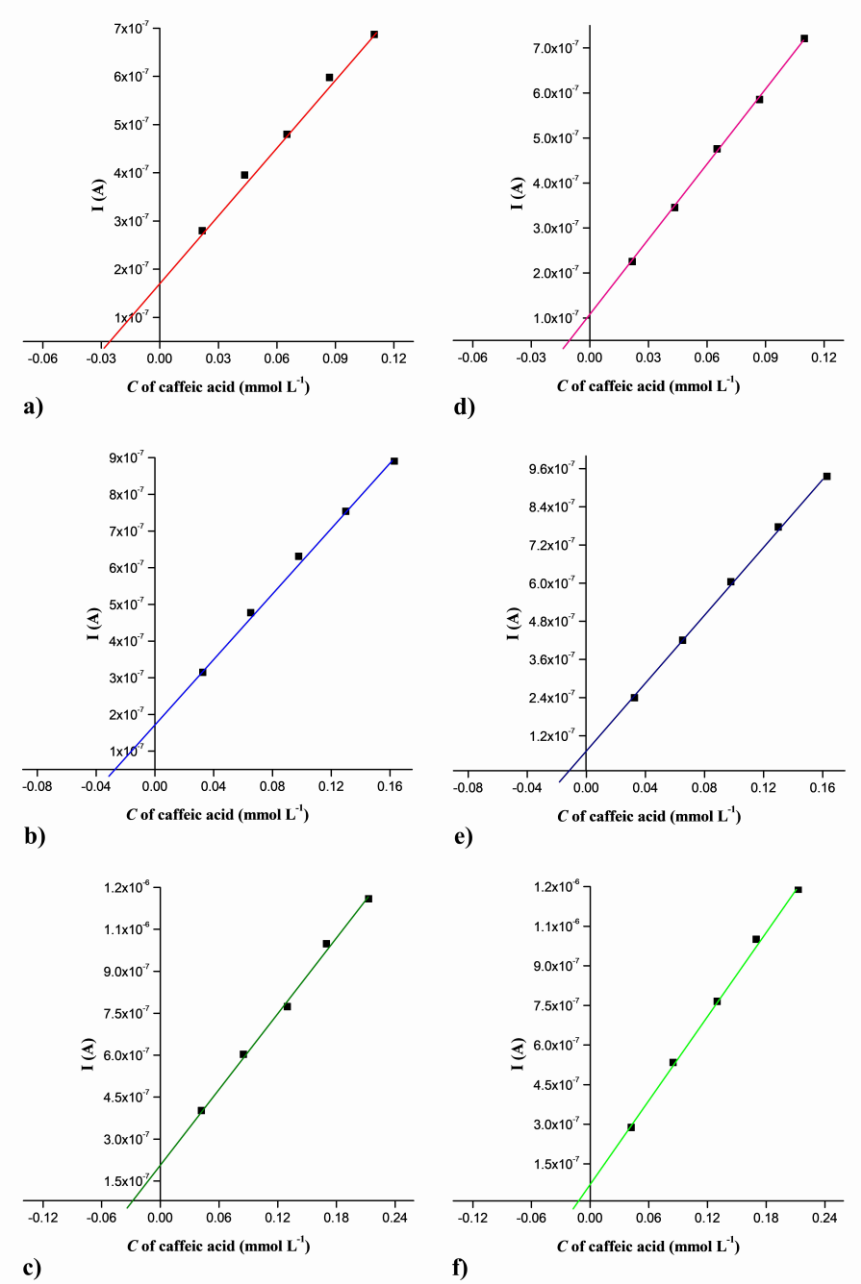

Figure 83. Standard addition method for wine samples. Plot of current intensity (*I*) *vs.* concentration of caffeic acid (*C*). Aliquots of 100 µL, 150 µL and 200 µL of red (***a-c***, respectively) and white wine (***d-f***, respectively) spiked five times with corresponding aliquots of 5 mmol L^{-1} caffeic acid.

4.2.3.4. Validation of developed amperometric method by GCE

The proposed amperometric method with developed SPCE/GNP@MnO_2/TvL/Naf was validated. The polyphenolic content in the same wine samples was determined using a GCE. The procedure was identical: different aliquots of red or white wine (100 µL, 150 µL and 200 µL) were spiked with standard additions of 5 mmol L^{-1} caffeic acid (100 µL, 150 µL and 200 µL) in 0.1 mol L^{-1} ABS (pH=4.60) as a supporting electrolyte. For quantification of polyphenolic index in wine samples was used optimized hydrodynamic chronoamperometric method. The potential of GCE was adjusted at optimal, 0.4 V. *Figure 84.* shows constructed calibration curves for each analyzed aliquot of red and white wine by GCE, respectively. The polyphenolic content was determined in the same way as in the case of the SPCE/GNP@MnO_2/TvL/Naf. *Table 9.* shows the EPI values in the wine samples.

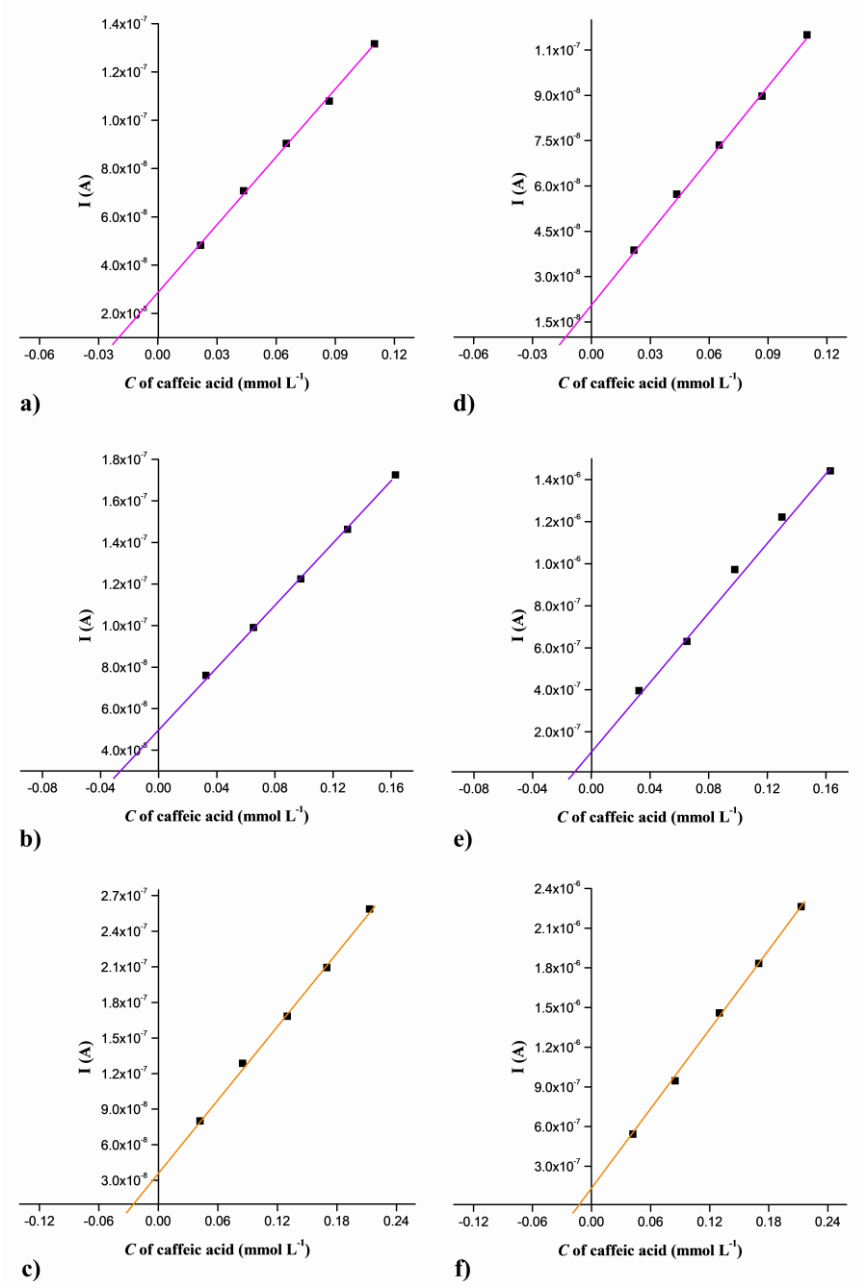

Figure 84. Standard addition method for wine samples obtained by GCE. Plot of current intensity (*I*) *vs.* concentration of caffeic acid (*C*). Aliquots of 100 µL, 150 µL and 200 µL of red (***a-c***, respectively) and white wine (***d-f***, respectively) spiked five times with corresponding aliquots of 5 mmol L^{-1} caffeic acid.

Table 9. EPI in wine samples obtained with GCE.

	Standard addition* **(μL)**	**a/b from calibration curve (mmol L^{-1})**	***m* of caffeic acid**** **(mg)**	**EPI***** **(mg/L)**
Red wine	100	0.0245	103.6	1036
	150	0.0259	109.6	1096
	200	0.0250	105.8	1058
White wine	100	0.0128	54.1	541
	150	0.0126	53.2	532
	200	0.0125	53.0	530

*5 mmol L^{-1} caffeic acid

** calculated in relation to a/b

***mg of caffeic acid per L of wine

Table 10. shows the average values of the polyphenolic index, with the corresponding standard deviations (SD) between the analyzed aliquots, obtained with developed biosensor and GCE. In order to compare the results, recovery values were calculated. As can be seen, the polyphenolic index in red wines obtained with SPCE/GNP@MnO_2/TvL/Naf and GCE matches 94%, while in the case of white wines the match is 95%. This indicates that the developed SPCE/GNP@MnO_2/TvL/Naf and the proposed amperometric method provide very satisfactory accuracy and precision during the quantification of polyphenols (caffeic acid as model compound) in wine samples, with minimal influence of the matrix effect.

Table 10. The polyphenolic content in wine samples shown as *average ± SD (RSD)* obtained with developed SPCE/GNP@MnO_2/TvL/Naf and GCE.

Wine samples	**BPI*** **(mg/L)**	**EPI**** **(mg/L)**	**Recovery (%)**
Red	1128 ± 25 (2.16%)	1063 ± 30 (2.82%)	94
White	507 ± 4 (0.64%)	534 ± 7 (1.17%)	95

*recorder with SPCE/GNP@MnO_2/TvL/Naf
**recorder with GCE

5. Conclusion

In this doctoral dissertation, new amperometric biosensors, for the detection of glucose and polyphenols in food samples, have been proposed. Combination of graphene nanomaterials and M_xO_y nanoparticles, as two highly promising nanomaterials with unique properties relevant for electrochemistry, were used for the construction of glucose and polyphenolic index biosensors. Amperometric biosensors offer a new solution for development of highly sensitive electrochemical methods that can be utilized for the detection of a wide range of chemical compounds. Modification of standard electrochemical sensors, such as Pt or Au electrodes, SPCE, GCE, CPE and BDD, with carefully selected combination of graphene@M_xO_y nanocomposites, significantly improves electrochemical performances of these electrodes. This kind of modification provides an opportunity for development of methods with higher sensitivity of determination (decreases LOD), increases selectivity during the detection of the target analyte, and enables simultaneous detection of compounds of similar structural formulas, as well as isomeric structures.

Glucose biosensor

Glucose biosensor was developed by application of GNR@Bi_2O_3 nanocomposite onto the surface of SPCE. The crystal structure of the nanocomposite was determined using XRPD and FE-SEM methods. Prior to the construction of the glucose biosensor, an optimization of the electrochemical system (which will later be used for glucose detection) with H_2O_2 was provided. Obtained results lead to few important conclusions:

- ✓ 10 µL of 1 mg mL^{-1} GNR@Bi_2O_3 was determined as the optimal amount of nanocomposite that should be applied to the surface SPCE;
- ✓ active surface area of unmodified SPCE and SPCE/GNR@Bi_2O_3 were 215 mm^2 and 785 mm^2, respectively;
- ✓ it was confirmed that SPCE/GNR@Bi_2O_3 electrode shows the best electrochemical performances for H_2O_2;
- ✓ the pH of 7.40 of 0.1 mol L^{-1} PBS was determined as optimal;
- ✓ by defining a cyclic voltammograms, after applying different scan rates, it was found that the diffusion-controlled process is responsible for the oxidation of H_2O_2 at SPCE/GNR@Bi_2O_3 surface;
- ✓ optimal working potential of hydrodynamic chronoamperometric method, for the determination of H_2O_2, was 0.6 V;
- ✓ at potential of 0.6 V, SPCE/GNR@Bi_2O_3 gave a wide working linear range for the detection of H_2O_2 (4 - 550 µmol L^{-1});
- ✓ during the determination of H_2O_2, SPCE/GNR@Bi_2O_3 showed good life-time, reproducibility, repeatability and precision;
- ✓ SPCE/GNR@Bi_2O_3 showed high selectivity during the detection of H_2O_2 in the presence of *Fru*, *Mal* and *Uric*, while *Asc* and *Dop*, at the applied concentrations, negatively affected the determination of H_2O_2.

After optimizing the system, GO_x was immobilized on the SPCE/GNR@Bi_2O_3 surface, in order to construct the biosensor. The amount of GO_x added to the electrode was optimized, as well as the amount of Naf added to the GO_x. The working linear range of the developed

SPCE/GNR@Bi_2O_3/GO_x/Naf biosensor, towards glucose, was fourther examined. The developed biosensor was utilized for the determination of glucose in honey sample. If considered together, from these results, it can be concluded:

- ✓ 5 µL of 10 mg L^{-1} GOx solution was determined as the optimal amount that should be applied to SPCE/GNR@Bi_2O_3, while 2.5 µL of 5% Naf proved to be optimal for enzyme coverage;
- ✓ under optimized experimental and instrumental conditions (0.1 mol L^{-1} PBS (pH=7.40) and working potential of 0.6 V), developed SPCE/GNR@Bi_2O_3/GO_x/Naf showed a linear working concentration range, towards glucose, starting from 0.28 and going to 1.70 mmol L^{-1};
- ✓ LOQ, LOD and sensitivity were 0.25 mmol L^{-1}, 0.07 mmol L^{-1} and 480 µA (µmol L^{-1}*cm^2)$^{-1}$, respectively;
- ✓ during the determination of glucose, the developed glucose biosensor showed good electroanalytical properties, such as reproducibility, repeatability and precision, as well as good and lasting activity during the examined period of one week;
- ✓ in contrast to SPCE/GNR@Bi_2O_3, the developed SPCE/GNR@Bi_2O_3/GO_x/Naf showed selectivity during the detection of glucose in the presence of sugars (*Fru* and *Mal*) and vitamin/metabolites (*Asc*/*Uric*), while *Dop*, in this case as well, showed its pronounced electroactivity at electrode surface;
- ✓ high accuracy and precision of the developed glucose biosensor was proven by means of glucose detection in a predefined honey sample (which represents *PT* scheme with declared glucose content of 32.6%).

Polyphenolic index biosensor

GNP and MnO_2 nanoparticles were rationally combined, in order to construct a polyphenolic index biosensor. Synthesized GNP@MnO_2 nanocomposite has been applied to the surface of SPCE. XRPD and FE-SEM methods were used to define the crystal structure of nanocomposites and resulting nanocomposite. Subsequently, cyclic voltammetry proved that SPCE/GNP@MnO_2 gives an excellent electrochemical response toward caffeic acid (taken as a model compound for the determination of polyphenolic content). Drawn by the experience, gained during glucose biosensor development, 5 µL 10 mg L^{-1} laccase solution has been immobilized on the surface of SPCE/GNP@MnO_2. The final construction step of the polyphenolic index biosensor was to cover the laccase with 2.5 µL of 5% Naf. Further electrochemical measurements followed. From the obtained results it was concluded:

- ✓ active surface area of unmodified SPCE and SPCE/GNP@MnO2 were 182 mm^2 and 400 mm^2, respectively;
- ✓ developed SPCE/GNP@MnO_2/Lac/Naf shows greater electrochemical response, for detection of caffeic acid, in 0.1 mol L^{-1} ABS, compared to 0.1 mol L^{-1} BRBS;
- ✓ the optimal pH of 0.1 mol L^{-1} ABS was determined to be 4.60, which is analogous to the pH of laccase activity;

- ✓ 0.4 V was the optimal working potential of hydrodynamic chronoamperometric method;

- ✓ although SPCE/GNP@MnO_2 showed excellent electrochemical characteristics during the detection of caffeic acid, the hydrodynamic chronoamperometric method suggested and confirmed that the developed SPCE/GNP@MnO_2/Lac/Naf is characterized with even more superior electrochemical characteristics toward the same analyte;

- ✓ at working potential 0.4 V, working linear range of SPCE/GNP@MnO_2/Lac/Naf for caffeic acid was in range from 5 to 320 μmol L^{-1};

- ✓ LOQ, LOD and sensitivity were 1.9 μmol L^{-1}, 5.8 μmol L^{-1} and 1840 μA (μmol L^{-1}*cm^2)$^{-1}$, respectively;

- ✓ during the determination of caffeic acid, SPCE/GNP@MnO_2/Lac/Naf showed good activity in the examined period of seven days, as well as excellent reproducibility, repeatability and precision;

- ✓ SPCE/GNP@MnO_2/Lac/Naf showed high selectivity during the determination of caffeic acid, in the presence of sugars (*Glu* and *Fru*), vitamins (*Asc*), metabolites (*Tart* and *Uric*) and pharmaceuticals (*Par* and *p-nPh*);

- ✓ BPI in red and white wines was determined by SPCE/GNP@MnO_2/Lac/Naf;

- ✓ by determining the polyphenolic content (EPI) in the same wine samples with GCE, under the same optimized experimental and instrumental condition, the developed polyphenolic index biosensor and the proposed amperometric method were validated;

- ✓ recovery values showed that the developed SPCE/GNP@MnO_2/Lac/Naf shows high accuracy and precision during the detection of caffeic acid in wine samples.

6. References

Adetayo, A., & Runsewe, D. (2019). Synthesis and Fabrication of Graphene and Graphene Oxide: A Review. *Open Journal of Composite Materials*, *9*, 207–229.

Ahmad, M., Pan, C., Luo, Z., & Zhu, J. (2010). A Single ZnO Nanofiber-Based Highly Sensitive Amperometric Glucose Biosensor. *The Journal of Physical Chemistry C*, *114*, 9308–9313.

Alonso-Lomillo, M. A., Domínguez-Renedo, O., & Arcos-Martínez, M. J. (2010). Screen-printed biosensors in microbiology; a review. *Talanta*, *82*, 1629–1636.

Anithaa, A. C., Lavanya, N., Asokan, K., & Sekar, C. (2015). WO3 nanoparticles based direct electrochemical dopamine sensor in the presence of ascorbic acid. *Electrochimica Acta*, *167*, 294–302.

Ansari, A. A., Kaushik, A., Solanki, P. R., & Malhotra, B. D. (2009). Electrochemical Cholesterol Sensor Based on Tin Oxide-Chitosan Nanobiocomposite Film. *Electroanalysis*, *21*, 965–972.

Anusha, J. R., Raj, C. J., Cho, B.-B., Fleming, A. T., Yu, K.-H., & Kim, B. C. (2015). Amperometric glucose biosensor based on glucose oxidase immobilized over chitosan nanoparticles from gladius of Uroteuthis duvauceli. *Sensors and Actuators B: Chemical*, *215*, 536–543.

Arregui, L., Ayala, M., Gómez-Gil, X., Gutiérrez-Soto, G., Hernández-Luna, C. E., Herrera de Los Santos, M., Levin, L., Rojo-Domínguez, A., Romero-Martínez, D., Saparrat, M. C. N., Trujillo-Roldán, M. A., & Valdez-Cruz, N. A. (2019). Laccases: Structure, function, and potential application in water bioremediation. *Microbial cell factories*, *18*, 200.

Arribas, A. S., Martínez-Fernández, M., Moreno, M., Bermejo, E., Zapardiel, A., & Chicharro, M. (2013). Analysis of total polyphenols in wines by FIA with highly stable amperometric detection using carbon nanotube-modified electrodes. *Food chemistry*, *136*, 1183–1192.

Arvand, M., Ghodsi, N., & Zanjanchi, M. A. (2016). A new microplatform based on titanium dioxide nanofibers/graphene oxide nanosheets nanocomposite modified screen printed carbon electrode for electrochemical determination of adenine in the presence of guanine. *Biosensors & bioelectronics*, *77*, 837–844.

Ashik, U.P.M., Kudo, S., & Hayashi, J.-i. (2018). An Overview of Metal Oxide Nanostructures. In *Synthesis of Inorganic Nanomaterials* (pp. 19–57): Elsevier.

Bahadır, E. B., & Sezgintürk, M. K. (2016). Applications of graphene in electrochemical sensing and biosensing. *TrAC Trends in Analytical Chemistry*, *76*, 1–14.

Balandin, A. A., Ghosh, S., Bao, W., Calizo, I., Teweldebrhan, D., Miao, F., & Lau, C. N. (2008). Superior thermal conductivity of single-layer graphene. *Nano letters*, *8*, 902–907.

Bang, J. H., Choi, M. S., Mirzaei, A., Kwon, Y. J., Kim, S. S., Kim, T. W., & Kim, H. W. (2018). Selective NO2 sensor based on Bi2O3 branched SnO2 nanowires. *Sensors and Actuators B: Chemical*, *274*, 356–369.

Banks, C. E., & Compton, R. G. (2005). Exploring the electrocatalytic sites of carbon nanotubes for NADH detection: An edge plane pyrolytic graphite electrode study. *The Analyst*, *130*, 1232–1239.

Bateni, F., Ghahremani, R., & Staser, J. A. (2020). Electrochemical oxidative valorization of lignin by the nanostructured PbO2/MWNTs electrocatalyst in a low-energy depolymerization process. *Journal of Applied Electrochemistry*, *110*, 3552.

Benvidi, A., Firouzabadi, A. D., Moshtaghiun, S. M., Mazloum-Ardakani, M., & Tezerjani, M. D. (2015). Ultrasensitive DNA sensor based on gold nanoparticles/reduced graphene oxide/glassy carbon electrode. *Analytical biochemistry*, *484*, 24–30.

Bergamini, M. F., Santos, D. P., & Zanoni, M. V. B. (2010). Determination of isoniazid in human urine using screen-printed carbon electrode modified with poly-L-histidine. *Bioelectrochemistry (Amsterdam, Netherlands)*, *77*, 133–138.

Beyene, N. (2004). (Bio)sensors based on manganese dioxide-modified carbon substrates: Retrospections, further improvements and applications*1. *Talanta*, *64*, 1151–1159.

Beyene, N. W., Kotzian, P., Schachl, K., Alemu, H., Turkušić, E., Čopra, A., Moderegger, H., Švancara, I., Vytřas, K., & Kalcher, K. (2004). (Bio)sensors based on manganese dioxide-modified carbon substrates: retrospections, further improvements and applications. *Talanta*, *64*, 1151-1159.

Bilgi, M., & Ayranci, E. (2016). Biosensor application of screen-printed carbon electrodes modified with nanomaterials and a conducting polymer: Ethanol biosensors based on alcohol dehydrogenase. *Sensors and Actuators B: Chemical*, *237*, 849–855.

Boopathy, G., Keerthi, M., Chen, S. M., Umapathy, M. J., Govindasamy, M., Chen, T. W., Ali, M. A., Al-Hemaid, F. M. A., & Elshikh, M. S. (2018). Graphene Oxide/α-MnO2 Binary Nanosheets Based Non-Enzymatic Biosensor for Pico-Molar Level Electrochemical Detection of Biomarker (Guanine) in DNA Sample. Journal of *The Electrochemical Society*, *165*, B651-B658.

Boujakhrout, A., Jimenez-Falcao, S., Martínez-Ruiz, P., Sánchez, A., Díez, P., Pingarrón, J. M., & Villalonga, R. (2016). Novel reduced graphene oxide-glycol chitosan nanohybrid for the assembly of an amperometric enzyme biosensor for phenols. *The Analyst*, *141*, 4162–4169.

Brasanac-Vukanovic, S., Mutic, J., Stankovic, D., Arsic, I., Blagojevic, N., Vukasinovic-Pesic, V., & Tadic, V. (2018). Wild Bilberry (Vaccinium myrtillus L., Ericaceae) from Montenegro as a Source of Antioxidants for Use in the Production of Nutraceuticals. *Molecules*, *23*, 1864.

Brenna, O. V., & Pagliarini, E. (2001). Multivariate analysis of antioxidant power and polyphenolic composition in red wines. *Journal of agricultural and food chemistry*, *49*, 4841–4844.

Bunaciu, A. A., Udriştioiu, E. G., & Aboul-Enein, H. Y. (2015). X-ray diffraction: Instrumentation and applications. *Critical Reviews in Analytical Chemistry*, *45*, 289–299.

Cabot, A., Marsal, A., Arbiol, J., & Morante, J. R. (2004). Bi2O3 as a selective sensing material for NO detection. *Sensors and Actuators B: Chemical*, *99*, 74–89.

Cai, J., Ruffieux, P., Jaafar, R., Bieri, M., Braun, T., Blankenburg, S., Muoth, M., Seitsonen, A. P., Saleh, M., Feng, X., Müllen, K., & Fasel, R. (2010). Atomically precise bottom-up fabrication of graphene nanoribbons. *Nature*, *466*, 470–473.

Çakıroğlu, B., Demirci, Y. C., Gökgöz, E., & Özacar, M. (2019). A photoelectrochemical glucose and lactose biosensor consisting of gold nanoparticles, MnO2 and g-C3N4 decorated TiO2. *Sensors and Actuators B: Chemical*, *282*, 282–289.

Cao, L., Fang, C., Zeng, R., Zhao, X., Zhao, F., Jiang, Y., & Chen, Z. (2017). A disposable paper-based microfluidic immunosensor based on reduced graphene oxide-tetraethylene pentamine/Au nanocomposite decorated carbon screen-printed electrodes. *Sensors and Actuators B: Chemical*, *252*, 44–54.

Castrovilli, M. C., Bolognesi, P., Chiarinelli, J., Avaldi, L., Calandra, P., Antonacci, A., & Scognamiglio, V. (2019). The convergence of forefront technologies in the design of laccase-based biosensors – An update. *TrAC Trends in Analytical Chemistry*, *119*, 115615.

Chabot, V., Higgins, D., Yu, A., Xiao, X., Chen, Z., & Zhang, J. (2014). A review of graphene and graphene oxide sponge: Material synthesis and applications to energy and the environment. *Energy & Environmental Science*, *7*, 1564.

Chaiyo, S., Mehmeti, E., Žagar, K., Siangproh, W., Chailapakul, O., & Kalcher, K. (2016). Electrochemical sensors for the simultaneous determination of zinc, cadmium and lead using a Nafion/ionic liquid/graphene composite modified screen-printed carbon electrode. *Analytica chimica acta*, *918*, 26–34.

Chawla, S., Rawal, R., Kumar, D., & Pundir, C. S. (2012a). Amperometric determination of total phenolic content in wine by laccase immobilized onto silver nanoparticles/zinc oxide nanoparticles modified gold electrode. *Analytical biochemistry*, *430*, 16–23.

Chawla, S., Rawal, R., Sharma, S., & Pundir, C. S. (2012b). An amperometric biosensor based on laccase immobilized onto nickel nanoparticles/carboxylated multiwalled carbon nanotubes/polyaniline modified gold electrode for determination of phenolic content in fruit juices. *Biochemical Engineering Journal*, *68*, 76–84.

Chen, D., Wu, S., Fang, J., Lu, S., Zhou, G., Feng, W., Yang, F., Chen, Y., & Fang, Z. (2018). A nanosheet-like α-Bi2O3/g-C3N4 heterostructure modified by plasmonic metallic Bi and oxygen vacancies with high photodegradation activity of organic pollutants. *Separation and Purification Technology*, *193*, 232–241.

Chen, H., He, J., Zhang, C., & He, H. (2007). Self-Assembly of Novel Mesoporous Manganese Oxide Nanostructures and Their Application in Oxidative Decomposition of Formaldehyde. *The Journal of Physical Chemistry C*, *111*, 18033–18038.

Chen, R., Shen, Z.-R., Wang, H., Zhou, H.-J., Liu, Y.-P., Ding, D.-T., & Chen, T.-H. (2011). Fabrication of mesh-like bismuth oxide single crystalline nanoflakes and their visible light photocatalytic activity. *Journal of Alloys and Compounds*, *509*, 2588–2596.

Chen, X., Jia, X., Han, J., Ma, J., & Ma, Z. (2013a). Electrochemical immunosensor for simultaneous detection of multiplex cancer biomarkers based on graphene nanocomposites. *Biosensors & bioelectronics*, *50*, 356–361.

Chen, Y.-C., Oteyza, D. G. de, Pedramrazi, Z., Chen, C., Fischer, F. R., & Crommie, M. F. (2013b). Tuning the band gap of graphene nanoribbons synthesized from molecular precursors. *ACS nano*, *7*, 6123–6128.

Chen, Z., Yu, A., Ahmed, R., Wang, H., Li, H., & Chen, Z. (2012). Manganese dioxide nanotube and nitrogen-doped carbon nanotube based composite bifunctional catalyst for rechargeable zinc-air battery. *Electrochimica Acta*, *69*, 295–300.

Cho, I.-H., Kim, D. H., & Park, S. (2020). Electrochemical biosensors: Perspective on functional nanomaterials for on-site analysis. *Biomaterials research*, *24*, 6.

Choi, W., Lahiri, I., Seelaboyina, R., & Kang, Y. S. (2010). Synthesis of Graphene and Its Applications: A Review. *Critical Reviews in Solid State and Materials Sciences*, *35*, 52–71.

Clark, L.C. (1956). Monitor and control of blood and tissue oxygen tensions. *Transactions - American Society for Artificial Internal Organs*, *2*, 41-48.

Clark, L. C., & Lyons, C. (1962). ELECTRODE SYSTEMS FOR CONTINUOUS MONITORING IN CARDIOVASCULAR SURGERY. *Annals of the New York Academy of Sciences*, *102*, 29–45.

Coroş, M., Pogăcean, F., Roşu, M.-C., Socaci, C., Borodi, G., Mageruşan, L., Biriş, A. R., & Pruneanu, S. (2016). Simple and cost-effective synthesis of graphene by electrochemical exfoliation of graphite rods. *RSC Advances*, *6*, 2651–2661.

Crouch, E., Cowell, D. C., Hoskins, S., Pittson, R. W., & Hart, J. P. (2005). Amperometric, screen-printed, glucose biosensor for analysis of human plasma samples using a biocomposite water-based carbon ink incorporating glucose oxidase. *Analytical biochemistry*, *347*, 17–23.

Dai, Y., Huang, J., Zhang, H., & Liu, C. C. (2019). Highly sensitive electrochemical analysis of tunnel structured MnO2 nanoparticle-based sensors on the oxidation of nitrite. *Sensors and Actuators B: Chemical*, *281*, 746–750.

Della Pelle, F., & Compagnone, D. (2018). Nanomaterial-Based Sensing and Biosensing of Phenolic Compounds and Related Antioxidant Capacity in Food. *Sensors (Basel, Switzerland)*, *18*.

Delle Noci, S., Frasconi, M., Favero, G., Tosi, M., Ferri, T., & Mazzei, F. (2008). Electrochemical Kinetic Characterization of Redox Mediated Glucose Oxidase Reactions: A Simplified Approach. *Electroanalysis*, *20*, 163–169.

Devaraj, M., Saravanan, R., Deivasigamani, R., Gupta, V. K., Gracia, F., & Jayadevan, S. (2016). Fabrication of novel shape Cu and Cu/Cu2O nanoparticles modified electrode for the determination of dopamine and paracetamol. *Journal of Molecular Liquids*, *221*, 930–941.

Devasenathipathy, R., Mani, V., Chen, S.-M., Huang, S.-T., Huang, T.-T., Lin, C.-M., Hwa, K.-Y., Chen, T.-Y., & Chen, B.-J. (2015). Glucose biosensor based on glucose oxidase immobilized at gold nanoparticles decorated graphene-carbon nanotubes. *Enzyme and microbial technology*, *78*, 40–45.

Dey, R. S., & Raj, C. R. (2013). A hybrid functional nanoscaffold based on reduced graphene oxide–ZnO for the development of an amperometric biosensing platform. *RSC Advances*, *3*, 25858.

Di Fusco, M., Tortolini, C., Deriu, D., & Mazzei, F. (2010). Laccase-based biosensor for the determination of polyphenol index in wine. *Talanta*, *81*, 235–240.

Diaconu, M., Litescu, S. C., & Radu, G. L. (2010). Laccase–MWCNT–chitosan biosensor—A new tool for total polyphenolic content evaluation from in vitro cultivated plants. *Sensors and Actuators B: Chemical*, *145*, 800–806.

Dimiev, A. M., Ceriotti, G., Metzger, A., Kim, N. D., & Tour, J. M. (2016). Chemical Mass Production of Graphene Nanoplatelets in ~100% Yield. *ACS nano*, *10*, 274–279.

Dong, Y., Li, K., Jiang, P., Wang, G., Miao, H., Zhang, J., & Zhang, C. (2014). Simple hydrothermal preparation of α-, β-, and γ-MnO 2 and phase sensitivity in catalytic ozonation. *RSC Adv*, *4*, 39167.

Dontsova, E. A., Zeifman, Y. S., Budashov, I. A., Eremenko, A. V., Kalnov, S. L., & Kurochkin, I. N. (2011). Screen-printed carbon electrode for choline based on MnO2 nanoparticles and choline oxidase/polyelectrolyte layers. *Sensors and Actuators B: Chemical*, *159*, 261–270.

Drago, R. S. (1992). Physical Methods for Chemists. Second edition. Surfside Scientific Publishers, Gainesville.

Đorđević, N. O., Pejin, B., Novaković, M. M., Stanković, D. M., Mutić, J. J., Pajović, S. B., & Tešević, V. V. (2017). Some chemical characteristics and antioxidant capacity of novel Merlot wine clones developed in Montenegro. *Scientia Horticulturae*, *225*, 505–511.

Drache, M., Roussel, P., & Wignacourt, J.-P. (2007). Structures and oxide mobility in Bi-Ln-O materials: Heritage of Bi2O3. *Chemical reviews*, *107*, 80–96.

Eichenbaum, G., Johnson, M., Kirkland, D., O'Neill, P., Stellar, S., Bielawne, J., DeWire, R., Areia, D., Bryant, S., Weiner, S., Desai-Krieger, D., Guzzie-Peck, P., Evans, D. C., & Tonelli, A. (2009). Assessment of the genotoxic and carcinogenic risks of p-nitrophenol when it is present as an impurity in a drug product. *Regulatory toxicology and pharmacology RTP*, *55*, 33–42.

ElKaoutit, M., Naranjo-Rodriguez, I., Temsamani, K. R., La Vega, M. D. de, & Cisneros, J. L. H.-H. de (2007). Dual laccase-tyrosinase based Sonogel-Carbon biosensor for monitoring polyphenols in beers. *Journal of agricultural and food chemistry*, *55*, 8011–8018.

Eremia, S. A. V., Vasilescu, I., Radoi, A., Litescu, S.-C., & Radu, G.-L. (2013). Disposable biosensor based on platinum nanoparticles-reduced graphene oxide-laccase biocomposite for the determination of total polyphenolic content. *Talanta*, *110*, 164–170.

Erogul, S., Bas, S. Z., Ozmen, M., & Yildiz, S. (2015). A new electrochemical sensor based on Fe3O4 functionalized graphene oxide-gold nanoparticle composite film for simultaneous determination of catechol and hydroquinone. *Electrochimica Acta*, *186*, 302–313.

Eslami, A., Hashemi, M., & Ghanbari, F. (2018). Degradation of 4-chlorophenol using catalyzed peroxymonosulfate with nano-MnO2/UV irradiation: Toxicity assessment and evaluation for industrial wastewater treatment. *Journal of Cleaner Production*, *195*, 1389–1397.

Fan, Y., Huang, K.-J., Niu, D.-J., Yang, C.-P., & Jing, Q.-S. (2011). TiO2-graphene nanocomposite for electrochemical sensing of adenine and guanine. *Electrochimica Acta*, *56*, 4685–4690.

Fanjul-Bolado, P., Hernández-Santos, D., Lamas-Ardisana, P. J., Martín-Pernía, A., & Costa-García, A. (2008). Electrochemical characterization of screen-printed and conventional carbon paste electrodes. *Electrochimica Acta*, *53*, 3635–3642.

Favero, G., Fusco, G., Mazzei, F., Tasca, F., & Antiochia, R. (2015). Electrochemical Characterization of Graphene and MWCNT Screen-Printed Electrodes Modified with AuNPs for Laccase Biosensor Development. *Nanomaterials (Basel, Switzerland)*, *5*, 1995–2006.

Fei, J., Wu, Y., Ji, X., Wang, J., Hu, S., & Gao, Z. (2003). An Amperometric Biosensor for Glucose Based on Electrodeposited Redox Polymer/Glucose Oxidase Film on a Gold Electrode. *Analytical Sciences*, *19*, 1259-1263.

Fletcher, S. (2015). Screen-printed carbon electrodes, in: Electrochemistry of carbon electrodes. Wiley-VCH, Weinheim.

Fernandes, C. I. S., & Rebelo, M. J. F. (2009). Polyphenolic Biosensors. Application in Red Wines. *Portugaliae Electrochimica Acta*, *27*, 457–462.

Ferri, S., Kojima, K., & Sode, K. (2011). Review of Glucose Oxidases and Glucose Dehydrogenases: A Bird's Eye View of Glucose Sensing Enzymes. *Journal of Diabetes Science and Technology*, *5*, 1068-1076.

Francke, R., & Little, R. D. (2014). Redox catalysis in organic electrosynthesis: Basic principles and recent developments. *Chemical Society reviews*, *43*, 2492–2521.

Freire, P. G., Montes, R. H.O., Romeiro, F. C., Lemos, S. C.S., Lima, R. C., Richter, E. M., & Munoz, R. A.A. (2016). Morphology of ZnO nanoparticles bound to carbon nanotubes affects

electrocatalytic oxidation of phenolic compounds. *Sensors and Actuators B: Chemical*, *223*, 557–565.

Freire, R. S., Thongngamdee, S., Durán, N., Wang, J., & Kubota, L. T. (2002). Mixed enzyme (laccase/tyrosinase)-based remote electrochemical biosensor for monitoring phenolic compounds. *The Analyst*, *127*, 258–261.

Fu, J., Qiao, H., Li, D., Luo, L., Chen, K., & Wei, Q. (2014). Laccase biosensor based on electrospun copper/carbon composite nanofibers for catechol detection. *Sensors (Basel, Switzerland)*, *14*, 3543–3556.

Galliez, K., Deniard, P., Lambertin, D., Jobic, S., & Bart, F. (2013). Influence of MnO2 polymorphism form on MnO2/Ag2O hydrogen getter. *Journal of Nuclear Materials*, *438*, 261–267.

Gamella, M., Campuzano, S., Reviejo, A. J., & Pingarrón, J. M. (2006). Electrochemical estimation of the polyphenol index in wines using a laccase biosensor. *Journal of agricultural and food chemistry*, *54*, 7960–7967.

Gan, N., Yang, X., Xie, D., Wu, Y., & Wen, W. (2010). A disposable organophosphorus pesticides enzyme biosensor based on magnetic composite nano-particles modified screen printed carbon electrode. *Sensors (Basel, Switzerland)*, *10*, 625–638.

Gao, C., Liu, L., Yu, T., & Yang, F. (2018). Development of a novel carbon-based conductive membrane with in-situ formed MnO2 catalyst for wastewater treatment in bio-electrochemical system (BES). *Journal of Membrane Science*, *549*, 533–542.

García-Guzmán, J. J., Hernández-Artiga, M. P., Palacios-Ponce de León, L., & Bellido-Milla, D. (2015). Selective methods for polyphenols and sulphur dioxide determination in wines. *Food chemistry*, *182*, 47–54.

George, J. M., Antony, A., & Mathew, B. (2018). Metal oxide nanoparticles in electrochemical sensing and biosensing: A review. *Mikrochimica acta*, *185*, 358.

Gerard, M. (2002). Application of conducting polymers to biosensors. *Biosensors and Bioelectronics*, *17*, 345–359.

Gil, D. M. A., & Rebelo, M. J. F. (2010). Evaluating the antioxidant capacity of wines: A laccase-based biosensor approach. *European Food Research and Technology*, *231*, 303–308.

Gnana Sundara Raj, B., Asiri, A. M., Qusti, A. H., Wu, J. J., & Anandan, S. (2014). Sonochemically synthesized MnO2 nanoparticles as electrode material for supercapacitors. *Ultrasonics sonochemistry*, *21*, 1933–1938.

Goldstein J. (2003). Scanning Electron Microscopy and X-ray Microanalysis. Third edition. Plenum Press, New York.

Gomes, S. A. S. S., Nogueira, J. M. F., & Rebelo, M. J. F. (2004). An amperometric biosensor for polyphenolic compounds in red wine. *Biosensors & bioelectronics*, *20*, 1211–1216.

Gujar, T. P., Shinde, V. R., Lokhande, C. D., & Han, S.-H. (2006). Electrosynthesis of Bi2O3 thin films and their use in electrochemical supercapacitors. *Journal of Power Sources*, *161*, 1479–1485.

Guo, T., Yao, M.-S., Lin, Y.-H., & Nan, C.-W. (2015). A comprehensive review on synthesis methods for transition-metal oxide nanostructures. *CrystEngComm*, *17*, 3551–3585.

Gupta, G., Rajendran, V., & Atanassov, P. (2003). Laccase Biosensor on Monolayer-Modified Gold Electrode. *Electroanalysis*, *15*, 1577–1583.

Gutierrez-Sanchez, C., Shleev, S., Lacey, A. L. de, & Pita, M. (2015). Third-generation oxygen amperometric biosensor based on Trametes hirsuta laccase covalently bound to graphite electrode. *Chemical Papers*, *69*, 7.

Haghighi, B., Gorton, L., Ruzgas, T., & Jönsson, L. J. (2003). Characterization of graphite electrodes modified with laccase from Trametes versicolor and their use for bioelectrochemical monitoring of phenolic compounds in flow injection analysis. *Analytica chimica acta*, *487*, 3–14.

Han, D., Fan, Q., Dai, J., Wang, T., Huang, J., Xu, Q., Ding, H., Hu, J., Feng, L., Zhang, W., Zeng, Z., Gottfried, J. M., & Zhu, J. (2020). On-Surface Synthesis of Armchair-Edged Graphene Nanoribbons with Zigzag Topology. *The Journal of Physical Chemistry C*, *124*, 5248–5256.

Han, X., Fang, X., Shi, A., Wang, J., & Zhang, Y. (2013). An electrochemical DNA biosensor based on gold nanorods decorated graphene oxide sheets for sensing platform. *Analytical biochemistry*, *443*, 117–123.

Homaei, A. A., Sariri, R., Vianello, F., & Stevanato, R. (2013). Enzyme immobilization: An update. *Journal of chemical biology*, *6*, 185–205.

Honeychurch, K. C., & Hart, J. P. (2003). Screen-printed electrochemical sensors for monitoring metal pollutants. *TrAC Trends in Analytical Chemistry*, *22*, 456–469.

Hou, S., Zhang, A., & Su, M. (2016). Nanomaterials for Biosensing Applications. *Nanomaterials (Basel, Switzerland)*, *6*.

Hu, C. C., & Tsou, Ta. W. (2002). Ideal capacitive behavior of hydrous manganese oxide prepared by anodic deposition. *Electrochemistry Communications*, *4*, 105-109.

Hu, Y., Li, F., Bai, X., Li, D., Hua, S., Wang, K., & Niu, L. (2011). Label-free electrochemical impedance sensing of DNA hybridization based on functionalized graphene sheets. *Chemical communications (Cambridge, England)*, *47*, 1743–1745.

Hu, Y. H., Wang, H., & Hu, B. (2010). Thinnest two-dimensional nanomaterial-graphene for solar energy. *ChemSusChem*, *3*, 782–796.

Hu, Z., Zhao, Y., Liu, J., Wang, J., Zhang, B., & Xiang, X. (2016). Ultrafine MnO2 nanoparticles decorated on graphene oxide as a highly efficient and recyclable catalyst for aerobic oxidation of benzyl alcohol. *Journal of colloid and interface science*, *483*, 26–33.

Huang, K.-J., Niu, D.-J., Sun, J.-Y., Han, C.-H., Wu, Z.-W., Li, Y.-L., & Xiong, X.-Q. (2011). Novel electrochemical sensor based on functionalized graphene for simultaneous determination of adenine and guanine in DNA. *Colloids and surfaces. B, Biointerfaces*, *82*, 543–549.

Huang, M., Zhao, X. L., Li, F., Zhang, L. L., & Zhang, Y. X. (2015a). Facile synthesis of ultrathin manganese dioxide nanosheets arrays on nickel foam as advanced binder-free supercapacitor electrodes. *Journal of Power Sources*, *277*, 36–43.

Huang, S.-H., Liao, H.-H., & Chen, D.-H. (2010). Simultaneous determination of norepinephrine, uric acid, and ascorbic acid at a screen printed carbon electrode modified with polyacrylic acid-coated multi-wall carbon nanotubes. *Biosensors & bioelectronics*, *25*, 2351–2355.

Huang, Y. H., Chen, J. H., Sun, X., Su, Z. B., Xing, H. T., Hu, S. R., Weng, W., Guo, H. X., Wu, W. B., & He, Y. S. (2015b). One-pot hydrothermal synthesis carbon nanocages-reduced graphene oxide composites for simultaneous electrochemical detection of catechol and hydroquinone. *Sensors and Actuators B: Chemical*, *212*, 165–173.

Hussain, A. M., Neppolian, B., Shim, H.-S., Kim, S. H., Kim, S.-K., Choi, H. C., Kim, W. B., Lee, K., & Park, S.-J. (2010). Efficiency Enhancement in Bulk Heterojunction Polymer Photovoltaic Cells Using ZrTiO 4 /Bi 2 O 3 Metal-Oxide Nanocomposites. *Japanese Journal of Applied Physics*, *49*, 42301.

Hwa, K.-Y., & Subramani, B. (2014). Synthesis of zinc oxide nanoparticles on graphene–carbon nanotube hybrid for glucose biosensor applications. *Biosensors and Bioelectronics*, *62*, 127–133.

Ibarra-Escutia, P., Gómez, J. J., Calas-Blanchard, C., Marty, J. L., & Ramírez-Silva, M. T. (2010). Amperometric biosensor based on a high resolution photopolymer deposited onto a screen-printed electrode for phenolic compounds monitoring in tea infusions. *Talanta*, *81*, 1636–1642.

Jakobek, L. (2015). Interactions of polyphenols with carbohydrates, lipids and proteins. *Food chemistry*, *175*, 556–567.

Jampasa, S., Wonsawat, W., Rodthongkum, N., Siangproh, W., Yanatatsaneejit, P., Vilaivan, T., & Chailapakul, O. (2014). Electrochemical detection of human papillomavirus DNA type 16 using a pyrrolidinyl peptide nucleic acid probe immobilized on screen-printed carbon electrodes. *Biosensors & bioelectronics*, *54*, 428–434.

Jia, N., Huang, B., Chen, L., Tan, L., & Yao, S. (2014). A simple non-enzymatic hydrogen peroxide sensor using gold nanoparticles-graphene-chitosan modified electrode. *Sensors and Actuators B: Chemical*, *195*, 165–170.

Jiang, L., Li, Z., Fan, G., Cao, L., & Di Zhang (2012). The use of flake powder metallurgy to produce carbon nanotube (CNT)/aluminum composites with a homogenous CNT distribution. *Carbon*, *50*, 1993–1998.

Jo, G., Choe, M., Lee, S., Park, W., Kahng, Y. H., & Lee, T. (2012). The application of graphene as electrodes in electrical and optical devices. *Nanotechnology*, *23*, 112001.

Joo, S. H., & Zhao, D. (2017). Environmental dynamics of metal oxide nanoparticles in heterogeneous systems: A review. *Journal of hazardous materials*, *322*, 29–47.

Jusman, Y., Ng, S. C., & Abu Osman, N. A. (2014). Investigation of CPD and HMDS sample preparation techniques for cervical cells in developing computer-aided screening system based on FE-SEM/EDX. *TheScientificWorldJournal*, *2014*, 289817.

Kalcher, K., Svancara, I., Buzuk, M., Vytras, K., & Walcarius, A. (2009). Electrochemical sensors and biosensors based on heterogeneous carbon materials. *Monatshefte für Chemie - Chemical Monthly*, *140*, 861–889.

Kapturski, P., & Bobrowski, A. (2008). The silver amalgam film electrode in catalytic adsorptive stripping voltammetric determination of cobalt and nickel. *Journal of Electroanalytical Chemistry*, *617*, 1–6.

Karimi-Maleh, H., Sheikhshoaie, M., Sheikhshoaie, I., Ranjbar, M., Alizadeh, J., Maxakato, N. W., & Abbaspourrad, A. (2019). A novel electrochemical epinine sensor using amplified CuO nanoparticles and a n -hexyl-3-methylimidazolium hexafluorophosphate electrode. *New Journal of Chemistry*, *43*, 2362–2367.

Kilmartin, P. A., Zou, H., & Waterhouse, A. L. (2001). A cyclic voltammetry method suitable for characterizing antioxidant properties of wine and wine phenolics. *Journal of agricultural and food chemistry*, *49*, 1957–1965.

Kim, S., Han, K., Lee, I., Yoon, Y., Park, W., Hong, S., Yang, W., & Hwang, W. (2017). A Zero-Power, Low-Cost Ultraviolet-C Colorimetric Sensor Using a Gallium Oxide and Reduced Graphene Oxide Hybrid via Photoelectrochemical Reactions. *Catalysts*, *7*, 248.

Korotkaya, E. (2014). Biosensors: Design, Classification, and Applications in the Food Industry. *Foods and Raw Materials*, *2*, 161–171.

Kosto, Y., Zanut, A., Franchi, S., Yakovlev, Y., Khalakhan, I., Matolín, V., Prince, K. C., Valenti, G., Paolucci, F., & Tsud, N. (2019). Electrochemical activity of the polycrystalline cerium oxide films for hydrogen peroxide detection. *Applied Surface Science*, *488*, 351–359.

Kotzian, P., Brázdilová, P., Kalcher, K., Handlíř, K., & Vytřas, K. (2007). Oxides of platinum metal group as potential catalysts in carbonaceous amperometric biosensors based on oxidases. *Sensors and Actuators B: Chemical*, *124*, 297–302.

Kotzian, P., Brázdilová, P., Kalcher, K., & Vytřas, K. (2005). Determination of Hydrogen Peroxide, Glucose and Hypoxanthine using (Bio)Sensors Based on Ruthenium Dioxide-Modified Screen-Printed Electrodes. *Analytical Letters*, *38*, 1099–1113.

Kotzian, P., Brázdilová, P., Řezková, S., Kalcher, K., & Vytřas, K. (2006). Amperometric Glucose Biosensor Based on Rhodium Dioxide-Modified Carbon Ink. *Electroanalysis*, *18*, 1499–1504.

Krishnan, S. K., Singh, E., Singh, P., Meyyappan, M., & Nalwa, H. S. (2019). A review on graphene-based nanocomposites for electrochemical and fluorescent biosensors. *RSC Advances*, *9*, 8778–8881.

Królicka, A., & Bobrowski, A. (2004). Bismuth film electrode for adsorptive stripping voltammetry – electrochemical and microscopic study. *Electrochemistry Communications*, *6*, 99–104.

Kuek Lawrence, C. S., Tan, S. N., & Floresca, C. Z. (2014). A "green" cellulose paper based glucose amperometric biosensor. *Sensors and Actuators B: Chemical*, *193*, 536–541.

Kurt Urhan, B., Oznuluer, T., Demir, U., & Ozturk Dogan, H. (2019). One-Pot Electrochemical Synthesis of Lead Oxide- Electrochemically Reduced Graphene Oxide Nanostructures and Their Electrocatalytic Applications. *IEEE Sensors Journal*, *19*, 4781–4788.

La, D. D., Bhargava, S., & Bhosale, S. V. (2016). Improved and A Simple Approach For Mass Production of Graphene Nanoplatelets Material. *ChemistrySelect*, *1*, 949–952.

Lamas-Ardisana, P. J., Martínez-Paredes, G., Añorga, L., & Grande, H. J. (2018). Glucose biosensor based on disposable electrochemical paper-based transducers fully fabricated by screen-printing. *Biosensors & bioelectronics*, *109*, 8–12.

Leskovac, V., Trivić, S., Wohlfahrt, G., Kandrac, J., & Pericin, D. (2005). Glucose oxidase from Aspergillus niger: The mechanism of action with molecular oxygen, quinones, and one-electron acceptors. *The international journal of biochemistry & cell biology*, *37*, 731–750.

Li, C., Liu, Y., Li, L., Du, Z., Xu, S., Zhang, M., Yin, X., & Wang, T. (2008). A novel amperometric biosensor based on NiO hollow nanospheres for biosensing glucose. *Talanta*, *77*, 455–459.

Li, L., Yang, Y.-W., Li, G.-H., & Zhang, L.-D. (2006). Conversion of a Bi nanowire array to an array of Bi-Bi2O3 core-shell nanowires and Bi2O3 nanotubes. *Small (Weinheim an der Bergstrasse, Germany)*, *2*, 548–553.

Li, M., Li, Y.-T., Li, D.-W., & Long, Y.-T. (2012). Recent developments and applications of screen-printed electrodes in environmental assays--a review. *Analytica chimica acta*, *734*, 31–44.

Li, Y., Zhang, J., Zhu, H., Yang, F., & Yang, X. (2010). Gold nanoparticles mediate the assembly of manganese dioxide nanoparticles for H2O2 amperometric sensing. *Electrochimica Acta*, *55*, 5123–5128.

Li, Y., Zhong, Y., Zhang, Y., Weng, W., & Li, S. (2015). Carbon quantum dots/octahedral Cu2O nanocomposites for non-enzymatic glucose and hydrogen peroxide amperometric sensor. *Sensors and Actuators B: Chemical*, *206*, 735–743.

Liang, K., Fu, X., Wu, L., Qin, Y., & Song, Y. (2016). A Novel Tyrosinase Biosensor based on Graphene and Co3O4 Nanocomposite Materials for Rapid Determining Catechol. *International Journal of Electrochemical Science*, *11*, 250-258.

Lin, L., Liu, Y., Tang, L., & Li, J. (2011). Electrochemical DNA sensor by the assembly of graphene and DNA-conjugated gold nanoparticles with silver enhancement strategy. *The Analyst*, *136*, 4732–4737.

Lin, W.-J., Liao, C.-S., Jhang, J.-H., & Tsai, Y.-C. (2009). Graphene modified basal and edge plane pyrolytic graphite electrodes for electrocatalytic oxidation of hydrogen peroxide and β-nicotinamide adenine dinucleotide. *Electrochemistry Communications*, *11*, 2153–2156.

Lino, F.M.A., Sá, L. Z. de, Torres, I.M.S., Rocha, M. L., Dinis, T.C.P., Ghedini, P. C., Somerset, V. S., & Gil, E. S. (2014). Voltammetric and spectrometric determination of antioxidant capacity of selected wines. *Electrochimica Acta*, *128*, 25–31.

Liu, G., Li, S., Lu, Y., Zhang, J., Feng, Z., & Li, C. (2016a). Controllable synthesis of α-Bi2O3 and γ-Bi2O3 with high photocatalytic activity by α-Bi2O3→γ-Bi2O3→α-Bi2O3 transformation in a facile precipitation method. *Journal of Alloys and Compounds*, *689*, 787–799.

Liu, G., & Lin, Y. (2006). Amperometric glucose biosensor based on self-assembling glucose oxidase on carbon nanotubes. *Electrochemistry Communications*, *8*, 251–256.

Liu, H., Gao, J., Xue, M., Zhu, N., Zhang, M., & Cao, T. (2009). Processing of graphene for electrochemical application: Noncovalently functionalize graphene sheets with water-soluble electroactive methylene green. *Langmuir the ACS journal of surfaces and colloids*, *25*, 12006–12010.

Liu, M., Du, Y., Miao, Y.-E., Ding, Q., He, S., Tjiu, W. W., Pan, J., & Liu, T. (2015). Anisotropic conductive films based on highly aligned polyimide fibers containing hybrid materials of graphene nanoribbons and carbon nanotubes. *Nanoscale*, *7*, 1037–1046.

Liu, N., Luo, F., Wu, H., Liu, Y., Zhang, C., & Chen, J. (2008). One-Step Ionic-Liquid-Assisted Electrochemical Synthesis of Ionic-Liquid-Functionalized Graphene Sheets Directly from Graphite. *Advanced Functional Materials*, *18*, 1518–1525.

Liu, P., Cottrill, A. L., Kozawa, D., Koman, V. B., Parviz, D., Liu, A. T., Yang, J., Tran, T. Q., Wong, M. H., Wang, S., & Strano, M. S. (2018). Emerging trends in 2D nanotechnology that are redefining our understanding of "Nanocomposites". *Nano Today*, *21*, 18–40.

Liu, Y., Zhang, X., He, D., Ma, F., Fu, Q., & Hu, Y. (2016b). An amperometric glucose biosensor based on a MnO 2 /graphene composite modified electrode. *RSC Advances*, *6*, 18654–18661.

Lopes, G. C., Perdigão, J., Baptista, D., & Ballarin, A. (2019). Does a Self-etching Ceramic Primer Improve Bonding to Lithium Disilicate Ceramics?: Bond Strengths and FESEM Analyses. *Operative Dentistry, 44*, 210–218.

Lorrain, B., Ky, I., Pechamat, L., & Teissedre, P.-L. (2013). Evolution of analysis of polyhenols from grapes, wines, and extracts. *Molecules (Basel, Switzerland), 18*, 1076–1100.

Lou, C., Jing, T., Zhou, J., Tian, J., Zheng, Y., Wang, C., Zhao, Z., Lin, J., Liu, H., Zhao, C., & Guo, Z. (2020). Laccase immobilized polyaniline/magnetic graphene composite electrode for detecting hydroquinone. *International journal of biological macromolecules, 149*, 1130–1138.

Lubert, K.-H., & Kalcher, K. (2010). History of Electroanalytical Methods. *Electroanalysis, 22*, 1937–1946.

Lugonja, N. M., Stanković, D. M., Spasić, S. D., Roglić, G. M., Manojlović, D. D., & Vrvić, M. M. (2014). Comparative Electrochemical Determination of Total Antioxidant Activity in Infant Formula with Breast Milk. *Food Analytical Methods, 7*, 337–344.

Luo, Z., Ma, X., Yang, D., Yuwen, L., Zhu, X., Weng, L., & Wang, L. (2013). Synthesis of highly dispersed titanium dioxide nanoclusters on reduced graphene oxide for increased glucose sensing. *Carbon, 57*, 470–476.

Makhotkina, O., & Kilmartin, P. A. (2010). The use of cyclic voltammetry for wine analysis: Determination of polyphenols and free sulfur dioxide. *Analytica chimica acta, 668*, 155–165.

Malhotra, B. D., & Ali, M. A. (2018). Nanomaterials in Biosensors. In *Nanomaterials for Biosensors* (pp. 1–74): Elsevier.

Mallakpour, S., & Madani, M. (2015). A review of current coupling agents for modification of metal oxide nanoparticles. *Progress in Organic Coatings, 86*, 194–207.

Manekkathodi, A., Lu, M.-Y., Wang, C. W., & Chen, L.-J. (2010). Direct growth of aligned zinc oxide nanorods on paper substrates for low-cost flexible electronics. *Advanced materials (Deerfield Beach, Fla.), 22*, 4059–4063.

Mani, P., Kumar, V. T. F., Keshavarz, T., Chandra, T. S., & Kyazze, G. (2018). The Role of Natural Laccase Redox Mediators in Simultaneous Dye Decolorization and Power Production in Microbial Fuel Cells. *Energies, 11*, 3455.

Mani, V., Devadas, B., Chen, S.-M., & Li, Y. (2013). Immobilization of Enzymes and Redox Proteins and Their Electrochemical Biosensor Applications. *ECS Transactions, 50*, 35–41.

Mani 2015, 6 mikro L enzima + 2mikro L naf.

Mano, N., Yoo, J. E., Tarver, J., Loo, Y.-L., & Heller, A. (2007). An electron-conducting cross-linked polyaniline-based redox hydrogel, formed in one step at pH 7.2, wires glucose oxidase. *Journal of the American Chemical Society, 129*, 7006–7007.

Manojlović, D., Mutić, J., & Šegan D. (2011). Fundamentals of electroanalytical chemistry. University of Belgrade, Faculty of Chemistry, Belgrade, Serbia. ISBN: 978-86-7220-042-3.

McCreery, R. L. (2008). Advanced carbon electrode materials for molecular electrochemistry. *Chemical reviews, 108*, 2646–2687.

Mehmeti, E., Stanković, D. M., Chaiyo, S., Zavasnik, J., Žagar, K., & Kalcher, K. (2017). Wiring of glucose oxidase with graphene nanoribbons: An electrochemical third generation glucose biosensor. *Microchimica Acta, 184*, 1127–1134.

Metters, J. P., Kadara, R. O., & Banks, C. E. (2011). New directions in screen printed electroanalytical sensors: An overview of recent developments. *The Analyst, 136*, 1067–1076.

Miller, J. N. (1991). Basic Statistical Methods for Analytical Chemistry. Part 2. Calibration and Regression Methods. A Review. *Analyst, 116*, 3-14.

Mistry, K. K., Layek, K., Mahapatra, A., RoyChaudhuri, C., & Saha, H. (2014). A review on amperometric-type immunosensors based on screen-printed electrodes. *The Analyst, 139*, 2289–2311.

Moccelini, S. K., Franzoi, A. C., Vieira, I. C., Dupont, J., & Scheeren, C. W. (2011). A novel support for laccase immobilization: Cellulose acetate modified with ionic liquid and application in biosensor for methyldopa detection. *Biosensors & bioelectronics, 26*, 3549–3554.

Mousty, C., Vieille, L., & Cosnier, S. (2007). Laccase immobilization in redox active layered double hydroxides: A reagentless amperometric biosensor. *Biosensors & bioelectronics, 22*, 1733–1738.

Nam, H.-S., Yoon, J.-K., Ko, J. M., & Kim, J.-D. (2010). Electrochemical capacitors of flower-like and nanowire structured MnO2 by a sonochemical method. *Materials Chemistry and Physics, 123*, 331–336.

Narita, A., Chen, Z., Chen, Q., & Müllen, K. (2019). Solution and on-surface synthesis of structurally defined graphene nanoribbons as a new family of semiconductors. *Chemical science*, *10*, 964–975.

Nawaz, M. A. H., Rauf, S., Catanante, G., Nawaz, M. H., Nunes, G., Marty, J. L., & Haya, A. (2016). One Step Assembly of Thin Films of Carbon Nanotubes on Screen Printed Interface for Electrochemical Aptasensing of Breast Cancer Biomarker. *Sensors*, *16*, 1651-1665.

Navarreto-Lugo, M., Lim, J. H., & Samia, A. C. S. (2018). Engineering of Au/Ag Nanostructures for Enhanced Electrochemical Performance. *Journal of The Electrochemical Society*, *165*, B83-B88.

Noorbakhsh, A., & Salimi, A. (2011). Development of DNA electrochemical biosensor based on immobilization of ssDNA on the surface of nickel oxide nanoparticles modified glassy carbon electrode. *Biosensors & bioelectronics, 30*, 188–196.

Norouzi, P., Ganjali, H., Larijani, B., Reza Ganjali, M., Faridbod, F., & Ali Zamani, H. (2011). A Glucose Biosensor Based on Nanographene and ZnO Nanoparticles Using FFT Continuous Cyclic Voltammetry. *International Journal of Electrochemical Science*, *6*, 5189-5199.

Novoselov, K. S. (2004). Electric Field Effect in Atomically Thin Carbon Films. *Science, 306*, 666–669.

Novoselov, K. S., & Castro Neto, A. H. (2012). Two-dimensional crystals-based heterostructures: Materials with tailored properties. *Physica Scripta*, *T146*, 14006.

Nunes, D., Pimentel, A., Gonçalves, A., Pereira, S., Branquinho, R., Barquinha, P., Fortunato, E., & Martins, R. (2019). Metal oxide nanostructures for sensor applications. *Semiconductor Science and Technology*, *34*, 43001.

Odaci, D., Timur, S., Pazarlioğlu, N., Kirgöz, U. A., & Telefoncu, A. (2006). Effects of mediators on the laccase biosensor response in paracetamol detection. *Biotechnology and applied biochemistry, 45*, 23–28.

Ognjanović, M., Stanković, D. M., Fabián, M., Vukadinović, A., Prijović, Ž., Dojčinović, B., & Antić, B. (2018). A Voltammetric Sensor Based on MgFe 2 O 4 Decorated on Reduced Graphene Oxide-modified Electrode for Sensitive and Simultaneous Determination of Catechol and Hydroquinone. *Electroanalysis, 30*, 2620–2627.

Ognjanović, M., Stanković, D. M., Jović, M., Krstić, M. P., Lesch, A., Girault, H. H., & Antić, B. (2020). Inkjet-Printed Carbon Nanotube Electrodes Modified with Dimercaptosuccinic Acid-Capped Fe 3 O 4 Nanoparticles on Reduced Graphene Oxide Nanosheets for Single-Drop Determination of Trifluoperazine. *ACS Applied Nano Materials, 3*, 4654–4662.

Oliveira, P. R. d., Oliveira, M. M., Zarbin, A. J.G., Marcolino-Junior, L. H., & Bergamini, M. F. (2012). Flow injection amperometric determination of isoniazid using a screen-printed carbon electrode modified with silver hexacyanoferrates nanoparticles. *Sensors and Actuators B: Chemical*, *171-172*, 795–802.

Omkaram, I., Hong, Y. K., & Kim, S. (2018). Transition Metal Dichalcogenide Photodetectors. In P. K. Nayak (Ed.), *Two-dimensional Materials for Photodetector*: InTech.

Oudghiri-Hassani, H., Rakass, S., Al Wadaani, F. T., Al-ghamdi, K. J., Omer, A., Messali, M., & Abboudi, M. (2018a). Synthesis, characterization and photocatalytic activity of α-Bi2O3 nanoparticles. *Journal of Taibah University for Science*, *9*, 508–512.

Oudghiri-Hassani, H., Rakass, S., Al Wadaani, F. T., Al-ghamdi, K. J., Omer, A., Messali, M., & Abboudi, M. (2018b). Synthesis, characterization and photocatalytic activity of α-Bi2O3 nanoparticles. *Journal of Taibah University for Science*, *9*, 508–512.

Pakapongpan, S., & Poo-Arporn, R. P. (2017). Self-assembly of glucose oxidase on reduced graphene oxide-magnetic nanoparticles nanocomposite-based direct electrochemistry for reagentless

glucose biosensor. *Materials science & engineering. C, Materials for biological applications*, *76*, 398–405.

Palanisamy, S., Ezhil Vilian, A. T., & Chen, S. M. (2012). Direct Electrochemistry of Glucose Oxidase at Reduced Graphene Oxide/Zinc Oxide Composite Modified Electrode for Glucose Sensor. *International Journal of Electrochemical Science*, *7*, 2153-2163.

Palanisamy, S., Ramaraj, S. K., Chen, S.-M., Yang, T. C. K., Yi-Fan, P., Chen, T.-W., Velusamy, V., & Selvam, S. (2017). A novel Laccase Biosensor based on Laccase immobilized Graphene-Cellulose Microfiber Composite modified Screen-Printed Carbon Electrode for Sensitive Determination of Catechol. *Scientific reports*, *7*, 41214.

Pan, C., Li, X., Wang, F., & Wang, L. (2008). Synthesis of bismuth oxide nanoparticles by the polyacrylamide gel route. *Ceramics International*, *34*, 439–441.

Pang, S. C., Anderson, M. A., & Chapman, T. W. (2000). Novel Electrode Materials for Thin-Film Ultracapacitors:
Comparison of Electrochemical Properties of Sol-Gel-Derived and Electrodeposited Manganese Dioxide. *Journal of The Electrochemical Society*, *147*, 444-450.

Park, S., Kim, S., Sun, G. J., & Lee, C. (2015). Synthesis, Structure, and Ethanol Gas Sensing Properties of In2O3 Nanorods Decorated with Bi2O3 Nanoparticles. *ACS Applied Materials & Interfaces*, *7*, 8138-8146.

Parveen, N., Mahato, N., Ansari, M. O., & Cho, M. H. (2016). Enhanced electrochemical behavior and hydrophobicity of crystalline polyaniline@graphene nanocomposite synthesized at elevated temperature. *Composites Part B: Engineering*, *87*, 281–290.

Patel, S. K.S., Anwar, M. Z., Kumar, A., Otari, S. V., Pagolu, R. T., Kim, S.-Y., Kim, I.-W., & Lee, J.-K. (2018). Fe2O3 yolk-shell particle-based laccase biosensor for efficient detection of 2,6-dimethoxyphenol. *Biochemical Engineering Journal*, *132*, 1–8.

Patris, S., & Kauffmann, J. M. (2015). Screen-printed electrodes (SPE) for drug compounds determination, in: Electroanalysis in biomedical and pharmaceutical sciences: Voltammetry, amperometry, biosensors, applications. Springer-Verlag, Berlin.

Pauliukaite, R., Metelka, R., Svancara, I., Królicka, A., Bobrowski, A., Vytras, K., Norkus, E., & Kalcher, K. (2002). Carbon paste electrodes modified with Bi(2)O(3) as sensors for the determination of Cd and Pb. *Analytical and bioanalytical chemistry*, *374*, 1155–1158.

Periasamy, A. P., Yang, S., & Chen, S.-M. (2011). Preparation and characterization of bismuth oxide nanoparticles-multiwalled carbon nanotube composite for the development of horseradish peroxidase based H_2O_2 biosensor. *Talanta*, *87*, 15–23.

Petković, B. B., Stanković, D., Milčić, M., Sovilj, S. P., & Manojlović, D. (2015). Dinuclear copper(II) octaazamacrocyclic complex in a PVC coated GCE and graphite as a voltammetric sensor for determination of gallic acid and antioxidant capacity of wine samples. *Talanta*, *132*, 513–519.

Ping, J., Wu, J., & Ying, Y. (2012). Determination of trace heavy metals in milk using an ionic liquid and bismuth oxide nanoparticles modified carbon paste electrode. *Chinese Science Bulletin*, *57*, 1781–1787.

Portaccio, M., Di Martino, S., Maiuri, P., Durante, D., Luca, P. de, Lepore, M., Bencivenga, U., Rossi, S., Maio, A. de, & Mita, D. G. (2006). Biosensors for phenolic compounds: The catechol as a substrate model. *Journal of Molecular Catalysis B: Enzymatic*, *41*, 97–102.

Prashanth, G. R., Goudar, V. S., Suran, S., Raichur, A. M., & Varma, M. M. (2012). Non-covalent functionalization using lithographically patterned polyelectrolyte multilayers for high-density microarrays. *Sensors and Actuators B: Chemical*, *171-172*, 315–322.

Pugno, N. M. (2009). The elasticity and strength of graphene. *Recent Res. Development of Materials Science*, *8*, 101-103.

Pumera, M. (2010). Graphene-based nanomaterials and their electrochemistry. *Chemical Society reviews*, *39*, 4146–4157.

Pumera, M. (2013). Electrochemistry of graphene, graphene oxide and other graphenoids: Review. *Electrochemistry Communications*, *36*, 14–18.

Pumera, M., Ambrosi, A., Bonanni, A., Chng, E. L. K., & Poh, H. L. (2010). Graphene for electrochemical sensing and biosensing. *TrAC Trends in Analytical Chemistry*, *29*, 954–965.

Qiao, K., & Hu, N. (2009). Direct electron transfer and electrocatalysis of myoglobin loaded in layer-by-layer films assembled with nonionic poly(ethylene glycol) and ZrO(2) nanoparticles. *Bioelectrochemistry (Amsterdam, Netherlands)*, *75*, 71–76.

Qu, J., Lou, T., Wang, Y., Dong, Y., & Xing, H. (2015). Determination of Catechol by a Novel Laccase Biosensor Based on Zinc-Oxide Sol-Gel. *Analytical Letters*, *48*, 1842–1853.

Radhakrishnan, S., Krishnamoorthy, K., Sekar, C., Wilson, J., & Kim, S. J. (2014). A highly sensitive electrochemical sensor for nitrite detection based on Fe2O3 nanoparticles decorated reduced graphene oxide nanosheets. *Applied Catalysis B: Environmental*, *148-149*, 22–28.

Rahman, M. M., Khan, S. B., Gruner, G., Al-Ghamdi, M. S., Daous, M. A., & Asiri, A. M. (2013). Chloride ion sensors based on low-dimensional α-MnO2–Co3O4 nanoparticles fabricated glassy carbon electrodes by simple I–V technique. *Electrochimica Acta*, *103*, 143–150.

Rakhi, R. B., Nayak, P., Xia, C., & Alshareef, H. N. (2016). Novel amperometric glucose biosensor based on MXene nanocomposite. *Scientific reports*, *6*, 36422.

Rao, D., Zhang, X., Sheng, Q., & Zheng, J. (2016). Highly improved sensing of dopamine by using glassy carbon electrode modified with MnO2, graphene oxide, carbon nanotubes and gold nanoparticles. *Microchimica Acta*, *183*, 2597–2604.

Rasheed, P. A., & Sandhyarani, N. (2014). Graphene-DNA electrochemical sensor for the sensitive detection of BRCA1 gene. *Sensors and Actuators B: Chemical*, *204*, 777–782.

Rastogi, A., Zivcak, M., Sytar, O., Kalaji, H. M., He, X., Mbarki, S., & Brestic, M. (2017). Impact of Metal and Metal Oxide Nanoparticles on Plant: A Critical Review. *Frontiers in chemistry*, *5*, 78.

Rawal, R., Chawla, S., & Pundir, C. S. (2011). Polyphenol biosensor based on laccase immobilized onto silver nanoparticles/multiwalled carbon nanotube/polyaniline gold electrode. *Analytical biochemistry*, *419*, 196–204.

Razmi, H., & Habibi, E. (2010). Amperometric detection of acetaminophen by an electrochemical sensor based on cobalt oxide nanoparticles in a flow injection system. *Electrochimica Acta*, *55*, 8731–8737.

Reddy, R. N., & Reddy, R. G. (2004). Synthesis and electrochemical characterization of amorphous MnO2 electrochemical capacitor electrode material. *Journal of Power Sources*, *132*, 315–320.

Reimer, L. (1998). Scanning Electron Microscopy. Physics of Image Formation and Microanalysis. Second edition. Springer-Verlag Berlin Heidelberg.

Riva, S. (2006). Laccases: Blue enzymes for green chemistry. *Trends in biotechnology*, *24*, 219–226.

Rizwan, S., & Fatima, S. (2018). Bismuth Ferrites/Graphene Nanoplatelets Nanohybrids for Efficient Organic Dye Removal. In Y. Zhou, F. Dong, & S. Jin (Eds.), *Bismuth - Advanced Applications and Defects Characterization*: InTech.

Rodríguez-Delgado, M. M., Alemán-Nava, G. S., Rodríguez-Delgado, J. M., Dieck-Assad, G., Martínez-Chapa, S. O., Barceló, D., & Parra, R. (2015). Laccase-based biosensors for detection of phenolic compounds. *TrAC Trends in Analytical Chemistry*, *74*, 21–45.

Roy, J. J., Abraham, T. E., Abhijith, K. S., Kumar, P. V. S., & Thakur, M. S. (2005). Biosensor for the determination of phenols based on cross-linked enzyme crystals (CLEC) of laccase. *Biosensors & bioelectronics*, *21*, 206–211.

Ruess, G., & Vogt, F. (1948). Hchstlamellarer Kohlenstoff aus Graphitoxyhydroxyd. *Monatshefte fr Chemie*, *78*, 222–242.

Ruffieux, P., Wang, S., Yang, B., Sánchez-Sánchez, C., Liu, J., Dienel, T., Talirz, L., Shinde, P., Pignedoli, C. A., Passerone, D., Dumslaff, T., Feng, X., Müllen, K., & Fasel, R. (2016). On-surface synthesis of graphene nanoribbons with zigzag edge topology. *Nature*, *531*, 489–492.

Sadeghi, S., Fooladi, E., & Malekaneh, M. (2015). A new amperometric biosensor based on Fe3O4/polyaniline/laccase/chitosan biocomposite-modified carbon paste electrode for determination of catechol in tea leaves. *Applied biochemistry and biotechnology*, *175*, 1603–1616.

Said, M. I., Rageh, A. H., & Abdel-aal, F. A. M. (2018). Fabrication of novel electrochemical sensors based on modification with different polymorphs of MnO 2 nanoparticles. Application to furosemide analysis in pharmaceutical and urine samples. *RSC Advances*, *8*, 18698–18713.

Saleem, H., Haneef, M., & Abbasi, H. Y. (2018). Synthesis route of reduced graphene oxide via thermal reduction of chemically exfoliated graphene oxide. *Materials Chemistry and Physics*, *204*, 1–7.

Salimi, A., Compton, R. G., & Hallaj, R. (2004). Glucose biosensor prepared by glucose oxidase encapsulated sol-gel and carbon-nanotube-modified basal plane pyrolytic graphite electrode. *Analytical biochemistry*, *333*, 49–56.

Salimi, A., Sharifi, E., Noorbakhsh, A., & Soltanian, S. (2007). Immobilization of glucose oxidase on electrodeposited nickel oxide nanoparticles: Direct electron transfer and electrocatalytic activity. *Biosensors & bioelectronics*, *22*, 3146–3153.

Sassolas, A., Blum, L. J., & Leca-Bouvier, B. D. (2012). Immobilization strategies to develop enzymatic biosensors. *Biotechnology Advances*, *30*, 489–511.

Schachl, K., Alemu, H., Kalcher, K., Jezkova, J., Svancara, I., & Vytras, K. (2006). Flow Injection Determination of Hydrogen Peroxide Using a Carbon Paste Electrode Modified with a Manganese Dioxide Film. *Analytical Letters*, *30*, 2655–2673.

Schachl, K., Alemu, H., Kalcher, K., Ježkova, J., Švancara, I., & Vytřas, K. (1997). Amperometric Determination of Hydrogen Peroxide With a Manganese Dioxide-modified Carbon Paste Electrode Using Flow Injection Analysis. *The Analyst*, *122*, 985–989.

Šeruga, M., Novak, I., & Jakobek, L. (2011). Determination of polyphenols content and antioxidant activity of some red wines by differential pulse voltammetry, HPLC and spectrophotometric methods. *Food chemistry*, *124*, 1208–1216.

Sethuraman, V., Muthuraja, P., Anandha Raj, J., & Manisankar, P. (2016). A highly sensitive electrochemical biosensor for catechol using conducting polymer reduced graphene oxide-metal oxide enzyme modified electrode. *Biosensors & bioelectronics*, *84*, 112–119.

Shahid, M. M., Rameshkumar, P., Pandikumar, A., Lim, H. N., Ng, Y. H., & Huang, N. M. (2015). An electrochemical sensing platform based on a reduced graphene oxide–cobalt oxide nanocube@platinum nanocomposite for nitric oxide detection. *Journal of Materials Chemistry A*, *3*, 14458–14468.

Shahrokhian, S., & Bozorgzadeh, S. (2006). Electrochemical oxidation of dopamine in the presence of sulfhydryl compounds: Application to the square-wave voltammetric detection of penicillamine and cysteine. *Electrochimica Acta*, *51*, 4271–4276.

Shahrokhian, S., & Zare-Mehrjardi, H. R. (2007). Application of thionine-nafion supported on multi-walled carbon nanotube for preparation of a modified electrode in simultaneous voltammetric detection of dopamine and ascorbic acid. *Electrochimica Acta*, *52*, 6310–6317.

Shahrokhian, S., & Zare-Mehrjardi, H. (2007). Cobalt salophen-modified carbon-paste electrode incorporating a cationic surfactant for simultaneous voltammetric detection of ascorbic acid and dopamine. *Sensors and Actuators B: Chemical*, *121*, 530–537.

Shang, N. G., Papakonstantinou, P., McMullan, M., Chu, M., Stamboulis, A., Potenza, A., Dhesi, S. S., & Marchetto, H. (2008). Catalyst-Free Efficient Growth, Orientation and Biosensing Properties of Multilayer Graphene Nanoflake Films with Sharp Edge Planes. *Advanced Functional Materials*, *18*, 3506–3514.

Shao, L., Li, W., Yang, S., Shi, Z., & Lü, S. (2007). Mineralogical characteristics of airborne particles collected in Beijing during a severe Asian dust storm period in spring 2002. *Science in China Series D: Earth Sciences*, *50*, 953–959.

Shao, Y., Wang, J., Wu, H., Liu, J., Aksay, I. A., & Lin, Y. (2010). Graphene Based Electrochemical Sensors and Biosensors: A Review. *Electroanalysis*, *22*, 1027–1036.

Sharon, M., & Sharon, M. (2015). *Graphene: An Introduction to the Fundamentals and Industrial Applications / Madhuri Sharon and Maheshwar Sharon ; foreword by Hisanori Shinohara.* Advanced Material Series. Hoboken, New Jersey: Wiley; Salem.

Shin, J., Seo, J. K., Yaylian, R., Huang, A., & Meng, Y. S. (2020). A review on mechanistic understanding of MnO 2 in aqueous electrolyte for electrical energy storage systems. *International Materials Reviews*, *65*, 356–387.

Si, W., Lei, W., Zhang, Y., Xia, M., Wang, F., & Hao, Q. (2012). Electrodeposition of graphene oxide doped poly(3,4-ethylenedioxythiophene) film and its electrochemical sensing of catechol and hydroquinone. *Electrochimica Acta*, *85*, 295–301.

Sirota, B., Reyes-Cuellar, J., Kohli, P., Wang, L., McCarroll, M. E., & Aouadi, S. M. (2012). Bismuth oxide photocatalytic nanostructures produced by magnetron sputtering deposition. *Thin Solid Films*, *520*, 6118–6123.

Song, Z., Ma, Y.-L., & Li, C.-E. (2019). The residual tetracycline in pharmaceutical wastewater was effectively removed by using MnO2/graphene nanocomposite. *The Science of the total environment*, *651*, 580–590.

Staiti, P., & Lufrano, F. (2009). Study and optimisation of manganese oxide-based electrodes for electrochemical supercapacitors. *Journal of Power Sources*, *187*, 284–289.

Stanković, A., Mihailović, J., Mirković, M., Radović, M., Milanović, Z., Ognjanović, M., Janković, D., Antić, B., Mijović, M., Vranješ-Đurić, S., & Prijović, Ž. (2020a). Aminosilanized flower-structured superparamagnetic iron oxide nanoparticles coupled to 131I-labeled CC49 antibody for combined radionuclide and hyperthermia therapy of cancer. *International journal of pharmaceutics*, *587*, 119628.

Stanković, D. M., Švorc, Ľ., Mariano, J. F. M. L., Ortner, A., & Kalcher, K. (2017). Electrochemical Determination of Natural Drug Colchicine in Pharmaceuticals and Human Serum Sample and its Interaction with DNA. *Electroanalysis*, *29*, 2276–2281.

Stanković, V., Đurđić, S., Ognjanović, M., Antić, B., Kalcher, K., Mutić, J., & Stanković, D. M. (2020b). Anti-human albumin monoclonal antibody immobilized on EDC-NHS functionalized carboxylic graphene/AuNPs composite as promising electrochemical HSA immunosensor. *Journal of Electroanalytical Chemistry*, *860*, 113928.

Stanković, V., Đurđić, S., Ognjanović, M., Mutić, J., Kalcher, K., & Stanković, D. M. (2020c). A novel nonenzymatic hydrogen peroxide amperometric sensor based on AgNp@GNR nanocomposites modified screen-printed carbon electrode. *Journal of Electroanalytical Chemistry*, *876*, 114487.

Stefano Ferri, PhD., Katsuhiro Kojima, Ph.D., & and Koji Sode. Review of Glucose Oxidases and Glucose Dehydrogenases: A Bird's Eye View of Glucose Sensing Enzymes.

Stradiotto, N. R., Yamanaka, H., & Zanoni, M. V. B. (2003). Electrochemical sensors: A powerful tool in analytical chemistry. *Journal of the Brazilian Chemical Society*, *14*, 159–173.

Su, D., Ahn, H.-J., & Wang, G. (2013). Hydrothermal synthesis of α-MnO2 and β-MnO2 nanorods as high capacity cathode materials for sodium ion batteries. *Journal of Materials Chemistry A*, *1*, 4845.

Suh-Cem Pang, Marc A. Anderson, and Thomas W. Chapman. Novel Electrode Materials for Thin-Film Ultracapacitors: Comparison of Electrochemical Properties of Sol-Gel-Derived and Electrodeposited Manganese Dioxide.

Sun, W., Qin, P., Gao, H., Li, G., & Jiao, K. (2010). Electrochemical DNA biosensor based on chitosan/nano-V2O5/MWCNTs composite film modified carbon ionic liquid electrode and its application to the LAMP product of Yersinia enterocolitica gene sequence. *Biosensors & bioelectronics*, *25*, 1264–1270.

Suresh, R., Giribabu, K., Manigandan, R., Kumar, S. P., Munusamy, S., Muthamizh, S., Stephen, A., & Narayanan, V. (2014). New electrochemical sensor based on Ni-doped V2O5 nanoplates modified glassy carbon electrode for selective determination of dopamine at nanomolar level. *Sensors and Actuators B: Chemical*, *202*, 440–447.

Švancara, I., & Kalcher, K. (2015). Carbon paste electrodes, in: Electrochemistry of carbon electrodes, Wiley-VCH, Weinheim, 2015.

Takai, K., Oga, M., Sato, H., Enoki, T., Ohki, Y., Taomoto, A., Suenaga, K., & Iijima, S. (2003). Structure and electronic properties of a nongraphitic disordered carbon system and its heat-treatment effects. *Physical Review B*, *67*, 199.

Takeda, H., Ueda, T., Kamada, K., Matsuo, K., Hyodo, T., & Shimizu, Y. (2015). CO-sensing properties of a NASICON-based gas sensor attached with Pt mixed with Bi2O3 as a sensing electrode. *Electrochimica Acta*, *155*, 8–15.

Talirz, L., Söde, H., Dumslaff, T., Wang, S., Sanchez-Valencia, J. R., Liu, J., Shinde, P., Pignedoli, C. A., Liang, L., Meunier, V., Plumb, N. C., Shi, M., Feng, X., Narita, A., Müllen, K., Fasel, R., & Ruffieux, P. (2017). On-Surface Synthesis and Characterization of 9-Atom Wide Armchair Graphene Nanoribbons. *ACS nano*, *11*, 1380–1388.

Tan, Y., Deng, W., Ge, B., Xie, Q., Huang, J., & Yao, S. (2009). Biofuel cell and phenolic biosensor based on acid-resistant laccase-glutaraldehyde functionalized chitosan-multiwalled carbon nanotubes nanocomposite film. *Biosensors & bioelectronics*, *24*, 2225–2231.

Tang, L., Wang, Y., Li, Y., Feng, H., Lu, J., & Li, J. (2009). Preparation, Structure, and Electrochemical Properties of Reduced Graphene Sheet Films. *Advanced Functional Materials*, *19*, 2782–2789.

Teixeira, F.S. M., Moraes, C. F., Fatibello-Filho, O., & Bocchi, N. (2001). Voltammetric determination of lithium ions in pharmaceutical formulation using a λ-MnO2-modified carbon-paste electrode. *Analytica Chimica Acta*, *443*, 249-255.

Teradal, N. L., & Seetharamappa, J. (2015). Bulk Modification of Carbon Paste Electrode with Bi 2 O 3 Nanoparticles and Its Application as an Electrochemical Sensor for Selective Sensing of Anti□HIV Drug Nevirapine. *Electroanalysis*, *27*, 2007–2016.

Tesarova, E., Baldrianova, L., Hocevar, S. B., Svancara, I., Vytras, K., & Ogorevc, B. (2009). Anodic stripping voltammetric measurement of trace heavy metals at antimony film carbon paste electrode. *Electrochimica Acta*, *54*, 1506–1510.

Teymourian, H., Salimi, A., & Firoozi, S. (2014). A High Performance Electrochemical Biosensing Platform for Glucose Detection and IgE Aptasensing Based on Fe 3 O 4 /Reduced Graphene Oxide Nanocomposite. *Electroanalysis*, *26*, 129–138.

Thiyagarajan, N., Chang, J.-L., Senthilkumar, K., & Zen, J.-M. (2014). Disposable electrochemical sensors: A mini review. *Electrochemistry Communications*, *38*, 86–90.

Tian, Y., Deng, P., Wu, Y., Li, J., Liu, J., Li, G., & He, Q. (2020). MnO 2 Nanowires-Decorated Reduced Graphene Oxide Modified Glassy Carbon Electrode for Sensitive Determination of Bisphenol A. *Journal of The Electrochemical Society*, *167*, 46514.

Tien, L.-C., & Peng, S.-H. (2019). Selective synthesis of α-Bi2O3/rGO and β-Bi2O3/rGO heterostructures as efficient visible-light-driven photocatalysts. *Ceramics International*, *45*, 15334–15342.

Truong, Q.-T., Pokharel, P., Song, G. S., & Lee, D.-S. (2012). Preparation and characterization of graphene nanoplatelets from natural graphite via intercalation and exfoliation with tetraalkylammoniumbromide. *Journal of nanoscience and nanotechnology*, *12*, 4305–4308.

Turkusić, E., Kalcher, K., Schachl, K., Komersova, A., Bartos, M., Moderegger, H., Svancara, I., & Vytras, K. (2001). Amperometric determination of glucose with an MnO2 and glucose oxidase bulk-modified screen-printed carbon ink biosensor. *Analytical Letters*, *34*, 2633–2647.

Turkusic, E., Kalcher, J., Kahrovic, E., Beyene, N., Moderegger, H., Sofic, E., Begic, S., & Kalcher, K. (2005). Amperometric determination of bonded glucose with an MnO and glucose oxidase bulk-modified screen-printed electrode using flow-injection analysis. *Talanta*, *65*, 559–564.

Uang, Y.-M., & Chou, T.-C. (2003). Fabrication of glucose oxidase/polypyrrole biosensor by galvanostatic method in various pH aqueous solutions. *Biosensors and Bioelectronics*, *19*, 141–147.

Ubbelohde, A. R., Lewis, F. A., & Rice, S. A. (1961). Graphite and Its Crystal Compounds. *Physics Today*, *14*, 66–68.

Umar, A., Rahman, M. M., Vaseem, M., & Hahn, Y.-B. (2009). Ultra-sensitive cholesterol biosensor based on low-temperature grown ZnO nanoparticles. *Electrochemistry Communications*, *11*, 118–121.

Vasić, V., Gašić, U., Stanković, D., Lušić, D., Vukić-Lušić, D., Milojković-Opsenica, D., Tešić, Ž., & Trifković, J. (2019). Towards better quality criteria of European honeydew honey: Phenolic profile and antioxidant capacity. *Food chemistry*, *274*, 629–641.

Vasilescu, I., Eremia, S. A. V., Kusko, M., Radoi, A., Vasile, E., & Radu, G.-L. (2016). Molybdenum disulphide and graphene quantum dots as electrode modifiers for laccase biosensor. *Biosensors & bioelectronics*, *75*, 232–237.

Veeralingam, S., & Badhulika, S. (2020). Surface functionalized β-Bi2O3 nanofibers based flexible, field-effect transistor-biosensor (BioFET) for rapid, label-free detection of serotonin in biological fluids. *Sensors and Actuators B: Chemical*, *321*, 128540.

Viculis, L. M., Mack, J. J., Mayer, O. M., Hahn, H. T., & Kaner, R. B. (2005). Intercalation and exfoliation routes to graphite nanoplatelets. *Journal of Materials Chemistry*, *15*, 974.

Vilian, A. T. E., Chen, S.-M., Ali, M. A., & Al-Hemaid, F. M. A. (2014a). Direct electrochemistry of glucose oxidase immobilized on ZrO 2 nanoparticles-decorated reduced graphene oxide sheets for a glucose biosensor. *RSC Adv*, *4*, 30358–30367.

Vilian, A. T. E., Mani, V., Chen, S.-M., Dinesh, B., & Huang, S.-T. (2014b). The Immobilization of Glucose Oxidase at Manganese Dioxide Particles-Decorated Reduced Graphene Oxide Sheets for the Fabrication of a Glucose Biosensor. *Industrial & Engineering Chemistry Research*, *53*, 15582–15589.

Viñas, P., Campillo, N., Martínez-Castillo, N., & Hernández-Córdoba, M. (2009). Solid-phase microextraction on-fiber derivatization for the analysis of some polyphenols in wine and grapes using gas chromatography-mass spectrometry. *Journal of chromatography. A*, *1216*, 1279–1284.

Vukojević, V., Djurdjić, S., Ognjanović, M., Antić, B., Kalcher, K., Mutić, J., & Stanković, D. M. (2018a). RuO2/graphene nanoribbon composite supported on screen printed electrode with enhanced electrocatalytic performances toward ethanol and NADH biosensing. *Biosensors & bioelectronics*, *117*, 392–397.

Vukojević, V., Djurdjić, S., Ognjanović, M., Fabián, M., Samphao, A., Kalcher, K., & Stanković, D. M. (2018b). Enzymatic glucose biosensor based on manganese dioxide nanoparticles decorated on graphene nanoribbons. *Journal of Electroanalytical Chemistry*, *823*, 610–616.

Vyskočil, V., & Barek, J. (2009). Mercury Electrodes–Possibilities and Limitations in Environmental Electroanalysis. *Critical Reviews in Analytical Chemistry*, *39*, 173–188.

Wang, J. (2000). Analytical electrochemistry. Second edition. Wiley-VCH, New York.

Wang, C.Y., Becker, R. W., Passow, T., Pletschen, W., Köhler, K., Cimalla, V., & Ambacher, O. (2011). Photon stimulated sensor based on indium oxide nanoparticles I: Wide-concentration-range ozone monitoring in air. *Sensors and Actuators B: Chemical*, *152*, 235–240.

Wang, H.-W., Hu, Z.-A., Chang, Y.-Q., Chen, Y.-L., Lei, Z.-Q., Zhang, Z.-Y., & Yang, Y.-Y. (2010). Facile solvothermal synthesis of a graphene nanosheet–bismuth oxide composite and its electrochemical characteristics. *Electrochimica Acta*, *55*, 8974–8980.

Wang, J. (2008). Electrochemical glucose biosensors. *Chemical reviews*, *108*, 814–825.

Wang, L., Wang, J., Wang, M., Li, P., Tong, J., & Yu, F. (2020). AgO-decorated multi-dimensional chrysanthemum-like NiCo2O4 mounted on nickel foam as a highly efficient and stable electrocatalyst for the oxygen evolution reaction. *Nanoscale*, *12*, 7180–7187.

Wang, S., Tan, Y., Zhao, D., & Liu, G. (2008). Amperometric tyrosinase biosensor based on Fe3O4 nanoparticles-chitosan nanocomposite. *Biosensors & bioelectronics*, *23*, 1781–1787.

Wang, S., Xu, L.-P., Liang, H.-W., Yu, S.-H., Wen, Y., Wang, S., & Zhang, X. (2015a). Self-interconnecting Pt nanowire network electrode for electrochemical amperometric biosensor. *Nanoscale*, *7*, 11460–11467.

Wang, S. G., Zhang, Q., Wang, R., Yoon, S. F., Ahn, J., Yang, D. J., Tian, J. Z., Li, J. Q., & Zhou, Q. (2003). Multi-walled carbon nanotubes for the immobilization of enzyme in glucose biosensors. *Electrochemistry Communications*, *5*, 800–803.

Wang, X., Luo, C., Li, L., & Duan, H. (2015b). Highly selective and sensitive electrochemical sensor for l -cysteine detection based on graphene oxide/multiwalled carbon nanotube/manganese dioxide/gold nanoparticles composite. *Journal of Electroanalytical Chemistry*, *757*, 100–106.

Wang, X.-Y., Narita, A., & Müllen, K. (2018a). Precision synthesis versus bulk-scale fabrication of graphenes. *Nature Reviews Chemistry*, *2*, 666.

Wang, Y., Huang, B., Dai, W., Ye, J., & Xu, B. (2016a). Sensitive determination of capsaicin on Ag/Ag2O nanoparticles/reduced graphene oxide modified screen-printed electrode. *Journal of Electroanalytical Chemistry*, *776*, 93–100.

Wang, Y., Li, Y., Tang, L., Lu, J., & Li, J. (2009). Application of graphene-modified electrode for selective detection of dopamine. *Electrochemistry Communications*, *11*, 889–892.

Wang, Y., Liu, X.-y., Xu, X., Yang, Y., Huang, L.-h., He, Z.-y., Xu, Y.-h., Chen, J.-j., & Feng, Z.-s. (2018b). Preparation and characterization of reduced graphene oxide/Fe3O4 nanocomposite by a facile in-situ deposition method for glucose biosensor applications. *Materials Research Bulletin*, *101*, 340–346.

Wang, Y., Yin, H., Li, X., Waterhouse, G. I. N., & Ai, S. (2019). Photoelectrochemical immunosensor for N6-methyladenine detection based on Ru@UiO-66, Bi2O3 and Black TiO2. *Biosensors & bioelectronics*, *131*, 163–170.

Wang, Y., Zhai, F., Hasebe, Y., Jia, H., & Zhang, Z. (2018c). A highly sensitive electrochemical biosensor for phenol derivatives using a graphene oxide-modified tyrosinase electrode. *Bioelectrochemistry (Amsterdam, Netherlands)*, *122*, 174–182.

Wang, Y., Zhang, S., Bai, W., & Zheng, J. (2016b). Layer-by-layer assembly of copper nanoparticles and manganese dioxide-multiwalled carbon nanotubes film: A new nonenzymatic electrochemical sensor for glucose. *Talanta*, *149*, 211–216.

Weber, M., Schlesinger, M., Walther, M., Zahn, D., Schalley, C. A., & Mehring, M. (2017). Investigations on the growth of bismuth oxido clusters and the nucleation to give metastable bismuth oxide modifications. *Zeitschrift für Kristallographie - Crystalline Materials*, *232*, 4218.

Wei, M.-Y., Huang, R., & Guo, L.-H. (2012). High catalytic activity of indium tin oxide nanoparticle modified electrode towards electro-oxidation of ascorbic acid. *Journal of Electroanalytical Chemistry*, *664*, 156–160.

Wu, B., Zhang, G., Shuang, S., & Choi, M. M. F. (2004). Biosensors for determination of glucose with glucose oxidase immobilized on an eggshell membrane. *Talanta*, *64*, 546–553.

Wu, H., Wang, J., Kang, X., Wang, C., Wang, D., Liu, J., Aksay, I. A., & Lin, Y. (2009). Glucose biosensor based on immobilization of glucose oxidase in platinum nanoparticles/graphene/chitosan nanocomposite film. *Talanta*, *80*, 403–406.

Wu, J., & Yin, L. (2011). Platinum nanoparticle modified polyaniline-functionalized boron nitride nanotubes for amperometric glucose enzyme biosensor. *ACS applied materials & interfaces*, *3*, 4354–4362.

Wu, S., Su, F., Dong, X., Ma, C., Pang, L., Peng, D., Wang, M., He, L., & Zhang, Z. (2017). Development of glucose biosensors based on plasma polymerization-assisted nanocomposites of polyaniline, tin oxide, and three-dimensional reduced graphene oxide. *Applied Surface Science*, *401*, 262–270.

Xiao, W., Wang, D., & Lou, X. W. (2010). Shape-Controlled Synthesis of MnO 2 Nanostructures with Enhanced Electrocatalytic Activity for Oxygen Reduction. *The Journal of Physical Chemistry C*, *114*, 1694–1700.

Xiaohong, W., Wei, Q., & Weidong, H. (2007). Thin bismuth oxide films prepared through the sol–gel method as photocatalyst. *Journal of Molecular Catalysis A: Chemical*, *261*, 167–171.

Xie, C., Xiao, L., Hu, M., Bai, Z., Xia, X., & Zeng, D. (2010). Fabrication and formaldehyde gas-sensing property of ZnO–MnO2 coplanar gas sensor arrays. *Sensors and Actuators B: Chemical*, *145*, 457–463.

Xin, Y., Fu-bing, X., Hong-wei, L., Feng, W., Di-zhao, C., & Zhao-yang, W. (2013). A novel H2O2 biosensor based on Fe3O4–Au magnetic nanoparticles coated horseradish peroxidase and

graphene sheets–Nafion film modified screen-printed carbon electrode. *Electrochimica Acta*, *109*, 750–755.

Xu, J.-J., Luo, X.-L., Du, Y., & Chen, H.-Y. (2004). Application of MnO2 nanoparticles as an eliminator of ascorbate interference to amperometric glucose biosensors. *Electrochemistry Communications*, *6*, 1169–1173.

Xu, J.-J., Zhao, W., Luo, X.-L., & Chen, H.-Y. (2005). A sensitive biosensor for lactate based on layer-by-layer assembling MnO2 nanoparticles and lactate oxidase on ion-sensitive field-effect transistors. *Chemical communications (Cambridge, England)*, 792–794.

Xu, M., Kong, L., Zhou, W., & Li, H. (2007). Hydrothermal Synthesis and Pseudocapacitance Properties of α-MnO 2 Hollow Spheres and Hollow Urchins. *The Journal of Physical Chemistry C*, *111*, 19141–19147.

Xu, X., Lu, P., Zhou, Y., Zhao, Z., & Guo, M. (2009). Laccase immobilized on methylene blue modified mesoporous silica MCM-41/PVA. *Materials Science and Engineering: C*, *29*, 2160–2164.

Yan, S., Wan, L., Li, Z., Zhou, Y., & Zou, Z. (2010). Synthesis of a mesoporous single crystal Ga2O3 nanoplate with improved photoluminescence and high sensitivity in detecting CO. *Chemical communications (Cambridge, England)*, *46*, 6388–6390.

Yan, Y., Liu, Q., Du, X., Qian, J., Mao, H., & Wang, K. (2015). Visible light photoelectrochemical sensor for ultrasensitive determination of dopamine based on synergistic effect of graphene quantum dots and TiO2 nanoparticles. *Analytica chimica acta*, *853*, 258–264.

Yang, C., van der Laak, N. K., Chan, K.-Y., & Zhang, X. (2012). Microwave-assisted microemulsion synthesis of carbon supported Pt-WO3 nanoparticles as an electrocatalyst for methanol oxidation. *Electrochimica Acta*, *75*, 262–272.

Yang, L., Liu, D., Huang, J., & You, T. (2014a). Simultaneous determination of dopamine, ascorbic acid and uric acid at electrochemically reduced graphene oxide modified electrode. *Sensors and Actuators B: Chemical*, *193*, 166–172.

Yang, L.-L., Han, Q.-F., Zhao, J., Zhu, J.-W., Wang, X., & Ma, W.-H. (2014b). Synthesis of Bi2O3 architectures in DMF–H2O solution by precipitation method and their photocatalytic activity. *Journal of Alloys and Compounds*, *614*, 353–359.

Yang, W., Ratinac, K. R., Ringer, S. P., Thordarson, P., Gooding, J. J., & Braet, F. (2010a). Carbon nanomaterials in biosensors: Should you use nanotubes or graphene? *Angewandte Chemie (International ed. in English)*, *49*, 2114–2138.

Yang, W., Zhang, J., Ma, Q., Zhao, Y., Liu, Y., & He, H. (2017). Heterogeneous Reaction of SO2 on Manganese Oxides: The Effect of Crystal Structure and Relative Humidity. *Scientific reports*, *7*, 4550.

Yang, X., Wu, F., Chen, D.-Z., & Lin, H.-W. (2014c). An electrochemical immunosensor for rapid determination of clenbuterol by using magnetic nanocomposites to modify screen printed carbon electrode based on competitive immunoassay mode. *Sensors and Actuators B: Chemical*, *192*, 529–535.

Yang, Y.-L., Chuang, M.-C., Lou, S.-L., & Wang, J. (2010b). Thick-film textile-based amperometric sensors and biosensors. *The Analyst*, *135*, 1230.

Ye, Y., & Ju, H. (2005). Rapid detection of ssDNA and RNA using multi-walled carbon nanotubes modified screen-printed carbon electrode. *Biosensors & bioelectronics*, *21*, 735–741.

Yin, H., Zhang, Q., Zhou, Y., Ma, Q., liu, T., Zhu, L., & Ai, S. (2011). Electrochemical behavior of catechol, resorcinol and hydroquinone at graphene–chitosan composite film modified glassy carbon electrode and their simultaneous determination in water samples. *Electrochimica Acta*, *56*, 2748–2753.

Yu, H., Yan, F., Dai, Z., & Ju, H. (2004). A disposable amperometric immunosensor for alpha-1-fetoprotein based on enzyme-labeled antibody/chitosan-membrane-modified screen-printed carbon electrode. *Analytical biochemistry*, *331*, 98–105.

Yuan, Y., He, K., Byles, B. W., Liu, C., Amine, K., Lu, J., Pomerantseva, E., & Shahbazian-Yassar, R. (2019). Deciphering the Atomic Patterns Leading to MnO2 Polymorphism. *Chem*, *5*, 1793–1805.

Zaidi, S. A., & Shin, J. H. (2015). A novel and highly sensitive electrochemical monitoring platform for 4-nitrophenol on MnO 2 nanoparticles modified graphene surface. *RSC Advances*, *5*, 88996–89002.

Zbiljić, J., Guzsvány, V., Vajdle, O., Prlina, B., Agbaba, J., Dalmacija, B., Kónya, Z., & Kalcher, K. (2015). Determination of H2O2 by MnO2 modified screen printed carbon electrode during Fenton and visible light-assisted photo-Fenton based removal of acetamiprid from water. *Journal of Electroanalytical Chemistry*, *755*, 77–86.

Zhang, H., Bo, X., & Guo, L. (2015a). Electrochemical preparation of porous graphene and its electrochemical application in the simultaneous determination of hydroquinone, catechol, and resorcinol. *Sensors and Actuators B: Chemical*, *220*, 919–926.

Zhang, L., Yuan, S.-m., Yang, L.-m., Fang, Z., & Zhao, G.-c. (2013). An enzymatic glucose biosensor based on a glassy carbon electrode modified with manganese dioxide nanowires. *Microchimica Acta*, *180*, 627–633.

Zhang, S., & Zheng, J. (2016). Synthesis of single-crystal α-MnO2 nanotubes-loaded Ag@C core-shell matrix and their application for electrochemical sensing of nonenzymatic hydrogen peroxide. *Talanta*, *159*, 231–237.

Zhang, W., Li, X., Zou, R., Wu, H., Shi, H., Yu, S., & Liu, Y. (2015b). Multifunctional glucose biosensors from Fe3O4 nanoparticles modified chitosan/graphene nanocomposites. *Scientific Reports*, *5*, 1417.

Zhang, Y., He, P., & Hu, N. (2004). Horseradish peroxidase immobilized in TiO2 nanoparticle films on pyrolytic graphite electrodes: Direct electrochemistry and bioelectrocatalysis. *Electrochimica Acta*, *49*, 1981–1988.

Zhang, Y., & Jiang, W. (2012). Decorating graphene sheets with gold nanoparticles for the detection of sequence-specific DNA. *Electrochimica Acta*, *71*, 239–245.

Zhao, G., Feng, J.-J., Xu, J.-J., & Chen, H.-Y. (2005). Direct electrochemistry and electrocatalysis of heme proteins immobilized on self-assembled ZrO2 film. *Electrochemistry Communications*, *7*, 724–729.

Zhao, Z. W., Chen, X. J., Tay, B. K., Chen, J. S., Han, Z. J., & Khor, K. A. (2007). A novel amperometric biosensor based on ZnO:Co nanoclusters for biosensing glucose. *Biosensors & bioelectronics*, *23*, 135–139.

Zheng, X., & Guo, Z. (2000). Potentiometric determination of hydrogen peroxide at MnO2-doped carbon paste electrode. *Talanta*, *50*, 1157-1162.

Zheng, Q., Wu, H., Shen, Z., Gao, W., Yu, Y., Ma, Y., Guang, W., Guo, Q., Yan, R., Wang, J., & Ding, K. (2015). An electrochemical DNA sensor based on polyaniline/graphene: High sensitivity to DNA sequences in a wide range. *The Analyst*, *140*, 6660–6670.

Zhou, M., Zhai, Y., & Dong, S. (2009). Electrochemical sensing and biosensing platform based on chemically reduced graphene oxide. *Analytical chemistry*, *81*, 5603–5613.

Zhou, Q., Yang, L., Wang, G., & Yang, Y. (2013). Acetylcholinesterase biosensor based on SnO2 nanoparticles-carboxylic graphene-nafion modified electrode for detection of pesticides. *Biosensors & bioelectronics*, *49*, 25–31.

Zhou, G., Sun, J., Yaseen, M., Zhang, H., He, H., & Wang, Y. (2018). Synthesis of Highly Selective Magnetite (Fe3O4) and Tyrosinase Immobilized on Chitosan Microspheres as Low Potential Electrochemical Biosensor. *Journal of The Electrochemical Society*, *165*, G11-G17.

Zhu, Z. (2017). An Overview of Carbon Nanotubes and Graphene for Biosensing Applications. *Nano-micro letters*, *9*, 25.

Zhuang, X., Chen, D., Wang, S., Liu, H., & Chen, L. (2017). Manganese dioxide nanosheet-decorated ionic liquid-functionalized graphene for electrochemical theophylline biosensing. *Sensors and Actuators B: Chemical*, *251*, 185–191.

Zidan, M., Tee, W. T. Abdullah, A. H., Zainal, Z., & Kheng, G. J. (2011a). Electrochemical Oxidation of Ascorbic Acid Mediated by Bi2O3 Microparticles Modified Glassy Carbon Electrode. *International Journal of Electrochemical Science*, *6*, 289-300.

Zidan, M., Tee, W. T. Abdullah, A. H., Zainal, Z., & Kheng, G. J. (2011b). Electrochemical Oxidation of Paracetamol Mediated by Nanoparticles Bismuth Oxide Modified Glassy Carbon Electrode. *International Journal of Electrochemical Science*, *6*, 279-288.

Biography of the author

Slađana Z. Đurđić was born on November 20th, 1991. in Čačak, Republic of Serbia. She finished elementary and high school in Lučani. She started at the Faculty of Chemistry - University of Belgrade in 2010. as a full-time student in the field of Environmental Chemistry, and graduated on September 29th, 2014., with GPA of 9.32. She started graduate academic studies (MSc) at the Faculty of Chemistry - University of Belgrade in 2014. She completed MSc studies in 2015. with GPA of 10.00 and in the same year she started her PhD studies at the Department of Analytical Chemistry at the Faculty of Chemistry - University of Belgrade. She passed all the exams provided for in the plan and program in PhD studies with GPA of 10.00.

In 2015., Slađana Z. Đurđić was participated as a teaching associate at the Faculty of Chemistry - University of Belgrade. During the period of 2017-2018, she was employed at the Innovation Center of the Faculty of Chemistry - University of Belgrade, as a graduate researcher. Since 2018., she has been employed at the Faculty of Chemistry - University of Belgrade, as an assistant at the Department of Analytical Chemistry. Since 2017., Slađana Z. Đurđić has participated as a researcher on the national project OI 172030 (*Application of advanced oxidation processes and nanostructured oxide materials for removing pollutants from the environment, development and optimization of instrumental techniques for monitoring efficiency*) funded by the Ministry of Education, Science and Technological Development of the Republic of Serbia. In 2020., she has participated as a researcher on the Serbian-French bilateral project "Pavle Savić" (*Magnetic electrochemiluminescent biosensors for ultrasensitive mycotoxins*), while since the beginning of 2021. she participates as a member of the IMPTOX project (*An Innovative Analytical Platform to Investigate the Effect and Toxicity of Micro and Nano Plastics Combined with Environmental Contaminants on the Risk of Allergic Disease in Preclinical and Clinical Studies*).

She was awarded as the Best Student of the Environmental Chemistry Study Program (school year 2013/2014.) As a part of the international CEEPUS Mobility Network, she participated in the *Seminar/workshop on SENSING IN ELECTROANALYSIS* (2017. and 2018.), Pardubice (Czech Republic) and, during the period of 2018-2020, she was granted three times with a one-month stay in Austria, at the Karl-Franzens - University of Graz.

Untill now, Slađana Z. Đurđić is the author and co-author of 26 scientific papers in international journals, as well as 12 papers published in the international conference proceedings as abstracts (M34) and 12 paper published in the national conference proceedings as abstracts. The doctoral dissertation resulted in 2 scientific papers (published in the top 30% of international journals) and one paper published in the international conference proceedings as abstracts.

List of scientific papers that are part of the doctoral dissertation:

S. Đurđić, V. Vukojević, F. Vlahović, M. Ognjanović, Ľ. Švorc, K. Kalcher, J. Mutić, D. M. Stanković. Application of bismuth(III) oxide decorated graphene nanoribbons for enzymatic glucose biosensing. *Journal of Electroanalytical Chemistry*, 850 (**2019**) 113400. [Journal of Electroanalytical Chemistry, IF_{2019}=3.519; (17/86)].

https://www.sciencedirect.com/science/article/pii/S157266571930668X

S. Đurđić, V. Stanković, F. Vlahović, M. Ognjanović, K. Kalcher, T. Ćirković Veličković, J. Mutić, D. M. Stanković. Laccase Polyphenolic Biosensor Supported on MnO_2@GNP Decorated SPCE: Preparation, Characterization, and Analytical Application. Journal of The Electrochemical Society, 168 (**2021**) 037510. [Journal of The Electrochemical Society, IF_{2019}=3.719; (5/21)].

https://iopscience.iop.org/article/10.1149/1945-7111/abeaf2

Биографија аутора

Слађана З. Ђурђић рођена је 20. новембра 1991. године у Чачку, Република Србија. Основу и средњу школу завршила је у Лучанима. Хемијски факултет - Универзитета у Београду уписала је 2010. године као редован студент на смеру Хемичар за животну средину, и дипломирала 29. септембра 2014. године, са просечном оценом 9.32. Мастер академске студије на Хемијском факултету - Универзитета у Београду уписала је 2014. године. Мастер студије је завршила 2015. године са просечном оценом 10.00 и исте године уписала докторске академске студије при Катедри за аналитичку хемију на Хемијском факултету - Универзитета у Београду. Положила је све планом и програмом предвиђене испите на докторским студијама са просечном оценом 10.00.

Слађана З. Ђурђић је 2015. године била ангажована као сарадник у настави на Хемијском факултету - Универзитета у Београду. Од 2017. до 2018. године је била запослена на Иновационом центру Хемијског факултета - Универзитета у Београду, као истраживач приправник. Од 2018. године је запослена на Хемијском факултету - Универзитета у Београду, као асистент при Катедри за аналитичку хемију. Од 2017. године Слађана З. Ђурђић је ангажована као истраживач на националном пројекту ОИ 172030 (*Примена унапређених оксидационих процеса и наноструктурисаних оксидних материјала за уклањање загађивача из животне средине , развој и оптимизација инструменталних техника за праћење ефикасности*) финансираном од стране Министарства просвете, науке и технолошког развоја Републике Србије. У 2020. години је ангажована као истраживач на српско-француском билатералном пројекту ”Павле Савић” (*Магнетни електрохемлуминисцентни биосензори за ултраосетљиве микотоксине*), док је од 2021. године ангажована на *IMPTOX* пројекту (*Иновативна аналитичка платформа за истраживање ефекта и токсичности микро и нано пластика у комбинацији са загађивачима животне средине на ризик од алергијске болести у претклиничкој и клиничкој студији*).

Добитник је дипломе за најбољег студента који је завршио студијски програм Хемичар за животну средину у школској 2013/2014. години. Такође је награђена неколико пута у оквиру међународне мреже *CEEPUS Mobility Network* (2017. и 2018. године за учешће на семинару *Seminar/workshop on SENSING IN ELECTROANALYSIS*, Пардубице (Чешка република); током периода 2018-2020. године три пута је награђивана једномесечним боравком у Аустрији, на *Karl-Franzens* - Универзитету у Грацу.

Слађана З. Ђурђић је, до сада, аутор и ко-аутор 26 научних радова у међународним часописима, као и 12 саопштења на научним скуповима међународног значаја штампана у изводу (М34) и 12 саопштења на научним скуповима националног значаја штампана у изводу (М64). Из докторске дисертације су проистекла 2 рада, објављена у часописима категорије М21, и једно саопштење на научним скуповима међународног значаја штампана у изводу (М34).

Списак научних радова који су део докторске дисертације:

S. Đurđić, V. Vukojević, F. Vlahović, M. Ognjanović, Ľ. Švorc, K. Kalcher, J. Mutić, D. M. Stanković. Application of bismuth(III) oxide decorated graphene nanoribbons for enzymatic glucose biosensing. *Journal of Electroanalytical Chemistry*, 850 (**2019**) 113400. [Journal of Electroanalytical Chemistry, IF_{2019}=3.519; (17/86)].

https://www.sciencedirect.com/science/article/pii/S157266571930668X

S. Đurđić, V. Stanković, F. Vlahović, M. Ognjanović, K. Kalcher, T. Ćirković Veličković, J. Mutić, D. M. Stanković. Laccase Polyphenolic Biosensor Supported on MnO_2@GNP Decorated SPCE: Preparation, Characterization, and Analytical Application. Journal of The Electrochemical Society, 168 (**2021**) 037510. [Journal of The Electrochemical Society, IF_{2019}=3.719; (5/21)].

https://iopscience.iop.org/article/10.1149/1945-7111/abeaf2

Изјава о ауторству

Име и презиме аутора: **Слађана З. Ђурђић**

Број индекса: **ДХ09/2015**

Изјављујем

да је докторска дисертација под насловом:

„Композити графена и наноструктурисаних оксида као компоненте биосензора глукозе и полифенола“.

„Graphene and nano-structured oxides composites as components of glucose and polyphenols biosensors“.

- резултат сопственог истраживачког рада;
- да дисертација у целини ни у деловима није била предложена за стицање друге дипломе према студијским програмима других високошколских установа;
- да су резултати коректно наведени и
- да нисам кршио ауторска права и користио интелектуалну својину других лица.

У Београду,

16.06.2021.

Потпис аутора

Слађана Ђурђић

Изјава о истоветности штампане и електронске верзије докторског рада

Име и презиме аутора: **Слађана З. Ђурђић**

Број индекса: **ДХ09/2015**

Студијски програм **Хемија**

Наслов рада:

„Композити графена и наноструктурисаних оксида као компоненте биосензора глукозе и полифенола".

„Graphene and nano-structured oxides composites as components of glucose and polyphenols biosensors".

Ментори:

Др Јелена Мутић, ванредни професор Хемијског факултета - Универзитета у Београду

Др Далибор Станковић, доцент Хемијског факултета - Универзитета у Београду

Изјављујем да је штампана верзија мог докторског рада истоветна електронској верзији коју сам предао ради похрањена у **Дигиталном репозиторијуму Универзитета у Београду**. Дозвољавам да се објаве моји лични подаци везани за добијање академског назива доктора наука, као што су име и презиме, година и место рођења и датум одбране рада. Ови лични подаци могу се објавити на мрежним страницама дигиталне библиотеке, у електронском каталогу и у публикацијама Универзитета у Београду.

У Београду,

16.06.2021.

Потпис аутора

Слађана Ђурђић

Изјава о коришћењу

Овлашћујем Универзитетску библиотеку „Светозар Марковић" да у **Дигитални репозиторијум Универзитета у Београду** унесе моју докторску дисертацију под насловом:

„Композити графена и наноструктурисаних оксида као компоненте биосензора глукозе и полифенола".

„Graphene and nano-structured oxides composites as components of glucose and polyphenols biosensors".

која је моје ауторско дело.

Дисертацију са свим прилозима предала сам у електронском формату погодном за трајно архивирање. Моју докторску дисертацију похрањену у Дигиталном репозиторијуму Универзитета у Београду и доступну у отвореном приступу могу да користе сви који поштују одредбе садржане у одабраном типу лиценце Креативне заједнице (Creative Commons) за коју сам се одлучила.

1. Ауторство (CC BY)
2. Ауторство – некомерцијално (CC BY-NC)
3. Ауторство – некомерцијално – без прерада (CC BY-NC-ND)
4. Ауторство – некомерцијално – делити под истим условима (CC BY-NC-SA)
5. Ауторство – без прерада (CC BY-ND)
6. Ауторство – делити под истим условима (CC BY-SA)

У Београду,
16.06.2021.

Потпис аутора

Слађана Дмитровић

1. Ауторство. Дозвољавате умножавање, дистрибуцију и јавно саопштавање дела, и прераде, ако се наведе име аутора на начин одређен од стране аутора или даваоца лиценце, чак и у комерцијалне сврхе. Ово је најслободнија од свих лиценци.

2. Ауторство - некомерцијално. Дозвољавате умножавање, дистрибуцију и јавно саопштавање дела, и прераде, ако се наведе име аутора на начин одређен од стране аутора или даваоца лиценце. Ова лиценца не дозвољава комерцијалну употребу дела.

3. Ауторство - некомерцијално - без прерада. Дозвољавате умножавање, дистрибуцију и јавно саопштавање дела, без промена, преобликовања или употребе дела у свом делу, ако се наведе име аутора на начин одређен од стране аутора или даваоца лиценце. Ова лиценца не дозвољава комерцијалну употребу дела. У односу на све остале лиценце, овом лиценцом се ограничава највећи обим права коришћења дела.

4. Ауторство - некомерцијално - делити под истим условима. Дозвољавате умножавање, дистрибуцију и јавно саопштавање дела, и прераде, ако се наведе име аутора на начин одређен од стране аутора или даваоца лиценце и ако се прерада дистрибуира под истом или сличном лиценцом. Ова лиценца не дозвољава комерцијалну употребу дела и прерада.

5. Ауторство - без прерада. Дозвољавате умножавање, дистрибуцију и јавно саопштавање дела, без промена, преобликовања или употребе дела у свом делу, ако се наведе име аутора на начин одређен од стране аутора или даваоца лиценце. Ова лиценца дозвољава комерцијалну употребу дела.

6. Ауторство - делити под истим условима. Дозвољавате умножавање, дистрибуцију и јавно саопштавање дела, и прераде, ако се наведе име аутора на начин одређен од стране аутора или даваоца лиценце и ако се прерада дистрибуира под истом или сличном лиценцом. Ова лиценца дозвољава комерцијалну употребу дела и прерада. Слична је софтверским лиценцама, односно лиценцама отвореног кода.